Long-lived neutralinos as probes of gravitino dark matter

———————————————

Dissertation zur Erlangung des Doktorgrades

des Department Physik der Universität Hamburg

vorgelegt von

Jan Hajer

aus Eckernförde

Hamburg

2013

Zusammenfassung

Supersymmetrische Erweiterungen des Standard Models mit kleiner R-Paritätsbrechung und leptonzahlverletzenden Kopplungen sind natürlicherweise konsistent mit primordialer Nukleosynthese, thermaler Leptogenese und dunkler Materie, bestehend aus Gravitinos. Wir untersuchen sowohl Supergravitationsmodelle mit universellen Randbedingungen an der Skala der großen Vereinheitlichung und skalaren Taus oder bino-artigen Neutralinos als zweitleichtesten supersymmetrischen Teilchen (NLSP) als auch Modelle mit gemischter Eich- und Gravitationsvermittlung mit higgsino-artigen Neutralinos als NLSP. Fermi-LAT Daten über den Fluss der isotropen und diffusen Gamma Strahlung führen zu einer unteren Schranke an die Gravitino Lebensdauer, die wir in eine untere Schranke an die NLSP Zerfallslänge von einigen Zentimetern übersetzen. Zusammen mit den Massen des Gravitinos und des Neutralinos erhält man eine mikroskopische Bestimmung der Planck Masse. Für supersymmetrische Massenparamter, die am Large Hadron Collider (LHC) messbar wären, würde die Entdeckung einer Photonlinie in der Größenordnung der Fermi-LAT Obergrenze eine NLSP Zerfallslänge von einigen hundert Metern nach sich ziehen. Dies wäre am LHC messbar. Daher untersuchen wir im Detail die Empfindlichkeit der LHC Experimente auf die Größe der R-Paritätsbrechung auf Modelle, deren Massen für farbgeladene Teilchen starke Produktion erlauben als auch Modelle, deren Massen nur Drell-Yan Produktion erlauben. Wir simulieren die Signale und deren Untergrund mit öffentlich zugänglichen Programmen, die wir um die endliche Lebensdauer der NLSPs erweitert haben. Wir stellen fest, dass Werte der R-Paritätsbrechenden Skala vermessen werden können, die ein bis zwei Größenordnungen unter der aus Astrophysik und Kosmologie abgeleiteten oberen Schranke liegen. Am Beispiel des Higgsinos zeigen wir, dass im Falle eines Signals die NLSP Masse durch die Rekonstruktion einer zwei-Muon-Kante gemessen werden kann.

Abstract

Supersymmetric extensions of the Standard Model with small R-parity and lepton-number violating couplings are naturally consistent with primordial nucleosynthesis, thermal leptogenesis and gravitino dark matter. We consider both supergravity models with universal boundary conditions at the grand unification scale and a scalar tau or bino-like neutralino as the next-to-lightest supersymmetric particle (NLSP) as well as hybrid gauge-gravity mediation models with a higgsino-like neutralino as the NLSP. Fermi-LAT data on the isotropic diffuse gamma-ray flux yield a lower bound on the gravitino lifetime, which we translate into a lower bound of the NLSP decay length of several centimeters. Together with gravitino and neutralino masses, one obtains a microscopic determination of the Planck mass. For supersymmetric mass parameters that can be tested at the Large Hadron Collider (LHC), the discovery of a photon line with an intensity close to the Fermi-LAT limit would imply a NLSP decay length of several hundred meters, which can also be measured at the LHC. We conduct a detailed investigation of the sensitivity of LHC experiments to the amount of R-parity breaking for models with masses of the coloured particles, which allow for strong production, as well as masses which only allow for Drell-Yang production. We perform a simulation of signal and background events using tools that are publicly available, which we have extended in order to also simulate the finite NLSP decay length. We find that values of the overall scale of R-parity violation can be probed which are one to two orders of magnitude smaller than the present upper bound obtained from astrophysics and cosmology. Using the example of higgsinos, we demonstrate that, given a signal, the NLSP mass can be determined by reconstructing the di-muon mass edge.

Contents

Chapter 1

Introduction

The Large Hadron Collider (LHC) at CERN has greatly extended the energy reach of experimental particle physics. The recent observation of the Higgs particle [5] by both the ATLAS and CMS experiments at $\sim 126\,\text{GeV}$ [6, 7] has confirmed the mechanism of spontaneous electroweak (EW) symmetry breaking. Although the discovery of the Higgs field completes the Standard Model (SM), the search for new physics at even higher energies is not over. Such a light scalar receives quadratically divergent corrections to its mass, leading to large fine-tuning within the SM. Furthermore, although the gravitational evidence for dark matter (DM) is strong (see *e.g.* [8]), its particle nature has yet to be determined.

The minimal supersymmetric standard model (MSSM) addresses both these issues but also faces new problems. While unbroken supersymmetry (SUSY) only introduces one new parameter, the higgsino mass parameter μ, soft SUSY breaking generally introduces many new parameters along with sources of large flavour- and CP-violation (see *e.g.* [9]). The latter problems would be alleviated if the superpartners had large (multi-TeV) masses. Indeed, this would be consistent with the relatively large value of the Higgs mass and the current absence of LHC signals for any other new particles.

Furthermore, the SM predicts massless neutrinos, which contradicts the observation of neutrino oscillations [10]. The most straightforward extension of the SM to concur with this finding is given by right-handed Majorana neutrinos. Additionally, this model leads to interesting cosmological consequences, as one is able to explain the baryon asymmetry of the universe via leptogenesis. In thermal leptogenesis, the lepton asymmetry is created through the decays of these heavy right-handed neutrinos and then transferred to a baryon asymmetry via sphaleron processes. In order to generate the amount of CP asymmetry which is needed for this process, as well as to account for the small neutrino masses generated via the seesaw mechanism, the right-handed neutrinos need to be very heavy and therefore a high reheating temperature is required to produce them thermally [11–14].

Locally supersymmetric extensions of the SM predict the existence of the gravitino, the gauge fermion of supergravity (SUGRA) [15]. The high reheating temperature needed for thermal leptogenesis also leads to gravitinos being produced in great abundance. Since the gravitino couplings are suppressed by the Planck scale, late decays of heavy unstable gravitinos may interfere with big bang nucleosynthesis (BBN) and, hence, cause what is called gravitino problem [16–21]. For some patterns of SUSY breaking, however, the gravitino is the lightest supersymmetric particle (LSP), and therefore a natural DM candidate [22]. Accordingly, gravitino DM has become an attractive alternative [23] to the standard scenario of weakly

interacting massive particles (WIMPs) [24]. If the gravitino is the LSP and a DM candidate, the BBN bounds instead apply to the next-to-lightest supersymmetric particle (NLSP), which is then meta-stable and might alter BBN predictions.

One possible solution to this problem is given by a slight breaking of R-parity. R-parity conserves baryon and lepton number and is imposed in the usual MSSM in order to forbid proton decay. Its conservation also renders the lightest supersymmetric particle stable, making *e.g.* the lightest neutralino a natural WIMP DM candidate. From a theoretical point of view, however, R-parity conservation is not particularly favoured and the stability of the proton can be ensured by demanding the absence of either baryon or lepton number violation. The requirement of successful baryogenesis puts an upper bound on the amount of R-parity violation (RPV) that can be allowed without erasing the baryon asymmetry before the EW phase transition sets in [25–28].

Following [29], we break R-parity spontaneously at the grand unification scale, which leads to a model with bilinear R-parity breaking [30–33]. A small amount of RPV leads to a decaying gravitino with a lifetime exceeding the age of the universe, due to the double suppression of gravitino decays by the Planck mass and the small R-parity violating coupling. The lifetime of the NLSP, however, is sufficiently short to be consistent with primordial nucleosynthesis. This makes it possible to have a good gravitino DM candidate even with the high reheating temperatures needed for leptogenesis, thus solving the gravitino problem [34].

It has been shown that the gravitino can account for the observed DM abundance for typical gluino masses and different types of NLSPs [35]. Gravitino decays lead to characteristic signatures in high-energy cosmic rays, in particular to a diffuse gamma-ray flux [29, 34, 36–42]. The search of the Fermi Large Area Telescope (Fermi-LAT) collaboration for monochromatic photon lines [43] and the measurement of the diffuse gamma-ray flux [44] severely constrain possible signals from decaying DM [45].

The nature of the NLSP is determined by the details of the SUSY breaking mechanism. The simplest class of SUGRA models with universal boundary conditions at the scale of grand unified theories (GUTs) leads to bino-like neutralino or scalar tau NLSPs. More involved models, such as hybrid gauge-gravity mediated SUSY breaking [46], lead to light higgsinos with masses around the EW scale and the other sparticles typically in the TeV range. Such models are motivated by ways of obtaining the MSSM and grand unification in string theory that feature a hidden sector of exotic states. They thus make use of the mechanism present in gravity-mediated SUSY breaking to generate an EW-scale higgsino mass parameter, as well as of the advantages of gauge mediation by providing a large number of messengers.

For a neutralino NLSP, the matrix elements for gravitino and NLSP decays are directly related. Together with the lower bound on the gravitino lifetime, and the corresponding upper bound on the value of R-parity breaking, which is derived from the diffuse gamma-ray flux observed by the Fermi-LAT collaboration [43, 44], one obtains a lower bound on the NLSP decay length, varying from a few centimeters to several hundred meters.

Large macroscopic decay lengths are extremely powerful in discriminating against SM backgrounds in searches for decaying NLSPs [54]. This remains true if the decay length is larger than the size of the detector since a sizeable fraction of NLSPs may still decay inside the detector. This has been studied for both neutral and charged NLSPs with decay lengths ranging from a few millimeters to hundreds of meters [47–53]. This will lead to displacements of decay vertices in the outer layers of the multi-purpose LHC detectors ATLAS and CMS, which motivates the muon signatures that are considered here.

This work is organized as follows. In Chapter 2 we give a short overview of SUSY and introduce the relevant formulas. Afterwards, in Chapter 3 we motivate RPV in general and present our detailed analysis of bilinear RPV and consequential decays. We propose a new description of bilinear RPV with vanishing sneutrino vacuum expectation values (VEVs) and show how this notation simplifies the calculation of R-parity breaking decays. In Chapter 4 we use these results in order to constrain the viable parameter range of bilinear RPV as well as the properties of the decaying particles. Subsequently, in Chapter 5 we perform detailed detector studies of three relevant scenarios. Firstly, we show that bounds on sparticle masses can be weakened due to RPV, thus providing a possible explanation as to why SUSY has not been discovered yet, even if it is already being produced at the LHC. Secondly, we demonstrate that RPV can also enable detection of weakly coupled new physics that is generally not probed by the usual LHC searches. Furthermore, we discuss why the signal we consider would hide from the LHC searches performed so far, and show that the search strategy that we propose here could reveal new physics in the data already accumulated during the LHC runs with proton collisions at 8 TeV center-of-mass energy. Finally, we summarize our work in Chapter 6.

Chapter 2

Supersymmetry basics

The mass parameter of the Higgs Lagrangian is the only dimensionful parameter of the SM and determines the overall scale of the EW SM. The SM, however, does not possess a symmetry to protect this scalar mass against quadratic divergences. Therefore, quantum corrections will push the Higgs mass towards the cut-off scale of the theory, which might be as high as the Planck scale. An elegant solution to this so-called hierarchy problem of the SM is the introduction of SUSY, which stabilises this hierarchy by relating all bosonic masses to fermionic masses and, moreover, is free of quadratic divergences. Furthermore SUSY leads naturally to a DM candidate, be it a WIMP or the gravitino. An interesting observation is the unification of the gauge couplings at the GUT scale within the MSSM, as opposed to the SM, which does not lead to gauge coupling unification (*cf.* Figure 2.1).

In this chapter we give a rough overview of topics related to SUSY, which we need in the following sections and introduce the notation we are using.

2.1 Supersymmetric multiplets

SUSY is a symmetry between bosons and fermions (for a review see *e.g.* [56]). To that end every particle is accompanied by an supersymmetric partner, which has exactly the same properties with exception of the spin. These pairs together with non-propagating bosonic auxiliary fields form so-called supermultiplets. A supersymmetric field theory can be described by extending the usual bosonic Lorentz spacetime with coordinates x_μ with two fermionic directions θ and $\bar{\theta}$ to superspace. A superfield is a function on superspace and can be decomposed into its component fields which are functions on the usual Lorentz spacetime, by means of a power series expansion in the Grassmann variables θ and $\bar{\theta}$. In order to find irreducible representations of the SUSY algebra one has to impose constraints on the general scalar superfield. Demanding that the superderivative of the superfields vanishes

$$\overline{D}\Phi = 0 \,, \qquad\qquad \overline{D} = -\frac{\partial}{\partial\bar{\theta}} - i\theta\sigma^\mu\partial_\mu \,, \qquad (2.1a)$$

$$D\overline{\Phi} = 0 \,, \qquad\qquad D = \frac{\partial}{\partial\theta} + i\sigma^\mu\bar{\theta}\partial_\mu \,, \qquad (2.1b)$$

leads to a chiral superfield Φ, which contains a complex scalar field ϕ, a Weyl fermion ψ and an auxiliary scalar field F as well as its conjugate $\overline{\Phi}$ containing the conjugate component fields.
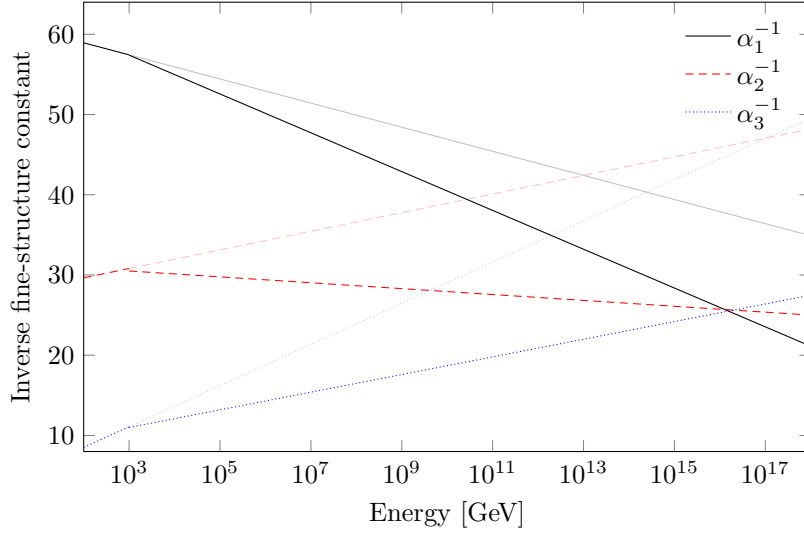
Figure 2.1: In contrast to the SM (light) the RGE running of the gauge couplings in the MSSM (strong) intersect in one point, which defines the GUT scale [55].

Requiring, on the other hand, that a superfield is real,

$$V^\dagger = V \ , \tag{2.2}$$

leads to a vector superfield V, which contains in the Wess-Zumino gauge a vector field A_μ, a Majorana fermion λ, as well as an auxiliary scalar field D.

The superpotential is a holomorphic function of chiral superfields

$$W(\Phi) = L_i \Phi_i + \frac{1}{2} M_{ij} \Phi_i \Phi_i + \frac{1}{6} y_{ijk} \Phi_i \Phi_j \Phi_k \ , \tag{2.3}$$

which, together with the real Kähler potential K, defines a renormalizable supersymmetric theory. For example the mass terms for Dirac fermions and the Yukawa coupling between two fermions and a scalar are given by the second derivative of the superpotential as a function of the scalar fields

$$\mathcal{L} \supset \frac{\partial^2 W(\phi)}{\partial \phi_i \partial \phi_j} \psi_i \psi_j + \text{h.c.} = W^{ij} \psi_i \psi_j + \text{h.c.} \tag{2.4}$$

Whereas the scalar potential is given by

$$V = \frac{\partial W(\phi)}{\partial \phi_i} \frac{\partial W^*(\phi)}{\partial \phi^i} = W^i W_i^* \ . \tag{2.5}$$

Furthermore we will need supersymmetric gauge interactions. The coupling between gauginos and the component fields of the chiral multiplet are given by the Lagrangian

$$-\mathcal{L} = \sqrt{2} g (\phi^\dagger T^a \psi) \lambda^a + \text{h.c.} \tag{2.6}$$

Name	Superfield	Scalar	Fermion	$(SU(3)_C, SU(2)_L)_{U(1)_Y}$
Quarks Squarks	Q	$\widetilde{q} = \begin{pmatrix} \widetilde{u}_L \\ \widetilde{d}_L \end{pmatrix}$	$q = \begin{pmatrix} u_L \\ d_L \end{pmatrix}$	$(\mathbf{3}, \mathbf{2})_{\frac{1}{6}}$
	U	$\widetilde{\overline{u}}_R$	$\overline{u}_R$	$(\overline{\mathbf{3}}, \mathbf{1})_{-\frac{2}{3}}$
	D	$\widetilde{\overline{d}}_R$	$\overline{d}_R$	$(\overline{\mathbf{3}}, \mathbf{1})_{\frac{1}{3}}$
Leptons Sleptons	L	$\widetilde{l} = \begin{pmatrix} \widetilde{\nu}_L \\ \widetilde{e}_L \end{pmatrix}$	$l = \begin{pmatrix} \nu_L \\ e_L \end{pmatrix}$	$(\mathbf{1}, \mathbf{2})_{-\frac{1}{2}}$
	E	$\widetilde{\overline{e}}_R$	$\overline{e}_R$	$(\mathbf{1}, \mathbf{1})_1$
	N	$\widetilde{\overline{\nu}}_R$	$\overline{\nu}_R$	$(\mathbf{1}, \mathbf{1})_0$
Higgs Higgsinos	H_u	$H_u = \begin{pmatrix} H_u^+ \\ H_u^0 \end{pmatrix}$	$h_u = \begin{pmatrix} h_u^+ \\ h_u^0 \end{pmatrix}$	$(\mathbf{1}, \mathbf{2})_{\frac{1}{2}}$
	H_d	$H_d = \begin{pmatrix} H_d^0 \\ H_d^- \end{pmatrix}$	$h_d = \begin{pmatrix} h_d^0 \\ h_d^- \end{pmatrix}$	$(\mathbf{1}, \mathbf{2})_{-\frac{1}{2}}$

Table 2.1: Chiral superfields of the MSSM including right-handed neutrinos.

2.2 Minimal supersymmetric standard model

The MSSM is the minimal consistent supersymmetric extension of the standard model (for a review see *e.g.* [57]). Every fermion and scalar of the SM is extended to a chiral supermultiplet, additionally a second Higgs multiplet is necessary (*cf.* Table 2.1) Therefore, the MSSM predicts many new scalar fields. The SM couplings are encoded in the superpotential

$$W_{\mathrm{RPC}} = \mu H_u H_d + h_{ij}^u Q_i U_j^c H_u + h_{ij}^d Q_i D_j^c H_d + h_{ij}^e L_i E_j^c H_d \ , \tag{2.7}$$

which conserves baryon and lepton number. The gauge fields of the SM are extended to gauge multiplets and therefore accompanied by gauginos (*cf.* Table 2.2).

2.3 Supergravity

Promoting SUSY to a local symmetry leads to SUGRA, which is a supersymmetric extension of general relativity. The supermultiplet of SUGRA contains, next to the usual graviton and some auxiliary fields, a spin three-half fermion, the gravitino ψ_μ.

2.3.1 Gravitino

Having spin three-half the gravitino possesses properties which distinguish it from usual fermions. In Appendix B.2 we derive the Lagrangian of a spinor-vector. In momentum space the mode functions are given by

$$\psi_\mu(x) = \psi_\mu^+(p, s) e^{-ipx} \ , \qquad \psi_\mu(x) = \psi_\mu^-(p, s) e^{-ipx} \ , \qquad s = \pm 3/2, \pm 1/2 \ . \tag{2.8}$$

Name	Superfield	Fermion	Vector	$(\mathrm{SU(3)_C}, \mathrm{SU(2)_L})_{\mathrm{U(1)_Y}}$
B, Bino	B	b	B_μ	$(\mathbf{1}, \mathbf{1})_0$
W, Wino	W	w	W_μ	$(\mathbf{1}, \mathbf{3})_0$
Gluon, Gluino	G	g	G_μ	$(\mathbf{8}, \mathbf{1})_0$

Table 2.2: Gauge supermultiplets of the MSSM.

The mode functions can be constructed from the usual spin-one-half fermion fields and the spin-one polarization vector ϵ_μ [58]

$$\psi_\mu^+(p,s) = \sum_{m,\lambda} \left\langle (1/2, m)(1, \lambda) \,\middle|\, (3/2, s) \right\rangle x(p, m)\epsilon_\mu(p, \lambda) \ , \tag{2.9a}$$

$$\psi_\mu^-(p,s) = \sum_{m,\lambda} \left\langle (1/2, m)(1, \lambda) \,\middle|\, (3/2, s) \right\rangle y(p, m)\epsilon_\mu(p, \lambda) \ , \tag{2.9b}$$

where the brackets are Clebsch-Gordan coefficients. In the following we will need the polarization tensor for gravitinos

$$P_{\mu\nu}^\pm(p) = \sum_s \psi_\mu^\pm(p,s)\psi_\nu^{\pm\dagger}(p,s) \ . \tag{2.10}$$

which we have derived in Appendix (B.4.3) and which is given in two-component notation by

$$P_{\mu\nu}^\pm(p) = (m_{3/2} \mp (\sigma p)) \left(\Pi_{\mu\nu}(p) - \frac{1}{3}\Pi_{\mu\sigma}(p)\Pi_{\nu\lambda}(p)\overline{\sigma}^\sigma \sigma^\lambda \right) \ , \tag{2.11}$$

where

$$\Pi_{\mu\nu}(p) = -g_{\mu\nu} + \frac{p_\mu p_\nu}{m_{3/2}^2} \ , \tag{2.12}$$

is the polarization tensor for a massive vector boson (*cf.* Equation (B.89)). The couplings of the gravitino are weaker than the couplings of usual fermions as they are suppressed by the Planck mass.

2.4   Supersymmetry breaking

As SUSY has not been discovered so far, it is obvious that SUSY cannot be an exact symmetry of an effective theory which extends the SM, but must be broken. The breaking of SUSY leads to masses for just the scalar field of the MSSM and, therefore, shifts the masses of these fields in so far unprobed energy regimes. SUSY can only be broken spontaneously by VEVs of the auxiliary fields of a supermultiplet. Therefore, one can distinguish between F-term breaking if the SUSY breaking is caused by the auxiliary field of a chiral multiplet, and D-term breaking if it is caused by the auxiliary field of a vector multiplet. Due to the supertrace theorem [59], it is, however, not possible to construct viable models which break SUSY in the auxiliary fields of the MSSM supermultiplets or any supermultiplet that couples renormalizable to the MSSM. Therefore, one has to assume that SUSY breaking happens in a hidden sector and is mediated to the MSSM.
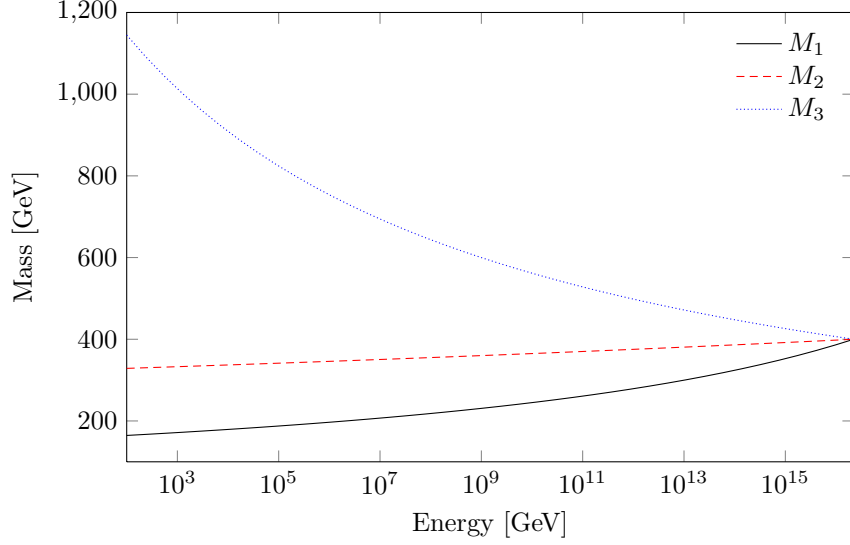
Figure 2.2: RGE running of gaugino masses under the CMSSM assumption of unified gaugino masses $m_{1/2}$ at the GUT scale [55].

2.4.1 Explicit supersymmetry breaking

The precise breaking mechanism is so far unknown, but can be parametrized by the explicit breaking terms collected in the soft SUSY breaking Lagrangian

$$
\begin{aligned}
-\mathcal{L}_{\text{soft}} = {} & m_u^2 H_u^\dagger H_u + m_d^2 H_d^\dagger H_d + (B H_u H_d + \text{h.c.}) \\
& + \widetilde{m}_{li}^2 \widetilde{l}_i^\dagger \widetilde{l}_i + \widetilde{m}_{ei}^2 \widetilde{e}_i^\dagger \widetilde{e}_i + \widetilde{m}_{qi}^2 \widetilde{q}_i^\dagger \widetilde{q}_i + \widetilde{m}_{ui}^2 \widetilde{u}_i^\dagger \widetilde{u}_i + \widetilde{m}_{di}^2 \widetilde{d}_i^\dagger \widetilde{d}_i \\
& + \frac{1}{2} \left(M_1 bb + M_2 ww + M_3 gg + \text{h.c.} \right) \\
& + \left(A_u \widetilde{q}_i H_u \widetilde{u}_j^\dagger + A_d \widetilde{q}_i H_d \widetilde{d}_j^\dagger + A_e \widetilde{l}_i H_u \widetilde{e}_j^\dagger + \text{h.c.} \right) \ .
\end{aligned}
\tag{2.13}
$$

In order to reduce this large number of new parameters, one has to assume a certain breaking mechanism or at least relate these parameter to just a few parameters at the mass scale of a unified theory.

2.4.2 Planck-suppressed mediation

One possible mediation mechanism is mediation by Planck-suppressed operators, which is usually called gravity mediation and originates in new physics including quantum gravity at the Planck scale. F-term breaking in this scenario would lead to soft SUSY breaking masses of order

$$
m_{\text{soft}} \simeq \frac{\langle F \rangle}{M_{\text{P}}} \ .
\tag{2.14}
$$

Therefore, the SUSY breaking scale for TeV-scale MSSM soft terms is of order $\sqrt{\langle F \rangle} \simeq 5 \times 10^{11} \, \text{GeV}$. The most severe problem of gravity mediated SUSY breaking is the introduction of new sources of flavour violation and therefore possible large flavour changing neutral currents

(FCNCs). Hence, a mechanism must be implemented which ensures flavour universality of the soft SUSY breaking terms. The CMSSM is the result of a popular assumption which reduced the number of parameters to four

$$M_1 = M_2 = M_3 = m_{1/2} \ , \tag{2.15a}$$

$$\widetilde{m}_q^2 = \widetilde{m}_u^2 = \widetilde{m}_d^2 = \widetilde{m}_L^2 = \widetilde{m}_e^2 = m_0^2 \mathbb{1} \ , \qquad m_{H_d}^2 = m_{H_u}^2 = m_0^2 \ , \tag{2.15b}$$

$$A_u = A_0 y_u \ , \qquad\qquad A_d = A_0 y_d \ , \qquad A_e = A_0 y_e \ , \tag{2.15c}$$

$$B = B_0 \mu \ . \tag{2.15d}$$

The ongoing searches for SUSY at the LHC have already excluded a large part of the parameter space of this overly simple model. The unification at the high energy scale leads to simple relations at the TeV scale. For example, assuming unified gaugino masses at the GUT scale the RGE running predicts mass ratios between the gaugino mass parameters at the TeV scale of[1]

$$\frac{M_2}{M_1} = \frac{3}{5}\frac{1}{t_w^2} \simeq 2 \ , \qquad\qquad \frac{M_3}{M_1} = \frac{3}{5}\frac{\alpha_s}{\alpha}c_w^2 \simeq 6 \ , \tag{2.16}$$

where c_w and t_w are the sine and tangent of the weak mixing angle, respectively. This can as well be seen in Figure 2.2.

2.4.3 Messenger gauge mediation

Another possibility to mediate the breaking of SUSY in the hidden sector to the MSSM is via messengers of mass M_m which are charged under the SM gauge group [60]. The soft masses are loop-suppressed and F-term breaking leads to a characteristic soft mass scale of

$$m_\mathrm{soft} \simeq \frac{\alpha_i}{4\pi}\frac{\langle F \rangle}{M_\mathrm{m}} \ , \tag{2.17}$$

where α_i are the fine-structure constants of the SM. If the masses of the messengers are comparable to the VEV responsible for SUSY breaking, then the SUSY breaking scale can be as low as $\sqrt{\langle F \rangle} \simeq M_\mathrm{m} \simeq 10^4\,\mathrm{GeV}$. In general, however, both scales can be much higher.

2.4.4 Hybrid gauge gravity mediation

If both the above mediation mechanism are present, the two contributions are of the same order as long as the messenger scale is only about a loop factor smaller than the Planck scale. In this case, gauge mediation is dominant for large numbers of messengers.

In certain grand-unified models which naturally emerge from string constructions, there is a large number of vector-like states in incomplete GUT multiplets which should decouple close to the GUT scale [46]. They serve as messengers for gauge-mediated supersymmetry breaking, inducing gaugino masses and scalar soft masses. The gravity-mediated contributions to the MSSM parameters are subdominant with respect to the gauge-mediated ones. The only exception are the μ and B parameters, to which (minimal) gauge mediation does not contribute at all. These two parameters are induced by gravitationally suppressed interactions through the Giudice-Masiero mechanism [61], leading to light higgsinos and otherwise heavy superparticles. Related models with mixed gauge-gravity mediation have previously been discussed in [62].

---

[1]Here and in the following we abbreviate the trigonometric functions by: $\cos(w) = c_w$, $\sin(w) = s_w$ and $\tan(w) = t_w$.

Light higgsinos

The main properties of the higgsino sector in our model of hybrid gauge gravity mediation can be summarized as follows. Since

$$|\mu| \ll |M_1|, \ |M_2| \ , \tag{2.18}$$

where M_1 and M_2 are the bino and wino masses of (2.13) respectively, there are three higgsino-like light states χ_1^0 , $\chi_1^\pm$ and χ_2^0 with masses close to $|\mu|$. Their mass splittings will be of the order $m_Z^2/M_{1,2}$, typically a few GeV for $|\mu| \gtrsim 100\,\mathrm{GeV}$ and for TeV-scale gaugino masses. A thermally produced χ_1^0 LSP is not a viable dark matter candidate, since its relic density is extremely low due to the large annihilation cross section. This same mechanism, on the other hand, can substantially ameliorate the gravitino BBN problem if dark matter consists of gravitinos instead. The χ_1^0 is then the NLSP, but it will be effectively stable on collider time scales.

Chapter 3

R-parity breaking

In this section we first give a short introduction to the concept of conserved R-symmetry and reasons for its breaking to the residual R-parity. Then we give two physical models which break R-parity, thereby we derive a thorough overview of bilinear R-parity breaking and its physical consequences. Finally, we derive the decays of scalar leptons, neutralinos and the gravitino which are induced by R-parity breaking.

3.1 Neutrino masses and lepton number violation

Despite the fact, that the SM predicts massless neutrinos, it is by now well established that neutrinos are massive, even so their mass is tiny [10]. Although many extensions of the SM which explain this observation have been proposed, the debate on the correct mechanism is still active. As we will show, broken R-parity leads to neutrino masses, as long as it is lepton number violating. This is an example for the general statement, that every lepton number violating operator leads to neutrino masses [63]. A more common mechanism, which does not depend on SUSY, is the seesaw mechanism which introduces a set of heavy right-handed neutrinos ν_R which are singlets under the SM gauge group (A.1). It is straightforward to extend this idea to SUSY, *i.e.* promote ν_R to a chiral multiplet N. The new fields allow new superpotential terms

$$W_N = h_{ij}^e L_i E_j^c H_d + h_{ij}^\nu L_i N_j^c H_u + \frac{1}{2} M_{ij}^N N_i^c N_j^c \ . \tag{3.1}$$

The Majorana mass term M^N is unique in the (minimal supersymmetric) SM as it is only allowed for gauge singlets. One consequence is the violation of lepton number by $\Delta L = 2$. We are assuming that the Majorana mass term is close to the GUT scale. Whereas the Dirac mass $m_D = h_{ij}^\nu v$ is of the order of the Higgs VEV v. Therefore the seesaw mechanism [64–66] leads to tiny neutrino masses which are to first order given by the eigenvalues of

$$M^\nu = -m_{\mathrm{D}}(M^N)^{-1} m_{\mathrm{D}}^T \ . \tag{3.2}$$

The SM Lagrangian with massless neutrinos conserves lepton and baryon number. Therefore the SM, barring non-perturbative effects, conserves these quantum numbers. Hence, basic extensions such as the R-parity conserving MSSM are assumed to be also lepton and baryon number conserving. The motivation to keep these accidental symmetries as well in supersymmetric extensions of the SM is reduced if even the non supersymmetric theory breaks lepton number.

3.2 From R-invariance to R-parity

In an attempt to extend the SM with SUSY one faces the problem of how to define baryon and lepton number in supersymmetric theories, especially as the concept of conserved baryon and lepton number is in the SM intrinsically connected with fermion fields. As it turns out, the $(\mathcal{N} = 1)$ super Poincaré-algebra has a unique Abelian extension, the $U(1)_R$-symmetry, which acts on the SUSY generators. Therefore, it is possible to introduce an additive conserved quantum number R [67], whose value differs by ± 1 unit for the two components of each SUSY multiplet, and might be connected to baryon and lepton number. Hence, as long as the R-charge is conserved, all potentially dangerous processes which connect different SM fermion fields via their scalar partners are forbidden.

With this symmetry imposed, however, Majorana masses are prohibited and gauginos and the gravitino stay massless, which contradicts experimental results, *e.g.* the non-observation of light R-hadrons. Furthermore an explicit higgsino mass term μ is forbidden as well. As spontaneously broken SUGRA requires a massive gravitino it has to break the $U(1)_R$. The remaining discrete $\mathbb{Z}_2$ subgroup is called R-parity [68] and can be expressed as a product of the spin quantum number S and matter parity $3B + L$

$$R_p = (-1)^R = (-1)^{2S}(-1)^{3B+L} = (-1)^{2S}(-1)^{3(B-L)} \ , \tag{3.3}$$

where B is the baryon number and L is the lepton number. R-parity allows not only for massive gravitinos but also for mass terms of gauginos and higgsinos. This intimate relationship of the breaking of R-invariance and these mass terms allows to build models where theses masses are of the same order [69].

In superspace R-parity can be interpreted as an invariance under reflection of the fermionic Grassmann coordinate $\theta \rightarrow -\theta$, in practice it distinguishes between particles and super particles. All terms of the superpotential (2.7) are invariant under R-parity.

In the SM of particle physics, baryon and lepton number conservation are accidental symmetries, therefore there is no theoretical reason to assume R-parity conservation (RPC), however observation of nature tells us that it must be at least a approximate symmetry of every supersymmetric low energy extension of the SM.

3.3 General R-parity breaking

If one abandons the requirement of R-parity conservation, new and potentially dangerous operators have to be considered. The most general gauge invariant superpotential of the MSSM particle content contains, next to the RPC terms (2.7), the R-parity breaking terms

$$W_{\text{RPV}} = \mu_i H_u L_i + \frac{1}{2}\lambda_{ijk} L_i E_j^c L_k + \lambda'_{ijk} D_i^c Q_j L_k + \frac{1}{2}\lambda''_{ijk} U_i^c D_j^c D_k^c \ . \tag{3.4}$$

Where the bilinear term and the first two trilinear terms leads to lepton number violation (LNV) and the last term to baryon number violation (BNV). After introducing R-parity breaking operators in the supersymmetric theory in general one has to extend the model of SUSY breaking as well. In order to stay agnostic about the concrete structure of SUSY breaking, we introduce all allowed explicit SUSY and R-parity breaking terms

$$-\mathcal{L}_{\text{RPV}} = B_i H_u \tilde{l}_i + m_{id}^2 \tilde{l}_i^\dagger H_d + \frac{1}{2}A_{ijk}\tilde{l}_i\tilde{l}_i\widetilde{e}_k^c + A'_{ijk}\tilde{l}_i\widetilde{g}_i\widetilde{d}_k^c + \frac{1}{2}A''_{ijk}\widetilde{u}_i^c\widetilde{d}_i^c\widetilde{d}_k^c + \text{h.c.} \tag{3.5}$$
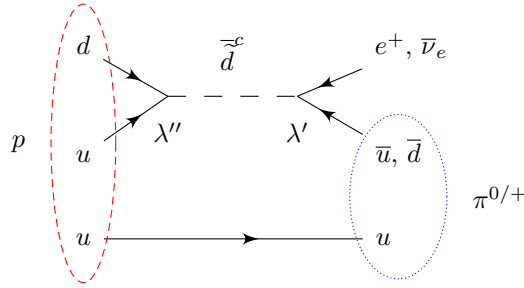
Figure 3.1: Proton decay in general RPV via the lepton number violating coupling λ' and the baryon number violating coupling λ''.

In general these new operators introduce 48 supersymmetric parameters and 51 SUSY breaking parameters.

3.3.1   Proton decay

Together, baryon number and lepton number violating processes lead to proton decay. In the case of RPV the largest contribution comes from an effective interaction of the form (*cf.* Figure 3.1) [32]

$$\mathcal{L} = \frac{\lambda'' \lambda'^*}{m_{\tilde{d}}^2} \left((u^c d^c)^\dagger (\nu d) - (u^c d^c)^\dagger (eu) \right) + \text{h.c.} \tag{3.6}$$

So far no evidence for proton decay have been found and the strongest constraint on the proton lifetime is given by [70]

$$\tau_{p \to \pi^0 e^+} \geq 5.5 \times 10^{23} \tau_{\text{Universe}} \; , \tag{3.7}$$

which leads to a stringent bound of

$$\sqrt{\lambda' \lambda''} \lesssim 4 \times 10^{-14} \; . \tag{3.8}$$

By forbidding either lepton or baryon number violating terms we are left with weaker bounds coming *e.g.* from neutrino-less double β decay.

3.4   Minimal flavour violating R-parity breaking

One way to control baryon and lepton number violating processes and to suppress flavour changing operators is to impose minimal flavour violation (MFV).

3.4.1   Spurious flavour symmetries

The largest possible flavour group of the SM matter content that still commutes with the SM gauge group (A.1) is given by [71, 72]

$$\text{U}(3)^5 \simeq G_q \times G_l \times G_A \; , \tag{3.9}$$

where we have defined

$$G_q = \mathrm{SU}(3)_Q \times \mathrm{SU}(3)_U \times \mathrm{SU}(3)_D \ , \tag{3.10a}$$

$$G_l = \mathrm{SU}(3)_L \times \mathrm{SU}(3)_E \ , \tag{3.10b}$$

$$G_A = \mathrm{U}(1)_\mathrm{B} \times \mathrm{U}(1)_\mathrm{L} \times \mathrm{U}(1)_\mathrm{Y} \times \mathrm{U}(1)_\mathrm{PQ} \times \mathrm{U}(1)_E \ . \tag{3.10c}$$

The charges of the Abelian symmetries are Baryon number (B), Lepton number (L), hypercharge (Y), a Peccei-Quinn (PQ) symmetry of two Higgs doublet models (2HDMs) and a global rotation of a single $\mathrm{SU}(2)_\mathrm{L}$ singlet (E). The SM Higgs mass keeps these symmetries intact, the Yukawa couplings, however, break these symmetries except for $\mathrm{U}(1)_\mathrm{B} \times \mathrm{U}(1)_\mathrm{L} \times \mathrm{U}(1)_\mathrm{Y}$. In order to recover the full flavour symmetry one promotes the Yukawa couplings to spurion fields, which transform under the flavour group in such a way that all gauge invariant terms of the superpotential are also flavour invariant

$$h^u = (\mathbf{3}, \overline{\mathbf{3}}, \mathbf{1})_{G_q} \ , \qquad h^d = (\mathbf{3}, \mathbf{1}, \overline{\mathbf{3}})_{G_q} \ , \qquad h^e = (\mathbf{3}, \overline{\mathbf{3}})_{G_l} \ . \tag{3.11}$$

In supersymmetric theories these spurion fields have to be superfields. Remembering that the superpotential terms must be holomorphic severely restricts the RPV terms which are allowed next to the usual RPC terms [73]. The only allowed RPV term is the BNV in (3.4)

$$W_\mathrm{MFV} = \frac{1}{2} a h^u U^c h^d D^c h^d D^c \ , \tag{3.12}$$

where a is a coupling which we assume to be of $\mathcal{O}(1)$. This superpotential term is naturally suppressed by $\mathcal{O}(h^3)$.

3.4.2 Minimal flavour violation and the seesaw mechanism

Adding the right-handed neutrino (3.1) increases the flavour symmetry. The lepton flavour group (3.10b) is now

$$G_l = \mathrm{SU}(3)_L \times \mathrm{SU}(3)_E \times \mathrm{SU}(3)_N \ . \tag{3.13}$$

The Majorana neutrino mass term (3.1) breaks the $\mathrm{SU}(3)_N$ [74]. In order to restore the spurious symmetries broken by the Yukawa couplings and the Majorana mass term three spurions are needed in the extended lepton sector

$$h^e = (\mathbf{3}, \overline{\mathbf{3}}, \mathbf{1})_{G_l} \ , \qquad h^\nu = (\mathbf{3}, \mathbf{1}, \overline{\mathbf{3}})_{G_l} \ , \qquad M^N = (\mathbf{1}, \mathbf{1}, \overline{\mathbf{6}})_{G_l} \ . \tag{3.14}$$

The two new spurions allow, in addition to the BNV term (3.12), just one holomorphic, lepton number violating superpotential term [73].

$$W_\mathrm{MFV}^\mathrm{seesaw} = \frac{1}{2\Lambda} c \det^2 h^\nu \, (LL) \left((h^\nu)^{-1} M^N (h^\nu)^{-1} \right) (h^e E^c) \ . \tag{3.15}$$

Therefore, all lepton number violating processes are suppressed by the small neutrino mass (3.2). which allows to keep processes leading to proton decays small enough to evade the proton bounds (3.8). Furthermore non-holomorphic bilinear RPV terms are generated and are as well suppressed by the neutrino mass, which leads to the usual RPV phenomenology induced by scalar neutrino VEVs.

	Ψ	H_u	H_d	N	N^c	Φ	X	Z
R	1	0	0	0	-2	-1	4	0

Table 3.1: R-charges of matter fields $\Psi = q,\ u^c,\ e^c,\ d^c,\ l,\ \nu^c$, Higgs fields and gauge singlets in spontaneous R-parity breaking.

3.5   Bilinear R-parity breaking

In this section we will discuss a further possibility to break R-parity in such a way that only couplings which are proportional to the SM Yukawa couplings are introduced. In models with bilinear R-parity breaking, only the mass mixing term between lepton and Higgs fields appears in the superpotential,

$$\Delta W = \mu_i H_u L_i \ . \tag{3.16}$$

Induced by SUSY breaking, the mixing between lepton and Higgs fields appears as well in the scalar potential,

$$\Delta \mathcal{L} = -B_i H_u \tilde{l}_i - m_{id}^2 \tilde{l}_i^\dagger H_d + \text{h.c.} \tag{3.17}$$

In the following we will discuss a model that introduces this kind of RPV and the consequences following from these mixing terms together with the RPC superpotential (2.7) and the SUSY breaking masses (2.13), where, for simplicity, we have assumed flavour diagonal mass matrices.

3.5.1   Spontaneous R-parity breaking

Let us now compute the parameters μ_i, B_i and m_{id}^2 in a specific example where the spontaneous breaking of R-parity is related to the spontaneous breaking of $\text{B} - \text{L}$, the difference of baryon and lepton number [29].

   We consider a supersymmetric extension of the SM with symmetrygroup

$$G = G_{\text{SM}} \times U(1)_{\text{B}-\text{L}} \times U(1)_{\text{R}} \ . \tag{3.18}$$

In addition to three quark lepton generations and the Higgs fields H_u and H_d the model contains three right-handed neutrinos ν_i^c, two non-Abelian singlets N^c and N, which transform as ν^c and its complex conjugate, respectively, and three gauge singlets X, Φ and Z. The part of the superpotential responsible for neutrino masses has the usual form

$$W_\nu = h_{ij}^\nu l_i \nu_j^c H_u + \frac{1}{M_{\text{P}}} h_{ij}^n \nu_i^c \nu_j^c N^2 \ , \tag{3.19}$$

where $M_{\text{P}} = 2.4 \times 10^{18}\,\text{GeV}$ is the Planck mass. The expectation value of H_u generates Dirac neutrino masses, whereas the expectation value of the singlet Higgs field N generates the Majorana mass matrix of the right-handed neutrinos ν_i^c. The superpotential responsible for $\text{B} - \text{L}$ breaking is chosen as

$$W_{\text{B}-\text{L}} = X \left(N N^c - \Phi^2 \right) \ , \tag{3.20}$$

where unknown Yukawa couplings have been set equal to one. Φ plays the role of a spectator field, which will finally be replaced by its VEV, $\langle \Phi \rangle = v_{\text{B}-\text{L}}$. Similarly, Z is a spectator

field which breaks SUSY and U(1)$_\mathrm{R}$, $\langle Z \rangle = F_Z \theta\theta$. The superpotential in Equation (3.19) and (3.20) is the most general one consistent with the R-charges listed in Table 3.1, up to nonrenormalizable terms which are irrelevant for our discussion.

The expectation value of Φ leads to the breaking of B − L,

$$\langle N \rangle = \langle N^c \rangle = \langle \Phi \rangle = v_{\mathrm{B-L}} \ , \tag{3.21}$$

where the first equality is a consequence of the U(1)$_\mathrm{B-L}$ D-term. This generates a Majorana mass matrix M for the right-handed neutrinos with three large eigenvalues, which we assume to fulfil $M_3 > M_2 > M_1$. If the largest eigenvalue of h^n is $\mathcal{O}(1)$, one has $M_3 \simeq v_{\mathrm{B-L}}^2 / M_\mathrm{P}$. Integrating out the heavy Majorana neutrinos one obtains the familiar dimension-5 seesaw operator which yields the light neutrino masses.

Since the field Φ carries R-charge −1, the VEV $\langle \Phi \rangle$ breaks R-parity, which is conserved by the VEV $\langle Z \rangle$. Thus, the breaking of B − L is tied to the breaking of R-parity, which is then transmitted to the low-energy degrees of freedom via higher-dimensional operators in the superpotential and the Kähler potential. Bilinear R-parity breaking is obtained from a correction to the Kähler potential,

$$\begin{aligned}
\Delta K = \ & \frac{1}{M_\mathrm{P}^3} \left(a_i Z^\dagger \Phi^\dagger N^c H_u l_i + a_i' Z^\dagger \Phi N^\dagger H_u l_i \right) \\
& + \frac{1}{M_\mathrm{P}^4} \left(b_i Z^\dagger Z \Phi^\dagger N^c H_u l_i + b_i' Z^\dagger Z \Phi N^\dagger H_u l_i \right. \\
& \left. + c_i Z^\dagger Z \Phi^\dagger N^c l_i^\dagger H_d + c_i' Z^\dagger Z \Phi N^\dagger l_i^\dagger H_d \right) + \mathrm{h.c.}
\end{aligned} \tag{3.22}$$

Replacing the spectator fields Z and Φ, as well as N^c and N by their expectation values, one obtains the correction to the superpotential

$$\Delta W = \mu_i H_u l_i \ , \tag{3.23}$$

with

$$\mu_i = \sqrt{3} \left(a_i + a_i' \right) m_{3/2} \Theta \ , \qquad \Theta = \frac{v_{\mathrm{B-L}}^2}{M_\mathrm{P}^2} \simeq \frac{M_3}{M_\mathrm{P}} \ , \qquad m_{3/2} = \frac{F_Z}{\sqrt{3} M_\mathrm{P}} \ . \tag{3.24}$$

Note that Θ can be increased or decreased by including appropriate Yukawa couplings in Equation (3.19) and (3.20). The corresponding corrections to the scalar potential are given by

$$-\Delta \mathcal{L} = B_i H_u \tilde{l}_i + m_{id}^2 \tilde{l}_i^\dagger H_d + \mathrm{h.c.} \ , \tag{3.25}$$

where

$$B_i = 3 \left(b_i + b_i' \right) m_{3/2}^2 \Theta \ , \qquad\qquad m_{id}^2 = 3 \left(c_i + c_i' \right) m_{3/2}^2 \Theta \ . \tag{3.26}$$

The corresponding R-parity conserving terms are generated by [61]

$$K \supset \frac{a_0}{M_\mathrm{P}} Z^\dagger H_u H_d + \frac{b_0}{M_\mathrm{P}^2} Z^\dagger Z H_u H_d + \mathrm{h.c.} \ , \tag{3.27}$$

which yields

$$\begin{aligned}
W &\supset \mu H_u H_d \ , & \mu &= \sqrt{3} a_0 m_{3/2} \ , & \text{(3.28a)} \\
-\mathcal{L} &\supset B H_u H_d + \mathrm{h.c.} \ , & B &= 3 b_0 m_{3/2}^2 \ . & \text{(3.28b)}
\end{aligned}$$

ψ_i	$\mathbf{10}_3$	$\mathbf{10}_2$	$\mathbf{10}_1$	Φ_3^*	Φ_2^*	Φ_1^*	ν_3^c	ν_2^c	ν_1^c	H_u	H_d	Φ	X	Z
Q_i	0	1	2	1	1	2	0	0	1	0	0	0	0	0

Table 3.2: Froggatt-Nielsen U(1) flavour charges. $\mathbf{10}_i = (q_i, u_i^c, e_i^c)$, $\Phi = (d_i^c, l_i)$, $i = 1 \dots 3$.

Higher dimensional operators yield further R-parity violating couplings between scalars and fermions. However, the cubic couplings allowed by the symmetries of our model are suppressed by one power of $M_{\rm P}$ compared to ordinary Yukawa couplings and cubic soft SUSY breaking terms. Note that the coefficients of the nonrenormalizable operators are free parameters, which are only fixed in specific models of SUSY breaking. In particular, one may have $\mu^2, \widetilde{m}_i^2 > m_{3/2}^2$ and hence a gravitino LSP. All parameters are defined at the GUT scale and have to be evolved to the EW scale by the renormalization group equations.

Flavour symmetry

The phenomenological viability of the model depends on the size of R-parity breaking mass mixings and therefore on the scale $v_{\rm B-L}$ of R-parity breaking as well as the parameters $a_i \dots c_i'$ in Equation (3.22). Any model of flavour physics, which predicts Yukawa couplings, will generically also predict the parameters $a_i \dots c_i'$. As a typical example, we use a model [75] for quark and lepton mass hierarchies based on a Froggatt-Nielsen U(1) flavour symmetry, which is consistent with thermal leptogenesis and all constraints from flavour changing processes [76].

The mass hierarchy is generated by the expectation value of a singlet field ϕ with charge $Q_\phi = -1$ via nonrenormalizable interactions with a scale

$$\Lambda = \frac{\langle \phi \rangle}{\eta} > \Lambda_{\rm GUT} \ , \qquad\qquad \eta \simeq 0.06 \ . \qquad\qquad (3.29)$$

The η-dependence of Yukawa couplings and bilinear mixing terms for multiplets ψ_i with charges Q_i is given by

$$h_{ij} \propto \eta^{Q_i+Q_j} \ , \qquad \mu_i \propto \eta^{Q_i} \ , \qquad B_i \propto \eta^{Q_i} \ , \qquad m_{id}^2 \propto \eta^{Q_i} \ . \qquad (3.30)$$

The charges Q_i for quarks, leptons, Higgs fields and singlets are listed in Table 3.2. The neutrino mass scale $m_\nu \simeq 0.01\,{\rm eV}$ implies for the heaviest right-handed neutrinos $M_2 \sim M_3 \sim 10^{12}\,{\rm GeV}$. The corresponding scales for B − L breaking and R-parity breaking are

$$v_{\rm B-L} \simeq 10^{15}\,{\rm GeV} \ , \qquad\qquad \Theta = \frac{v_{\rm B-L}^2}{M_{\rm P}^2} \simeq 10^{-6} \ . \qquad (3.31)$$

For the small R-parity breaking considered in this paper the neutrino masses are dominated by the conventional seesaw contribution [29].

The R-parity breaking parameters μ_i, B_i and m_{id}^2 strongly depend on the mechanism of SUSY breaking. In the example considered in this section all mass parameters are $\mathcal{O}(m_{3/2})$, which corresponds to gravity or gaugino mediation. From Equation (3.24), (3.26) and (3.30) one reads off

$$\mu_i = \widehat{a}\eta^{Q_i}m_{3/2}\Theta \ , \qquad B_i = \widehat{b}\eta^{Q_i}m_{3/2}^2\Theta \ , \qquad m_{id}^2 = \widehat{c}\eta^{Q_i}m_{3/2}^2\Theta \ , \qquad (3.32)$$

with $\widehat{a}, \widehat{b}, \widehat{c} = \mathcal{O}(1)$.

Loop corrections

Depending on the mechanism of SUSY breaking, the R-parity breaking soft terms may vanish at the GUT scale [31], therefore, we choose

$$B_i\left(\Lambda_{\mathrm{GUT}}\right) = m_{id}^2\left(\Lambda_{\mathrm{GUT}}\right) = 0 \ . \tag{3.33}$$

Non-zero values of these parameters at the EW scale are then induced by radiative corrections. The renormalization group equations for the bilinear R-parity breaking mass terms read (*cf.* Reference [31]):

$$16\pi^2 \frac{d\mu_i}{d\ln\Lambda} = 3\mu_i\left(h_{jk}^u h_{jk}^{u*} - \frac{1}{5}g_1^2 - g_2^2\right) + \mu_k h_{ij}^e h_{kj}^{e*} - \mu\left(\lambda_{ijk}h_{kj}^{e*} + 3\lambda'_{kji}h_{kj}^{d*}\right) \ , \tag{3.34a}$$

$$\begin{aligned}
16\pi^2 \frac{dB_i}{d\ln\Lambda} = {}&3B_i\left(h_{jk}^u h_{jk}^{u*} - \frac{1}{5}g_1^2 - g_2^2\right) + 6\mu_i\left(\frac{1}{5}g_1^2 M_1 + g_2^2 M_2\right) \\
&+ B_k h_{ij}^e h_{kj}^{e*} - B\left(\lambda_{ijk}h_{kj}^{e*} + 3\lambda'_{kji}h_{kj}^{d*}\right) \ ,
\end{aligned} \tag{3.34b}$$

$$\begin{aligned}
16\pi^2 \frac{dm_{id}^2}{d\ln\Lambda} = {}&\lambda_{kji}^* h_{kj}^e m_d^2 - m_{jd}^2 h_{jk}^e h_{ik}^{e*} - 3\lambda'_{kji}h_{kj}^d m_d^2 + h_{jk}^e h_{jk}^{e*} m_{id}^2 \\
&+ 3h_{kj}^{d*}h_{kj}^d m_{id}^2 + \widetilde{m}_{li}^2 \lambda_{nki}^* h_{nk}^e - 3\widetilde{m}_{li}^2 \lambda'^*_{nki} h_{nk}^e \\
&+ 2\lambda_{kji}^* \widetilde{m}_{lk}^2 \lambda_{kj} + 2\lambda_{kji}^* h_{kj}^e \widetilde{m}_{ej}^2 - 6\lambda_{kji}^{\prime*} h_{kj}^d \widetilde{m}_{dk}^2 - 6\lambda'_{kji}\widetilde{m}_{qj}^2 h_{kj}^d \ .
\end{aligned} \tag{3.34c}$$

In bilinear R-parity breaking, the R-parity violating Yukawa couplings vanish at the GUT scale. One-loop radiative corrections then yield for the soft terms at the EW scale (*cf.* Equations (3.34a) and (3.34b))

$$B_i\left(\Lambda_{\mathrm{EW}}\right) = \frac{\mu_i}{16\pi^2}6\left(\frac{1}{5}g'^2 M_1 + g^2 M_2\right)\ln\frac{\Lambda_{\mathrm{GUT}}}{\Lambda_{\mathrm{EW}}} \ , \qquad m_{id}^2\left(\Lambda_{\mathrm{EW}}\right) = 0 \ . \tag{3.35}$$

This illustrates that the bilinear R-parity breaking terms μ_i^2, B_i and m_{id}^2 are not necessarily of the same order of magnitude at the EW scale.

3.5.2 Generic parameter choice

For a generic choice of parameters μ_i, B_i and m_{id}^2 the EW symmetry is broken by VEVs of all scalar SU(2) doublets,

$$\left\langle H_u^0\right\rangle = v_u \ , \qquad\qquad \left\langle H_d^0\right\rangle = v_d \ , \qquad\qquad \langle\widetilde{\nu}_i\rangle = v_i \ , \tag{3.36}$$

with the usual 2HDM VEV relations (A.15) and a new relation including the scalar neutrino VEVs [77] [1]

$$\widehat{\epsilon}_i \equiv \frac{v_i}{v_d} = \frac{B_i t_\beta - m_{id}^2 - \mu\mu_i^*}{\widetilde{m}_{li}^2 + \frac{1}{2}m_Z^2 c_{2\beta}} \ , \tag{3.37}$$

where higher order terms in the R-parity breaking parameters have been neglected.

---

[1]Note that our result for $\widehat{\epsilon}_i = v_i/v_d$ holds at all renormalization scales, contrary to different expressions used in the literature.

3.5.3 Superfield rotation

It is convenient to discuss the predictions of the model in a basis of $SU(2)$ doublets where the R-parity breaking mass mixing between Higgs and lepton fields μ_i, B_i and m_{id}^2 in the superpotential (3.16) and the Lagrangian (3.17) are traded for R-parity breaking Yukawa couplings of the form (3.4) and (3.5). This can easily be achieved by field redefinitions. First one rotates the superfields H_d and L_i,

$$H_d = H_d' - \epsilon_i L_i' \;, \qquad\qquad L_i = L_i' + \epsilon_i H_d' \;, \qquad\qquad \epsilon_i = \frac{\mu_i}{\mu} \;. \qquad (3.38)$$

Then the bilinear term in the superpotential (3.16) vanishes for the new fields and the sneutrino VEVs depends solely on soft SUSY and EW symmetry breaking parameters

$$\mu_i' = 0 \;, \qquad\qquad \widehat{\epsilon}_i' = \frac{B_i t_\beta - m_{id}^2}{\widetilde{m}_{li}^2 + \frac{1}{2} m_Z^2 c_{2\beta}} \;. \qquad (3.39)$$

One obtains instead cubic R-parity and lepton number violating terms[2]

$$\Delta W' = \frac{1}{2} \lambda_{ijk} l_i' e_j^c l_k' + \lambda_{ijk}' d_i^c q_j l_k' \;. \qquad (3.40)$$

where the R-parity breaking Yukawa couplings are functions of the rotation parameter ϵ_i and the R-parity conserving Yukawa couplings

$$\lambda_{ijk} = -h_{ij}^e \epsilon_k + h_{kj}^e \epsilon_i \;, \qquad\qquad \lambda_{ijk}' = -h_{ij}^d \epsilon_k \;. \qquad (3.41)$$

Applying the supersymmetric rotation (3.38) to the RPV scalar masses (3.17) leads to new R-parity breaking mass mixing given by

$$B_i' = B_i - B\epsilon_i \;, \qquad\qquad m_{id}^{2\prime} = m_{id}^2 + \epsilon_i \left(\widetilde{m}_{li}^2 - m_d^2 \right) \;. \qquad (3.42)$$

The corrections for R-parity conserving mass terms are negligible. Note that the Higgs mass terms m_u^2 and m_d^2 contain the contributions both from the superpotential (2.7) and the soft SUSY breaking terms.

3.5.4 Scalar field rotation

In a second step one can perform a non-supersymmetric rotation among all scalar $SU(2)$ doublets,

$$H_d' = H_d'' - \epsilon_i' \tilde{l}_i'' \;, \qquad \varepsilon H_u^* = \varepsilon H_u'^* - \epsilon_i'' \tilde{l}_i'' \;, \qquad \tilde{l}_i' = \tilde{l}_i'' + \epsilon_i' H_d'' + \epsilon_i'' \varepsilon H_u'^* \;, \qquad (3.43)$$

where ε is the usual $SU(2)$ matrix, $\varepsilon = i\sigma^2$. After this rotation the bilinear R-parity breaking mass mixing terms (3.17) become

$$B_i'' = B_i' - \epsilon_i' B + \left(m_u^2 - \widetilde{m}_{li}^2 \right) \epsilon_i'' \;, \qquad m_{id}^{2\prime\prime} = m_{id}^{2\prime} + \epsilon_i'' B + \left(\widetilde{m}_{li}^2 - m_d^2 \right) \epsilon_i' \;. \qquad (3.44)$$

Choosing for the two parameters of the scalar rotation

$$\epsilon_i' = -\frac{B_i' B + m_{id}^{2\prime} \left(\widetilde{m}_{li}^2 - m_u^2 \right)}{\left(\widetilde{m}_{li}^2 - m_u^2 \right) \left(\widetilde{m}_{li}^2 - m_d^2 \right) - B^2} \;, \qquad \epsilon_i'' = \frac{B_i' \left(\widetilde{m}_{li}^2 - m_d^2 \right) + B m_{id}^{2\prime}}{\left(\widetilde{m}_{li}^2 - m_u^2 \right) \left(\widetilde{m}_{li}^2 - m_d^2 \right) - B^2} \;, \qquad (3.45)$$

---

[2]The term proportional to $H_d E_i^c H_d$ vanishes due to $SU(2)$ symmetry.

leads to vanishing mixing terms between $H_u \tilde{l}_i$ and $\tilde{l}_i^\dagger H_d$ in the new basis of doublets. According to (3.39) also the scalar lepton VEVs $\langle \tilde{\nu}_i \rangle$ vanish in this basis.

$$B_i'' = 0 , \qquad\qquad m_{id}^{2''} = 0 , \qquad\qquad \hat{\epsilon}_i'' = \langle \tilde{\nu}_i \rangle'' = 0 . \qquad (3.46)$$

Consequently we have eliminated all bilinear RPV terms in both the superpotential (3.16) and the Lagrangian (3.17).

Trilinear couplings

It is straightforward to work out the R-parity violating Yukawa couplings which are induced by applying the rotation (3.43) on the Lagrangian which follows from applying standard procedures (2.4) on the RPC superpotential (2.7). The corresponding couplings read, after dropping prime and double-prime superscripts on all fields

$$-\Delta\mathcal{L} = \frac{1}{2}\lambda_{ijk}l_i\tilde{e}_j^c l_k + \hat{\lambda}_{ijk}l_i e_j^c \tilde{l}_k + h_{ij}^e \left(\epsilon' H_d + \epsilon'' \varepsilon H_u^*\right) e_j^c h_d$$
$$+ \lambda' l_i \left(\tilde{q}_j d_k + q_j \tilde{d}_k\right) + \hat{\lambda}' d_i^c q_j \tilde{l}_k + \tilde{\lambda}_{ijk} q_i u_j^c \varepsilon \tilde{l}_k^* + \text{h.c.} , \qquad (3.47)$$

where the Yukawa couplings are given by the supersymmetric expressions (3.41) as well as by the new non-supersymmetric terms

$$\hat{\lambda}_{ijk} = -h_{ij}^e(\epsilon_k + \epsilon_k') + h_{kj}^e \epsilon_i , \qquad \hat{\lambda}_{ijk}' = -h_{ij}^d(\epsilon_k + \epsilon_k') , \qquad \tilde{\lambda}_{ijk} = h_{ij}^u \epsilon_k'' . \qquad (3.48)$$

Note that a new coupling of right-handed up-quarks, $\tilde{\lambda}_{ijk}$, has been generated which is not present in the usual RPV Lagrangian (3.5).

Electroweak phenomenology

After shifting the Higgs fields around their VEVs (A.14) and omitting the primes the rotated scalar lepton fields (3.43) read

$$\tilde{l}_i = \tilde{l}_i + \epsilon_i' H_d + \epsilon_i'' \varepsilon H_u^* = \tilde{l}_i + \epsilon_i' \begin{pmatrix} v_d - \frac{s_\alpha}{\sqrt{2}} h^0 \\ 0 \end{pmatrix} + \epsilon_i'' \begin{pmatrix} 0 & 1 \\ -1 & 0 \end{pmatrix} \begin{pmatrix} 0 \\ v_u + \frac{c_\alpha}{\sqrt{2}} h^{0*} \end{pmatrix}$$
$$= \tilde{l}_i + \begin{pmatrix} \epsilon_i' v_d + \epsilon_i'' v_u \\ 0 \end{pmatrix} + \frac{1}{\sqrt{2}} \begin{pmatrix} -\epsilon_i' s_\alpha h^0 + \epsilon_i'' c_\alpha h^{0*} \\ 0 \end{pmatrix}$$
$$= \begin{pmatrix} \tilde{\nu}_i + \zeta_i v + \frac{\kappa_i}{\sqrt{2}} h^0 \\ \tilde{l}_i \end{pmatrix} , \qquad (3.49)$$

where we have taken only the lightest Higgs state into account and have introduced

$$\zeta_i = \epsilon_i' c_\beta + \epsilon_i'' s_\beta , \qquad\qquad \kappa_i = -\epsilon_i' s_\alpha + \epsilon_i'' c_\alpha . \qquad (3.50)$$

Finally, we can assume the Higgs decoupling limit (A.16) which simplifies the result further

$$\kappa_i \simeq \zeta_i , \qquad\qquad \tilde{l}_i \simeq \begin{pmatrix} \tilde{\nu}_i + \zeta_i \left(v + \frac{1}{\sqrt{2}} h^0\right) \\ \tilde{l}_i \end{pmatrix} . \qquad (3.51)$$

After EW symmetry breaking the term containing the Higgs fields in the Lagrangian (3.47) leads together with this result to a mass mixing between charged down type higgsinos and right-handed leptons

$$\mathcal{L} = h_{ij}^e \left(\epsilon' H_d + \epsilon'' \varepsilon H_u^* \right) e_j^c h_d = h_{ij}^e \begin{pmatrix} \zeta_i (v + \frac{1}{\sqrt{2}} h^0) \\ 0 \end{pmatrix} e_j^c \begin{pmatrix} h_d^0 \\ h_d^- \end{pmatrix}$$
$$= m_{ij}^e c_\beta^{-1} \zeta_i h_d^- e_j^c \, , \qquad\qquad\qquad\qquad\qquad (3.52)$$

where we have introduced the usual lepton mass matrix

$$m_{ij}^e = h_{ij}^e v_d \, . \qquad\qquad\qquad\qquad\qquad (3.53)$$

Therefore, we can conclude this section by noting that $\zeta_i v$ plays a similar role as the sneutrino VEVs in the general basis of RPV.

3.5.5 Comparison between the general and the rotated basis

Given the Yukawa couplings h_{ij}^u, h_{ij}^d and h_{ij}^e, the bilinear RPV phenomenology is governed by 9 independent parameters which may be chosen as either of the combinations

$$\mu_i, \ B_i, \ m_{id}^2 \, , \qquad\qquad\qquad\qquad \epsilon_i, \ \epsilon_i', \ \epsilon_i'' \, . \qquad\qquad (3.54)$$

These parameters determine lepton-gaugino mass mixing, lepton-slepton and quark-slepton Yukawa couplings, and therefore the low-energy phenomenology. The values of these parameters depend on the pattern of SUSY breaking and the flavour structure of the supersymmetric SM. In terms of the parameters of the SUSY breaking model (3.24), (3.26) and (3.28a) as well as the Froggatt-Nielsen flavour model (3.30) one obtains for the ϵ-parameters

$$\epsilon_i = a\eta^{Q_i} \Theta \, , \qquad\qquad \epsilon_i' = b\eta^{Q_i} \Theta \, , \qquad\qquad \epsilon_{id}'' = c\eta^{Q_i} \Theta \, , \qquad (3.55)$$

with $a, b, c = \mathcal{O}(1)$. For R-parity violating phenomenology concerning EW symmetry breaking it is sufficient to consider the linear combination $\zeta_i \propto \eta^{Q_i} \Theta$.

3.6 Neutralino and chargino mass matrices

The mass eigenstates of the neutral gauginos and higgsinos are called neutralinos. The new operators introduced by RPV lead to mixing terms between neutralinos and neutrinos. Hence the RPV neutralino eigenstates are mixtures of gauginos, higgsinos and neutrinos. The mass eigenstates of charged wino and higgsino are called charginos. RPV mixes the charginos with charged leptons of the SM.

3.6.1 Gaugino couplings

The Lagrangian which couples the components of the chiral multiplet to gauginos (2.6) leads for the lepton and Higgs doublets after the non supersymmetric rotation to the R-parity breaking couplings of bino and wino to

$$-\mathcal{L} = \frac{1}{\sqrt{2}} \left(\left(\epsilon' H_d''^\dagger + \epsilon'' H_u'^T \varepsilon \right) l_i - \epsilon'' L_i''^\dagger h_u - \epsilon' L_i''^\dagger h_d \right) \left(-g' b + g\sigma^a w^a \right) \, . \qquad (3.56)$$

taking additionally to the Higgs VEV only the couplings to the lightest neutral Higgs state into account leads after dropping the primes to the mixing

$$-\mathcal{L} = \frac{1}{\sqrt{2}} \left(\begin{pmatrix} \zeta_i^*(v + \frac{1}{\sqrt{2}} h^{0\dagger}) \\ 0 \end{pmatrix} l_i - \epsilon'' L_i^\dagger h_u - \epsilon' L_i h_d \right) (g'b + g\sigma^a w^a) + \text{h.c.}$$

$$\supset -\zeta_i^* s_w m_Z \nu_i b + \zeta_i^* m_W \nu_i w^3 + \sqrt{2} \zeta_i^* m_W e_i w^+$$

$$- \frac{1}{2} \zeta_i^* g' h^{0\dagger} \nu_i b + \frac{1}{2} \zeta_i^* g h^{0\dagger} \nu_i w^3 + \frac{1}{\sqrt{2}} \zeta_i^* g e_i w^+ + \text{h.c.} \tag{3.57}$$

Where we have for simplicity omitted the RPV scalar lepton couplings.

3.6.2 Neutralino mass matrix

The higgsino mass term μ of the superpotential (2.7), the SUSY braking gaugino masses M_1 and M_2 (2.13) and a possible right-handed neutrino mass M_{ij}^ν (3.2) together with the gaugino higgsino mixing terms in the Lagrangian (2.6) especially the RPV contributions in the Lagrangian (3.57) represent the 7×7 neutralino mass matrix in the basis of gauginos b, w^3, higgsinos h_u^0, h_d^0 and the three gauge eigenstates of the neutrino ν_i

$$\mathcal{M}_N = \begin{pmatrix} M_1 & 0 & m_Z s_\beta s_w & -m_Z c_\beta s_w & -\zeta_i m_Z s_w \\ 0 & M_2 & -m_Z s_\beta c_w & m_Z c_\beta c_w & \zeta_i m_Z c_w \\ m_Z s_\beta s_w & -m_Z s_\beta c_w & 0 & -\mu & 0 \\ -m_Z c_\beta s_w & m_Z c_\beta c_w & -\mu & 0 & 0 \\ -\zeta_i m_Z s_w & \zeta_i m_Z c_w & 0 & 0 & M_{ij}^\nu \end{pmatrix}. \tag{3.58}$$

Before diagonalizing the neutralino matrix, it is instructive to first analyse the neutralino matrix in the basis of photino $\widetilde{\gamma}$, zino z and higgsino $h^{1,2}$ eigenstates

$$\widetilde{\gamma} = s_w w^3 + c_w b , \qquad z = c_w w^3 - s_w b , \qquad h^{1,2} = \frac{1}{\sqrt{2}} (h_d \mp h_u) . \tag{3.59}$$

where the higgsinos $h^{1,2}$ are defined in such a way that their supersymmetric mass term is diagonalized. These eigenstates are defined by the unitary transformation

$$U = \begin{pmatrix} -s_w & c_w & 0 & 0 & 0 \\ c_w & s_w & 0 & 0 & 0 \\ 0 & 0 & -\frac{1}{\sqrt{2}} & \frac{1}{\sqrt{2}} & 0 \\ 0 & 0 & \frac{1}{\sqrt{2}} & \frac{1}{\sqrt{2}} & 0 \\ 0 & 0 & 0 & 0 & 1 \end{pmatrix}. \tag{3.60}$$

This transformation leads to a basis in which only the zino mixes with the other neutralino eigenstates

$$\mathcal{M}'_N = \begin{pmatrix} M_z & \frac{s_{2w}}{2}(M_2 - M_1) & \frac{c_\beta + s_\beta}{\sqrt{2}} m_Z & \frac{c_\beta - s_\beta}{\sqrt{2}} m_Z & \zeta_j m_Z \\ \frac{s_{2w}}{2}(M_2 - M_1) & M_\gamma & 0 & 0 & 0 \\ \frac{c_\beta + s_\beta}{\sqrt{2}} m_Z & 0 & \mu & 0 & 0 \\ \frac{c_\beta - s_\beta}{\sqrt{2}} m_Z & 0 & 0 & -\mu & 0 \\ \zeta_i m_Z & 0 & 0 & 0 & M_{ij}^\nu \end{pmatrix}, \tag{3.61}$$

where we have defined the photino and zino mass parameters

$$M_\gamma = M_1 c_w^2 + M_2 s_w^2 \ , \qquad\qquad M_z = M_1 s_w^2 + M_2 c_w^2 \ . \qquad (3.62)$$

The neutralino mass matrix is fully diagonalized by an unitary matrix

$$U^{(n)T} \mathcal{M}_N U^{(n)} = \mathcal{M}_N^{\mathrm{diag}} \ , \qquad\qquad U^{(n)\dagger} U^{(n)} = \mathbb{1} \ , \qquad (3.63)$$

which relates the neutral gauge eigenstates to the mass eigenstates[3]

$$\begin{pmatrix} b \\ w^3 \\ h_u^0 \\ h_d^0 \\ \nu_i \end{pmatrix} = U^{(n)} \begin{pmatrix} \chi_b^0 \\ \chi_w^0 \\ \chi_{h_u}^0 \\ \chi_{h_d}^0 \\ \nu_i' \end{pmatrix} \ . \qquad (3.64)$$

Our convention for the separation of the transformation matrices into RPC and RPV parts is

$$U^{(n)} = \left(\begin{array}{c|c} U_{ab}^{(\chi^0)} & U_{ai}^{(\chi^0,\nu)} \\ \hline U_{ia}^{(\nu,\chi^0)} & U_{ij}^{(\nu)} \end{array} \right) \ . \qquad (3.65)$$

This diagonalisation leads to masses for the four neutralinos and a R-parity breaking mass term for the neutrinos. The diagonalisation can only be accomplished approximately in $m_Z/\tilde{m}$, where $\tilde{m}$ is the largest out of the supersymmetric mass parameters M_1, M_2 and μ. Hence the approximated diagonalisation does not depend on the details of the supersymmetric spectrum, but in fact its accuracy depends only on the ratio between the EW scale and the largest supersymmetric parameter. The mass eigenstates are given by

$$m_b = M_1 - m_Z^2 s_w^2 \frac{\mu s_{2\beta} + M_1}{\mu^2 - M_1^2} \left(1 + \mathcal{O}\left(\frac{m_Z^2}{\tilde{m}^2} \right) \right) \ , \qquad (3.66\mathrm{a})$$

$$m_{w^0} = M_2 - m_W^2 \frac{\mu s_{2\beta} + M_2}{\mu^2 - M_2^2} \left(1 + \mathcal{O}\left(\frac{m_Z^2}{\tilde{m}^2} \right) \right) \ , \qquad (3.66\mathrm{b})$$

$$m_{h_1^0} = -\mu - m_Z^2 \frac{\mu + M_1 c_w^2 + M_2 s_w^2}{2(\mu + M_1)(\mu + M_2)} (1 - s_{2\beta}) \left(1 + \mathcal{O}\left(\frac{m_Z^2}{\tilde{m}^2} \right) \right) \ , \qquad (3.66\mathrm{c})$$

$$m_{h_2^0} = \mu + m_Z^2 \frac{\mu - M_1 c_w^2 - M_2 s_w^2}{2(\mu - M_1)(\mu - M_2)} (1 + s_{2\beta}) \left(1 + \mathcal{O}\left(\frac{m_Z^2}{\tilde{m}^2} \right) \right) \ , \qquad (3.66\mathrm{d})$$

$$m_{ij}^\nu = M_{ij}^\nu - \zeta^2 m_Z^2 \left(\frac{s_w^2}{M_1} + \frac{c_w^2}{M_2} \right) \left(1 + \mathcal{O}\left(\frac{m_Z^2}{\tilde{m}^2} \right) \right) \ . \qquad (3.66\mathrm{e})$$

where we have introduced the overall R-parity breaking parameter ζ

$$\zeta^2 = \sum_i \zeta_i^2 \ . \qquad (3.67)$$

The names of the mass eigenstates indicate that they are closely related to the gauge eigenstates this holds only as long as the three supersymmetric mass parameters involved are non-degenerate.

---

[3]Usually the mass eigenstates are already at this stage called $\chi_{1\ldots4}^0$, we will use this notation after we have settled on a specific hierarchy between the mass parameters M_1, M_2 and μ.

Neutrino masses

The R-parity violating contribution to the neutrino masses (3.66e) can be derived without the approximation in the differences between the EW scale and the largest of the SUSY mass parameters and reads in this case

$$m_\nu^{\text{RPV}} = \zeta^2 \left(\frac{s_{2\beta}}{\mu} - \frac{M_1 M_2}{M_\gamma m_Z^2} \right)^{-1} (1 + \mathcal{O}(\zeta)) \ . \tag{3.68}$$

In order to generate neutrino Masses of order 50–200 meV mostly by RPV, a model with GeV to TeV scale gauginos needs ζ to be approximately 2×10^{-4}–2×10^{-5}

$$\zeta \simeq 3 \times 10^{-5} \left(\frac{m_\nu}{100\,\text{meV}} \right)^{\frac{1}{2}} \left(\frac{M_1}{100\,\text{GeV}} \right)^{\frac{1}{2}} \ . \tag{3.69}$$

Hence, for fixed gaugino masses an upper limit on neutrino masses leads to an upper limit on ζ.

3.6.3 Chargino mass matrix

The higgsino mass parameter μ of the superpotential (2.7), the soft SUSY breaking wino mass M_2 (2.13) together with the lepton masses m_{ij}^e (3.52) and the mixing terms in Lagrangian (3.57) lead to the 5×5 chargino mass matrix of gaugino, higgsino and the gauge eigenstates of the charged leptons[4]

$$\mathcal{M}_C = \begin{pmatrix} M_2 & \sqrt{2} m_Z s_\beta c_w & 0 \\ \sqrt{2} m_Z c_\beta c_w & \mu & \zeta_i h_{ij}^e \mu \\ \sqrt{2} \zeta_i m_Z c_w & 0 & h_{ij}^e v c_\beta \end{pmatrix} \ , \qquad h_{ij}^e = \text{diag}(h_1^e, h_2^e, h_3^e) \ . \tag{3.70}$$

This matrix is diagonalized by a bi-unitary transformation,

$$U^{(c)\dagger} \mathcal{M}_C \widetilde{U}^{(c)} = \mathcal{M}_C^{\text{diag}} \ , \qquad\qquad U^{(c)\dagger} U^{(c)} = \widetilde{U}^{(c)\dagger} \widetilde{U}^{(c)} = \mathbb{1} \ , \tag{3.71}$$

which relates charged gauge eigenstates to the mass eigenstates

$$\begin{pmatrix} w^- \\ h_d^- \\ e_i \end{pmatrix} = U^{(c)} \begin{pmatrix} \chi_w^- \\ \chi_h^- \\ e_i' \end{pmatrix} \ , \qquad\qquad \begin{pmatrix} w^+ \\ h_u^+ \\ e_i^c \end{pmatrix} = \widetilde{U}^{(c)} \begin{pmatrix} \chi_w^+ \\ \chi_h^+ \\ e_i^{c'} \end{pmatrix} \ . \tag{3.72}$$

Our convention for the separation of the transformation matrices into RPC and violating parts is

$$U^{(c)} = \left(\begin{array}{c|c} U_{\alpha\beta}^{(\chi^-)} & U_{\alpha i}^{(\chi^-,e)} \\ \hline U_{i\alpha}^{(e,\chi^-)} & U_{ij}^{(e)} \end{array} \right) \ , \qquad \widetilde{U}^{(c)} = \left(\begin{array}{c|c} \widetilde{U}_{\alpha\beta}^{(\chi^+)} & \widetilde{U}_{\alpha i}^{(\chi^+,e^c)} \\ \hline \widetilde{U}_{i\alpha}^{(e^c,\chi^+)} & \widetilde{U}_{ij}^{(e^c)} \end{array} \right) \ . \tag{3.73}$$

---

[4]Note the extra factors of $\sqrt{2}$ in the charged mass matrix compared to [1].

The chargino and lepton mass eigenstates[5] are to leading order (LO) in $m_Z/\tilde{m}$

$$m_{w^\pm} = M_2 + \frac{m_W^2}{M_2 - \mu} s_{2\beta} \left(1 + \mathcal{O}\left(\frac{m_W^2}{\tilde{m}^2} \right) \right) \tag{3.74a}$$

$$m_{h^\pm} = \mu + \frac{m_W^2}{\mu - M_2} s_{2\beta} \left(1 + \mathcal{O}\left(\frac{m_W^2}{\tilde{m}^2} \right) \right) \tag{3.74b}$$

$$m_{ei} = h_{ij}^e v c_\beta \left(1 + \mathcal{O}\left(\zeta^2 \right) \right) \tag{3.74c}$$

It is unambiguous to call the mass eigenstates wino and higgsino as long as the two parameters are non-degenerate. The RPV contributes to the lepton masses can safely be neglected. The mass difference between the charginos is given by

$$m_{w^\pm} - m_{h^\pm} = M_2 - \mu + \frac{m_W^2}{M_2 - \mu}(s_{2\beta} + 1) + \mathcal{O}\left(\frac{m_Z^2}{\tilde{m}^2} \right) \tag{3.75}$$

3.6.4 Currents in mass eigenstate basis

The basis change from gauge eigenstates to mass eigenstates modifies the currents which couple gauge fields to neutralinos and charginos (A.32). As shown in Appendix A.4 the currents in the mass eigenstate basis depend on CKM-type matrix elements for the neutral $V^{(\chi^0, \nu)}$ and the charged $V^{(\chi^0, e)}$ currents, which are functions of the transformation matrices U (3.65) and (3.73).

$$
\begin{aligned}
J_{e\mu} &= \overline{\chi}_\alpha^- \overline{\sigma}_\mu V_{\alpha\beta}^{(\chi^-)} \chi_\beta^- + \overline{\chi}_\alpha^+ \overline{\sigma}_\mu V_{\alpha\beta}^{(\chi^+)} \chi_\beta^+ + \overline{e}_i \overline{\sigma}_\mu V_{ij}^{(e)} e_j + \overline{e}_i^c \overline{\sigma}_\mu V_{ij}^{(e^c)} e_j^c \\
&\quad + \left(\overline{\chi}_\alpha^- \overline{\sigma}_\mu V_{\alpha j}^{(\chi^-, e)} e_j + \overline{\chi}_\alpha^+ \overline{\sigma}_\mu V_{\alpha j}^{(\chi^+, e^c)} e_j^c + \text{h.c.} \right) ,
\end{aligned} \tag{3.76a}
$$

$$
\begin{aligned}
J_{Z\mu} &= \overline{\chi}_a^0 \overline{\sigma}_\mu V_{ab}^{(\chi^0)} \chi_b^0 + \overline{\chi}_\alpha^- \overline{\sigma}_\mu V_{\alpha\beta}^{(\chi^-)} \chi_\beta^- + \overline{\chi}_\alpha^+ \overline{\sigma}_\mu V_{\alpha\beta}^{(\chi^+)} \chi_\beta^+ \\
&\quad + \overline{\nu}_i \overline{\sigma}_\mu V_{ij}^{(\nu)} \nu_j + \overline{e}_i \overline{\sigma}_\mu V_{ij}^{(e)} e_j + \overline{e}_i^c \overline{\sigma}_\mu V_{ij}^{(e^c)} e_j^c \\
&\quad + \left(\overline{\chi}_a^0 \overline{\sigma}_\mu V_{aj}^{(\chi, \nu)} \nu_j + \overline{\chi}_\alpha^- \overline{\sigma}_\mu V_{\alpha j}^{(\chi^-, e)} e_j + \overline{\chi}_\alpha^+ \overline{\sigma}_\mu V_{\alpha j}^{(\chi^+, e^c)} e_j^c + \text{h.c.} \right) - s_w^2 J_{e\mu} ,
\end{aligned} \tag{3.76b}
$$

$$
\begin{aligned}
J_\mu^- &= \overline{\chi}_a^0 \overline{\sigma}_\mu V_{a\beta}^{(\chi)} \chi_\beta^- + \overline{\chi}_\alpha^+ \overline{\sigma}_\mu V_{\alpha b}^{(\chi)} \chi_b^0 + \overline{\chi}_a^0 \overline{\sigma}_\mu V_{aj}^{(\chi, e)} e_j + \overline{e}_i^c \overline{\sigma}_\mu V_{ib}^{(\chi, e)} \chi_b^0 \\
&\quad + \overline{\nu}_i \overline{\sigma}_\mu V_{i\beta}^{(\nu, \chi)} \chi_\beta^- + \overline{\chi}_\alpha^+ \overline{\sigma}_\mu V_{\alpha j}^{(\nu, \chi)} \nu_j + \overline{\nu}_i \overline{\sigma}_\mu V_{ij}^{(\nu, e)} e_j + \overline{e}_i^c \overline{\sigma}_\mu V_{ij}^{(\nu, e)} \nu_j ,
\end{aligned} \tag{3.76c}
$$

The R-parity conserving part of these matrices is well known from SUSY introductions. The R-parity breaking part is given in Appendix A.4.2.

3.7 Gravitino interactions

In order to calculate RPV gravitino decays we have to derive the corresponding coupling. To that end, we start with the RPC coupling of gravitino to gauginos and higgsinos given by the Lagrangian [34, 45, 56, 78]

$$\mathcal{L} = -\frac{i}{4M_{\mathrm{P}}} \overline{\psi}_\mu \gamma^{\nu\rho} \gamma^\mu \lambda^a F_{\nu\rho}^a - \frac{i}{\sqrt{2}M_{\mathrm{P}}} \left(\overline{\psi}_\mu \gamma^\nu \gamma^\mu \chi D_\nu \phi^* + \text{c.c.} \right) , \tag{3.77}$$

---

[5]Also in this case it is more common to name the mass eigenstates $\chi_{1\ldots 2}^\pm$, we will do so after choosing a hierarchy between the mass parameters M_2 and μ.

where our definition of the antisymmetric product of two gamma matrices is given by (B.28). The coupling to gauge fields and gauginos of the supersymmetric EW SM reads after the RPV rotations

$$
\begin{aligned}
\mathcal{L} = & -\frac{i}{4M_{\mathrm{P}}}\overline{\psi}_\mu \gamma^{\nu\rho}\gamma^\mu \left(B_{\nu\rho}b + W^a_{\nu\rho}w^a \right) \\
= & -\frac{i}{4M_{\mathrm{P}}}\overline{\psi}_\mu \gamma^{\nu\rho}\gamma^\mu \left[F_{\nu\rho}\left(c_w b + s_w w^3 \right) + Z_{\nu\rho}\left(c_w w^3 - s_w b \right) + W^-_{\nu\rho}w^+ + W^+_{\nu\rho}w^- \right] \\
= & -\frac{i}{4M_{\mathrm{P}}}\overline{\psi}_\mu \gamma^{\nu\rho}\gamma^\mu \left[F_{\nu\rho}\left(s_w U^{w,\nu}_i + c_w U^{b,\nu}_i \right)\nu_i + Z_{\nu\rho}\left(c_w U^{w,\nu}_i - s_w U^{b,\nu}_i \right)\nu_i \right. \\
& \left. \qquad\qquad + W^-_{\nu\rho}U^{w,e^c}_i e^c_i + W^+_{\nu\rho}U^{w,e}_i e_i \right] \\
= & -\frac{i}{2M_{\mathrm{P}}}\overline{\psi}_\mu \gamma^{\nu\rho}\gamma^\mu \left[\left(\partial_\nu A_\rho U^{\gamma,\nu}_i + \partial_\nu Z_\rho U^{z,\nu}_i \right)\nu_i + \partial_\nu W^-_\rho U^{w,e^c}_i e^c_i + \partial_\nu W^+_\rho U^{w,e}_i e_i \right] \;, \quad (3.78)
\end{aligned}
$$

where we have used the RPV transformation matrices mixing gauginos and neutrinos (3.65) as well as gauginos and charged leptons (3.73). In the last step we have introduced the mixing of photino and zino with neutrinos

$$
U^{(\gamma,\nu)}_i = c_w U^{(b,\nu)}_i + s_w U^{(w,\nu)}_i \;, \qquad\qquad U^{(z,\nu)}_i = -s_w U^{(b,\nu)}_i + c_w U^{(w,\nu)}_i \;. \qquad (3.79)
$$

Furthermore, we have used the fact that $\gamma^{\mu\nu}$ and the field strength tensors $F_{\mu\nu}$ are both antisymmetric

$$
\gamma^{\mu\nu}F_{\mu\nu} = 2\gamma^{\mu\nu}\partial_\mu A_\nu = 2\gamma^\mu \partial_\mu \gamma^\nu A_\nu - 2\partial^\mu A_\mu \;. \qquad (3.80)
$$

The coupling of gravitino to the components of chiral superfields H_u, H_d and L_i reads with the covariant derivative of the supersymmetric Higgs fields (A.17b) and the non supersymmetric rotation of the scalar lepton field (3.51)

$$
\begin{aligned}
\mathcal{L} = & -\frac{i}{\sqrt{2}M_{\mathrm{P}}}\overline{\psi}_\mu \gamma^\nu \gamma^\mu \left(h_u D_\nu H^*_u + h_d D_\nu H^*_d + l_i D_\nu \tilde{l}^\dagger_i \right) + \mathrm{h.c.} \\
= & -\frac{i}{\sqrt{2}M_{\mathrm{P}}}\overline{\psi}_\mu \gamma^\nu \gamma^\mu \left[\left(\partial_\nu - \frac{i}{2}\begin{pmatrix} \sqrt{2}g W^-_\mu \\ -\sqrt{g^2+g'^2}Z_\mu \end{pmatrix} \right) s_\beta \left(v + \frac{1}{\sqrt{2}}h^0 \right) h_u \right. \\
& \left. \quad + \left(\partial_\nu - \frac{i}{2}\begin{pmatrix} \sqrt{g^2+g'^2}Z_\mu \\ \sqrt{2}g W^+_\mu \end{pmatrix} \right)\left(c_\beta h_d + \zeta_i l_i \right)\left(v + \frac{1}{\sqrt{2}}h^0 \right) \right] + \mathrm{h.c.} \\
= & \frac{1}{2M_{\mathrm{P}}}\overline{\psi}_\mu \gamma^\nu \gamma^\mu \left[m_Z Z_\nu \left(-s_\beta U^{h_u\nu} + c_\beta U^{h_d\nu} + \zeta_i \right)\nu_i - i\partial_\nu h^0 \left(s_\beta U^{h_u\nu} + c_\beta U^{h_d\nu} + \zeta_i \right)\nu_i \right. \\
& \left. \quad + \sqrt{2}m_W W^-_\nu s_\beta U^{h_u e}e^c_i + \sqrt{2}m_W W^+_\nu \left(c_\beta U^{h_d e} + \zeta_i \right)e_i \right] + \mathrm{h.c.} \qquad (3.81)
\end{aligned}
$$

For the gravitino coupling to Z and neutrino as well as the coupling to W and lepton we will use in the following the abbreviations

$$
\kappa^W_i = \zeta_i + c_\beta U^{(h_d,e)}_i + s_\beta U^{(h_u,e^c)}_i \;, \qquad\qquad \kappa^Z_i = \zeta_i + c_\beta U^{(h_d,\nu)}_i - s_\beta U^{(h_u,\nu)}_i \;. \qquad (3.82)
$$

The gravitino coupling to Higgs and neutrino simplifies due to the symmetry between the transformations of the two different Higgs types, which is simplest to observe in the neutralino
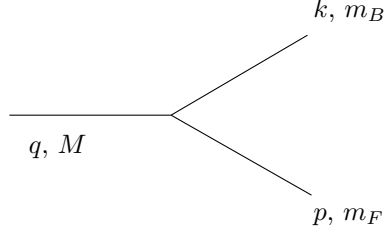
Figure 3.2: General two body decay of a particle with mass M and momentum q in two particles with masses $m_{B,F}$ and momenta k and p.

mass matrix in the photino-zino basis (3.61)

$$c_\beta U_i^{(h_d,\nu)} + s_\beta U_i^{(h_u,\nu)} = 0 \, , \qquad\qquad \zeta_i + c_\beta U_i^{(h_d,\nu)} + s_\beta U_i^{(h_u,\nu)} = \zeta_i \, . \qquad (3.83)$$

Combining the RPV coupling of gravitino to the components of chiral and gauge superfields after EW symmetry breaking leads to

$$\mathcal{L} = \frac{1}{2M_{\mathrm{P}}} \left\{ \overline{\psi}_\mu \gamma^\nu \gamma^\mu \left[\left(m_Z \kappa_i^Z Z_\nu - i\zeta_i \partial_\nu h^0 \right) \nu_i + \sqrt{2} m_W \kappa_i^W W_\nu^+ e_i \right] \right.$$
$$\left. - i\overline{\psi}_\mu \gamma^{\nu\rho} \gamma^\mu \left[\left(U_i^{(z,\nu)} \partial_\nu Z_\rho + U_i^{(\gamma,\nu)} \partial_\nu A_\rho \right) \nu_i + U_i^{(w,e)} \partial_\nu W_\rho^+ e_i \right] \right\} + \mathrm{h.c.} \qquad (3.84)$$

Where the RPV mixing between gauginos and higgsinos with leptons are to first order in ζ and $m_Z/\tilde{m}$ given by

$$U_i^{(\gamma,\nu)} = \zeta_i s_w m_W \frac{M_2 - M_1}{M_1 M_2} \, , \qquad\qquad (3.85a)$$

$$U_i^{(w,e)} = -\sqrt{2}\zeta_i \frac{m_W}{M_2} = \sqrt{2}\xi_i^W \, , \qquad \kappa_i^W = \zeta_i \left(1 + \frac{m_W^2}{\mu M_2} s_{2\beta} \right) \, , \qquad (3.85b)$$

$$U_i^{(z,\nu)} = -\zeta_i m_Z \left(\frac{c_w^2}{M_2} + \frac{s_w^2}{M_1} \right) \, , \qquad \kappa_i^Z = \zeta_i \left(1 + \frac{m_Z^2}{\mu} s_{2\beta} \left(\frac{c_w^2}{M_2} + \frac{s_w^2}{M_1} \right) \right) \, , \qquad (3.85c)$$

As the mixing of the lepton doublet with the three components of the wino is uniform before the rotation into mass eigenstates we are able to verify that this uniformity holds via the relation[6]

$$c_w U_i^{(z,\nu)} + s_w U_i^{(\gamma,\nu)} = \frac{1}{\sqrt{2}} U_i^{(w,e)} = \xi_i^W \, , \qquad (3.86)$$

as well after the rotation [40].

3.8 Decays of the lightest supersymmetric particles

The two body decay width of a particle with mass M ($cf.$ Figure 3.2) as a function of the Lorentz-invariant matrix element $\mathcal{M}$ is given by [79, 80]

$$\Gamma = \frac{1}{16\pi} |\mathcal{M}|^2 \frac{\lambda}{M^3} \, , \qquad (3.87)$$

---

[6]The trigonometric factors in this relation are due to the rotation into the neutral gauge mass eigenstates and the factor $\sqrt{2}$ is due to the rotation into charged mass eigenstates.
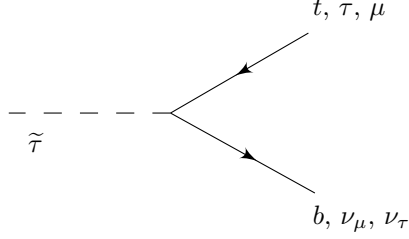
Figure 3.3: Stau decays into top and bottom as well as leptons and neutrinos.

where the phase space is parametrized by

$$\lambda^2 = \left(M^2 - (m_B + m_F)^2 \right) \left(M^2 - (m_B - m_F)^2 \right) \ , \qquad |p_B| = |p_F| = \frac{\lambda}{2M} \ . \tag{3.88}$$

In the following we will calculate the two body decays of neutralino and gravitino in the two spinor notation, the derivation and details of the treatment of two component spinors can be found *e.g.* in [80].

3.8.1 Scalar lepton decays

The Lagrangian (3.47) leads to decays of sleptons into two leptons. Our interest lies in the decays of the lightest slepton, usually the stau, which decays either hadronically into a top and a bottom quark or leptonically into a tau lepton and a muon neutrino or a muon and a tau neutrino (*cf.* Figure 3.3). The leptonic decay is governed by the amplitude

$$i\mathcal{M} = -i\lambda y_\tau x_\nu \ . \tag{3.89}$$

The square of this amplitude is then given by

$$|\mathcal{M}|^2 = |\lambda| \, y_\tau x_\nu x_\nu^\dagger x_\tau^\dagger \ . \tag{3.90}$$

Summing over the final state fermion spins leads to

$$\sum_f |\mathcal{M}|^2 = |\lambda|^2 \, \text{tr}(k_\tau \sigma)(p_\nu \bar{\sigma}) = |\lambda|^2 \left(m_{\tilde{\tau}}^2 - m_\tau^2 - m_\nu^2 \right) \ . \tag{3.91}$$

The decay width is, finally, given by

$$\Gamma_{\tilde{\tau}} \simeq \frac{|\lambda|^2}{16\pi} m_{\tilde{\tau}} f_S(m_{\tilde{\tau}}, m_\tau) \ , \tag{3.92}$$

where we have neglected the neutrino mass and have introduced the scalar phase space suppression factor, which is normalized to one

$$f_S(m_1, m_2) = (1-r)^2 = \left(1 - \frac{m_2^2}{m_1^2} \right)^2 \ , \qquad\qquad r = \frac{m_2^2}{m_1^2} \ . \tag{3.93}$$

The energy dependence of the scalar phase space factor for the coloured channel is depicted in Figure 4.4.
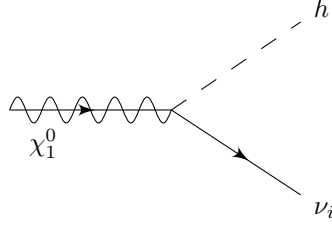
Figure 3.4: Neutralino decay into the lightest Higgs boson and neutrino.

3.8.2   Neutralino decays

A neutralino with a mass larger than $100\,\mathrm{GeV}$ decays predominantly via two-body channels either into W boson and charged lepton (see Figure 3.5a), Z boson and neutrino [81] (see Figure 3.5b) or Higgs boson and neutrino [82] (see Figure 3.4).

Decay into Higgs and neutrino

The Lagrangian (3.57) couples the gauge eigenstates of the neutralino to Higgs and neutrino and gives rise to the amplitude

$$i\mathcal{M} = \frac{i}{2}g\widetilde{V}_{i1}^{(\nu\chi)}x_iy_j \; , \tag{3.94}$$

where $V_{i1}^{(\nu\chi)}$ is the matrix element coupling the lightest Higgs state to neutralino and neutrino (A.44).[7] The square of this amplitude is

$$|\mathcal{M}|^2 = \frac{1}{4}g^2\left|\widetilde{V}_{i1}^{(\nu\chi)}\right|^2 x_iy_jy_j^\dagger x_i^\dagger \; . \tag{3.95}$$

Summing over outgoing neutrinos (B.83)

$$\sum_j |\mathcal{M}|^2 = \frac{1}{4}g^2\left|\widetilde{V}_{i1}^{(\nu\chi)}\right|^2 x_ik_j\sigma x_i^\dagger \; , \tag{3.96}$$

and averaging over incoming neutralinos (B.83) leads to

$$\frac{1}{2}\sum |\mathcal{M}|^2 = \frac{1}{4}g^2\left|\widetilde{V}_{i1}^{(\nu\chi)}\right|^2 \operatorname{tr} k_j\sigma p_i\overline{\sigma} = \frac{1}{4}g^2\left|\widetilde{V}_{i1}^{(\nu\chi)}\right|^2 k_jp_i$$
$$= \frac{1}{8}g^2\left|\widetilde{V}_{i1}^{(\nu\chi)}\right|^2 (m_{\chi_1^0}^2 - m_h^2) \; , \tag{3.97}$$

where we have simplified the traces over sigma matrices using (B.84) and have applied the momentum and mass relations

$$m_{\chi_1^0}^2 = m_h^2 + m_\nu^2 + 2k_jp_i \; , \qquad\qquad m_\nu \ll m_{\chi_1^0}, m_h \; . \tag{3.98}$$

Using the formula for a general two body decay (3.87) this leads finally to the decay width of a neutralino decaying into the lightest Higgs and neutrino

$$\Gamma(\chi_1^0 \to h^0\nu_i) = \frac{1}{32}\frac{\alpha}{s_w^2}\left|\widetilde{V}_{i1}^{(\nu\chi)}\right|^2 m_{\chi_1^0}\left(1 - \frac{m_h^2}{m_{\chi_1^0}^2}\right) = \frac{1}{32}\frac{\alpha}{s_w^2}\left|\widetilde{V}_{i1}^{(\nu\chi)}\right|^2 m_{\chi_1^0}f_S(m_{\chi_1^0}, m_h) \; . \tag{3.99}$$

In the last step we have used the scalar phase space factor (3.93).

---

[7]Here we are using the usual definition that χ_1^0 is the lightest neutralino.

(a) $\chi_1^0 \to W^\pm l_i^\mp$
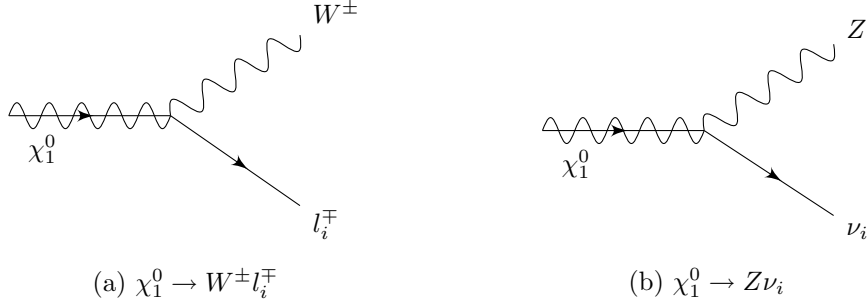
(b) $\chi_1^0 \to Z\nu_i$

Figure 3.5: Neutralino decays into W boson and charged lepton (a) as well as Z boson and neutrino (b).

Decay into gauge boson and lepton

The Lagrangian (A.21) which couples gauge bosons via RPV currents (3.76a) to neutralino and lepton leads to neutralino decays into Z boson and neutrino via the amplitude

$$i\mathcal{M} = -i\frac{g}{c_w}V_{1i}^{(\chi,\nu)}\epsilon_\mu^* x_i \sigma^\mu x_j^\dagger \ . \tag{3.100}$$

The square of this amplitude is

$$|\mathcal{M}|^2 = \frac{g^2}{c_w^2}\left|V_{1i}^{(\chi,\nu)}\right|^2 \epsilon_\mu^* \epsilon_\nu x_i \sigma^\mu x_j^\dagger x_j \sigma^\nu x_i^\dagger \ . \tag{3.101}$$

Summing over final state neutrinos (B.83) leads to

$$\sum_j |\mathcal{M}|^2 = \frac{g^2}{c_w^2}\left|V_{1i}^{(\chi,\nu)}\right|^2 \epsilon_\mu^* \epsilon_\nu x_i \sigma^\mu (k_j\overline{\sigma})\sigma^\nu x_i^\dagger \ . \tag{3.102}$$

Averaging over initial states neutralinos (B.83) and using the spin sum for gauge bosons (B.89) simplifies this expression to

$$\begin{aligned}\frac{1}{2}\sum |\mathcal{M}|^2 &= \frac{1}{2}\frac{g^2}{c_w^2}\left|V_{1i}^{(\chi,\nu)}\right|^2 \epsilon_\mu^* \epsilon_\nu \operatorname{tr}\sigma^\mu (k_j\overline{\sigma})\sigma^\nu (p_i\overline{\sigma}) \\ &= \frac{1}{2}\frac{g^2}{c_w^2}\left|V_{1i}^{(\chi,\nu)}\right|^2 (k_j p_i + 2k_j k_Z p_i k_Z) \\ &= \frac{1}{4}\frac{g^2}{c_w^2}\left|V_{1i}^{(\chi,\nu)}\right|^2 \left(m_{\chi_1^0}^2 - m_Z^2\right)\left(\frac{m_{\chi_1^0}^2}{m_Z^2} + 2\right) \ . \end{aligned} \tag{3.103}$$

Finally, the decay width is

$$\begin{aligned}\Gamma\left(\chi_1^0 \to Z\nu\right) &= \frac{1}{4}\frac{\alpha}{s_{2w}^2}\left|V_{1i}^{(\chi,\nu)}\right|^2 m_{\chi_1^0}\left(1 - \frac{m_Z^2}{m_{\chi_1^0}^2}\right)^2\left(2 + \frac{m_{\chi_1^0}^2}{m_Z^2}\right) \\ &= \frac{1}{4}\frac{\alpha}{s_{2w}^2}\left|V_{1i}^{(\chi,\nu)}\right|^2 \frac{m_{\chi_1^0}^3}{m_Z^2} f_V(m_{\chi_1^0}, m_Z) \ . \end{aligned} \tag{3.104}$$
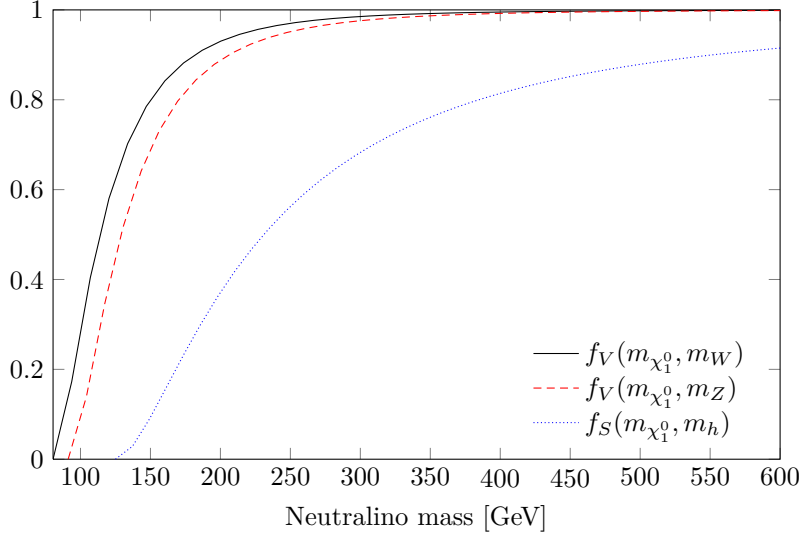
Figure 3.6: Phase space suppression factors for neutralino decays into W and Z bosons (*cf.* Equation (3.105)) as well as the lightest Higgs (*cf.* Equation (3.93)).

Note the Nambu-Goldstone enhancement factor m_χ^2/m_Z^2 for the longitudinal polarizations of the gauge bosons [83]. In the last step we we have introduced the normalized vector boson phase space factor

$$f_V(m_1, m_2) = f_S(m_1, m_2)\,(1 + 2r) = \left(1 - \frac{m_2^2}{m_1^2}\right)^2 \left(1 + 2\frac{m_2^2}{m_1^2}\right) \;, \qquad (3.105)$$

which is depicted in Figure 3.6. Compared to the decay into scalar bosons (3.99), the normalization leads to the extra factor of $m_{\chi_1^0}^2/m_Z^2$ in the decay width (3.104). The calculation of the decay into W boson is analogue to the decay into Z boson.

Total decay width

Summarizing, the partial decay widths, taking also decays into antiparticles into account, are given by

$$\Gamma\left(\chi_1^0 \to W^\pm l^\mp\right) = \frac{G_F}{4\sqrt{2}\pi} m_{\chi_1^0}^3 \sum_i \left|V_{1i}^{(\chi^0,e)}\right|^2 f_V(m_{\chi_1^0}, m_W) \;, \qquad (3.106a)$$

$$\Gamma\left(\chi_1^0 \to Z\nu\right) = \frac{G_F}{2\sqrt{2}\pi} m_{\chi_1^0}^3 \sum_i \left|V_{1i}^{(\chi^0,\nu)}\right|^2 f_V(m_{\chi_1^0}, m_Z) \;, \qquad (3.106b)$$

$$\Gamma\left(\chi_1^0 \to h\nu\right) = \frac{\alpha}{16 s_w^2} m_{\chi_1^0} \sum_i \left|\widetilde{V}_{1i}^{(\nu,\chi^0)}\right|^2 f_S(m_{\chi_1^0}, m_h) \;, \qquad (3.106c)$$

where $V_{1i}^{(\chi^0,e)}$ and $V_{1i}^{(\chi^0,\nu)}$ are the charged and neutral current matrix elements, whereas $\widetilde{V}_{1i}^{(\nu,\chi^0)}$ is the matrix element for the decay into the Higgs boson. The total neutralino decay width is given by the sum

$$\Gamma_{\chi_1^0} = \Gamma(\chi_1^0 \to W^\pm l^\mp) + \Gamma(\chi_1^0 \to Z\nu) + \Gamma(\chi_1^0 \to h\nu) \;, \qquad (3.107)$$

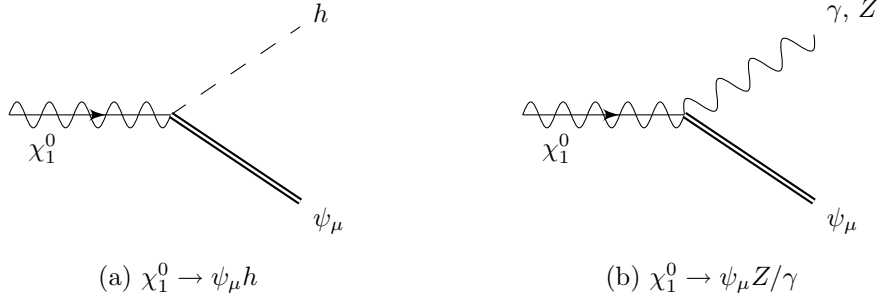(a) $\chi_1^0 \to \psi_\mu h$ (b) $\chi_1^0 \to \psi_\mu Z/\gamma$

Figure 3.7: Neutralino decays into gravitino and Higgs boson (a) as well as gravitino and neutral gauge boson (b).

and depends on the character of the lightest neutralino. In Section 4 we will give detailed formulas for the cases where the lightest neutralino is the bino-, wino- or higgsino-like.

R-parity conserving decays

The neutralino may also decay via RPC channel into a light gravitino. For example the decay width into gravitino and photon is given by [84–88]

$$\Gamma(\chi \to \gamma \psi_\mu) = \frac{1}{48\pi} |U_{11}c_w + U_{12}s_w|^2 \frac{m_{\chi_1^0}^5}{M_P^2 m_{3/2}^2} f_S^{3/2}(m_{\chi_1^0}, m_{3/2}) \left(1 + 3\frac{m_{3/2}^2}{m_{\chi_1^0}^2}\right) . \tag{3.108}$$

Dividing the total RPV decay width by the total RPC decay width leads in the gaugino NLSP case to

$$\frac{\Gamma_{\mathrm{RPV}}}{\Gamma_{\mathrm{RPC}}} = 8\pi \frac{\alpha}{c_w^4} \zeta^2 \frac{m_{3/2}^2 M_P^2}{m_{\chi_1^0}^4} \frac{f_{\mathrm{RPV}}}{f_{\mathrm{RPC}}} . \tag{3.109}$$

The RPC decay becomes dominant for

$$\zeta \lesssim 7 \times 10^{-16} \left(\frac{m_{3/2}}{10\,\mathrm{GeV}}\right) \left(\frac{m_{\chi_1^0}}{100\,\mathrm{GeV}}\right)^{-2} \left(\frac{f_{\mathrm{RPC}}}{f_{\mathrm{RPV}}}\right)^{\frac{1}{2}} , \tag{3.110}$$

hence, it dominates only for very small RPV and extremely large mass splitting between the mass of the lightest neutralino and the mass of the gravitino.

3.8.3 Gravitino decays

The Lagrangian (3.84) leads to RPV gravitino decays. These decays are not only suppressed by the smallness of RPV but also by the Planck mass.

Decay into photon and neutrino

The Lagrangian which couples gravitino to gauge boson and neutrino (3.84) reads in two component notation

$$\mathcal{L} = \frac{i}{2M_P} U_i^{(\gamma,\nu)} \psi_\mu^\dagger \sigma^{\nu\rho} \sigma^\mu \partial_\nu A_\rho \nu_i , \tag{3.111}$$
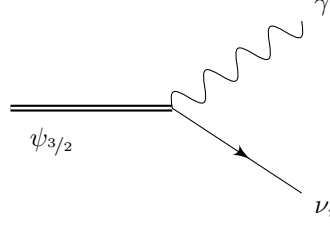
Figure 3.8: Gravitino decay into photon and neutrino.

and leads with the momentum assignment of Figure 3.2 to the amplitude

$$i\mathcal{M} = -\frac{1}{2M_\mathrm{P}} U_i^{(\gamma,\nu)} \epsilon_\rho^* \psi_\mu^+ (\sigma k) \overline{\sigma}^\rho \sigma^\mu x_i^\dagger \ , \tag{3.112}$$

where we have used the antisymmetry of $\sigma^{\mu\nu}$ (3.80) and the polarization of the gauge boson. The square of this amplitude is

$$|\mathcal{M}|^2 = -\frac{i}{4M_\mathrm{P}^2} \left| U_i^{(\gamma,\nu)} \right|^2 \epsilon_\rho^* \epsilon_\lambda \psi_\mu^+ (\sigma k) \overline{\sigma}^\rho \sigma^\mu x^\dagger x \sigma^\kappa \overline{\sigma}^\lambda (\sigma k) \psi_\kappa^{+\dagger} \ . \tag{3.113}$$

Summing over the final state neutrinos

$$|\mathcal{M}|^2 = \frac{i}{4M_\mathrm{P}^2} \left| U_i^{(\gamma,\nu)} \right|^2 \epsilon_\rho^* \epsilon_\lambda \psi_\mu^+ (\sigma k) \overline{\sigma}^\rho \sigma^\mu (p\overline{\sigma}) \sigma^\kappa \overline{\sigma}^\lambda (\sigma k) \psi_\kappa^{+\dagger} \ , \tag{3.114}$$

and averaging over initial states gravitino leads to

$$\frac{1}{4} \sum |\mathcal{M}|^2 = -\frac{1}{16M_\mathrm{P}^2} \left| U_i^{(\gamma,\nu)} \right|^2 \epsilon_\rho^* \epsilon_\lambda \operatorname{tr} \left((\sigma k) \overline{\sigma}^\rho \sigma^\mu (p\overline{\sigma}) \sigma^\kappa \overline{\sigma}^\lambda (\sigma k) P_{\kappa\mu}^+ \right) \ . \tag{3.115}$$

Using the sum over gravitino spins (B.94) and gauge boson spins (B.90) and solving the following traces over σ-matrices

$$\operatorname{tr} \left((\sigma k) \overline{\sigma}^\rho \sigma^\mu (p\overline{\sigma}) \sigma_\mu \overline{\sigma}_\rho (\sigma k)(\overline{\sigma} q) \right) = 16(kp)(kq) - 8k^2(pq) \ , \tag{3.116a}$$

$$\operatorname{tr} \left((\sigma k) \overline{\sigma}^\rho (\sigma q) (p\overline{\sigma}) (\sigma q) \overline{\sigma}_\rho (\sigma k)(\overline{\sigma} q) \right) = 8q^2(kp)(kq) - 16(kq)^2(pq) + 4k^2 q^2(pq) \ , \tag{3.116b}$$

$$\operatorname{tr} \left((\sigma k) \overline{\sigma}^\rho \sigma^\mu (p\overline{\sigma}) \sigma^\kappa \overline{\sigma}_\rho (\sigma k)(\overline{\sigma} q) \sigma_\kappa \overline{\sigma}_\mu \right) = -16k^2(pq) \ , \tag{3.116c}$$

$$\operatorname{tr} \left((\sigma k) \overline{\sigma}^\rho (\sigma q) (p\overline{\sigma}) \sigma_\kappa \overline{\sigma}_\rho (\sigma k)(\overline{\sigma} q) \sigma_\kappa (\overline{\sigma} q) \right) = 16q^2(kp)(kq) - 32(kq)^2(pq) \ , \tag{3.116d}$$

$$\operatorname{tr} \left((\sigma k) \overline{\sigma}^\rho \sigma^\mu (p\overline{\sigma}) (\sigma q) \overline{\sigma}_\rho (\sigma k)(\overline{\sigma} q) (\sigma q) \overline{\sigma}_\mu \right) = 8k^2 q^2(pq) \ , \tag{3.116e}$$

leads to

$$\frac{1}{4} \sum |\mathcal{M}|^2 = \frac{1}{12} \frac{1}{M_\mathrm{P}^2 m_{3/2}^2} \left| U_i^{(\gamma,\nu)} \right|^2 (m_{3/2}^2 - m_\nu^2)^2 (3m_{3/2}^2 + m_\nu^2)$$

$$\simeq \frac{1}{4} \frac{m_{3/2}^4}{M_\mathrm{P}^2} \left| U_i^{(\gamma,\nu)} \right|^2 \ . \tag{3.117}$$

Finally, the decay width reads

$$\Gamma(\psi_{3/2} \to \gamma\nu) = \frac{1}{64\pi} \frac{m_{3/2}^3}{M_P^2} \left| U_i^{(\gamma,\nu)} \right|^2 \ . \tag{3.118}$$
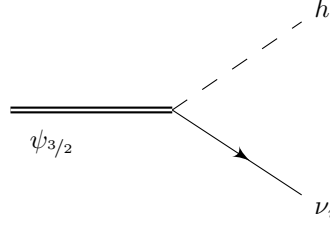
Figure 3.9: Gravitino decay into the lightest Higgs boson and neutrino.

Decay into Higgs and neutrino

The part of the Lagrangian (3.84) which couples gravitino to Higgs and photon reads in two component notation

$$\mathcal{L} = -\frac{i}{2}\frac{\zeta_i}{M_P}\psi_\mu^\dagger\overline{\sigma}^\nu\sigma^\mu\partial_\nu h^0\overline{\nu}_i \ , \tag{3.119}$$

which leads to the matrix element

$$i\mathcal{M} = \frac{i}{2}\frac{\zeta_i}{M_P}\psi_\mu(k\overline{\sigma})\sigma^\mu x_l^\dagger \ . \tag{3.120}$$

The square is

$$|\mathcal{M}|^2 = \frac{1}{4}\frac{\zeta^2}{M_P^2}\psi_\mu(\overline{\sigma}k)\sigma^\mu x_l^\dagger x_l\sigma^\nu(\overline{\sigma}k)\psi_\nu^\dagger \ , \tag{3.121}$$

summing over the final states

$$|\mathcal{M}|^2 = \frac{1}{4}\frac{\zeta^2}{M_P^2}\psi_\mu(\overline{\sigma}k)\sigma^\mu(p\overline{\sigma})\sigma^\nu(k\overline{\sigma})\psi_\nu^\dagger \ , \tag{3.122}$$

and averaging over the initial states leads to

$$\frac{1}{4}|\mathcal{M}|^2 = \frac{1}{16}\frac{\zeta^2}{M_P^2}\operatorname{tr}\left((\overline{\sigma}k)\sigma^\mu(p\overline{\sigma})\sigma^\nu(\overline{\sigma}k)P_{\nu\mu}^+\right) \ . \tag{3.123}$$

Hence after solving the traces of sigma matrices

$$\operatorname{tr}\left(\overline{\sigma}^\mu(k\sigma)(p\overline{\sigma})(\sigma k)\overline{\sigma}_\mu(\sigma q)\right) = 4k^2(pq) - 8(kp)(kq) \ , \tag{3.124a}$$

$$\operatorname{tr}\left((q\overline{\sigma})(k\sigma)(p\overline{\sigma})(\sigma k)(\overline{\sigma}q)(\sigma q)\right) = 4q^2(kq)(kp) - 2k^2q^2(pq) \ , \tag{3.124b}$$

$$\operatorname{tr}\left(\overline{\sigma}^\mu(k\sigma)(p\overline{\sigma})(\sigma k)\overline{\sigma}^\nu(\overline{\sigma}q)\sigma_\mu\sigma_\nu\right) = 16(kp)(kq) - 8k^2(pq) \ , \tag{3.124c}$$

$$\operatorname{tr}\left(\overline{\sigma}^\mu(k\sigma)(p\overline{\sigma})(\sigma k)(q\overline{\sigma})(\sigma q)\overline{\sigma}_\mu(\sigma q)\right) = 4k^2q^2(pq) - 8q^2(kp)(kq) \ , \tag{3.124d}$$

$$\operatorname{tr}\left((q\overline{\sigma}^\mu)(k\sigma)(p\overline{\sigma})(\sigma k)\overline{\sigma}^\nu(\sigma q)(\overline{\sigma}q)\right) = 16q^2(kq)(kp) - 16k^2q^2(pq) \ , \tag{3.124e}$$

the square of the matrix element reads

$$\frac{1}{4}|\mathcal{M}|^2 = -\frac{1}{24}\frac{\zeta^2}{M_P^2 m_{3/2}^2}(m_{3/2} - m_h - m_\nu)(m_{3/2} + m_h - m_\nu)(m_{3/2} - m_h + m_\nu)$$

$$\times (m_{3/2} + m_h + m_\nu)(m_{3/2}^2 - m_h^2 + m_\nu^2)$$

$$\simeq -\frac{1}{24}\frac{\zeta^2}{M_P^2 m_{3/2}^2}(m_{3/2}^2 - m_h^2)^3 \ . \tag{3.125}$$

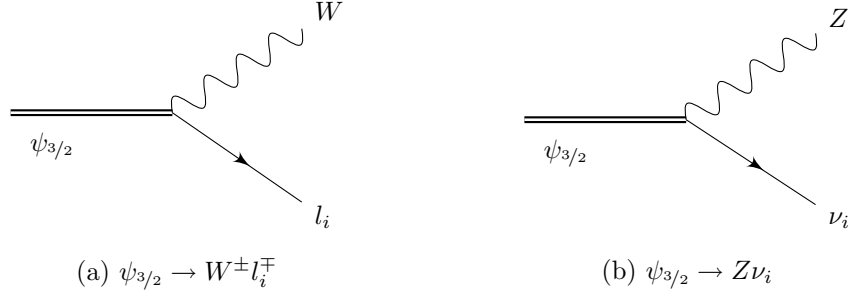(a) $\psi_{3/2} \to W^{\pm} l_i^{\mp}$ (b) $\psi_{3/2} \to Z \nu_i$

Figure 3.10: Gravitino decays into W boson and charged lepton as well as Z boson and neutrino.

Finally, the decay width is

$$\Gamma(\psi_{3/2} \to h\nu) = \frac{1}{384\pi} \frac{m_{3/2}^3}{M_P^2} \zeta^2 f_S^2(m_{3/2}, m_h) \ , \tag{3.126}$$

where we have used the scalar phase space suppression factor (3.93), which shows up quadratically.

Decay into massive gauge bosons and leptons

The decay width for gauge bosons is more complicated as the coupling of gravitino to gauge bosons is governed by two independent parts in the Lagrangian (3.84) For the Z bosons these parts read in two component notation

$$\mathcal{L} = \frac{1}{2M_{\mathrm{P}}} \overline{\psi}_\mu \left(m_Z \kappa_i^Z \overline{\sigma}^\nu \sigma^\mu - i U_i^{(z,\nu)} \sigma^{\rho\nu} \sigma^\mu \partial_\rho \right) Z_\nu \nu_i + \mathrm{h.c.} \tag{3.127}$$

which leads to the matrix element

$$i\mathcal{M} = \frac{i}{2M_{\mathrm{P}}} \epsilon_\nu^* \psi_\mu^\dagger \left(a + b(k\sigma) \right) \overline{\sigma}^\nu \sigma^\mu x_i^\dagger \ , \tag{3.128}$$

where

$$a = m_Z \kappa_i^Z \ , \qquad\qquad b = U_i^{(z,\nu)} \ . \tag{3.129}$$

The square of the matrix element is

$$|\mathcal{M}|^2 = \frac{1}{4M_{\mathrm{P}}^2} \epsilon_\nu^* \epsilon_\lambda \psi_\mu^\dagger \left(a + b(k\sigma) \right) \overline{\sigma}^\nu \sigma^\mu x_i^\dagger x_i \sigma_\kappa \overline{\sigma}^\lambda \left(a^* + b^*(k\sigma) \right) \psi_\kappa \ . \tag{3.130}$$

Summing over final state neutrinos

$$\sum_p |\mathcal{M}|^2 = \frac{1}{4M_{\mathrm{P}}^2} \epsilon_\nu^* \epsilon_\lambda \psi_\mu^\dagger \left(a + b(k\sigma) \right) \overline{\sigma}^\nu \sigma^\mu (p\overline{\sigma}) \sigma_\kappa \overline{\sigma}^\lambda \left(a^* + b^*(k\sigma) \right) \psi_\kappa \ , \tag{3.131}$$

and averaging over the initial state gravitinos leads to

$$\frac{1}{4} \sum_{pq} |\mathcal{M}|^2 = \frac{1}{16M_{\mathrm{P}}^2} \epsilon_\nu^* \epsilon_\lambda \operatorname{tr} \left(\left(a + b(k\sigma) \right) \overline{\sigma}^\nu \sigma^\mu (p\overline{\sigma}) \sigma_\kappa \overline{\sigma}^\lambda \left(a^* + b^*(k\sigma) \right) P_{\kappa\mu} \right) \ . \tag{3.132}$$
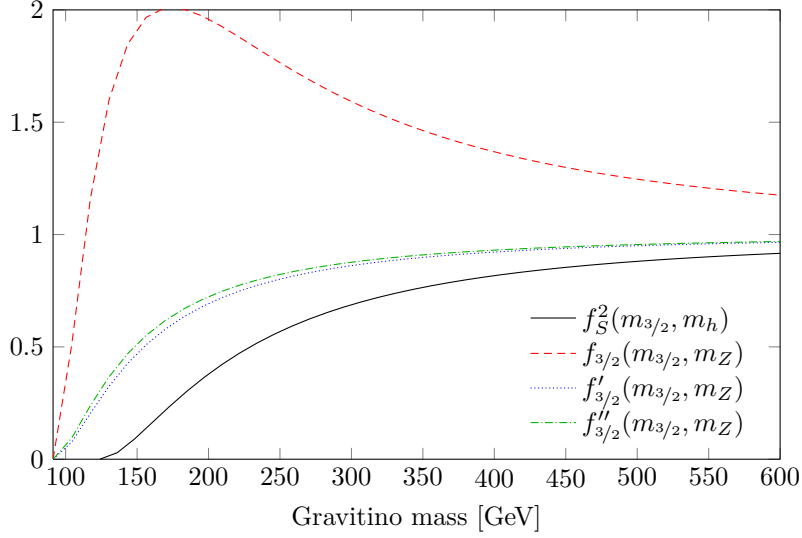
Figure 3.11: Gravitino phase space suppression factors for massive neutral particle. The decay into W boson is governed by the same factors as the decay into Z boson, just the masses have to be replaced. Note the maximum at $f_{3/2}(m_{3/2} \simeq 1.9 m_V) \simeq 2$.

Fortunately we have already solved one half of the traces we have to calculate in (3.116) the other half is given by

$$\text{tr}\left((\sigma k)(\overline{\sigma} k)\sigma^\mu(p\overline{\sigma})\sigma_\mu(\overline{\sigma} k)(\sigma k)(\overline{\sigma} q)\right) = 16k^2(kp)(kq) - 8k^4(pq) \, , \tag{3.133a}$$

$$\text{tr}\left((\sigma k)(\overline{\sigma} k)(\sigma q)(p\overline{\sigma})(\sigma q)(\overline{\sigma} k)(\sigma k)(\overline{\sigma} q)\right) = 8k^2 q^2(kp)(kq) - 16k^2(kq)^2(pq) + 4k^4 q^2(pq) \, , \tag{3.133b}$$

$$\text{tr}\left((\sigma k)(\overline{\sigma} k)\sigma^\mu(p\overline{\sigma})\sigma^\kappa(\overline{\sigma} k)(\sigma k)(\overline{\sigma} q)\sigma_\mu\overline{\sigma}_\kappa\right) = 32k^2(kp)(kq) \, , \tag{3.133c}$$

$$\text{tr}\left((\sigma k)(\overline{\sigma} k)\sigma^\mu(p\overline{\sigma})(\sigma q)(\overline{\sigma} k)(\sigma k)(\overline{\sigma} q)\sigma_\mu(\overline{\sigma} q)\right) = 16k^2 q^2(kp)(kq) - 32k^2(kq)^2(pq) \, , \tag{3.133d}$$

$$\text{tr}\left((\sigma k)(\overline{\sigma} k)(\sigma q)(p\overline{\sigma})\sigma_\kappa(\overline{\sigma} k)(\sigma k)(\overline{\sigma} q)(\sigma q)\overline{\sigma}_\kappa\right) = 8k^4 q^2(pq) \, . \tag{3.133e}$$

Therefore, the result for the amplitude is

$$\frac{1}{4}|\mathcal{M}|^2 = -\frac{1}{24}\frac{1}{m_{3/2}^2 M_P^2}\left\{\left|\kappa_i^Z\right|^2\left(m_{3/2}^2 - m_Z^2 + m_l^2\right)\left[\left(m_l^2 - m_{3/2}^2 - m_Z^2\right)^2 + 8m_{3/2}^2 m_Z^2\right]\right.$$

$$+ 8\,\text{Re}\,\kappa_i^Z U_i^{(z,\nu)} m_{3/2} m_Z\left[m_{3/2}^2\left(-2m_{3/2}^2 + m_Z^2 + m_l^2\right) + \left(m_Z^2 - m_l^2\right)^2\right] \tag{3.134}$$

$$\left. + 2\left|U_i^{(z,\nu)}\right|^2\left[m_{3/2}^4\left(3m_{3/2}^2 - m_Z^2 - 5m_l^2\right) + m_{3/2}^2\left(m_l^4 - m_Z^4\right) - \left(m_Z^2 - m_l^2\right)^3\right]\right\} \, .$$

Finally, the decay rate into Z bosons is given by

$$\Gamma(\psi_{3/2} \to Z\nu) = \frac{1}{384\pi}\frac{m_{3/2}^3}{M_P^2} \tag{3.135}$$

$$\times \left(\left|\kappa_i^Z\right|^2 f_{3/2}(m_{3/2}, m_Z) + 16\frac{m_Z}{m_{3/2}}\,\text{Re}\,\kappa_i^Z U_i^{(z,\nu)} f'_{3/2}(m_{3/2}, m_Z) + 6\left|U_i^{(z,\nu)}\right|^2 f''_{3/2}(m_{3/2}, m_Z)\right) ,$$

where we have introduced three phase space suppression factors for gravitino decays into gauge bosons

$$f_{3/2}(m_1, m_2) = f_S(m_1, m_2)\left(1 + 10r + r^2\right) = \left(1 - \frac{m_2^2}{m_1^2}\right)^2\left(1 + 10\frac{m_2^2}{m_1^2} + \frac{m_2^4}{m_1^4}\right) , \quad (3.136a)$$

$$f'_{3/2}(m_1, m_2) = f_S(m_1, m_2)\left(1 + \frac{1}{2}r\right) = \left(1 - \frac{m_2^2}{m_1^2}\right)^2\left(1 + \frac{1}{2}\frac{m_2^2}{m_1^2}\right) , \quad (3.136b)$$

$$f''_{3/2}(m_1, m_2) = f_S(m_1, m_2)\left(1 + \frac{2}{3}r + \frac{1}{3}r^2\right) = \left(1 - \frac{m_2^2}{m_1^2}\right)^2\left(1 + \frac{2}{3}\frac{m_2^2}{m_1^2} + \frac{1}{3}\frac{m_2^4}{m_1^4}\right) , \quad (3.136c)$$

which are normalized to one and shown in Figure 3.11. The decay into W bosons is calculated in the same manner.

Total decay width and branching ratios

Summarizing, the two body decays of gravitino resulting from the Lagrangian (3.84) are after summing over particles and antiparticles given by [45, 89, 90]

$$\Gamma(\psi_{3/2} \to \gamma\nu) = \frac{1}{32\pi}\frac{m_{3/2}^3}{M_P^2}\left|U_i^{(\gamma,\nu)}\right|^2 , \quad (3.137a)$$

$$\Gamma(\psi_{3/2} \to h\nu) = \frac{1}{192\pi}\frac{m_{3/2}^3}{M_P^2}\zeta_i^2 f_S^2(m_{3/2}, m_h) , \quad (3.137b)$$

$$\Gamma(\psi_{3/2} \to W^\pm l^\mp) = \frac{1}{96\pi}\frac{m_{3/2}^3}{M_P^2} \quad (3.137c)$$

$$\times \left(\left|\kappa_i^W\right|^2 f_{3/2}(m_{3/2}, m_W) + 16\frac{m_W}{m_{3/2}}\operatorname{Re}\kappa_i^W\xi_i^W f'_{3/2}(m_{3/2}, m_W) + 6\left|\xi_i^W\right|^2 f''_{3/2}(m_{3/2}, m_W)\right) ,$$

$$\Gamma(\psi_{3/2} \to Z\nu) = \frac{1}{192\pi}\frac{m_{3/2}^3}{M_P^2} \quad (3.137d)$$

$$\times \left(\left|\kappa_i^Z\right|^2 f_{3/2}(m_{3/2}, m_Z) + 16\frac{m_Z}{m_{3/2}}\operatorname{Re}\kappa_i^Z U_i^{(z,\nu)} f'_{3/2}(m_{3/2}, m_Z) + 6\left|U_i^{(z,\nu)}\right|^2 f''_{3/2}(m_{3/2}, m_Z)\right) .$$

The total decay width is the sum of these partial decay widths

$$\Gamma_{\psi_\mu} = \Gamma(\psi_\mu \to W^\pm l^\mp) + \Gamma(\psi_\mu \to Z\nu) + \Gamma(\psi_\mu \to h\nu) + \Gamma(\psi_\mu \to \gamma\nu) , \quad (3.138)$$

and the branching ratios are shown in Figure 3.12. For large gravitino mass the branching ratio into photon and neutrino approaches zero, and the branching ratio into Z boson and neutrino as well as Higgs boson and neutrino are identical and half the size of the branching ratio into W boson and lepton.
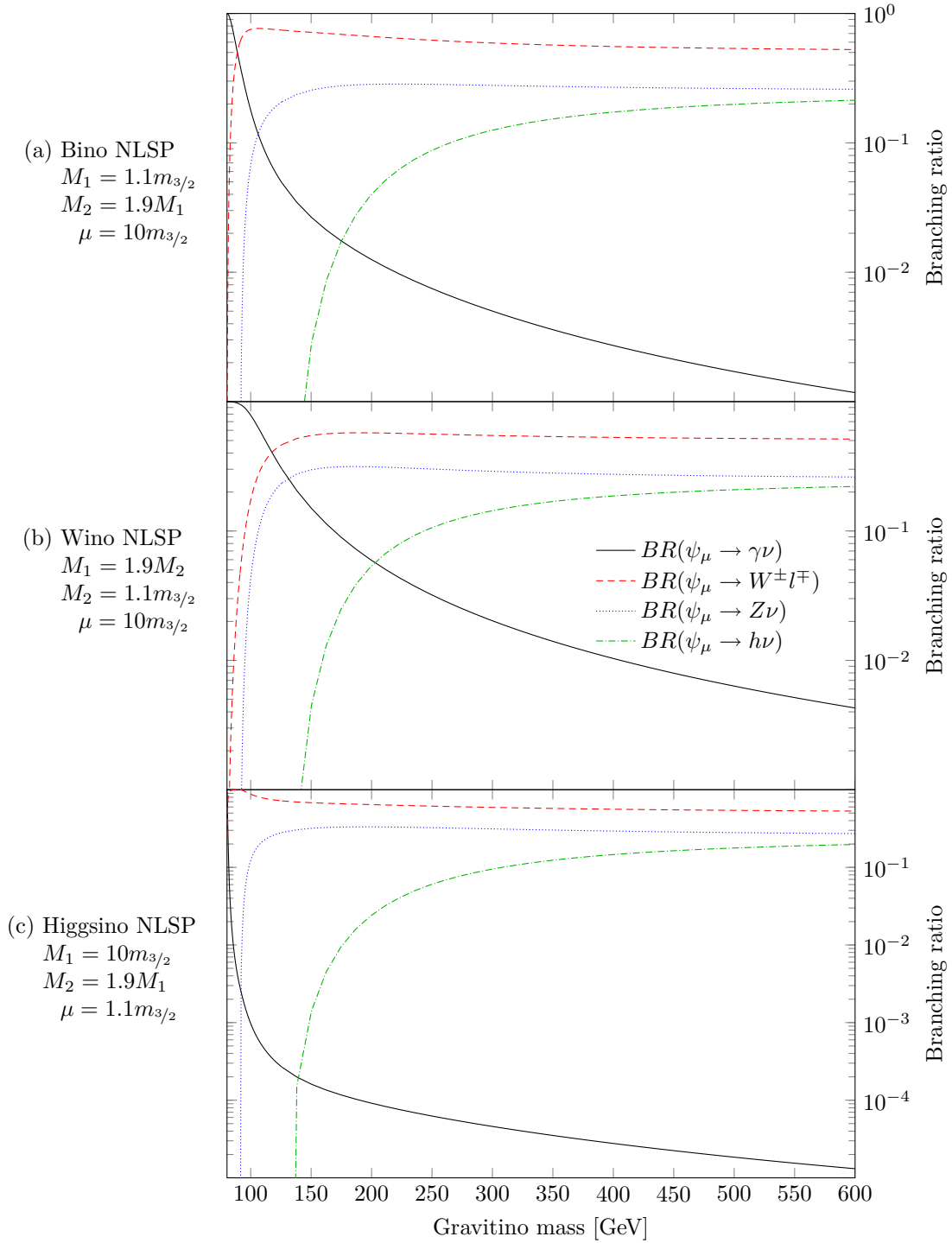
(a) Bino NLSP
$M_1 = 1.1m_{3/2}$
$M_2 = 1.9M_1$
$\mu = 10m_{3/2}$

(b) Wino NLSP
$M_1 = 1.9M_2$
$M_2 = 1.1m_{3/2}$
$\mu = 10m_{3/2}$

$BR(\psi_\mu \to \gamma\nu)$
$BR(\psi_\mu \to W^\pm l^\mp)$
$BR(\psi_\mu \to Z\nu)$
$BR(\psi_\mu \to h\nu)$

(c) Higgsino NLSP
$M_1 = 10m_{3/2}$
$M_2 = 1.9M_1$
$\mu = 1.1m_{3/2}$

Gravitino mass [GeV]

Figure 3.12: Gravitino branching ratio for the decays into photon and neutrino, W boson and lepton, Z boson and neutrino and Higgs boson and neutrino (*cf.* Equation (3.137)). We distinguish the three case where the NLSP is bino- (a), wino- (b) or higgsino-like (c).

Chapter 4

Constraining neutralino decays via gravitino decays

In this section we first analyse the dependence of the gravitino decay width on the RPV parameter ζ and the gaugino masses. Afterwards we relate neutralino NLSP to gravitino decay widths and derive lower bounds on the NLSP decay lengths. Knowing the lifetimes of the LSPs we are able to constrain the parameters with cosmological and astrophysical observations. Finally we analyse the behaviour of scalar tau NLSP.

4.1 Gravitino dark matter

Inserting the matrix element (3.85a) into the partial decay width for a gravitino decaying into a photon and a neutrino (3.118) and summing over neutrinos and anti-neutrinos one obtains for the gravitino lifetime to LO[1] in $m_Z/\tilde{m}$

$$\Gamma_{3/2}(\gamma\nu) = \frac{1}{32\pi}\zeta^2 s_w^2 m_W^2 \frac{m_{3/2}^3}{M_P^2}\left(\frac{M_2 - M_1}{M_1 M_2}\right)^2 \; . \tag{4.1}$$

Whenever the NLSP is bino- or wino-like the gravitino lifetime depends directly on the value of the RPV parameter ζ (3.50), the mass of the NLSP as well as the ratio of the two gaugino mass parameter. In the case of higgsino-like NLSP, however, the gravitino lifetime depends on the mass of the possibly much heavier gauginos instead of the NLSP mass. Nevertheless, one can invert the relation (4.1) with respect to the R-parity breaking parameter

$$\zeta^2 = 32\pi \frac{1}{s_w^2 m_W^2}\frac{M_P^2}{m_{3/2}^3 \tau_{3/2}}\left(\frac{M_1 M_2}{M_2 - M_1}\right)^2 \; , \tag{4.2}$$

and constrain its value from the bounds on the gravitino lifetime (see Section 4.3.3). For a gravitino lifetime comparable to the age of the Universe and reasonable assumptions on the masses of the gauginos and the gravitino ζ becomes

$$\zeta \simeq 0.005 \left(\frac{M_1}{100\,\text{GeV}}\right)\left(\frac{m_{3/2}}{10\,\text{GeV}}\right)^{-3/2}\left(\frac{\tau_{3/2}}{\tau_{\text{Universe}}}\right)^{-\frac{1}{2}} \; . \tag{4.3}$$

---

[1] Where $\widetilde{m}$ is the largest out of the three supersymmetric neutralino mass parameters M_1, M_2, μ.

Comparing this to the upper bound derived from the RPV contribution to the neutrino mass (3.69) leads to the conclusion that the lifetime of gravitinos, which are not too heavy, must be much larger than the age of the universe

$$\tau_{3/2} = \frac{128\pi}{s_{2w}^2} \frac{M_{\rm P}^2}{m_{3/2}^3 m_\nu} \frac{M_1 M_2 M_\gamma}{(M_1 - M_2)^2}$$

$$\simeq 10^7\,\tau_{\rm Universe} \left(\frac{M_1}{100\,{\rm GeV}} \right) \left(\frac{m_{3/2}}{10\,{\rm GeV}} \right)^{-3} \left(\frac{m_\nu}{100\,{\rm meV}} \right)^{-1}\,. \tag{4.4}$$

For fixed $m_{3/2}$ this expression represents a lower bound on the lifetime of gravitino as the value for M_1 is a lower bound on the bino mass parameter and the value of m_ν is an upper bound on the RPV contribution to the neutrino mass.

4.1.1   Microscopic determination of the Planck mass

In principle, one can determine the Planck mass from decay properties of the NLSP together with the observation of a photon line in the diffuse gamma-ray flux, which is produced by gravitino decays. This has been proposed for $\widetilde{\tau}$-NLSP in [29] based on a similar analysis for stable gravitino [91].

   In our analysis of NLSP decays in Section 3.8.2 we have seen that the value of RPV ζ can be determined by the mass and the lifetime of the lightest gaugino. Therefore, it is clear that gaugino NLSP decays are particularly well suited for a measurement of the Planck mass

$$M_{\rm P} = \frac{1}{8\sqrt{2\pi}} m_Z s_{2w} \zeta \frac{M_2 - M_1}{M_1 M_2} m_{3/2}^{3/2} \tau_{3/2}^{1/2}\,. \tag{4.5}$$

$M_{\rm P}$ will be a function of the masses and lifetimes of the LSPs only.

4.2   Quasi stable next-to lightest neutralinos

After having determined the lifetime of the gravitino LSP we are in the position to analyse the properties of the NLSP. In this section we will restrict ourselves to neutralino NLSPs and will give analytic formulas for the three cornering cases where one of the three parameters M_1, M_2, μ is notably lighter than the other two.

4.2.1   Bino-like

If M_1 is the lightest of the supersymmetric mass parameter, the NLSP is bino-like. As long as the masses of the two EW gauginos are identical at the GUT scale, we can expect the ratio of their masses to be roughly two at the TeV scale (*cf.* Equation (2.16)). If we further assume that the higgsino mass parameter μ is also larger than the bino mass parameter we are in a pure bino NLSP scenario.

   In the extreme case ($\mu \gg m_{1/2}$) the masses of the next-to lightest neutralino and the lightest chargino are degenerate and the mass difference to the lightest neutralino is given by

$$m_{\chi_1^\pm} - m_{\chi_1^0} = m_{\chi_2^0} - m_{\chi_1^0} = M_2 - M_1 - c_{2w} \frac{m_Z^2}{\mu} c_{2\beta} + \mathcal{O}\left(\frac{m_{\chi_1^0}}{\mu} \right)\,. \tag{4.6}$$
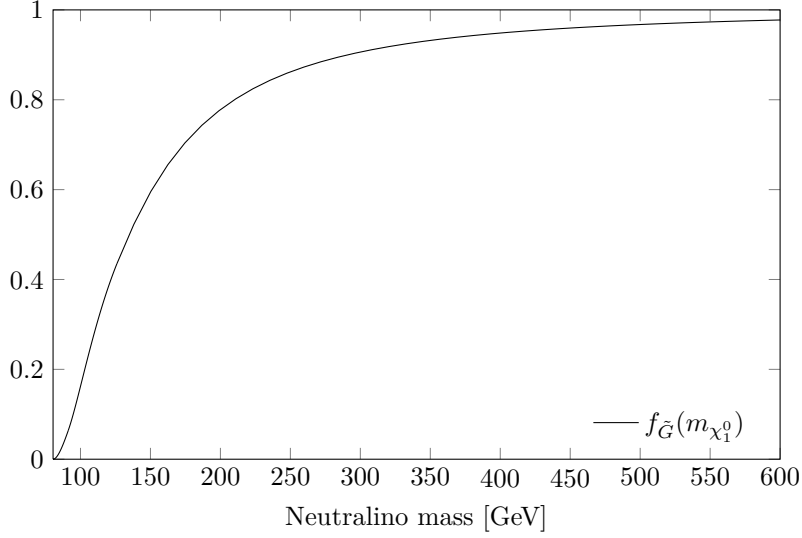
Figure 4.1: Gaugino phase space suppression factor.

In the bino-like neutralino NLSP scenario the decays of the χ_1^0 into Z, W and Higgs bosons as well as leptons is up to order $m_Z^2/\tilde{m}^2$ governed by the three matrix elements (*cf.* Appendix A.4.2)

$$V_{1i}^{(\chi^0,\nu)} = -\zeta_i \frac{s_w}{2} \frac{m_Z}{M_1} \ , \qquad V_{1i}^{(\chi^-,e)} = -\zeta_i s_w \frac{m_Z}{M_1} \ , \qquad \widetilde{V}_{i1}^{(\nu,\chi^0)} = -\zeta_i t_w \ . \tag{4.7}$$

Using these matrix elements in the total decay width (3.107) leads under the assumptions that $m_{\chi_1^0} \simeq M_1$ to first order in $m_Z/\tilde{m}$ to the bino-like neutralino decay width

$$\Gamma_{\chi_1^0} = \frac{1}{4} \frac{\alpha}{c_w^2} \zeta^2 m_{\chi_1^0} f_{\tilde{G}}(m_{\chi_1^0}) \ , \tag{4.8}$$

where we have introduced the gaugino phase space suppression factor (*cf.* Equations (3.93) and (3.105))

$$f_{\tilde{G}}(m_{\chi_1^0}) = \frac{1}{2} f_V(m_{\chi_1^0}, m_W) + \frac{1}{4} f_V(m_{\chi_1^0}, m_Z) + \frac{1}{4} f_S(m_{\chi_1^0}, m_h) \ , \tag{4.9}$$

which approaches one for large neutralino masses and is depicted in Figure 4.1. In this case the branching ratios for the decay into Z and Higgs are equal and half the size as the branching ratio into W, as one can as well see in Figure 4.2. The lifetime is for reasonable assumptions given by

$$c\tau_{\chi_1^0} \simeq 7.7 \,\mathrm{m} \left(\frac{m_{\chi_1^0}}{100 \,\mathrm{GeV}} \right)^{-1} \left(\frac{\zeta}{10^{-8}} \right)^{-2} f_{\tilde{G}}^{-1}(m_{\chi_1^0}) \ . \tag{4.10}$$

Using the Gravitino decay width (4.2) in order to eliminate the RPV coupling ζ the neutralino lifetime can be directly related to the gravitino lifetime

$$\tau_{\chi_1^0} = \frac{1}{8} \frac{c_w^2 s_w^2 m_W^2}{\alpha} \left(\frac{M_2 - M_1}{M_1 M_2} \right)^2 \frac{m_{3/2}^3 \tau_{3/2}}{M_{\mathrm{P}}^2 m_{\chi_1^0}} f_{\tilde{G}}^{-1}(m_{\chi_1^0}) \ , \tag{4.11}$$
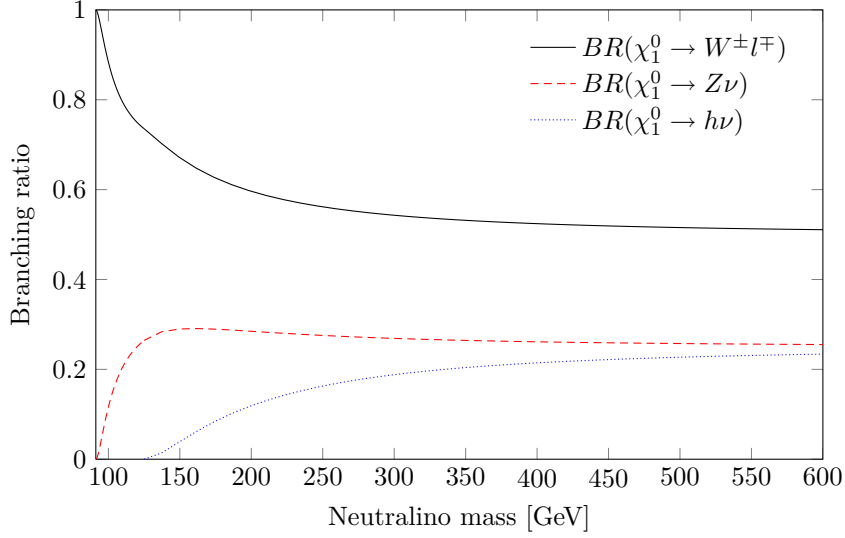
Figure 4.2: Branching ratios for gaugino decays into W-, Z- and the lightest Higgs boson as well as leptons.

We obtain for a typical neutralino decay length the relation

$$c\tau_{\chi_1^0} \simeq 4.3\,\text{m} \left(\frac{m_{\chi_1^0}}{100\,\text{GeV}}\right)^{-3} \left(\frac{m_{3/2}}{10\,\text{GeV}}\right)^3 \left(\frac{\tau_{3/2}(\gamma\nu)}{6\times10^{28}\,\text{s}}\right) f_{\tilde{G}}^{-1}(m_{\chi_1^0})\,. \tag{4.12}$$

The formula for the microscopic determination of the Planck mass (4.5) reads in the case of a bino-like NLSP

$$M_\text{P} = \frac{1}{4\sqrt{2\pi}} \frac{m_W s_{2w}}{\sqrt{\alpha}} \left(\frac{\tau_{3/2}}{\tau_{\chi_1^0}}\right)^{\frac{1}{2}} \left(\frac{m_{3/2}}{m_{\chi_1^0}}\right)^{\frac{3}{2}} \frac{M_2 - M_1}{M_2} f_{\tilde{G}}^{-\frac{1}{2}}(m_{\chi_1^0}) \tag{4.13}$$

$$\simeq 2.4\times10^{18}\,\text{GeV} \left(\frac{m_{3/2}}{m_{\chi_1^0}}\right)^{\frac{3}{2}} \left(\frac{\tau_{3/2}}{10^{28}\,\text{s}}\right)^{\frac{1}{2}} \left(\frac{c\tau_{\chi_1^0}}{700\,\text{m}}\right)^{\frac{1}{2}} f_{\tilde{G}}^{-\frac{1}{2}}(m_{\chi_1^0})\,.$$

It is remarkable that the observation of a photon line in the diffuse gamma-ray flux, together with a measurement of the neutralino lifetime at the LHC, can provide a microscopic determination of the Planck mass.

4.2.2   Wino-like

In the case of wino-like NLSP the mass of the lightest neutralino is to first order in $m_Z^2/\tilde{m}^2$ degenerate with the mass of the lightest chargino. This constitutes the most optimistic case for three body decays. Compared to the two body decays, however, the three body decays can still be neglected, as these are not only suppressed by the larger phase space but also by two coupling constants. Keep in mind that a, albeit suppressed, decay channel into photons opens up. For wino-like NLSP the matrix elements leading to two body wino decays are up to order $m_Z^2/\tilde{m}^2$ given by

$$V_{1i}^{(\chi^0,\nu)} = \frac{1}{2}\zeta_i c_w \frac{m_Z}{M_2}\,, \qquad V_{1i}^{(\chi^0,e)} = -\zeta_i c_w \frac{m_Z}{M_2}\,, \qquad \widetilde{V}_{i1}^{(\nu,\chi^0)} = \zeta_i\,. \tag{4.14}$$

This leads under the assumption $m_{\chi_1^0} \simeq M_2$ to the total decay width of

$$\Gamma_{\chi_1^0} = \frac{1}{4} \frac{\alpha}{s_w^2} \zeta^2 m_{\chi_1^0} f_{\tilde{G}}(m_{\chi_1^0}) \; , \tag{4.15}$$

which is as well governed by the gaugino phase space suppression factor (4.9) and leads to the same branching ratios as in the bino-like NLSP case. As the total decay length differ only by a factor of $t_w^2 \simeq 0.3$, the numerical values for the decay length are similar to the bino-like case

$$c\tau_{\chi_1^0} \simeq 2.3 \, \mathrm{m} \left(\frac{m_{\chi_1^0}}{120 \, \mathrm{GeV}} \right)^{-1} \left(\frac{\zeta}{10^{-8}} \right)^{-2} f_{\tilde{G}}^{-1}(m_{\chi_1^0}) \; . \tag{4.16}$$

With the Gravitino decay width (4.1) also the wino-like neutralino lifetime can be expressed directly in terms of the gravitino lifetime

$$\tau_{\chi_1^0} = \frac{1}{8} \frac{s_w^4 m_W^2}{\alpha} \left(\frac{M_1 - M_2}{M_1 M_2} \right)^2 \frac{m_{3/2}^3 \tau_{3/2}}{M_\mathrm{P}^2 m_{\chi_1^0}} f_{\tilde{G}}^{-1}(m_{\chi_1^0}) \; , \tag{4.17}$$

We obtain for a typical neutralino decay length

$$c\tau_{\chi_1^0} \simeq 1.2 \, \mathrm{m} \left(\frac{m_{\chi_1^0}}{100 \, \mathrm{GeV}} \right)^{-3} \left(\frac{m_{3/2}}{10 \, \mathrm{GeV}} \right)^3 \left(\frac{\tau_{3/2}(\gamma\nu)}{6 \times 10^{28} \, \mathrm{s}} \right) f_{\tilde{G}}^{-1}(m_{\chi_1^0}) \; . \tag{4.18}$$

Also in the wino-like neutralino NLSP case on is able to determine the Planck mass microscopically

$$M_\mathrm{P} = \frac{1}{2\sqrt{2\pi}} \frac{m_W s_w^2}{\sqrt{\alpha}} \left(\frac{\tau_{3/2}}{\tau_{\chi_1^0}} \right)^{\frac{1}{2}} \left(\frac{m_{3/2}}{m_{\chi_1^0}} \right)^{\frac{3}{2}} \frac{M_1 - M_2}{M_1} f_{\tilde{G}}^{-\frac{1}{2}}(m_{\chi_1^0})$$

$$\simeq 2.4 \times 10^{18} \, \mathrm{GeV} \left(\frac{m_{3/2}}{m_{\chi_1^0}} \right)^{\frac{3}{2}} \left(\frac{\tau_{3/2}}{10^{28} \, \mathrm{s}} \right)^{\frac{1}{2}} \left(\frac{c\tau_{\chi_1^0}}{200 \, \mathrm{m}} \right)^{\frac{1}{2}} f_{\tilde{G}}^{-\frac{1}{2}}(m_{\chi_1^0}) \tag{4.19}$$

4.2.3   Higgsino-like

In the light higgsino scenario (LHS) motivated by hybrid gauge-gravity mediation μ is the lightest of the supersymmetric parameters: $\mu \ll M_1, M_2$. In this case the matrix elements governing the RPV neutralino decays are more complicated than in the gaugino case and read to first order in $m_Z/\tilde{m}$ (cf. Appendix A.4.2)

$$V_{1i}^{(\chi^0,\nu)} = \frac{\zeta_i m_Z^2}{2\sqrt{2}\mu} \left(\left(\frac{s_w^2}{M_1} + \frac{c_w^2}{M_2} \right) (s_\beta - c_\beta) - \frac{M_\gamma - \mu}{(M_1 - \mu)(M_2 - \mu)} (s_\beta + c_\beta) \right) \; , \tag{4.20a}$$

$$V_{1i}^{(\chi^0,e)} = \frac{\zeta_i m_Z^2}{\sqrt{2}\mu} \left(2 \frac{\mu c_w^2 (s_\beta + c_\beta)}{M_2(M_2 - \mu)} - \frac{M_\gamma - \mu}{(M_1 - \mu)(M_2 - \mu)} (s_\beta + c_\beta) - 2 \frac{c_w^2}{M_2} s_\beta \right) \; , \tag{4.20b}$$

$$\widetilde{V}_{i1}^{(\nu,\chi^0)} = -\frac{\zeta_i m_Z}{\sqrt{2}} \left(\frac{c_w}{M_2 - \mu} + \frac{s_w t_w}{M_1 - \mu} \right) (s_\beta + c_\beta) \; . \tag{4.20c}$$

The evaluation of the partial decay widths in the case of a higgsino-like neutralino (see Figure 4.3) leads to the conclusion that the lifetime of the lightest higgsino can be estimated solely from the decay into a W boson and a charged lepton. In the following, we only provide
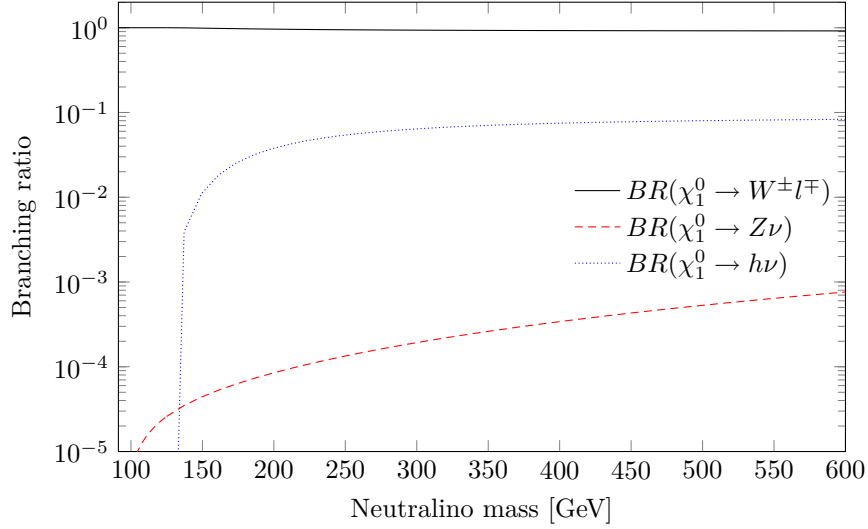
Figure 4.3: Branching ratios for higgsino decays into W-, Z-, and the lightest Higgs boson as wel as leptons.

the approximate formulae, where we have taken into account that $\tan\beta$ in hybrid gauge-gravity mediation is in general large. In the numerical evaluation, however, we use the full results. The lifetime of the lightest higgsino reads as a function of ζ

$$\tau_{\chi_1^0} \simeq 16 \frac{c_w^2 s_w^2}{\alpha m_Z^2} \frac{1}{\zeta^2} \frac{1}{m_{\chi_1^0}} f_V^{-1}(m_{\chi_1^0}, m_W) \tag{4.21}$$
$$\times \left(2 \frac{\mu c_w^2}{M_2(M_2 - \mu)}(s_\beta + c_\beta) - \frac{M_\gamma - \mu}{(M_1 - \mu)(M_2 - \mu)}(s_\beta + c_\beta) - 2\frac{c_w^2}{M_2}s_\beta \right)^{-2} ,$$

here and in the rest of this section we have set $m_{\chi_1^0} \simeq \mu$. Expanding the higgsino lifetime in $\mu/\tilde{m}$ we arrive at a formula which is to first order independent of the gaugino mass scale $\tilde{m} \sim M_1 \sim M_2$

$$\tau_{\chi_1^0} \simeq 16 \frac{c_w^2 s_w^2}{\alpha m_Z^2} \frac{1}{\zeta^2} \frac{1}{m_{\chi_1^0}} f_V^{-1}(m_{\chi_1^0}, m_W) \left(\frac{M_1 M_2}{3M_1 c_w^2 + M_2 s_w^2} \right)^2 \left(1 + \mathcal{O}\left(\frac{m_{\chi_1^0}}{m_{\chi_4^0}} \right) \right) . \tag{4.22}$$

The factor including the gaugino masses M_1 and M_2 depends only on their ratio and is *e.g.* in the case of unified GUT masses very close to ¹/₂. For reasonable assumptions the decay length is given by

$$c\tau_{\chi_1^0} \gtrsim 4.3\,\mathrm{m} \left(\frac{\zeta}{10^{-7}} \right)^{-2} \left(\frac{m_{\chi_1^0}}{400\,\mathrm{GeV}} \right)^{-1} \left(\frac{m_{\chi_3^0}}{2\,\mathrm{TeV}} \right)^2 f_V^{-1}(m_{\chi_1^0}, m_W) . \tag{4.23}$$

Expressing ζ in terms of the gravitino lifetime using Equation (4.2) together with the assumption of large $\tan\beta$ and large branching ratio into W bosons leads to following expression for

the higgsino-like neutralino lifetime

$$\tau_{\chi_1^0} \simeq \frac{1}{2\pi} \frac{c_w^4 s_w^4}{\alpha} \frac{m_{3/2}^3 \tau_{3/2}}{M_P^2} \left(\frac{M_1 - M_2}{M_1 M_2} \right)^2 \frac{1}{m_{\chi_1^0}} f_V^{-1}(m_{\chi_1^0}, m_W) \tag{4.24}$$

$$\times \left(2\frac{\mu c_w^2}{M_2(M_2 - \mu)}(s_\beta + c_\beta) - \frac{M_\gamma - \mu}{(M_1 - \mu)(M_2 - \mu)}(s_\beta + c_\beta) - 2\frac{c_w^2}{M_2}s_\beta \right)^{-2} .$$

The neutralino lifetime depends on the neutralino mass, the gravitino mass and its lifetime, and additionally on the bino and wino mass parameters. Expanding the higgsino lifetime in $\mu/\tilde{m}$ allows us to arrive at a formula which is to first order independent of the higher neutralino mass scale $\tilde{m} \sim M_1 \sim M_2$

$$\tau_{\chi_1^0} \simeq \frac{1}{2\pi} \frac{m_{3/2}^3 \tau_{3/2}}{M_P^2} \frac{s_w^4 c_w^4}{\alpha} \frac{1}{f_V(m_{\chi_1^0}, m_W)} \frac{1}{m_{\chi_1^0}} \left(\frac{M_2 - M_1}{3M_1 c_w^2 + M_2 s_w^2} \right)^2 \left(1 + \mathcal{O}\left(\frac{m_{\chi_1^0}}{m_{\chi_4^0}} \right) \right) . \tag{4.25}$$

The term consisting of the gaugino masses M_1 and M_2 and the weak mixing angle depends only on the ratio of the gaugino masses and is at the TeV scale $e.g.$ in the case of unified GUT masses very close to $1/8$. The relation for the decay length is now

$$c\tau_{\chi_1^0} \simeq 0.4\,\mathrm{m} \left(\frac{m_{3/2}}{10\,\mathrm{GeV}} \right)^3 \left(\frac{m_{\chi_1^0}}{100\,\mathrm{GeV}} \right)^{-1} \left(\frac{\tau_{3/2}}{10^{28}\,\mathrm{s}} \right) f_V^{-1}(m_{\chi_1^0}, m_W) . \tag{4.26}$$

Finally, we are able to give a relation for the microscopic determination of the Planck scale in the case of higgsino-like NLSP

$$M_P = \sqrt{2} \frac{s_w^2 c_w^2}{e} \left(\frac{m_{3/2}^3}{m_{\chi_1^0}} \frac{\tau_{3/2}}{\tau_{\chi_1^0}} \right)^{\frac{1}{2}} \frac{M_2 - M_1}{3M_1 c_w^2 + M_2 s_w^2} f_V^{-\frac{1}{2}}(m_{\chi_1^0}, m_W) \tag{4.27}$$

$$\simeq 2.4 \times 10^{18}\,\mathrm{GeV} \left(\frac{m_{3/2}}{10\,\mathrm{GeV}} \right)^{\frac{3}{2}} \left(\frac{m_{\chi_1^0}}{100\,\mathrm{GeV}} \right)^{-\frac{1}{2}} \left(\frac{\tau_{3/2}}{10^{28}\,\mathrm{s}} \right)^{\frac{1}{2}} \left(\frac{c\tau_{\chi_1^0}}{73\,\mathrm{cm}} \right)^{-\frac{1}{2}} f_V^{-\frac{1}{2}}(m_{\chi_1^0}, m_W) .$$

In the LHS, higgsino-like charginos and neutralinos would be pair produced at the LHC via virtual Z and W bosons. Heavier higgsinos decay into lighter ones, the lightest one being the neutralino-like NLSP. The mass difference between the lightest chargino and the lightest neutralino is

$$m_{\chi_1^\pm} - m_{\chi_1^0} \overset{m_Z \ll \tilde{m}}{\simeq} \frac{1}{2} m_Z^2 \left(\frac{(1 + s_{2\beta})(M_\gamma - \mu)}{(M_1 - \mu)(M_2 - \mu)} - \frac{2c_w^2(M_2 s_{2\beta} + \mu)}{(M_2 + \mu)(M_2 - \mu)} \right)$$

$$\overset{\mu \ll \tilde{m}}{\simeq} \frac{1}{2} m_Z^2 \left(\frac{M_1 c_1 + M_2 c_2}{M_1 M_2} + \mu \frac{M_1^2 c_1 + M_2^2 c_2}{M_1^2 M_2^2} + \mathcal{O}\left(\frac{\mu}{\tilde{m}} \right)^2 \right) , \tag{4.28}$$

where we have introduced

$$c_1 = (1 - s_{2\beta})c_w^2 , \qquad\qquad c_2 = (1 + s_{2\beta})s_w^2 . \tag{4.29}$$

The mass difference between the next-to-lightest neutralino and the lightest neutralino is

$$m_{\chi_2^0} - m_{\chi_1^0} \overset{m_Z \ll \tilde{m}}{\simeq} \frac{1}{2} m_Z^2 \left(\frac{(1 + s_{2\beta})(M_\gamma - \mu)}{(M_1 - \mu)(M_2 - \mu)} + \frac{(1 - s_{2\beta})(M_\gamma + \mu)}{(M_1 + \mu)(M_2 + \mu)} \right)$$

$$\overset{\mu \ll \tilde{m}}{\simeq} m_Z^2 \frac{M_{\tilde{\gamma}}}{M_1 M_2} \left(1 + \mu s_{2\beta} \left(\frac{1}{M_1} + \frac{1}{M_2} - \frac{1}{M_\gamma} \right) + \mathcal{O}\left(\frac{\mu}{\tilde{m}} \right)^2 \right) . \tag{4.30}$$

Hence, in the case of heavy gauginos the mass difference is rather small and to first order proportional to $m_Z/\tilde{m}$. Therefore, SM products at this stage of the decay chain will be too soft to be detectable. In the presence of RPV, however, the NLSP would propagate in the detector and further decay, prominently into a W boson and a lepton, yielding detectable SM objects coming from a displaced vertex.

4.3   Cosmological bounds

Both lower and upper bounds on ζ can be derived from cosmology. The lower bound comes from the BBN constraints on the NLSP when the gravitino is the LSP. An upper bound can in principle be derived by demanding that the baryon asymmetry generated by leptogenesis is not washed out before the EW phase transition in the early universe [25–28]. However, the bound from the constraints on decaying DM from the Fermi gamma-ray searches is stronger. As we will see, for our analysis the lower bound is not very constraining while the upper bound will be the motivation for our LHC search strategy.

Having derived the decay widths of the gravitino LSP and the neutralino-like NLSP, we are now ready to estimate the gravitino mass range allowing for gravitino DM and successful leptogenesis [35]. This allows us to connect the results from gamma-ray searches with displaced neutralino decays at the LHC.

4.3.1   Big bang nucleosynthesis

To start with, we need to make sure that the decays of neutralino NLSPs do not interfere with BBN. Hence we demand that all neutralinos decay during the first 100 seconds of the universe [20, 92, 93]. Deriving the neutralino lifetime without substituting the R-parity violating parameter ζ for the gravitino mass and lifetime leads (*cf.* Equations (4.8) and (4.22)) in the case of bino-like NLSP to

$$\zeta \simeq 1.6 \times 10^{-13} \left(\frac{\tau_{\chi_1^0}}{100\,\mathrm{s}} \right)^{-\frac{1}{2}} \left(\frac{m_{\chi_1^0}}{100\,\mathrm{GeV}} \right)^{-\frac{1}{2}} f_{\tilde{G}}^{-\frac{1}{2}}(m_{\chi_1^0}) \,. \qquad (4.31)$$

In the LHS this bound becomes stronger due to the larger gaugino masses

$$\zeta \simeq 4.2 \times 10^{-12} \left(\frac{\tau_{\chi_1^0}}{100\,\mathrm{s}} \right)^{-\frac{1}{2}} \left(\frac{m_{\chi_1^0}}{100\,\mathrm{GeV}} \right)^{-\frac{1}{2}} \left(\frac{m_{\chi_3^0}}{2\,\mathrm{TeV}} \right) f_V^{-\frac{1}{2}}(m_{\chi_1^0}, m_W) \,, \qquad (4.32)$$

which then characterizes the model depend lower bounds on ζ.

4.3.2   Gravitino dark matter mass

The minimal gravitino mass is limited by the requirement that the gravitino abundance does not overclose the universe. Since gravitinos are produced in thermal SQCD scatterings $gg \to \tilde{g}\psi_\mu$ [94], the gravitino mass must increase with increasing gluino mass for a given reheating temperature.

As we are interested in models in which the coloured particles are massive enough to have evaded detection at the LHC, gluinos will typically be heavy. For example, in the hybrid gauge-gravity mediation scenario in [95], which gives rise to a Higgs mass close to the LHC result, the gluino mass is close to 4 TeV. In order to still allow for small gravitino masses, we

will assume that the hot phase of the universe was created in the decay of the false vacuum of unbroken $B - L$ [96, 97]. Since right-handed neutrinos are created from $B - L$ Higgs decays, this scenario allows for gravitino DM, leptogenesis and the correct values for the neutrino mass parameters while requiring lower reheating temperatures compared to the thermal leptogenesis case. The lower bound on the gravitino mass obtained in [97] for $m_{\tilde{g}} = 1\,\text{TeV}$ is $m_{3/2}^{\min} = 10\,\text{GeV}$. It is possible to scale this bound to other gluino masses using [96]

$$m_{3/2} = m_{3/2}^{\min} \left(\frac{m_{\tilde{g}}}{1\,\text{TeV}} \right)^2 \; . \tag{4.33}$$

Assuming *e.g.* a gluino mass of $2\,\text{TeV}$, the minimal gravitino mass is $40\,\text{GeV}$ and therefore a neutralino NLSP with a mass of $100\,\text{GeV}$ is still viable.

4.3.3   Fermi-LAT bound on the gravitino lifetime

With the help of the data of Fermi-LAT we are able to restrict the lifetime of gravitinos for a given mass. Using the isotropic diffuse gamma-ray flux one can derive a lower bound of $\tau_{3/2} \gtrsim 3 \times 10^{28}$ seconds. A stronger bound of $\tau_{3/2} \gtrsim 6 \times 10^{28}\,\text{s}$ can be derived as a consequence of the non-observation of any gamma-ray lines [98–100].

For bino-like neutralino this translate into a bound of $\zeta \lesssim 2.3 \times 10^{-8}$ and $\zeta \lesssim 1.6 \times 10^{-8}$, respectively. For a LHS with a bino mass of roughly $M_1 \sim 2\,\text{TeV}$ this translates via (4.2) into an upper bound on the RPV of $\zeta \lesssim 4.70 \times 10^{-8}$ and $\zeta \lesssim 3.32 \times 10^{-8}$, respectively.[2]

In Section 4.2 we have used this bounds in order to derive the decay lengths of neutralino NLSPs as a function of the gravitino mass and lifetime. We would like to remind the reader that the resulting neutralino decay lengths (4.12), (4.18) and (4.26) are well within the reach of the multi-purpose detectors at the LHC. Even when the neutralino decay length is larger than the detector dimensions, some neutralinos would, due to the statistical nature of the process, decay inside the detector.

4.4   Scalar tau as next-to-lightest supersymmetric particle

Contrary to the neutralino NLSP decay, the R-parity violating decays of a $\tilde{\tau}_1$-NLSP strongly depend on the flavour structure and the supersymmetry breaking parameters. Since the R-parity breaking Yukawa couplings are proportional to the ordinary Yukawa couplings, decays into fermions of the second and third generation dominate. The leading partial decay widths of left- and right-handed $\tilde{\tau}$-leptons are given by Equation (3.92). Inserting the appropriate Yukawa-like RPC couplings (3.47), neglecting the τ mass and multiplying the colour factors for the decay into top and bottom results for the left-handed $\tilde{\tau}$-lepton in

$$\Gamma_{\tilde{\tau}_R}(\tau_L \nu) = \Gamma_{\tilde{\tau}_R}(\mu_L \nu) = \frac{1}{16\pi} \sum_i |\lambda_{i33}|^2 \, m_{\tilde{\tau}_R} \; , \tag{4.34a}$$

$$\Gamma_{\tilde{\tau}_L}(\tau_R \nu) = \frac{1}{16\pi} \sum_i \left| \widehat{\lambda}_{i33} \right|^2 m_{\tilde{\tau}_L} \; , \tag{4.34b}$$

---

[2]This stringent RPV bound implies that the RPV contribution to the neutrino masses can be neglected compared to the contribution from right-handed neutrinos [29].
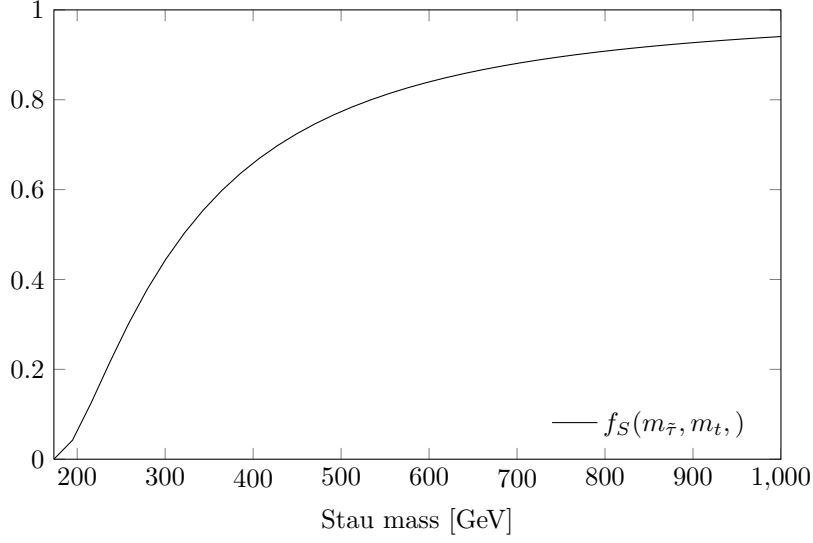
Figure 4.4: Phase space suppression factor for stau decays into top and bottom quarks.

and for the right-handed $\widetilde{\tau}$-lepton in

$$\Gamma_{\widetilde{\tau}_L}(\bar{t}_L b_R) = \Gamma_{\widetilde{\tau}_L}(\bar{t}_L s_R) = \frac{3}{16\pi} \left| \widehat{\lambda}'_{333} \right|^2 m_{\widetilde{\tau}_L} f_S(m_{\widetilde{\tau}}, m_t) \; , \tag{4.35a}$$

$$\Gamma_{\widetilde{\tau}_L}(\bar{t}_R b_L) = \frac{3}{16\pi} \left| \widetilde{\lambda}_{333} \right|^2 m_{\widetilde{\tau}_L} f_S(m_{\widetilde{\tau}}, m_t) \; . \tag{4.35b}$$

The dependence of the phase space suppression factor for stau decays into top and bottom quark on the stau mass is shown in Figure 4.4. In the flavour model discussed in Section 3.5.1, the order of magnitude of the various decay widths is determined by the power of the hierarchy parameter η ($\eta^2 \simeq 1/300$),

$$\Gamma_{\widetilde{\tau}_L}(\tau_R \nu) \sim \Gamma_{\widetilde{\tau}_R}(\tau_L \nu) = \Gamma_{\widetilde{\tau}_R}(\mu_L \nu) \sim \Gamma_{\widetilde{\tau}_L}(\bar{t}_L b_R) = \Gamma_{\widetilde{\tau}_L}(\bar{t}_L s_R) \sim \eta^4 \Theta^2 m_{\widetilde{\tau}} \; , \tag{4.36a}$$

$$\Gamma_{\widetilde{\tau}_L}(\bar{t}_R b_L) \sim \eta^2 \Theta^2 m_{\widetilde{\tau}} \; . \tag{4.36b}$$

The lightest mass eigenstate $\widetilde{\tau}_1$ is a linear combination of $\widetilde{\tau}_L$ and $\widetilde{\tau}_R$,

$$\widetilde{\tau}_1 = s_\tau \widetilde{\tau}_L + c_\tau \widetilde{\tau}_R \; . \tag{4.37}$$

From the above equations one obtains the $\widetilde{\tau}_1$-decay width

$$\Gamma_{\widetilde{\tau}_1} = s_\tau^2 \left(\Gamma_{\widetilde{\tau}_L}(\tau_R \nu) + \left(2\Gamma_{\widetilde{\tau}_L}(\bar{t}_L b_R) + \Gamma_{\widetilde{\tau}_L}(\bar{t}_R b_L) \right) f_S(m_{\widetilde{\tau}}, m_t) \right) + 2c_\tau^2 \Gamma_{\widetilde{\tau}_R}(\tau_L \nu) \; . \tag{4.38}$$

The total width is dominated by the contributions $\widetilde{\tau}_R \to \tau_L \nu$, $\mu_L \nu$ and $\widetilde{\tau}_L \to \bar{t}_R b_L$, respectively,

$$\Gamma_{\widetilde{\tau}_1} = s_\tau^2 \Gamma_{\widetilde{\tau}_L}(\bar{t}_R b_L) f_S(m_{\widetilde{\tau}}, m_t) + 2c_\tau^2 \Gamma_{\widetilde{\tau}_R}(\tau_L \nu) \; , \tag{4.39}$$

and it can be directly expressed in terms of the τ-lepton and top-quark masses,[3]

$$\Gamma_{\widetilde{\tau}_1} = \frac{\epsilon^2}{16\pi v^2} \left(3m_t^2 s_\tau^2 f_S(m_{\widetilde{\tau}}, m_t) + 2m_\tau^2 t_\beta^2 c_\tau^2 \right) m_{\widetilde{\tau}_1} \; , \tag{4.40}$$

_____

[3]Note the additional phase space factor $f_S(m_{\widetilde{\tau}}, m_t)$ compared to [1, 82], which can only be neglected for $m_{\widetilde{\tau}} \gg m_t$.
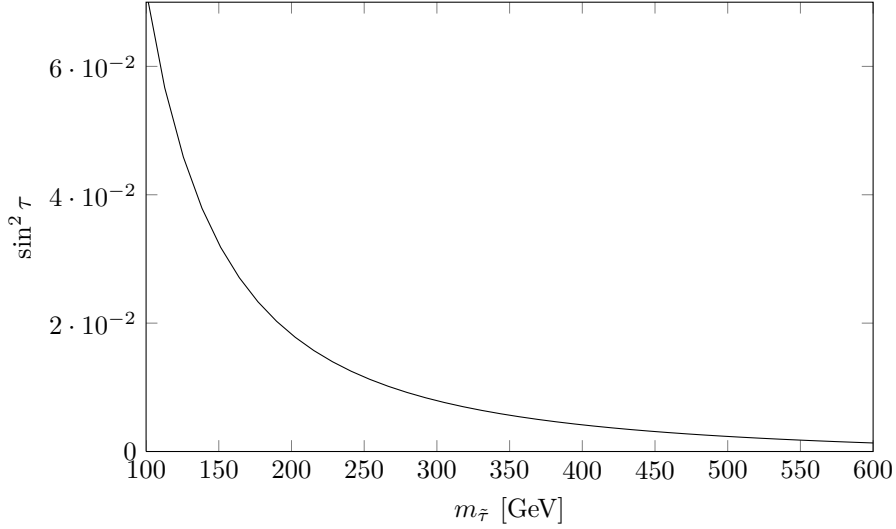
Figure 4.5: $\widetilde{\tau}$-mixing angle: $\sin^2 \tau$ as function of the lightest $\widetilde{\tau}$-mass $m_{\widetilde{\tau}_1}$.

where we have assumed

$$\epsilon_{2,3} = \epsilon'_{2,3} = \epsilon''_{2,3} \equiv \epsilon \ . \tag{4.41}$$

This corresponds to the parameter choice $a = b = c = 1$ in Equation (3.55). Note that $\widetilde{\tau}_1$-decay width and branching ratios have a considerable uncertainty since these parameters depend on the unspecified mechanism of supersymmetry breaking. From Equation (3.24) and $\eta \simeq 0.06$, one obtains for the R-parity breaking parameter

$$\epsilon \simeq \zeta \simeq \eta\Theta \simeq 6 \times 10^{-8} \ , \tag{4.42}$$

which is consistent with the present upper bound derived in Section (4.3.3) within the theoretical uncertainties.

The dependence of the mixing angle τ on $m_{\widetilde{\tau}_1}$ is shown in Figure 4.5 for the boundary conditions

$$m_0 = 0 \ , \qquad\qquad a_0 = 0 \ , \qquad\qquad \tan\beta = 10 \ . \tag{4.43}$$

For masses below the top-bottom threshold only leptonic $\widetilde{\tau}_1$-decays are possible. When the decay into top-bottom pairs becomes kinematically allowed, $\sin^2 \tau$ is small. However, the suppression by a small mixing angle is compensated by the larger Yukawa coupling compared to the leptonic decay mode. This is a direct consequence of the RPV couplings to up quarks $\widetilde{\lambda}$ which were not taken into account in previous analyses.

Due to the competition between mixing angle suppression and hierarchical Yukawa couplings, the top-bottom threshold is clearly visible in the $\widetilde{\tau}_1$-decay length as well as the branching ratios into leptons and heavy quarks. This is illustrated in Figures 4.6 and 4.7, respectively, where these observables are plotted as functions of $m_{\widetilde{\tau}_1}$. Representative values of the $\widetilde{\tau}_1$-decay lengths below and above the top-bottom threshold are

$$m_{\widetilde{\tau}_1} < m_t + m_b \ : \qquad\qquad c\tau_{\widetilde{\tau}_1}|_{150\,\text{GeV}} = 1.4\,\text{m} \left(\frac{\epsilon}{5 \times 10^{-8}} \right)^{-2} \ , \tag{4.44a}$$

$$m_{\widetilde{\tau}_1} > m_t + m_b \ : \qquad\qquad c\tau_{\widetilde{\tau}_1}|_{250\,\text{GeV}} = 0.6\,\text{m} \left(\frac{\epsilon}{5 \times 10^{-8}} \right)^{-2} \ . \tag{4.44b}$$
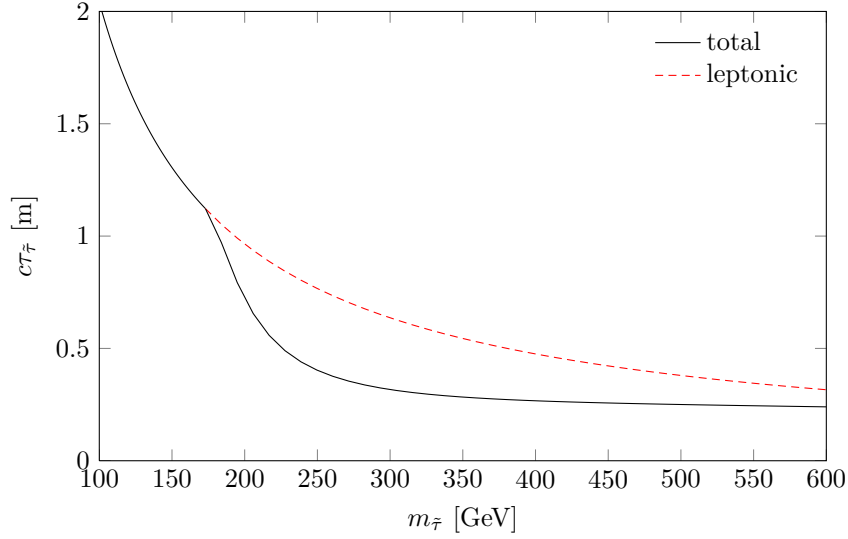
Figure 4.6: $\widetilde{\tau}_1$-decay length as function of $m_{\widetilde{\tau}_1}$. Above the top-bottom threshold hadronic decays decrease the $\widetilde{\tau}_1$-lifetime.
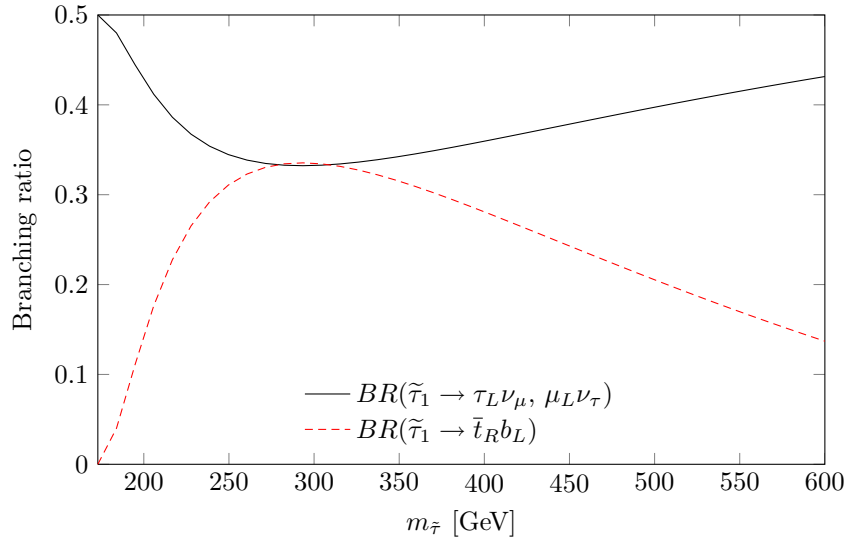

Figure 4.7: Lightest scalar tau branching ratios as functions of $m_{\widetilde{\tau}_1}$. The dependence on the $\widetilde{\tau}_1$-mass is determined by the top-bottom threshold and the mass dependence of the $\widetilde{\tau}_1$-mixing angle.

Choosing for ϵ a representative value from gravitino decay, $\epsilon = \zeta_{\mathrm{obs}} = 10^{-9}$, one obtains $c\tau_{\tilde{\tau}_1} = 4\,\mathrm{km}\ (1\,\mathrm{km})$ for $m_{\tilde{\tau}_1} = 150\,\mathrm{GeV}\ (250\,\mathrm{GeV})$. It is remarkable that such lifetimes can be measured at the LHC [47, 48].

Is it possible to avoid the severe constraint from gravitino decays on the $\tilde{\tau}_1$-decay length? In principle, both observables are independent, and the unknown constants in the definition of ϵ, ϵ' and ϵ'' can be adjusted such that $\zeta = 0$. However, this corresponds to a strong fine-tuning, unrelated to an underlying symmetry. To illustrate this, consider the case where the soft R-parity breaking parameters vanish at the GUT scale, $B_i = m_{id}^2 = 0$, which was discussed in Section 3.5.1. In bilinear R-parity breaking, also the R-parity violating Yukawa couplings vanish at the GUT scale. With the one-loop radiative corrections at the EW scale (cf. Equation (3.35); $\epsilon_i = \mu_i/\mu$),

$$B_i(\Lambda_{\mathrm{EW}}) = \frac{\epsilon_i \mu}{16\pi^2} 6 \left(\frac{1}{5} g'^2 M_1 + g^2 M_2 \right) \ln \frac{\Lambda_{\mathrm{GUT}}}{\Lambda_{\mathrm{EW}}} \ , \qquad m_{id}^2(\Lambda_{\mathrm{EW}}) = 0 \ , \qquad (4.45)$$

and $M_{1,2} \sim \mu$, one reads off from Equations (3.42) and (3.45)

$$\epsilon_i', \ \epsilon_i'' = \mathcal{O}\left(\epsilon_i\right) \ . \qquad (4.46)$$

Hence, all R-parity breaking parameters are naturally of the same order, unless the fine-tuning also includes radiative corrections between the GUT and the EW scale.

Even if one accepts the fine-tuning $\zeta = 0$, one still has to satisfy the cosmological bounds on R-parity violating couplings, which yield $\epsilon_i = \mu_i/\mu \lesssim 10^{-6}$ [28]. In the flavour model discussed in Section 3.5.1 this corresponds to the choice $a = 20$ in Equation (3.32). For the smaller $\tilde{\tau}_1$-mass, which is preferred by electroweak precision tests, one then obtains the lower bound on the decay length

$$c\tau_{\tilde{\tau}_1}\big|_{150\,\mathrm{GeV}} \gtrsim 4\,\mathrm{mm} \ . \qquad (4.47)$$

However, let us emphasize again that current constraints from Fermi-LAT on the diffuse gamma-ray spectrum indicate decay lengths several orders of magnitude larger.

Chapter 5

Neutralino at the LHC

Having laid the groundwork we are prepared to investigate possible signatures of light neutralinos with and without conserved R-parity at the LHC. First we introduce in Section 5.1 the software we are using to analyse the signatures of neutralinos. Then we introduce in Section 5.2 two benchmark models featuring light higgsinos and propose a search for RPC signatures. Afterwards, in Section 5.3, we describe the extension of the software we have implemented in order to work with displaced vertices. Finally we demonstrate the power of searches for displaced vertices using the example of strongly produced bino-like neutralino NLSP and weakly produced higgsino-like neutralino NLSP in Section 5.4 and 5.5, respectively.

5.1 Event simulation

Our simulation of the signal events relied on the following procedure. First, supersymmetric mass spectra were calculated with a modified version of `SOFTSUSY` 3.1.5 [101, 102]. The `SOFTSUSY` version was modified in order to produce if needed additionally to the spectrum the R-parity violating decay widths and branching ratios of the lightest neutralino. All other RPV decays are neglectable due to the tiny amount of R-parity breaking we introduce. The `SOFTSUSY` mass spectra were fed into `SDECAY` 1.3b [103] in order to calculate the decay widths of the SUSY particles (besides the neutralino LSP). In the next step the possible neutralino decay information was included into the `SDECAY` output. The signal process as well as the background was simulated with `MADGRAPH` 4.4.44 [104] and then given to `PYTHIA` 6.4.22 [105] for computation of all subsequent decays according to the `SDECAY` output as well as for parton showering and hadronization. All Monte Carlo samples were generated using parton distribution functions given by CTEQ6L1 [106]. The generic detector simulation `DELPHES` 1.9 [107], tuned to the CMS detector[1], was used in order to account for effects of event reconstruction at the detector level.

5.2 Search for light higgsinos with b-jets and missing leptons

The MSSM with RPC, light higgsinos and otherwise heavy superparticles has previously been studied *e.g.* in [108]. Recently some models were constructed which predict precisely this pattern, such as the "lopsided gauge mediation" models of [109, 110], as well as the

---

[1]As discussed in Section 5.5.1, our results would be similar for the ATLAS detector.

mixed gauge-gravity mediation models of [46] which this analysis will be concerned with (*cf.* Section 2.4.4).

5.2.1   Benchmark points

The precise details of the spectrum depend on the messenger content of the model, on the exact choice of messenger scale and SUSY breaking scale, and on the assumptions about the gravity-mediated contributions to the soft terms. For our purposes of a first tentative study of collider phenomenology, it is convenient to adopt a simplified parametrization: We fix the gravitino mass to be $m_{3/2} = 100\,\mathrm{GeV}$, and choose a common messenger mass just below the GUT scale, $M_\mathrm{m} = 5 \times 10^{15}\,\mathrm{GeV}$. Then the essential free parameters are the gaugino masses M_1, M_2 and M_3, the Higgs soft mass mixing B_μ, and the higgsino mass μ. At the GUT scale we expect

$$|B_\mu| \simeq |\mu|^2 \simeq m_{3/2}^2 \;, \qquad\qquad\qquad |M_{1,2,3}| \gg m_{3/2} \;. \qquad (5.1)$$

Scalar soft masses are dominated by the gauge-mediated contribution, which is completely fixed after prescribing the gaugino masses. Explicitly, they are given by the standard minimal gauge mediation formula

$$m_\Phi^2 = 2 \left(\frac{g^2}{16\pi^2} \right)^2 \left(\sum_a C_a n_a \right) \left| \frac{F}{M_\mathrm{m}} \right|^2 \;, \qquad (5.2)$$

where $a = 1$, 2, 3 labels the SM gauge factors, C_a is the corresponding quadratic Casimir of Φ, the SUSY breaking scale F is

$$F = \sqrt{3}\,m_{3/2} M_\mathrm{P} = \left(2 \times 10^{10}\,\mathrm{GeV} \right)^2 \;, \qquad (5.3)$$

and the effective messenger numbers n_a are obtained by inverting the standard gaugino mass formula

$$M_a = \frac{g^2}{16\pi^2} n_a \frac{F}{M_\mathrm{m}} \;. \qquad (5.4)$$

We are neglecting the running of the gauge couplings between M_m and M_GUT, as well as the subdominant gravity-mediated contributions. Trilinear terms are again dominated by gravity mediation; for simplicity we choose them to be universal and set $A_0 = \mu$.

Having thus fixed the MSSM parameters at the messenger scale, we evolve them to the weak scale by means of their RGEs using `SOFTSUSY`. Reproducing the correct value of the Z mass further reduces the number of free parameters by one. In the end, within our simplified ansatz the mass spectrum is entirely determined by the five parameters M_1, M_2, M_3, μ and B_μ at the messenger scale. These are subject to the conditions that EW symmetry should be broken with $m_Z = 91\,\mathrm{GeV}$, and that there should be a separation of mass scales according to

$$\mu \sim \sqrt{B_\mu} \sim m_{3/2} \;\ll\; M_1 \sim M_2 \sim M_3 \;. \qquad (5.5)$$

Table 5.1 shows two examples for low-energy spectra, both with $\mu = 150\,\mathrm{GeV}$ and $\sqrt{B_\mu} = 200\,\mathrm{GeV}$ and with equal values for M_1 and M_2.

$$\text{Spectrum I}\;:\qquad\qquad M_1 = M_2 = 1250\,\mathrm{GeV} \;, \qquad\qquad M_3 = 428\,\mathrm{GeV} \;. \qquad (5.6)$$

particle	model				
	Spectrum I	Spectrum II	HH50	HH50'	simplified
h_0	116	121	115	117	117
χ_1^0	124	117	206	207	125
$\chi_1^\pm$	129	119	389	395	
χ_2^0	134	121	389	395	
χ_3^0	559	1 319	635	771	
χ_4^0	1 059	2 453	649	778	
$\chi_2^\pm$	1 059	2 453	648	779	
H_0	641	660	861	958	
A_0	642	666	861	958	
$H^\pm$	648	672	865	962	
$\tilde{g}$	1 063	2 485	1 167	1 167	
$\tilde{t}_1$	665	1 558	860	660	659
$\tilde{b}_1$	797	1 614	1 034	943	
$\tilde{u}_1$	1 155	2 438	1 122	1 130	
$\tilde{d}_1$	1 065	2 294	1 119	1 127	
other squarks	1 070–1 500	2 300–3 100	1 120–1 160	990–1 270	
$\tilde{\tau}_1$	509	669	528	520	
other sleptons	790–1 160	1 400–2 300	530–600	530–600	

Table 5.1: A light and a heavy spectrum, with a CMSSM point HH50, a CMSSM-like point HH50' and a simplified model for comparison. The parameters defining these models are listed in Table 5.2. Particle masses are in GeV.

These parameters were chosen such that the model was close to the former LHC exclusion limits.[2]

$$\text{Spectrum II}\ :\qquad M_1 = M_2 = 3\,\text{TeV}\ ,\qquad M_3 = 1130\,\text{GeV}\ ,\qquad (5.7)$$

for which the model would be invisible at the early LHC and quite difficult to find even at 14 TeV. Our analysis will be mostly concerned with the phenomenology of Spectrum I at $\sqrt{s} = 7\,\text{TeV}$.[3]

---

[2]This parameter point is ruled out by now.

[3]The Higgs mass chosen for these models does not coincide with the mass measured at ATLAS and CMS, adjusting the Higgs mass, however, would not have a large effect on the analysis.

model	μ	$\sqrt{B_\mu}$	$M_1 = M_2$	M_3	m_0	$m_0^{(3)}$	A_0	$A_0^{(3)}$	$\tan\beta$
Spectrum I	150	200	1 250	428					46
Spectrum II	150	200	3 000	1 130					53
HH50			500	500	500	500	0	0	10
HH50'			500	500	500	300	0	−1 000	10

Table 5.2: Defining parameters for a light and a heavy spectrum, with a CMSSM point and a CMSSM-like point for comparison. Particle masses are in GeV. In HH50' third-generation squarks and sleptons were given a universal soft mass $m_0^{(3)}$ and a trilinear A-parameter $A_0^{(3)}$.

For comparison, we have also included a similar CMSSM benchmark point HH50 and a CMSSM-like benchmark point HH50'.

$$\text{HH50} \; : \quad m_0 = M_{1,2} = 500\,\text{GeV} \; , \quad \tan\beta = 10 \; , \quad \text{sign}(\mu) = +1 \; , \quad A_0 = 0 \; . \quad (5.8)$$

HH50' is defined in the same way, but with the soft terms of the third generation chosen differently: Third-generation squarks and sleptons were given a universal soft mass $m_0^{(3)} = 300\,\text{GeV}$ and a trilinear A-parameter $A_0^{(3)} = -1\,\text{TeV}$. This choice was made in order to have a reference spectrum whose $\tilde{t}_1 \tilde{t}_1^*$ production cross section is comparable to that of Spectrum I, while closely resembling the CMSSM. Finally, we also list a comparable simplified model, containing only the $\tilde{t}_1$ and a bino-like neutralino LSP. The model definitions are summarized in Table 5.2.

5.2.2 Signatures

The light higgsinos of our scenario will be produced in copious numbers in EW processes at the LHC. The Drell-Yan process gives rise to $\chi_1^+\chi_1^-$, $\chi_1^\pm\chi_{1,2}^0$ and $\chi_1^0\chi_2^0$ final states, and W boson fusion can give like-sign $\chi_1^\pm\chi_1^\pm$ pairs. The subsequent decays of χ_2^0 and $\chi_1^\pm$ into χ_1^0 will lead to events with missing energy and soft jets or leptons.

Unfortunately, with the higgsino mass splittings in the range of only a few GeV, most of these jets and leptons are too soft to even trigger on, and those events with high enough transverse momentum (p_T) (PT) to be detected are completely swamped by the SM background. Demanding large missing transverse energy ($\not{E}_T$) (MET) does not help much, since also the MET spectrum falls very rapidly. For illustration, the lepton PT and MET distributions for Spectrum I are shown in Figure 5.1. We have also studied events with additional jets from initial-state gluon radiation, in order to increase the number of events with larger PT and MET. While this somewhat enhances the tails of the distributions, it also reduces the overall cross section, and the combined effect does very little to improve the overall situation. In conclusion we confirm the findings of [111] that, in order to find evidence for our scenario in EW processes, a linear collider would be far better suited.[4]

---

[4]For the LHC, a mono-jet (from initial-state gluon radiation) together with large MET might perhaps be a useful signal, in combination with other searches. We will however not pursue this possibility in the present work because of the difficulties in accurately estimating the background without a full detector simulation.

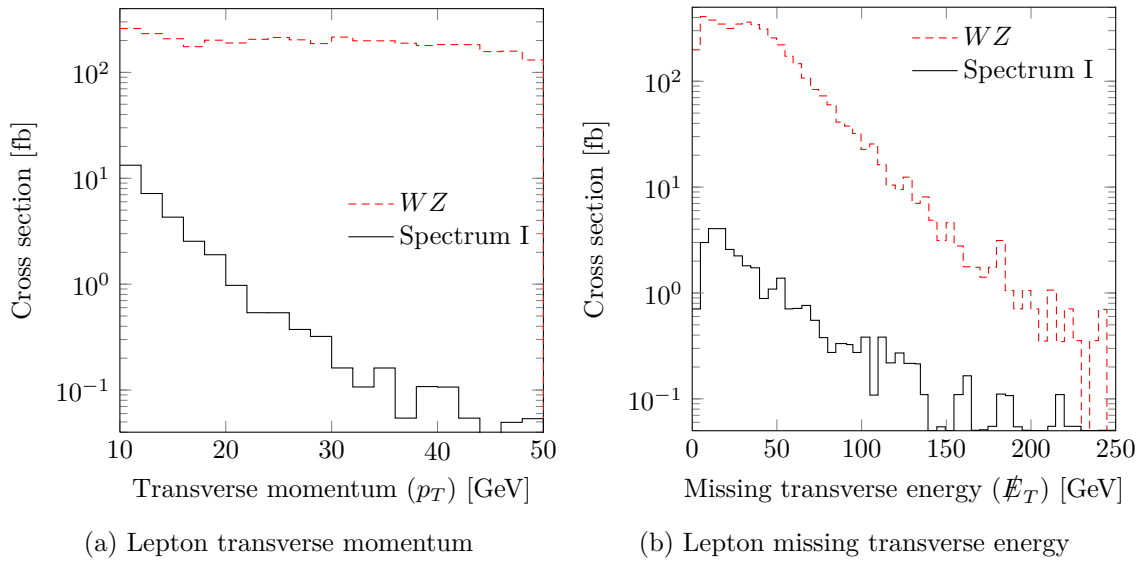(a) Lepton transverse momentum (b) Lepton missing transverse energy

Figure 5.1: Lepton transverse momentum and MET distributions of leptonic events from electroweakly produced higgsino decays within Spectrum I. For comparison, the SM background from WZ production (which is just one of the several contributing processes) is also shown. See Section 5.2.3 for details of the event simulation.

We are therefore led to consider those regions of parameter space where some coloured superparticles are still light enough to be produced at the LHC. The lightest coloured superparticle in our class of models is always the lighter of the scalar top quarks $\tilde{t}_1$. At the LHC it may be produced in pairs, or it may appear in cascade decays of first-generation squarks and gluinos if these are kinematically accessible. It turns out that processes involving the $\tilde{t}_1$ are particularly well suited to find evidence for our scenario (or to constrain it), and also to distinguish it from more generic incarnations of the MSSM.

For definiteness we will from now on focus on the Spectrum I benchmark point[5]

$$M_1 = M_2 = 1250\,\text{GeV}\ ,\qquad M_3 = 428\,\text{GeV}\ ,\qquad \mu = 150\,\text{GeV}\ ,\qquad \sqrt{B_\mu} = 200\,\text{GeV}\ . \qquad (5.9)$$

With superparticle masses as in Spectrum I, the clearest signatures at the early LHC will be jets with MET. We will see that the cross sections for stop pair production on the one hand and the more familiar $\tilde{q}\tilde{q}$, $\tilde{q}\tilde{q}^*$, $\tilde{q}\tilde{g}$ and $\tilde{g}\tilde{g}$ production (where $\tilde{q}$ stands for any first-generation squark) on the other hand are comparable; all these processes contribute to the signal.

More importantly, once there is evidence for supersymmetry in searches for jets plus MET, our model can also be distinguished experimentally from generic variants of the MSSM which lack its characteristic features of light and near-degenerate higgsinos. This is achieved by focussing on the stop pair production channel. In Spectrum I, stop decays do not involve hard leptons, since possible leptons from χ_2^0 or $\chi_1^\pm$ decays are too soft to be detected. The signature of a $\tilde{t}_1$ is therefore always a hard b-jet plus MET; a typical stop pair event is shown in Figure 5.2. By contrast, in generic supersymmetric models one usually expects also events with jets, MET and isolated leptons, be it from cascade decays of squarks and gluinos or from

---

[5]In a sense this was a maximally optimistic set of parameters, chosen such that it was still marginally allowed by former search limits.
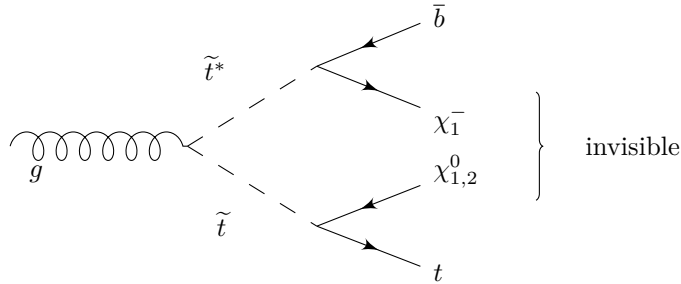
Figure 5.2: An example for a stop pair production event, showing up as to two high-energetic b-jets and missing energy.

$\tilde{t}$ decaying into charginos or non-LSP neutralinos. Once a signal is found in the jets + MET channel, we could use the absence of signals with leptons to severely constrain interpretations in terms of generic supersymmetry, thus providing further indirect evidence for our scenario.

We may even be able to discriminate between our model and a "simplified model" comprising only a $\tilde{t}_1$ and a bino-like χ_1^0 . In such a framework, likewise, no events with hard isolated leptons are expected. However, because the only possible $\tilde{t}_1$ decay is then $\tilde{t}_1 \rightarrow t\chi_1^0$ with the t decaying further into bW, the b-jet spectrum turns out to be significantly different from that of our model, where about half of the stops decay directly into a b quark without an intermediate top.

In the following Sections we present the results of three simulated searches. The first is for jets and large MET, in order to show that early LHC will be able to find evidence for our model. The second also includes leptons, to show that early LHC will, furthermore, be able to distinguish our model from a comparable CMSSM-like model. More precisely, our model will be compared both with the CMSSM point HH50, which has similar $\tilde{g}$ and $\tilde{q}$ production cross sections, and with the CMSSM-like point HH50', which in addition has also a comparable $\tilde{t}_1$ pair production cross section. Finally, we present a search with the cuts optimized to select events from $\tilde{t}_1$ pair production, and compare the result with the simplified model mentioned above.

5.2.3   Simulation of signal and background

The signal production cross sections and generated luminosities are listed in Table 5.3. The corresponding figures for SM backgrounds are listed in Table 5.4. It turns out that $t\bar{t}$ is the most important background. Since, consequently, the best statistics is needed for this channel, we have simulated about three times more events than expected. For the remaining backgrounds, the number of simulated events roughly matches the number of expected events, or exceeds it in the case of tri-bosons (where the cross sections are small) in order to avoid large Monte Carlo errors. An exception are background events with vector bosons plus jets, where we have only simulated a small fraction of the expected events. However, as will become clear when we present the cut flows, this background is very efficiently removed by our cuts. Therefore, it can be safely neglected without having to simulate the full sample.

model	partial cross sections [fb]						$\sigma(\text{tot})$[fb]	$\mathcal{L}_{\text{gen}}$ [fb^{-1}]
	$\sigma(\tilde{q}\tilde{q}^*)$	$\sigma(\tilde{q}\tilde{q})$	$\sigma(\tilde{t}\tilde{t}^*)$	$\sigma(\tilde{b}\tilde{b}^*)$	$\sigma(\tilde{g}\tilde{g})$	$\sigma(\tilde{g}\tilde{q})$		
Spectrum I	0.388	3.83	5.61	0.6	2.9	8.45	21.78	2000
HH50	1.79	12	0.682	0.044	1	9.3	24.8	403
HH50'	1.65	11.5	5.96	0.136	0.979	8.9	29	345

Table 5.3: Production cross sections of different models in fb calculated with `PROSPINO`. The cross section for $\tilde{b}\tilde{b}^*$-production is given at the lowest order, all other cross sections are calculated at NLO.

5.2.4 Event selection and analysis

Discovery with all-hadronic search

The first analysis serves to show that LHC will be able to find evidence for our model, *i.e.* to distinguish its signatures from the SM background.

In the first stage, candidate events with multiple high-energetic jets and MET are selected with the following pre-selection cuts at the level of the detector simulation:

- $1 < N(j) < 5$, where $p_T(j) > 100\,\text{GeV}$,

- $\not{E}_T > 50\,\text{GeV}$.

Furthermore, all events with an isolated lepton (electron or muon) with $p_T > 10\,\text{GeV}$ are rejected in order to suppress events with genuine missing energy from neutrinos:

- $N(l) = 0$.

After imposing these pre-selection cuts, we use a set of cuts optimized for discriminating between signal and background. Events are required to satisfy

- $HT' > 500\,\text{GeV}$,

where HT' is the sum of the PTs of the two most energetic jets,

$$HT' = \sum_{i=1}^{2} p_T(j_i) \, . \tag{5.10}$$

Following the experimental analyses, we use the α_T variable [115–117] as the main discriminator against quantum chromo dynamics (QCD) multi-jet production, defined for di-jet events as:

$$\alpha_T = \frac{E_T(j_2)}{M_T} = \frac{E_T(j_2)}{\sqrt{\left(\sum_{i=1}^{2} E_T(j_i)\right)^2 - \left(\sum_{i=1}^{2} p_x(j_i)\right)^2 - \left(\sum_{i=1}^{2} p_y(j_i)\right)^2}} \, , \tag{5.11}$$

where j_2 denotes the next-to-leading jet. In our analysis we use PT of the jets provided by `DELPHES` instead of E_T, and require the event to have

- $\alpha_T > 0.55$

sample	σ [pb]	$\mathcal{L}_{\mathrm{gen}}$ [fb^{-1}]
$t\bar{t}$	163	69.3
single top	85.1	20
$W + \mathrm{jet}$	826	0.06
W^+W^-	44.974	22.2
W^+Z	11.580	22.3
W^-Z	6.342	
ZZ	6.195	24.2
$W^+W^-W^+$	4×10^{-2}	375
W^+W^-Z	3×10^{-2}	500
W^+ZZ	9×10^{-3}	1670
ZZZ	3×10^{-3}	1876

Table 5.4: Cross sections and generated luminosity of SM background used in the present analysis. The single top production cross section includes all LHC production channels. The cross sections for the tri-boson events are calculated at the Born level with `MADGRAPH`, all other cross sections are taken from [112–114]

in order to pass the cut. In events with jet multiplicity $N(j) > 2$, two pseudo jets are formed following the CMS strategy [117] and the α_T variable is constructed from the pseudojets. Finally, in order to further suppress the $t\bar{t}$ background, we demand a very high value of MET:

- $\not{E}_T > 400\,\mathrm{GeV}$.

Because of the high MET cut in combination with the selection based on α_T, we can safely neglect QCD di- and multi-jet background contributions. The resulting cut flow is shown in Table 5.5.

Evidently, with this analysis it will be possible to discriminate between our model and the SM background. The same is true for the HH50 and HH50' models.

Model discrimination: CMSSM-like models

The more interesting question is that of model discrimination. For this a fully hadronic search such as the one we just presented is not suitable, even though the number of events passing the above cuts is significantly different between our model and HH50 / HH50'. This difference could, after all, be accounted for by slightly different squark and gluino production cross sections — for instance, the HH50 and HH50' spectra would just need to be slightly heavier in order to reproduce the 42 events after cuts which we found for our model.

In fact, some information can be gained already by requesting, in addition to the cuts presented above, that at least one jet should be b-tagged. We assume a PT-independent b-tagging efficiency of $40\,\%$, and a mistagging probability of $10\,\%$ as implemented in `DELPHES`. The additional cut is then

			pre-cuts				
		$N(j)$	$\not{E}_T$	$N(l)$	HT'	α_T	$\not{E}_T$
Spectrum I	$\tilde{q}\tilde{q}^*$	0.307	0.299	0.226	0.216	0.0463	0.042
	$\tilde{q}\tilde{q}$	3.21	3.16	2.39	2.29	0.46	0.381
	$\tilde{t}\tilde{t}^*$	4.45	4.36	3.85	2.56	0.537	0.432
	$\tilde{b}\tilde{b}^*$	0.497	0.491	0.433	0.346	0.081	0.069
	$\tilde{g}\tilde{g}$	2.34	2.31	1.79	1.63	0.405	0.316
	$\tilde{g}\tilde{q}$	6.71	6.63	5.12	4.83	1.04	0.843
sum							**2.08**
HH50		22.1	21.9	17.7	17.1	4.68	**4.39**
HH50'		25.5	25.2	19.9	18.1	4.59	**4.25**
SM	$t\bar{t}$	46200	13400	7360	865	4.5	0.923
	t	8020	1190	755	103	0.3	0.1
	$W + \text{jet}$	1980	82.6	33	0	0	0
	di-bosons	1640	170	102	18	0.178	0.134
	tri-bosons	14.7	4.47	2.78	0.761	0.0146	0.00162
sum							**1.21**

Table 5.5: Cut flow of general all-hadronic analysis for different signals and backgrounds at $\sqrt{s} = 7\,\text{TeV}$ in fb. Figures are given for all events that were simulated. The cut flow for the Spectrum I is shown separately for each different production channel.

- $N(b\text{-jets}) \geq 1$.

The cut flow is shown in Table 5.6. Note that the number of events from both HH50 and HH50' is dramatically reduced. This is partly because, in our model, a sizeable fraction of events was due to $\tilde{t}$ pair production, and the gluino can only decay into $\tilde{t}_1$ or $\tilde{b}_1$. By contrast, in HH50 and HH50' most events involve $\tilde{q}$ decays which do not necessarily lead to b-jets. Moreover, by vetoing events with isolated leptons, fewer $\tilde{t}_1$ events in our model are cut away than in HH50 and HH50' — these models tend to produce more leptonic events, which we will now put to use in a separate semi-leptonic analysis.

More precisely, as explained in Section 5.2.2, $\tilde{t}_1$ decays in our model can give hard isolated leptons at most from secondary top decays (which is, incidentally, also true for $\tilde{b}_1$ and even $\tilde{g}$ decays, since the gluino can only decay into $\tilde{t}_1$ or $\tilde{b}_1$). In HH50 and HH50' many more leptons are expected, jets with MET and isolated leptons being one of the hallmark signatures for generic supersymmetry. This motivates a semi-leptonic search for better model discrimination.

An event is selected for further analysis if it contains exactly one lepton (muon or electron) candidate

		After pre-cuts	b-tag	HT'	α_T	$\not{E}_T$
Spectrum I	$\tilde{q}\tilde{q}^*$	0.226	0.042	0.0415	0	0
	$\tilde{q}\tilde{q}$	2.39	0.577	0.563	0.113	0.0915
	$\tilde{t}\tilde{t}^*$	3.85	1.93	1.63	0.417	0.281
	$\tilde{b}\tilde{b}^*$	0.433	0.225	0.203	0.056	0.0435
	$\tilde{g}\tilde{g}$	1.79	0.922	0.897	0.233	0.176
	$\tilde{g}\tilde{q}$	5.12	1.97	1.93	0.423	0.326
	sum					**0.918**
HH50		17.7	1.56	1.54	0.308	0.268
HH50'		19.9	2.70	2.44	0.458	0.360
SM	$t\bar{t}$	7360	2880	701	5.64	0.361
	t	755	240	32.8	0.15	0.10
	sum					**0.461**

Table 5.6: Cut flow of the hadronic analysis with b-tagging for different signals and the relevant backgrounds at $\sqrt{s} = 7\,\text{TeV}$. The remaining signal and background events, scaled to an integrated luminosity of $20\,\text{fb}^{-1}$, are printed in bold. The cut flow for Spectrum I is shown separately for each different production channel.

- $N(l) = 1$, $\quad p_T(l) > 15\,\text{GeV}$.

Other than that, our pre-selection cuts are as before,

- $N(j) > 1$, $\quad p_T(j) > 100\,\text{GeV}$,

- $\not{E}_T > 50\,\text{GeV}$.

The actual cuts are now as follows. We select events with exactly two high-energetic jets,

- $N(j) = 2$.

This criterion selects preferably the $\tilde{t}\tilde{t}^*$ production channel, since usually more than two jets are expected to appear in channels involving $\tilde{q}$ or $\tilde{g}$. Furthermore, we employ the transverse mass variable

$$m_T = \sqrt{2p_T(l)\not{E}_T \left(1 - \cos\Delta\phi(l, \not{E}_T)\right)} \ , \qquad (5.12)$$

where $\Delta\phi(l, \not{E}_T)$ is the angle between MET and the momentum of the lepton in the transverse plane. This variable is bounded by the W-boson mass if the lepton and MET originate in W-boson decay. We select events with

- $m_T > 100\,\text{GeV}$,

		pre-cuts						
		$N(l)$	$N(j)$	$\not{E}_T$	$N(j)$	m_T	Iso	HT'	$\not{E}_T$
Spectrum I	$\tilde{q}\tilde{q}^*$	0.128	0.126	0.123	0.0140	0.00916	0.00323	0.00323	0.000539
	$\tilde{q}\tilde{q}$	1.35	1.33	1.31	0.19	0.136	0.065	0.0615	0.037
	$\tilde{t}\tilde{t}^*$	2.03	1.6	1.57	1.10	0.851	0.115	0.045	0.02
	$\tilde{b}\tilde{b}^*$	0.225	0.184	0.184	0.122	0.09	0.0125	0.008	0.004
	$\tilde{g}\tilde{g}$	1.11	1.1	1.09	0.129	0.104	0.0265	0.023	0.0145
	$\tilde{g}\tilde{q}$	3.20	3.17	3.13	0.345	0.268	0.085	0.071	0.038
sum									**0.114**
HH50		6.03	5.83	5.78	1.53	1.09	0.600	0.558	**0.365**
HH50'		7.83	7.31	7.24	2.31	1.67	0.893	0.713	**0.426**
SM	$t\bar{t}$	57700	14400	6350	5050	657	432	18.3	**0.0433**

Table 5.7: Cut flow of semi-leptonic analysis for different signals and relevant background at $\sqrt{s} = 7\,\text{TeV}$. All cross sections are in fb. The cut flow for Spectrum I is shown separately for each different production channel.

and ensure that the leptons in these events are isolated. Furthermore, as in the previous analysis we demand that the two jets have high PT and high MET,

- $HT' > 500\,\text{GeV}$,

- $\not{E}_T > 400\,\text{GeV}$.

The resulting cut flow is displayed in Table 5.7. As advertised, the number of leptonic events to survive the cuts is not significantly above the SM background, whereas a significant number of events survive in HH50 and HH50' (*cf.* Figure 5.3). This set of cuts therefore serves to discriminate between our model and CMSSM-like models.

Model discrimination: a simplified model

The analysis of the previous section relies on the presence of intermediate states (in the case of HH50 and HH50', the wino-like $\chi_1^\pm$ and χ_2^0) whose decay into the LSP produces isolated leptons. In models with non-unified gaugino masses, the LSP could still be bino-like while all remaining charginos and neutralinos are much heavier. Can we still distinguish our model from a generic model with a comparably heavy $\tilde{t}_1$ and only a light bino LSP below it? It turns out that this is rather more difficult, but still possible.

The simplified model in Table 5.1 has been designed to reproduce the relevant collider signals. We use the production cross section of stop pairs taken from Spectrum I. The only active states are a moderately heavy $\tilde{t}_1$ and a light bino-like χ_1^0. Stops that are produced in pairs will decay as $\tilde{t}_1 \rightarrow t\chi_1^0$, with the t further decaying into bW. The signature is therefore
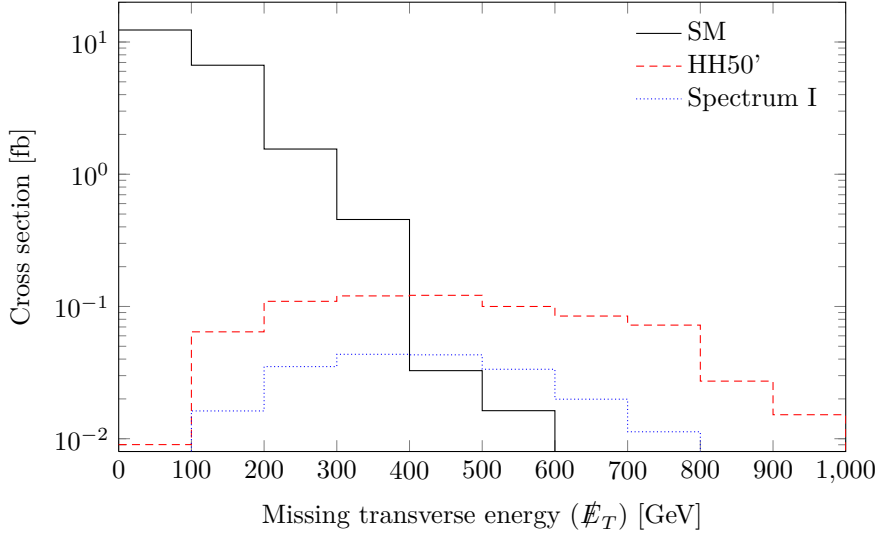
Figure 5.3: MET distribution in the semi-leptonic analysis before the final MET cut. SM events are black, events in Spectrum I are blue and events in HH50' are red.

b-jets and missing energy. A similar decay chain is also open in our model (as in the lower branch in Figure 5.2). However, in our model about $50\,\%$ of the stops will decay directly into b quarks and missing energy (as in the upper branch). These latter events will produce slightly harder b-jets than those involving an intermediate top.

To select the stop pair production channel in our model, we impose a series of simple cuts. At the pre-selection cut level, we select event with at least two and at most four high-energetic jets with PT larger than $100\,\mathrm{GeV}$, similar to the all-hadronic analysis:

- $1 < N(j) < 5$, where $\quad p_T(j) > 100\,\mathrm{GeV}$,

- $\not{E}_T > 50\,\mathrm{GeV}$.

Heavy squarks and gluinos will decay via long decay chains, typically giving rise to a large number of high-energetic jets. Therefore, we select events with exactly two high-energetic jets in order to single out stop pair production. Furthermore, we demand that at least one of these jets is a b-jet:

- $N(j) = 2$, where $\quad p_T(j) > 100\,\mathrm{GeV}$,

- $N(b\text{-jets}) \geq 1$.

The invariant mass of the 2-jet system originating in such decays is sensitive to the masses of the parent particles. We select events with relatively small 2-jet transverse mass:

- $m_{jj}^T \equiv \sqrt{2p_T(j_1)p_T(j_2)\left(1 - \cos\Delta\phi(j_1, j_2)\right)} < 500\,\mathrm{GeV}$

In order to suppress the SM background we employ following cuts:

- $HT' > 400\,\mathrm{GeV}$,

- $\Delta\phi\left(\not{E}_T, j_2\right) > 1$,

- $\not{E}_T > 400\,\mathrm{GeV}$,

		pre-cuts								
		$N(j)$	$\not{E}_T$	$N(j)$	b-tag	m^T_{jj}	HT'	$\Delta\phi$	$\not{E}_T$	$N(l)$
Spectrum I	$\tilde{q}\tilde{q}^*$	0.307	0.299	0.0383	0.00647	0.00162	0.00162	0.00108	0.00108	0.00108
	$\tilde{q}\tilde{q}$	3.21	3.16	0.489	0.0895	0.0275	0.0265	0.024	0.0165	0.012
	$\tilde{t}\tilde{t}^*$	4.45	4.36	3.05	1.58	0.964	0.689	0.619	0.319	0.288
	$\tilde{b}\tilde{b}^*$	0.497	0.492	0.326	0.166	0.076	0.0625	0.058	0.036	0.0315
	$\tilde{g}\tilde{g}$	2.34	2.31	0.329	0.174	0.072	0.0575	0.052	0.039	0.029
	$\tilde{g}\tilde{q}$	6.71	6.63	0.903	0.342	0.122	0.101	0.089	0.0605	0.0385
sum										**0.4**
simplified		4.34	4.24	2.83	1.12	0.711	0.415	0.354	0.168	0.129
SM	$t\bar{t}$	48900	16300	12060	4730	4370	555	141	0.554	0.261
	t	8020	1190	1060	343	317	45.4	8.81	0.30	0.15
sum										**0.41**

Table 5.8: Cut flow of the analysis in which we examine the possibility to distinguish $\tilde{t}$ decays via bino-like neutralinos from decays via higgsino-like neutralinos at $\sqrt{s} = 7\,\text{TeV}$. All cross sections are given in fb.

- $N(l) = 0$.

MET in QCD di- and multi-jet events can only appear due to the mismeasurement of one of the jets. We assume that, in events with very large MET and exactly two high-energetic jets, the mismeasured jet is the next-to-leading one. We therefore expect that no QCD event will survive the cuts on $\Delta\phi\left(\not{E}_T, j_2\right)$ and MET. The resulting cut flow is displayed in Table 5.8.

Evidently, these cuts can discriminate between Spectrum I and the simplified model. Of course the latter is not a realistic scenario, and in a fully-fledged model cascade decays of heavier states may also be relevant. However, since the cuts single out the stop pair production channel in our model quite efficiently, it seems reasonable to expect that this remains true for a generic full model which the simplified model is taken to represent here. The cuts are even tight enough to remove almost all of the stop decay events in the simplified model, while leaving a substantial excess above the SM background in our model (presumably coming from direct $\tilde{t}_1 \to b\chi_1^\pm$ decays). Note, however, that this analysis will be rather challenging with real data: Only few events survive, and the discrimination is not mainly due to a single cut, but rather to the combined effects of all of them.

5.3   R-parity violation leading to displaced muon vertices

There are two multipurpose experiments at the LHC, the ATLAS and CMS detectors. Each detector consists of several subdetectors, from the inner detector, for track reconstruction

and primary and secondary vertex reconstruction, to the calorimeters and outermost the muon system. Since the models under study here give rise to rather large displacements, we will choose to rely on the identification of muon objects in our search strategy. ATLAS has larger dimensions than CMS, with its muon system stretching out to a radius of about 20 m [118]. In our analysis, we choose to use requirements on the radial and beam-line coordinates corresponding to the CMS detector geometry, which will then be the somewhat more conservative choice. We do not expect our results to depend much on which of the two detectors is considered. The different detector layers of the CMS detector are [119]:

- The inner detector or tracker, which stretches out to a radius of $r \sim 110\,\mathrm{cm}$ transverse to the beam. Its innermost part, the pixel detector, covers $r \leq 11\,\mathrm{cm}$.

- The electromagnetic calorimeter which measures electron and photon energies and stretches to $r \lesssim 2\,\mathrm{m}$.

- The hadronic calorimeter, for measuring strongly interacting particles and identification of jets, which stretches out to $r \lesssim 3\,\mathrm{m}$.

- The magnet, stretching out to $r \sim 4\,\mathrm{m}$.

- The system of muon detectors or muon chambers, for identification of muons and measurement of their momentum, out to radius of $r \sim 7.4\,\mathrm{m}$.

In our analyses we are using the detector simulation `DELPHES`, tuned to the CMS detector, in order to account for effects of event reconstruction at the detector level. However, `DELPHES` describes the detector geometry solely in terms of angular variables, *i.e.* the detector is stretched infinitely in the radial direction. This approximation is sufficient for most studies involving prompt decays but is untenable in the case of late decaying particles. We overcome this obstacle by adding vertex information from particles at the generator level to objects at the detector level. Usually, this information is provided by the detector simulation. Our procedure is described in detail in the following section. We emphasize that a full detector simulation, which includes vertex reconstruction, needs to be done to improve our analyses.

5.3.1   Muon reconstruction process

Particles produced in the late decay of the neutralino will not be properly reconstructed in a real detector if the position of their vertex is beyond or even within the crucial detector component responsible for the respective identification. For example, an electron produced inside of the electromagnetic calorimeter will leave no track in the tracker and will therefore be identified as a photon or jet. In order to simulate the detector response to such events we use a detector geometry in the (r, z) coordinates, which is inspired by the CMS detector at the LHC (see Figure 5.4). The angular position of the detector components is given by the CMS tune of `DELPHES`.

In order to be as conservative as possible we only use muon and track objects for the present analysis, since these objects allow a simple simulation of detection efficiency losses due to the finite size of the detector. Namely, we assume that a muon can be reconstructed as long as its vertex is in front of the muon chambers, and analogously a track can be reconstructed if it originates approximately in the first third of the tracker (This region is called pixel detector in Figure 5.4). For the matching between generator level particles and objects
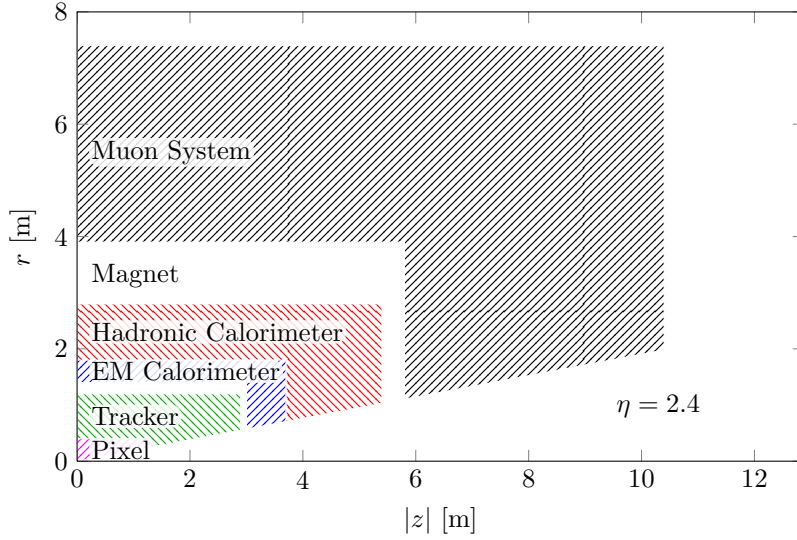
Figure 5.4: Layout of one quarter of the generic detector used for particle identification.

reconstructed by `DELPHES` we use the distance in pseudorapidity η and azimuthal angle ϕ, defined as $\Delta R = \sqrt{(\Delta\phi)^2 + (\Delta\eta)^2}$.

In the following we will call generator level muons, produced by `PYTHIA`, *GenMuons*, muons reconstructed initially by `DELPHES` *muon candidates*, and track objects reconstructed by `DELPHES` *RecoTracks*. Only GenMuons and RecoTracks have the coordinates of their vertex.

First, we perform the following PT cuts on muon candidates and RecoTracks:

- $p_T(\mu) > 20\,\text{GeV}$,

- $p_T(\text{Track}) > 15\,\text{GeV}$.

These cuts are guided by our SUSY search strategies, since we expect that muons coming from boson decays have high PT, and a sufficiently high PT cut can effectively suppress QCD fake leptons. Furthermore, `DELPHES` itself reconstructs only muons with PT above $10\,\text{GeV}$. Additionally, these cuts were optimized in order to get a realistic muon reconstruction efficiency (see Section 5.3.2).

In the second step vertex information is added to the muon candidates by matching with GenMuons:

- A GenMuon is selected for matching with muon candidates if its vertex lies in front of the muon system : $r_{(\mu)} = \sqrt{x^2 + y^2} < 4000\,\text{mm}$, $|z_{(\mu)}| < 6000\,\text{mm}$ (see Figure 5.4).

- The ΔR distance between each selected GenMuon and all muon candidates is computed.

- A GenMuon vertex is added to the muon candidate closest in ΔR, if $\Delta R < 0.1$ and GenMuon and muon candidate have the same charge.

- Muon candidates with added vertex information are called *RecoMuons*.

In the final step, muons with or without signal in the tracker are distinguished:
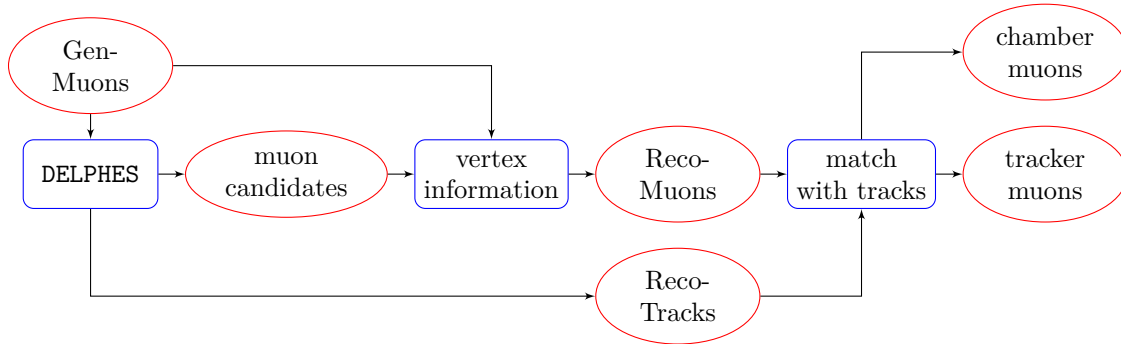
Figure 5.5: Muon reconstruction process.

- A RecoTrack is selected for matching with RecoMuons if the track vertex lies in the following range: $r_T < 400\,\text{mm}$, $|z_T| < 1300\,\text{mm}$.

- Each selected RecoTrack is matched with the RecoMuon closest in ΔR, if $\Delta R < 0.1$.

- Matched RecoTracks and RecoMuons are called *tracker muons*. RecoMuons which cannot be matched with RecoTracks are called *chamber muons*. Each RecoMuon is therefore either a tracker muon or a chamber muon.

After the reconstruction procedure one is left with two kinds of muon objects: (i) chamber muons which have no track in the tracker and are therefore reconstructed solely by the muon chambers, and (ii) tracker muons which have a track. The muon reconstruction process is depicted in Figure 5.5. The ΔR matching condition has been optimized in order to get a realistic muon reconstruction efficiency (see next section).

5.3.2   Muon reconstruction efficiency

In order to test our method of obtaining physically sensible objects we compute the muon reconstruction efficiency in the following way:

- Muons are created as described above.

- GenMuons are matched with RecoMuons without any constraints on the position of the GenMuon vertex.

- The number of successfully matched objects is compared bin-wise (in bins of r and $|z|$) with the number of all GenMuons.

The second condition is necessary in order to see whether the assignment between RecoMuons and GenMuons is correct. Since the matching procedure only relies on angular variables, it is possible that a RecoMuon originally matched with a GenMuon created in front of the muon chamber belongs in fact (*i.e.* has smaller angular distance) to a GenMuon coming from a decay inside the muon chamber or even outside of the detector. Such wrong matchings would be seen in the efficiency plot as efficiencies not equal to zero in regions where muons could not be detected by the detector defined above ($r_{(\mu)} > 4000\,\text{mm}$, $\left|z_{(\mu)}\right| > 6000\,\text{mm}$).

Figure 5.6 shows the computed muon efficiency in bins of r and $|z|$. As expected one sees a sharp decline in efficiency in the r plot at $r_{(\mu)} = 4000\,\text{mm}$, where the hard cut applies. The
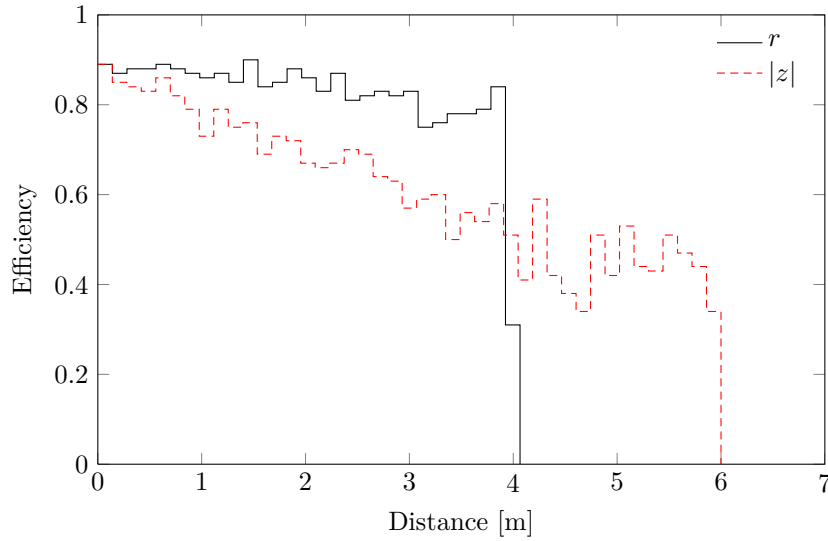
Figure 5.6: Muon reconstruction efficiency for the benchmark point HH27 in radial (r) and axial ($|z|$) directions.

decline in the z plot is gradually, since physical particles have to fulfil both r and $|z|$ criteria. The particles originating at small values of r and large values of $|z|$ are not reconstructed due to the limited pseudorapidity coverage of the muon detector. The efficiency stays at zero beyond $r = 4000\,\text{mm}$ and $|z| = 6000\,\text{mm}$ as expected, confirming our method of muon reconstruction. We expect that the computed muon efficiency agrees within $15\,\%$ with efficiencies of present LHC detectors including losses due to muon-jet separation requirements.

5.4 Strong production using the example of binos

In this section we present a search strategy for strongly produced bino-like neutralinos at the LHC. We show that for small values of the R-parity breaking parameter ζ usual SUSY searches are insufficient to find the signal. However, RPV leads to new signals including striking secondary vertices at large distances from the primary interaction point.

5.4.1 Decay signatures

Consider for simplicity, the following cascade process:

$$qg \to \widetilde{q}\widetilde{g} \to jjj\chi_1^0\chi_1^0 \,, \tag{5.13}$$

where $\widetilde{q}$ is a squark, $\widetilde{g}$ is a gluino, and j denotes a jet. The final state neutralinos decay in a secondary vertex into W bosons and leptons as well as into Z bosons and neutrinos. Figure 5.7 shows an example of a decay cascade with muons in final state. The distance between the collision point and the secondary vertex depends on the decay width of the neutralino (3.107) and hence on the R-parity breaking parameter ζ.

Table 5.9 summarizes the LHC signatures of the process (5.13) for sufficiently large values of ζ such that it is probable that both neutralinos decay inside of the tracker volume. All signatures contain at least three jets from the antecedent supersymmetric decays. In general

category	χ_1^0 decays	LHC signature
leptonic	$W^+W^-l\bar{l} \to \bar{l}ll\bar{l}\nu\nu$	
	$W^+W^+ll \to \bar{l}\bar{l}ll\nu\nu$	
	$W^-W^-\bar{l}\bar{l} \to ll\bar{l}\bar{l}\nu\nu$	
	$ZW^-\bar{l}\nu \to l\bar{l}l\bar{l}\nu\nu$	$3j + 2l + 2\bar{l} + \not{E}_T$
	$ZW^+l\nu \to l\bar{l}\bar{l}l\nu\nu$	
	$ZZ\nu\nu \to l\bar{l}l\bar{l}\nu\nu$	
(opposite sign, $\not{E}_T$ from Z)	$ZW^+l\nu \to \nu\nu\bar{l}l\nu\nu$	
	$ZW^-\bar{l}\nu \to \nu\nu l\bar{l}\nu\nu$	$3j + 1l + 1\bar{l} + \not{E}_T$
	$ZZ\nu\nu \to \nu\nu l\bar{l}\nu\nu$	
semi-leptonic	$W^+W^-l\bar{l} \to jjl l\bar{l}\nu$	
	$W^+W^+ll \to jj\bar{l}ll\nu$	$5j + 2l + 1\bar{l} + \not{E}_T$
	$ZW^+l\nu \to l\bar{l}jjl\nu$	
	$W^+W^-l\bar{l} \to jj\bar{l}l\bar{l}\nu$	
	$W^-W^-\bar{l}\bar{l} \to jjl\bar{l}\bar{l}\nu$	$5j + 1l + 2\bar{l} + \not{E}_T$
	$ZW^-\bar{l}\nu \to l\bar{l}jj\bar{l}\nu$	
	$ZW^+l\nu \to jj\bar{l}l\nu\nu$	
	$ZW^-\bar{l}\nu \to jjl\bar{l}\nu\nu$	$5j + 1l + 1\bar{l} + \not{E}_T$
	$ZZ\nu\nu \to jjl\bar{l}\nu\nu$	
	$W^+W^-l\bar{l} \to jjjjl\bar{l}$	$7j + 1l + 1\bar{l}$
(same sign, no $\not{E}_T$)	$W^+W^+ll \to jjjjll$	$7j + 2l$
	$W^-W^-\bar{l}\bar{l} \to jjjj\bar{l}\bar{l}$	$7j + 2\bar{l}$
single lepton	$ZW^+l\nu \to jjjjl\nu$	$7j + 1l + \not{E}_T$
($\not{E}_T$ from Z)	$ZW^-\bar{l}\nu \to jjjj\bar{l}\nu$	$7j + 1\bar{l} + \not{E}_T$
	$ZW^+l\nu \to \nu\nu jjl\nu$	$5j + 1l + \not{E}_T$
	$ZW^-\bar{l}\nu \to \nu\nu jj\bar{l}\nu$	$5j + 1\bar{l} + \not{E}_T$
all-hadronic	$ZZ\nu\nu \to jjjj\nu\nu$	$7j + \not{E}_T$
($\not{E}_T$ from Z)	$ZZ\nu\nu \to \nu\nu jj\nu\nu$	$5j + \not{E}_T$
invisible ($\not{E}_T$ from 2 Z)	$ZZ\nu\nu \to \nu\nu\nu\nu\nu\nu$	$3j + \not{E}_T$

Table 5.9: Possible final states assuming process (5.13) if both neutralinos decay inside the tracking volume. In general more complicated signatures can arise.
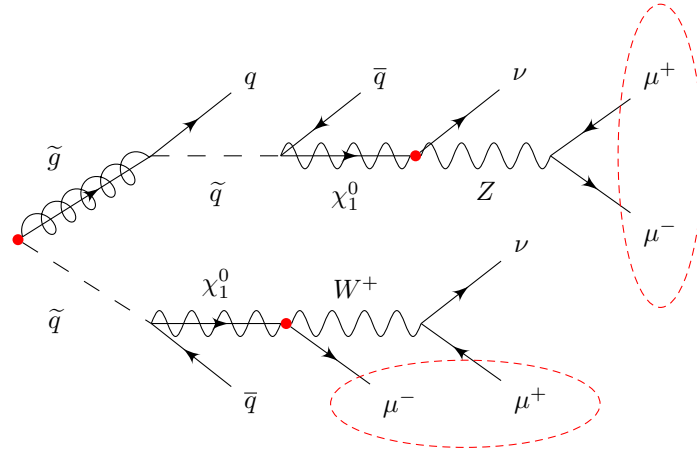
Figure 5.7: Typical strongly produced RPV decay chain at the LHC. The primary and secondary vertices as well as displaced muons are highlighted.

more complicated signatures can arise. Intermediate chargino decays can lead to additional gauge bosons in the final state, which then produce more jets or leptons. These decay chains as well as all production processes were taken into account in the simulation of the signal.

The signatures are classified according to the final states in the neutralino decays: leptonic signatures involving only leptons in the final state, semi-leptonic signatures involving at least two charged leptons and jets, single lepton signatures containing only one lepton, all-hadronic signatures where only jets accompanied by neutrinos are present, and finally invisible channels where both neutralinos decay solely to neutrinos. Additionally we single out channels having a considerable amount of MET from Z boson decays, since MET is one of the main features searched for in usual searches for new physics. Furthermore the channels labelled as *opposite sign* could be found in usual SUSY searches as they include a considerable amount of MET, many jets and one isolated lepton pair with different signs. However, some searches remove events with muon pairs having invariant mass around the Z pole in order to dispose of Drell-Yan $Z/\gamma^* \to l\bar{l}$ processes. Note that in the model presented in this work this cut would lead to a suppression of the signal. Other leptonic and semi-leptonic channels also contain opposite-sign lepton pairs but only small amount of MET and therefore they are not considered in the usual searches, (*cf.* References [120, 121]). Neutralino decays lead also to signatures containing same-sign lepton pairs but since no MET is present in these channels they are usually discarded in order to suppress various backgrounds [122].

If the value of ζ is rather small one of the neutralinos will decay outside of the detector leading to signatures with large amount of MET as shown in Table 5.10. The leptonic decays of one of the neutralinos inside the detector lead to a perfect opposite-sign signature. As mentioned above this signature can be hidden if one rejects events where the invariant mass distribution of the lepton pair is in the range of the Z boson mass. Another strategy is the search for single lepton events with large amount of MET.

Thus the applicability and the reach of the usual SUSY searches applied to the model presented in this work depends crucially on the size of R-parity breaking. In order to further evaluate this statement we investigated a number of characteristic variables in supersymmetric

category	χ_1^0 decays	LHC signature
leptonic	$W^+ l \to \bar{l} l \nu$	
(opposite sign)	$W^- \bar{l} \to l \bar{l} \nu$	$3j + 1l + 1\bar{l} + \not{E}_T$
	$Z \nu \to l \bar{l} \nu$	
single lepton	$W^+ l \to jjl$	$5j + 1l + \not{E}_T$
	$W^- \bar{l} \to jj\bar{l}$	$5j + 1\bar{l} + \not{E}_T$
all-hadronic	$Z \nu \to jj\nu$	$5j + \not{E}_T$
invisible	$Z \nu \to \nu\nu\nu$	$3j + \not{E}_T$

Table 5.10: Possible final states assuming process (5.13) if one of the neutralinos decays outside the tracking volume. In general more complicated signatures can arise.

events. The events were generated with `PYTHIA` with the CMSSM boundary conditions[6]

$$m_{1/2} = m_0 = 270 \, \text{GeV} \; , \qquad \tan\beta = 10 \; , \qquad a_0 = 0 \; , \qquad \text{sign} \, \mu = +1 \; . \qquad (5.14)$$

R-parity violating neutralino decays were taken into account.

Figure 5.8 shows the distribution of the $\beta\gamma$ factors of the neutralinos. This factor enters the formula for the neutralino decay length and one sees from the plot that analytic results in the literature, which have been computed with $\beta\gamma = 1$, are correct within one order of magnitude. The most important kinematic property connected with the neutralino decay length is the amount of missing transverse momentum ($\not{p}_T$) which is shown in Figure 5.9 for different values of the RPV parameter ζ. The MPT was computed as the sum of the PTs of all neutrinos produced in the detector before the hadronic calorimeter ($r < 1800 \, \text{mm}$, $|z| < 3700 \, \text{mm}$) and the PTs of the neutralinos decaying outside the hadronic calorimeter. The MPT distribution of the R-parity conserving model $\zeta = 0$ cannot be distinguished from the model with $\zeta = 1 \times 10^{-9}$. However, the distribution is significantly different for $\zeta = 3 \times 10^{-8}$ since in this case most events have only very little MPT due to early neutralino decays. This suggests that our model could only hardly be discovered in usual searches relying on MET. A further analysis with full detector simulation is needed in order to properly evaluate the discovery potential of usual SUSY searches.

Another general feature of models with relatively large ζ is the large possible number of leptons in the final state, illustrated in Figure 5.10. The generator level particles selected for this plot had to fulfil the criteria shown in Table 5.11 imposed in order to select leptons from hard processes which could be reconstructed in a realistic detector. The cuts on the vertex position represent a pessimistic estimate of the reconstruction efficiency (see Section 5.3.2).

5.4.2   Search strategies

As mentioned in the previous section one of the striking features of the presented model are events with secondary vertices and possibly many leptons in the final state. The search for

---

[6]By now this parameter point is already ruled out by the LHC experiments.
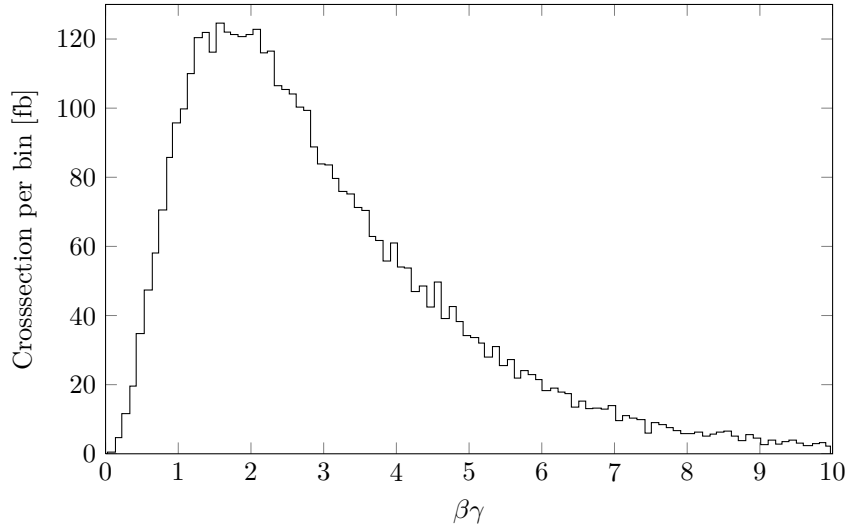
Figure 5.8: $\beta\gamma$ distribution of neutralinos at generator level for benchmark point HH27 (see Table 5.12). The number of neutralinos corresponds to twice the number of the events scaled to $10\,\mathrm{fb}^{-1}$ at $\sqrt{s} = 7\,\mathrm{TeV}$.
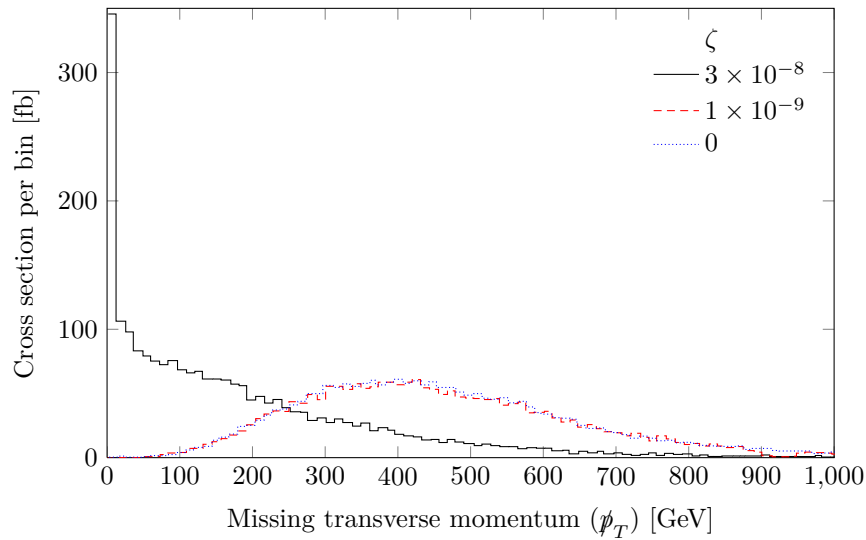

Figure 5.9: MPT distribution at generator level for benchmark point HH27 (see Table 5.12) and different values of the R-parity breaking parameter ζ. Generator level MPT is defined as sum over the PT of i) neutralinos decaying outside of the detector (see Section 5.3.1) and ii) all neutrinos produced inside of the detector. The number of events is scaled to $10\,\mathrm{fb}^{-1}$ at $\sqrt{s} = 7\,\mathrm{TeV}$.

(a) Number of electrons.

(b) Number of muons.
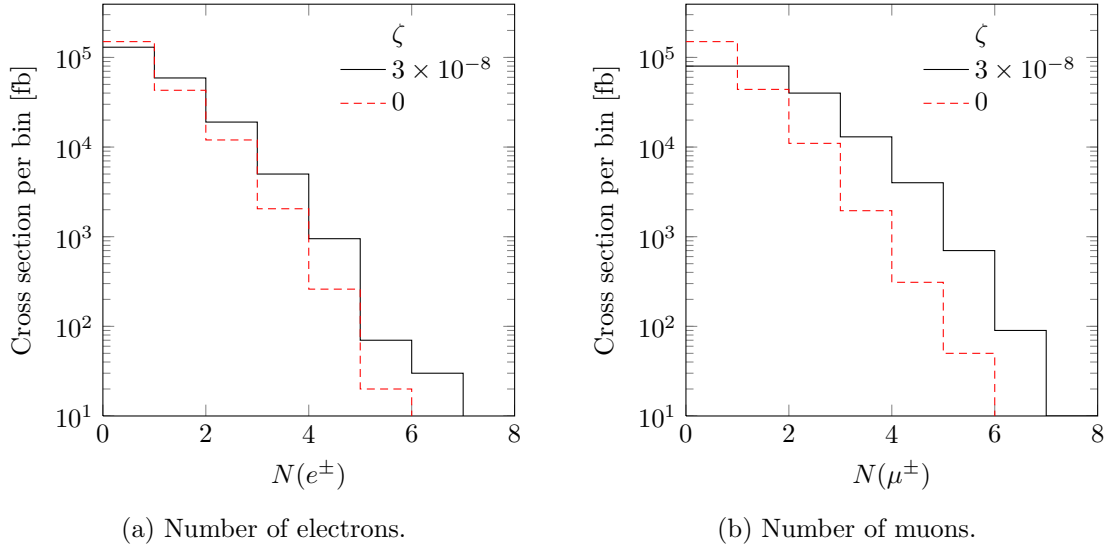
Figure 5.10: The number of generated particles per event for the benchmark point HH27 after selection cuts described in Table 5.11 at $\sqrt{s} = 7\,\text{TeV}$.

a secondary vertex is crucial in order to ensure the R-parity violating nature of the decays. Possible search strategies can be optimized in order to find some of the channels described in Tables 5.9 and 5.10. It is remarkable that many channels allow for the full reconstruction of the neutralino mass: all decay chains including Z bosons or hadronically decaying W bosons. The reconstruction of the neutralino mass from the particles produced in the Z boson decay depends crucially on the full reconstruction of the secondary vertex, which is beyond the scope of this work[7]. This method of neutralino mass reconstruction works also in R-parity conserving models where the neutralino decays into Z boson and gravitino [50].

For example, one promising search strategy working for all ζ values considered in this work is based on *single lepton* events with some number of hard jets and MET larger than $90\,\text{GeV}$. After the preselection one could look for events where the lepton is coming from a secondary vertex and try to reconstruct the W boson mass from a jet pair. In the final step one could try to reconstruct the neutralino mass from the jets selected in the previous step and the lepton. However such study depends crucially on the knowledge of the detector response in the case of late decaying particles. A neutralino can decay in various detector components and lead to unusual signals. Furthermore the mass resolution is limited by the uncertainty in the jet energy scale and by the uncertainty in the determination of the jet momentum direction.

We will focus our study on leptonic final states, which have a particularly clean signature, and reconstruct the Z boson coming from a secondary vertex. We will use only muon and track objects for which we assume to have modelled a realistic detector response (see Section 5.3.2). A possible background for this search are cosmic muons leaving no track in the detector. It is important to note that one would miss the signal in this channel entirely if one imposes a cosmic muon veto which rejects all events with muon pairs having no associated tracks (*cf.* Reference [120]).

---

[7]The four-vector pointing to the secondary vertex and the three-momenta of the leptons or jets from the Z boson provide sufficient information for the reconstruction of the neutralino mass.

particle	transverse momentum (p_T)	pseudorapidity	vertex position	
electron	$p_T > 7\,\text{GeV}$	$|\eta| < 2.5$	$r < 400\,\text{mm}$	$|z| < 1300\,\text{mm}$
muon	$p_T > 6\,\text{GeV}$	$|\eta| < 2.5$	$r < 4000\,\text{mm}$	$|z| < 6000\,\text{mm}$

Table 5.11: Cuts for the generator level particle selection for the study of particle multiplicity.

5.4.3 Simulation of signal and background

In this section we define a set of representative points in the parameter space of our model and describe the generation of the signal and dominant SM background samples. In particular we examine the simulation of detector effects using the generic detector simulation DELPHES on signal and background in the presence of secondary vertices.

Benchmark points

A typical set of boundary conditions for the SUSY breaking parameters of the MSSM at the grand unification scale is given by equal scalar and gaugino masses, $m_0 = m_{1/2}$. These boundary conditions lead to a bino-like neutralino χ_1^0 as NLSP. We choose a representative value of $\tan\beta$ and set the scalar trilinear couplings to zero,

$$a_0 = 0 \,, \qquad\qquad \tan\beta = 10 \,. \qquad\qquad (5.15)$$

Thus the universal gaugino mass remains the only independent SUSY breaking parameter which will be varied in the present study.

EW precision tests lead to lower bounds on the supersymmetric particle spectrum. In the present study the LSP spectrum corresponds to the choice $m_0 = m_{1/2} = 270\,\text{GeV}$ (HH27). At this benchmark point the NLSP is a neutralino with mass $m_{\chi_1^0} = 105.8\,\text{GeV}$.

In order to probe the region of gluino and squark masses accessible at the LHC [123] we increase the gaugino mass parameter in four steps: $m_{1/2} = 350, 500, 650, 800\,\text{GeV}$. Some particle masses at these points are shown in Table 5.12. For the different benchmark points the production cross sections, calculated with PROSPINO 2.1 [124] at $\sqrt{s} = 7\,\text{TeV}$, are given in Table 5.13. For the R-parity breaking parameter ζ we choose the following values:

$$\zeta = 3 \times 10^{-8},\ 2 \times 10^{-8},\ 1 \times 10^{-8},\ 5 \times 10^{-9},\ 1 \times 10^{-9},\ 5 \times 10^{-10},\ 1 \times 10^{-10} \,. \qquad (5.16)$$

Note that for gravitino masses $m_{3/2} = \mathcal{O}(100\,\text{GeV})$ one has $\zeta \lesssim 1 \times 10^{-9}$.

Major backgrounds

Neutralino decays usually have W- and Z bosons in the final state (*cf.* Figure 3.5). In our study we focus on the reconstruction of Z boson decays to muon pairs. Therefore, we only consider SM backgrounds which lead to at least two muons in the final state originating from W or Z bosons:

- $t\bar{t}$ production: W bosons from top quark decays.

- Z production

	GUT masses		particle masses			
	m_0	$m_{1/2}$	$m_{\chi_1^0}$	m_h	$m_{\tilde{g}}$	$m_{\tilde{u}}$
HH27	270	270	105.8	110.5	662.4	653.4
HH35	350	350	140.5	112.5	841.7	831.8
HH50	500	500	205.7	115.1	1170	1160
HH65	650	650	271.5	116.7	1492	1481
HH80	800	800	337.8	117.9	1809	1798

Table 5.12: Definition of the benchmark points together with some particle masses, which are given in GeV.

- Di-boson production (WW, WZ, ZZ)

- Tri-boson production (WWW, WWZ, ZZW, ZZZ)

Table 5.14a gives an overview of the background samples used in our analysis. We have simulated 10 times more signal events for small values of ζ than for large values of ζ in order to improve the statistics. We assume that pure QCD background can be efficiently suppressed in multi-lepton final states with high PT, particularly after imposing lepton isolation criteria (*cf.* References [121, 127]).

5.4.4 Search for the neutralino decays into Z boson and neutrino

As described in Section 5.4.2 this search proposal is focused on the channel $\chi_1^0 \to Z\nu \to \mu^+\mu^-\nu$. This channel possesses certain physical and technical advantages. On the physical side reliable muon identification is possible already in the early stage of the LHC data taking and one can assume that QCD background can hardly fake two muons at the same time. Furthermore this signal leads to spectacular events and has no easily identifiable SM background at all, as shown in this section. Additionally, the muon chamber is the detector component which is farthermost away from the primary vertex and hence one can expect that it will be possible to detect a significant number of clean late time decays even for very small R-parity breaking. On the technical side, muons seem to be the simplest objects for which a realistic detector response can be modelled within DELPHES (see Section 5.3.1), due to the limitations of this simulation in the presence of secondary vertices.

The spectacular feature of this signal are opposite sign muon pairs with invariant mass close to the Z boson mass, which have either associated tracks in the tracker with clearly visible secondary vertices or no associated tracks at all. Such muon pairs cannot be generated by usual SM background as will be shown in the following. However, a similar signal can arise from cosmic muons traversing the detector. We could not create a Monte Carlo background sample for cosmic muons, and we simply assume that such background can be suppressed by use of the full timing information of the event: cosmic muons will first cause a signal in the muon chamber which is closest to the ceiling of the experimental hall followed by a signal in the opposite direction.

	partial cross-sections [fb]				σ(tot) [fb]
	$\sigma(\widetilde{q}\widetilde{g})$	$\sigma(\widetilde{q}\widetilde{q})$	$\sigma(\widetilde{q}\overline{\widetilde{q}})$	$\sigma(\widetilde{g}\widetilde{g})$	
HH27	1090 (739)	682 (570)	256 (174)	208 (83)	2236 (1566)
HH35	172 (105)	149 (126)	38 (25.2)	26 (8.47)	385 (265)
HH50	8.91 (4.36)	11.8 (10.1)	1.7 (1.02)	0.95 (0.206)	23.36 (15.7)
HH65	0.579 (0.216)	1.01 (0.877)	0.0943 (0.0458)	0.0466 (6.37×10^{-3})	1.73 (1.145)
HH80	0.0379 (0.0109)	0.0805 (0.0723)	5.37×10^{-3} (1.98×10^{-3})	2.44×10^{-3} (0.203×10^{-3})	0.126 (0.0854)

Table 5.13: Production cross sections at NLO (LO) at the benchmark points calculated with `PROSPINO`.

Sample	σ [pb]	$\mathcal{L}$ [pb^{-1}]
$t\bar{t}$	163	1230
Z	977	716
W^+W^-	47	1060
ZZ	6.46	7740
W^+Z	11.88	4210
W^-Z	6.69	7480
W^+W^-Z	0.182	82000
W^+ZZ	0.040	375000
$W^+W^-W^+$	0.146	103000
ZZZ	0.015	375000

(a) Samples of SM background. The production cross sections are taken from [112, 113, 125, 126].

	ζ	$\mathcal{L}$ [fb^{-1}]
HH27	$\geq 5 \times 10^{-9}$	9.96
	$\leq 1 \times 10^{-9}$	99.6
HH35	$\geq 5 \times 10^{-9}$	26.0
	$\leq 1 \times 10^{-9}$	259
HH50	$\geq 5 \times 10^{-9}$	428
	$\leq 1 \times 10^{-9}$	4280
HH65	$\geq 5 \times 10^{-10}$	5780
	1×10^{-10}	57800
HH80	all ζ	79400

(b) Samples of signal events for different benchmark points (see Table 5.12) and $\zeta = \alpha \times 10^{-9}$ ($\alpha = 0.1, 0.5, 1, 5, 10, 20, 30$).

Table 5.14: Monte Carlo samples of SM background and signal events used for our analysis.

An intrinsic background for the presented search are muon pairs from R-parity violating decays, where one muon is coming from the W boson decay while the other muon is coming either from the neutralino decay into the W boson in either of the two branches or from the W or Z boson decay in the second branch (*cf.* Figure 5.7). This background can be suppressed if one has access to the corresponding tracks by demanding that both of them originate from the same vertex. In the case of muons without tracks this background is irreducible. However it belongs itself to the signal one is looking for.

5.4.5   Event selection

In order to find the signal we now employ a series of simple cuts on the reconstructed objects (muons, tracker muons, and chamber muons). First, we perform a selection cut on the number of muons in the event:

- $N(\text{muons}) \geq 2$.

We define two event classes depending on the number of tracker muons:

- Class 1: the event contains at least two tracker muons $N(\text{tracker muons}) \geq 2$.

- Class 2: otherwise.

From the description of the signal presented above, we implement additionally two sets of cuts depending on the class of the event. The cuts for Class 1 events are:

- All possible invariant masses of opposite sign tracker muons are computed. The event passes the cut if at least one invariant mass is in the range of the Z boson mass: $80\,\text{GeV} < M_{\mu^+\mu^-} < 100\,\text{GeV}$. If the event contains more than one appropriate combination of the tracker muons then the muons from the combination with invariant mass closest to the Z boson mass are selected for further analysis.

- $d(\text{Vertex}) > 5\,\text{mm}$: Each of the tracks associated with the two selected tracker muons should have a vertex which is further than $5\,\text{mm}$ away from the primary vertex. This value is approximately one order of magnitude larger than the current resolution of the inner tracker (*cf.* References [119, 127]).

- $\Delta d(\text{Vertex})_{ij} < 5\,\text{mm}$: The distance between the two track vertices should be less than $5\,\text{mm}$.

- If the event fails one of the cuts it is classified as a Class 2 event.

The cuts for Class 2 events are:

- $N(\text{chamber muons}) \geq 2$: If an event has less than two tracker muons then it should have at least two chamber muons.

- All possible invariant masses of opposite sign chamber muons are computed. An event passes the cut if at least one invariant mass is in the range of the Z boson mass: $80\,\text{GeV} < M_{\mu^+\mu^-} < 100\,\text{GeV}$.

Cuts		Background				Signal	
		$t\bar{t}$	Z	di-	tri-	ζ	
					boson	3×10^{-8}	10^{-9}
	$N(\text{muons}) \geq 2$	2480	13200	1360	14.2	292	44.8
Class 1	$80\,\text{GeV} < M_{\mu^+\mu^-} < 100\,\text{GeV}$	275	12700	1160	9.91	19.6	9.96
	$d(\text{Vertex}) > 5\,\text{mm}$	7.34	0	0	0	4.92	0.132
	$\Delta d(\text{Vertex})_{ij} < 5\,\text{mm}$	0	0	0	0	3.61	0
Cl. 2	$N(\text{chamber muons}) \geq 2$	0	0	0	0	105	0.183
	$80\,\text{GeV} < M_{\mu^+\mu^-} < 100\,\text{GeV}$	0	0	0	0	13.8	0.0203
	Total	0	0	0	0	17.5	0.0203

Table 5.15: Cut flow for HH27 at $\sqrt{s} = 7\,\text{TeV}$. All cross sections are given in fb.

Since each Class 1 event is classified as a Class 2 event if it fails one of the cuts, no signal event is discarded because of the presence of muons with tracks not coming from neutralino decay.

Most events will fall into the second class. The analysis is then very simple and amounts to the search for events with muons without associated track in which the invariant mass of a muon pair lies in the Z boson mass range. The cut flow is given in Table 5.15. As expected, no background events survived the cuts, since no SM process should produce secondary vertices so far away from the primary interaction point. Although our background estimate has an uncertainty due to the limited statistics, we assume on physical grounds that no background events will pass the cuts if we increase the number of simulated events. However, the major uncertainty in this study, the number of the background events from cosmic muons, cannot be estimated with the present software. Therefore, a full fledged analysis with full detector simulation which takes into account the cosmic muon background is needed. In the following we assume that this background can be efficiently suppressed with the full timing information of the event as described in the introduction to Section 5.4.4. Furthermore, we only estimate the systematic uncertainty due to the background and neglect statistical errors and the uncertainty of the muon reconstruction efficiency.

The significance of the signal is computed with the profile likelihood method [128] incorporated in the SIGCALC code [129]. We assume an integrated luminosity of $1\,\text{fb}^{-1}$ at $\sqrt{s} = 7\,\text{TeV}$ LHC and a ten times higher Monte Carlo luminosity $\mathcal{L}_{\text{MC}} = {}^{N_b}/\sigma_b = 10\,\text{fb}^{-1}$ for all the background events. At this integrated luminosity 17 signal events and no background events survive the cuts, which corresponds to a significance $Z_{PL} = 9.03$. Instead, if one makes the pessimistic estimate that 1 background event from the cosmic muons passes the cuts one finds a significance $Z_{PL} = 6.39$.
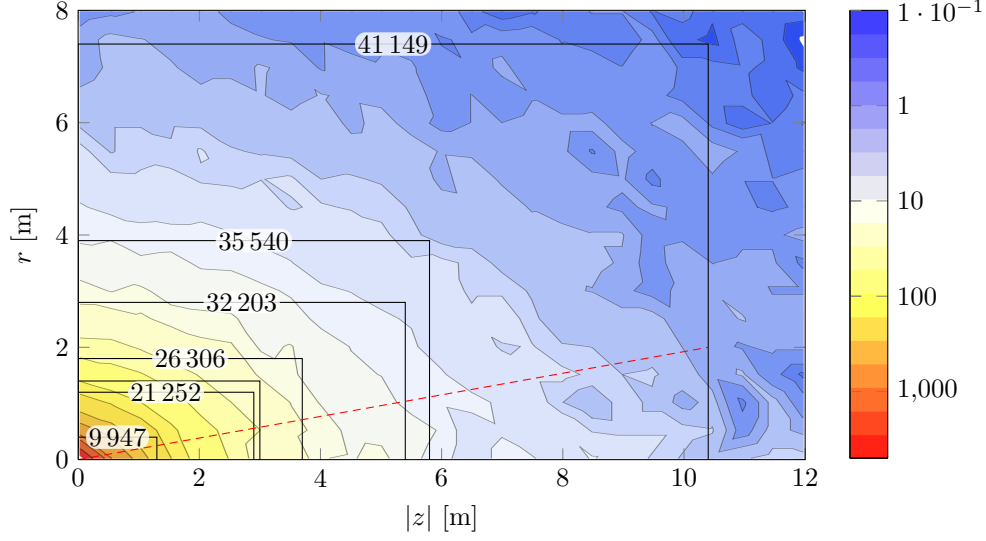
Figure 5.11: Contour plot showing the density of neutralino decays inside the detector per m^{-3} for HH27. The numbers on the horizontal boundaries of the detector components correspond to the total number of decays in the enclosed volume; $\zeta = 3 \times 10^{-8}$ and $\mathcal{L} = 10\,\mathrm{fb}^{-1}$.

5.4.6   Discovery reach at the LHC

In the previous section we have studied in detail the benchmark point HH27: $m_{1/2} = m_0 = 270\,\mathrm{GeV}$, which yields the rather small superparticle masses $m_{\chi_1^0} = 106\,\mathrm{GeV}$, $m_{\tilde{g}} \simeq 660\,\mathrm{GeV}$ and $m_{\tilde{q}} \simeq 650\,\mathrm{GeV}$ for the light quark flavours (*cf.* Table 5.12). From the decay rates given in Section 3.8.2 and the phase space factors shown in Figure 3.6 one obtains for decay length and branching ratio into Z boson/neutrino final states:

$$c\tau_{\chi_1^0} \simeq 31\,\mathrm{m} \left(\frac{\zeta}{10^{-8}}\right)^{-2} , \qquad\qquad BR(\chi_1^0 \to Z\nu) \simeq 0.17 . \qquad (5.17)$$

Based on the production cross sections listed in Table 5.13 an integrated luminosity $\mathcal{L} = 10\,\mathrm{fb}^{-1}$ yields about 22000 events and therefore 44000 NLSPs.

We have studied this benchmark point for two different values of the R-parity breaking parameter: $\zeta = 3 \times 10^{-8}$ and $\zeta = 1 \times 10^{-9}$. For the larger value of ζ one has $c\tau_{\chi_1^0} \simeq 3.5\,\mathrm{m}$. Hence, essentially all neutralinos decay inside the detector, most of them close to the origin. The spacial distribution of secondary vertices is displayed in the contour plot Figure 5.11. Using $BR(Z \to \mu^+\mu^-) \simeq 0.034$ and the branching ratio given in Equation (5.17), one concludes that there are 251 events with a secondary χ_1^0-decay vertex, which contain a $\mu^+\mu^-$ pair with $M_{\mu^+\mu^-} \simeq M_Z$. This is consistent with the simulation which yields 282 events in the detector volume (*cf.* Figure 5.12) and 174 events passing all cuts (*cf.* Table 5.15). The locations of the secondary vertices of these events are shown in Figure 5.12.

For the smaller value of the R-parity breaking parameter, $\zeta = 1 \times 10^{-9}$, the decay length increases to $c\tau_{\chi_1^0} \simeq 3.1\,\mathrm{km}$. Now most neutralino NLSPs decay outside the detector. This is apparent from Figure 5.13 where the total number of decays in the different sub-volumes of the detector are given. Compared to $\zeta = 3 \times 10^{-8}$, the number of decays inside the detector is
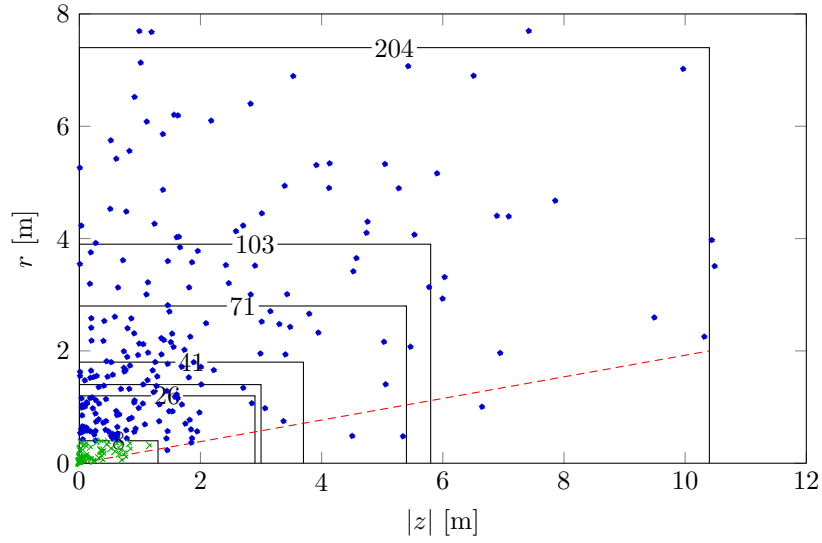
Figure 5.12: Location of secondary vertices for the decays $\chi_1^0 \to Z\nu$ with $Z \to \mu^+\mu^-$ (green crosses: inside pixel detector, blue dots: outside pixel detector); the numbers on the horizontal boundaries of the detector components give the number of decays in the enclosed volume; $m_{1/2} = m_0 = 270\,\mathrm{GeV}$, $\zeta = 3 \times 10^{-8}$ and $\mathcal{L} = 10\,\mathrm{fb}^{-1}$.
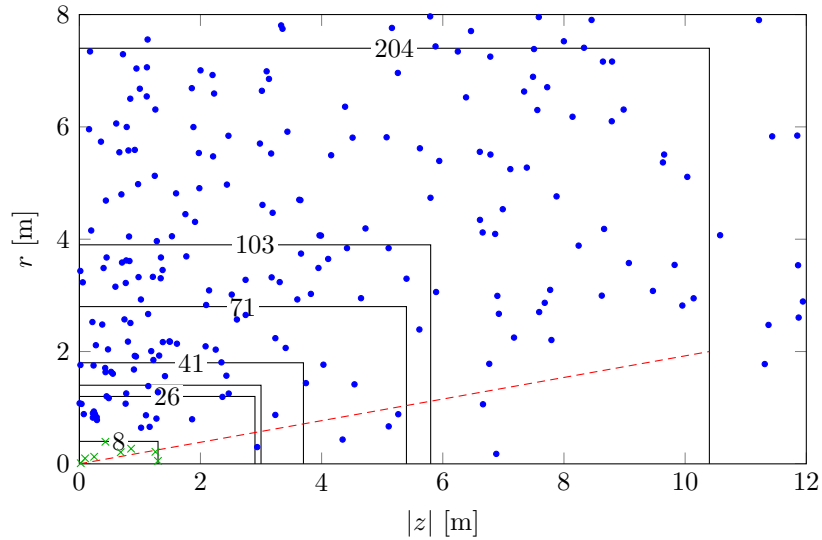

Figure 5.13: Location of all neutralino decays inside of the detector (blue crosses: decays inside pixel detector; black dots: decays outside pixel detector); the numbers on the horizontal boundaries of the detector components correspond to the total number of decays in the enclosed volume; $m_{1/2} = m_0 = 270\,\mathrm{GeV}$, $\zeta = 1 \times 10^{-9}$ and $\mathcal{L} = 10\,\mathrm{fb}^{-1}$.

smaller by a factor ~ 200, which roughly corresponds to the ratio of the decay lengths, as suggested in [47].

According to the simulation described in the previous section, for $\zeta = 1 \times 10^{-9}$ an integrated luminosity of $100 \, \text{fb}^{-1}$ is needed to obtain 2 signal events $\chi_1^0 \to Z\nu \to \mu^+\mu^-\nu$, which is consistent with the naive estimate within the statistical uncertainty and the detector efficiency. The number is very small compared to the total number of about 1000 decays in the detector volume used in the present analysis (*cf.* Section 5.3.1), which is a consequence of the tiny branching ratio into the chosen specific final state. It is likely that a substantially larger fraction of the events can be used in the search for a decaying neutralino. In [47] it has been argued that already 10 χ_1^0 decays inside the detector may be sufficient for the discovery of a decaying NLSP. It remains to be seen whether for events with a secondary vertex and jets, signal and background can be sufficiently well separated.

Let us now consider the benchmark point

$$\text{HH50:} \qquad\qquad\qquad m_{1/2} = m_0 = 500 \, \text{GeV} \; , \qquad\qquad\qquad (5.18)$$

which implies the heavier superparticle masses $m_{\chi_1^0} = 206 \, \text{GeV}$ and $m_{\tilde{g}} \simeq m_{\tilde{q}} \simeq 1200 \, \text{GeV}$ for the light quark flavours (*cf.* Table 5.12). The phase space suppression is now negligible, $f_W \simeq f_Z \simeq 1$, and one obtains for decay length and branching ratio into Z boson/neutrino final states:

$$c\tau_{\chi_1^0} \simeq 5.4 \, \text{m} \left(\frac{\zeta}{10^{-8}}\right)^{-2} \; , \qquad\qquad BR(\chi_1^0 \to Z\nu) \simeq 0.32 \; . \qquad (5.19)$$

The total production cross section for these heavier gluino/squark pairs is about two orders of magnitude smaller (*cf.* Table 5.13), and therefore an integrated luminosity $\mathcal{L} = 10 \, \text{fb}^{-1}$ only yields 460 NLSP.

We have studied this benchmark point again for the two different values of the R-parity breaking parameter $\zeta = 3 \times 10^{-8}$ and $\zeta = 1 \times 10^{-9}$. For the larger value of ζ one has $c\tau_{\chi_1^0} \simeq 60 \, \text{cm}$, and essentially all neutralinos decay inside the detector. The branching ratio into the considered final state is now somewhat larger, $BR(\chi_1^0 \to Z\nu \to \mu^+\mu^-\nu) \simeq 0.01$, so that one expects about 5 events with this final state, which is consistent with our simulation.

For $\zeta = 1 \times 10^{-9}$, the decay length is $c\tau_{\chi_1^0} \simeq 540 \, \text{m}$ and most neutralino NLSPs decay outside the detector. The spacial distribution of secondary vertices inside the detector, in total 12 for $10 \, \text{fb}^{-1}$, is shown in Figure 5.14. Due to the $1\,\%$ branching ratio into the $Z\nu \to \mu^+\mu^-\nu$ final state one then estimates that $1000 \, \text{fb}^{-1}$ will be needed for a discovery, which is consistent with our simulation.

In Figure 5.15 we have summarized the results of our simulations for the decay chain $\chi_1^0 \to Z\nu$ with $Z \to \mu^+\mu^-$. The benchmark points HH27–HH80 correspond to gluino and squark masses ranging from $650 \, \text{GeV}$ to $1800 \, \text{GeV}$ (*cf.* Table 5.12). The bands reflect the different number of events required for a 5σ discovery depending on the simulated background. The central value corresponds to 6 signal events (with luminosity $\mathcal{L}$) with no background events for a simulated luminosity of $10 \times \mathcal{L}$; the lower (upper) boundary represents 3 (13) signal events (with luminosity $\mathcal{L}$) with no (1) background event for a simulated luminosity of $100 \times \mathcal{L}$ ($10 \times \mathcal{L}$). We conclude that with $10 \, \text{fb}^{-1}$ a 5σ discovery of a quasi-stable neutralino is possible for squark and gluino masses of $830 \, \text{GeV}$ (*cf.* HH35) and an R-parity breaking parameter $\zeta = 3 \times 10^{-9}$, which is one order of magnitude smaller than the present astrophysical bound [98].
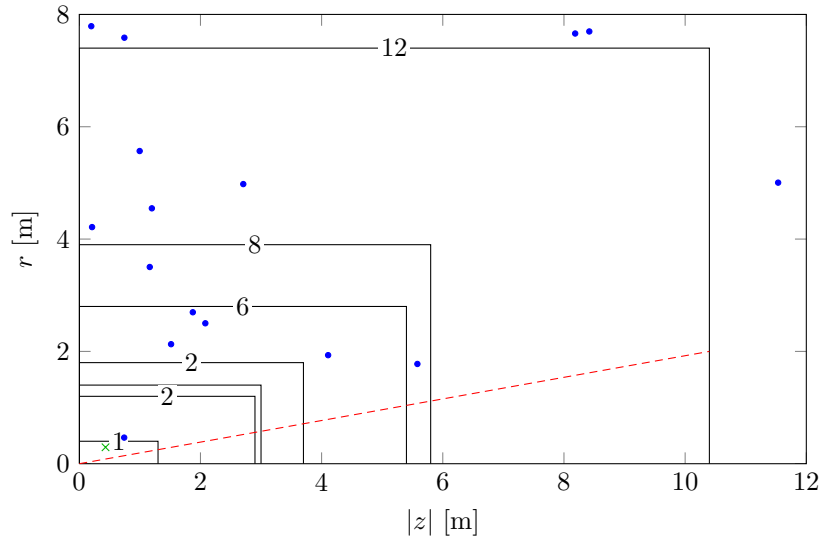
Figure 5.14: Location of all neutralino decays inside of the detector (blue cross: decay inside pixel detector; black dots: decays outside pixel detector); the numbers on the horizontal boundaries of the detector components correspond to the total number of decays in the enclosed volume; $m_{1/2} = m_0 = 500\,\mathrm{GeV}$, $\zeta = 1 \times 10^{-9}$ and $\mathcal{L} = 10\,\mathrm{fb}^{-1}$.
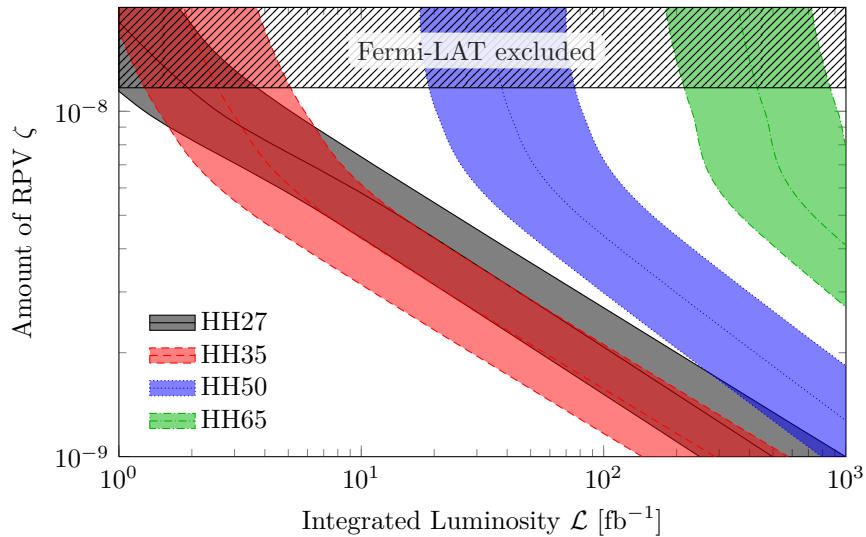

Figure 5.15: 5σ discovery reach in ζ for quasi-stable neutralino NLSP via the decays $\chi_1^0 \to Z\nu$ with $Z \to \mu^+\mu^-$. The different bench mark points correspond to gluino and squark masses between $650\,\mathrm{GeV}$ and $1800\,\mathrm{GeV}$; the bands represent different assumptions about the background (see text).
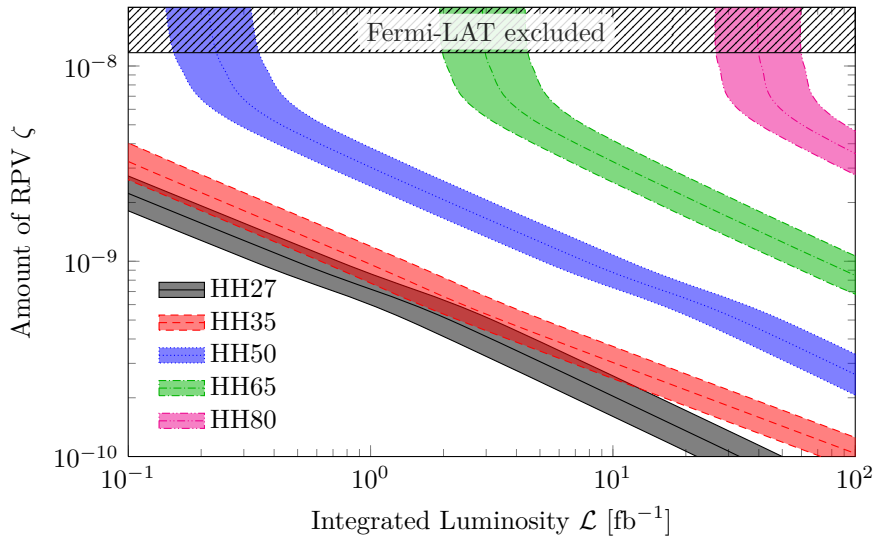
Figure 5.16: Estimate of the 5σ discovery reach in ζ for quasi-stable neutralino NLSP at the LHC; the lower (upper) boundary of the bands corresponds to 10 (20) decays inside the detector. The different bench mark points correspond to gluino and squark masses between $650\,\text{GeV}$ and $1800\,\text{GeV}$.

We expect that the sensitivity in the parameter ζ can be significantly improved if also neutralino decays with jets are taken into account. Figure 5.16 represents an estimate of the discovery reach for quasi-stable neutralino NLSPs at the LHC, assuming 10–20 decays inside the detector (*cf.* Reference [47]). The parameter space, which can be probed, is now significantly extended. As an example, with $10\,\text{fb}^{-1}$ and squark and gluino masses of $830\,\text{GeV}$ (*cf.* HH35), one is now sensitive to $\zeta = 3 \times 10^{-10}$, which lies two orders of magnitude below the present astrophysical bound. Correspondingly, for heavier gluinos and squarks, $m_{\tilde{g}} \simeq m_{\tilde{q}} \simeq 1480\,\text{GeV}$ (*cf.* HH65), one can probe values of the R-parity breaking parameter down to $\zeta = 3 \times 10^{-9}$.

5.5 Drell-Yan production using the example of higgsinos

As shown in section 4.2.3, higgsinos that are produced in proton collisions at the LHC decay in a secondary vertex into a W boson and a charged lepton in almost $100\,\%$ of all decays. In the model we are studying in this section the coloured particles are too heavy to be produced at the LHC, therefore we have to rely on Drell-Yan production of light higgsinos. Figure 5.17 shows an example of a cascade decay with muons in the final state. The distance between the collision point and the secondary vertex depends on the decay width of the neutralino (3.106), and hence on the R-parity breaking parameter ζ.

5.5.1 Signatures and search strategy

Table 5.16 summarizes all possible LHC signatures if the NLSP is a higgsino-like neutralino in the case when both neutralinos decay inside of the tracker volume. The signatures are classified according to the final states in the neutralino decays. Unlike the previously studied case of bilinear RPV in the MSSM in Section 5.4, when the spectra contain light squarks and gluinos and a bino-like neutralino NLSP, there are only two types of signatures: leptonic signatures
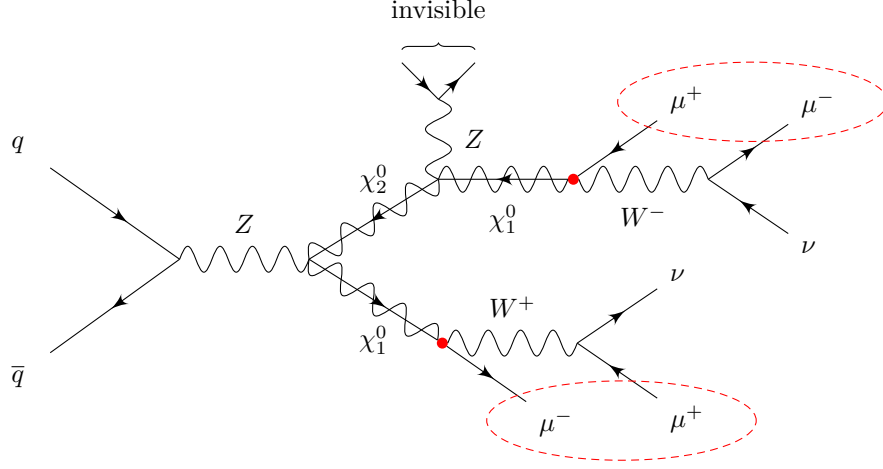
Figure 5.17: Typical R-parity violating decay chain involving higgsino-like neutralinos at the LHC. The secondary vertices as well as the two possibilities of interesting muon combinations are highlighted. The Z boson decay is invisible, due to the small mass difference between the heavier higgsinos and the lightest higgsino (see Equation (4.28), (4.30) and Table 5.19). The signature is essentially the same for chargino production, since also in this case the decays into the lightest higgsino lead only to particles with small PT.

category	χ_1^0 decays	LHC signature
leptonic	$W^+W^-l^+l^- \to l^+\nu l^-\bar{\nu}l^+l^-$	
	$W^+W^+l^-l^- \to l^+\nu l^+\nu l^-l^-$	$2l^- + 2l^+ + \not{E}_T$
	$W^-W^-l^+l^+ \to l^-\bar{\nu}l^-\bar{\nu}l^+l^+$	
semi-leptonic	$W^+W^-l^+l^- \to jjl^-\bar{\nu}l^+l^-$	$2j + 2l^- + 1l^+ + \not{E}_T$
	$W^+W^+l^-l^- \to jjl^+\nu l^-l^-$	
	$W^+W^-l^+l^- \to jjl^-\bar{\nu}l^+l^-$	$2j + 1l^- + 2l^+ + \not{E}_T$
	$W^-W^-l^+l^+ \to jjl^-\bar{\nu}l^+l^+$	
	$W^+W^-l^-l^+ \to jjjjl^-l^+$	$4j + 1l^- + 1l^+$
(same sign, no $\not{E}_T$)	$W^+W^+l^-l^- \to jjjjl^-l^-$	$4j + 2l^-$
	$W^-W^-l^+l^+ \to jjjjl^+l^+$	$4j + 2l^+$

Table 5.16: All possible final states in the higgsino-like neutralino case if both neutralinos decay inside the tracking volume.

category	χ_1^0 decays	LHC signature
leptonic	$W^+l^- \rightarrow l^+\nu l^-$	$1l^- + 1l^+ + \not{E}_T$
(opposite sign)	$W^-l^+ \rightarrow l^-\overline{\nu}l^+$	
single lepton	$W^+l^- \rightarrow jjl^-$	$2j + 1l^- + \not{E}_T$
	$W^-l^+ \rightarrow jjl^+$	$2j + 1l^+ + \not{E}_T$

Table 5.17: All possible final states in the higgsino-like neutralino case if one of the neutralinos decays outside the tracking volume.

involving only charged leptons in the final state, and semi-leptonic signatures involving at least two charged leptons and jets.

Most SUSY searches for such final states at the LHC so far rely on the large production cross sections of the strongly interacting squarks and/or gluinos. The searches that are starting to probe direct EW production of charginos and neutralinos have been interpreted in R-parity conserving models with a stable neutralino LSP [130–132]. They rely on leptonic signatures with larger MET than what would be present in our scenario in the case of both neutralinos decaying inside the tracker. Searches in the first LHC data for RPV have also been performed [133–141] but because of differences in the scenarios considered and differing signatures they do not apply here. Searches for long-lived neutral particles have been carried out as well but do not apply to our model as they assume either the wrong event topologies [142, 143], final states [144] and/or size of the displacements [143, 145].

For smaller values of ζ, one of the neutralinos may decay inside or after the muon system leading to signatures with a larger amount of MET as shown in Table 5.17. We show in Figure 5.18 how this possibly gives rise to a missing energy signature as ζ decreases. However, this situation would still not be covered by the current direct neutralino- and chargino searches by ATLAS and CMS [130–132] since the lepton reconstruction in these searches requires a track in the pixel detector, often with a certain maximum impact parameter to the primary vertex. For the same reason that we obtain missing energy from one of the neutralinos decaying outside of the detector, it will also be less probable that the other neutralino decays early enough for the leptons to fulfil such requirements on their inner tracks, as will be illustrated below.

For very small RPV both neutralinos may escape the detector without being observed. This case cannot be distinguished from the one with R-parity conservation. As we argue in Section 5.2.2 this is for stable higgsinos and heavy coloured particles very challenging to detect [111]. This can as well be understood just by looking at the typical LHS process shown in Figure 5.17 and trying to imagine possible signatures in the case of the lightest neutralino being stable.

We illustrate in Table 5.18 how often the different situations of none, one or two of the neutralinos, produced in processes like in Figure 5.17, decaying inside the detector occurs depending on the RPV and the higgsino mass. We also check how often the events would give inner tracks, possibly with a small impact parameter to the primary vertex, since this is a common requirement on lepton objects in existing searches. Table 5.18 illustrates:

- For decreasing ζ, we approach a situation indistinguishable from the case of R-parity
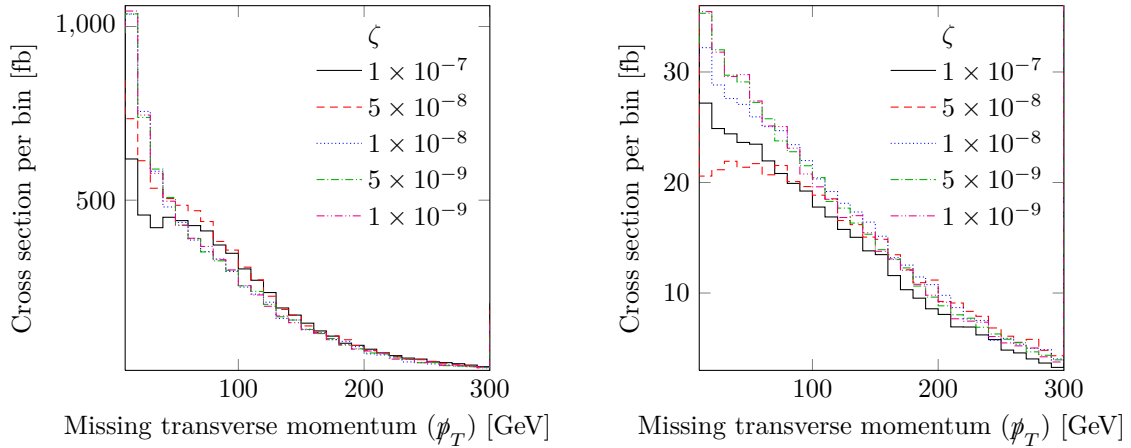
(a) For $\mu = 100\,\mathrm{GeV}$ and $\zeta = 1 \times 10^{-7}, 5 \times 10^{-8}$ most often one neutralino remains undetected, corresponding to an increased MPT around the neutralino mass $m_{\chi_1^0} = 102\,\mathrm{GeV}$. For smaller values of ζ most of the time both neutralinos leave the detector leading to small MPT.

(b) For $\mu = 200\,\mathrm{GeV}$ and $\zeta = 5 \times 10^{-8}, 1 \times 10^{-8}$ most often one neutralino leads to MPT around the neutralino mass $m_{\chi_1^0} = 205\,\mathrm{GeV}$. For smaller values of ζ most of the time both neutralinos leave the detector undetected.

Figure 5.18: MPT at the generator level, defined as the sum of the PT of all neutrinos and of the neutralinos that decay after they have left the detector. In the case where only one of the two neutralinos escapes the detector, corresponding to a large value in the second columns in Table 5.18b, we notice an increased MPT around the neutralino mass. In the case where both neutralino decay outside the detector corresponding to a large value in the first columns in Table 5.18b, the values for small MPT are increased. This reflects that the neutralinos are mostly back-to-back, due to the absence of other high PT objects in the decay cascade.
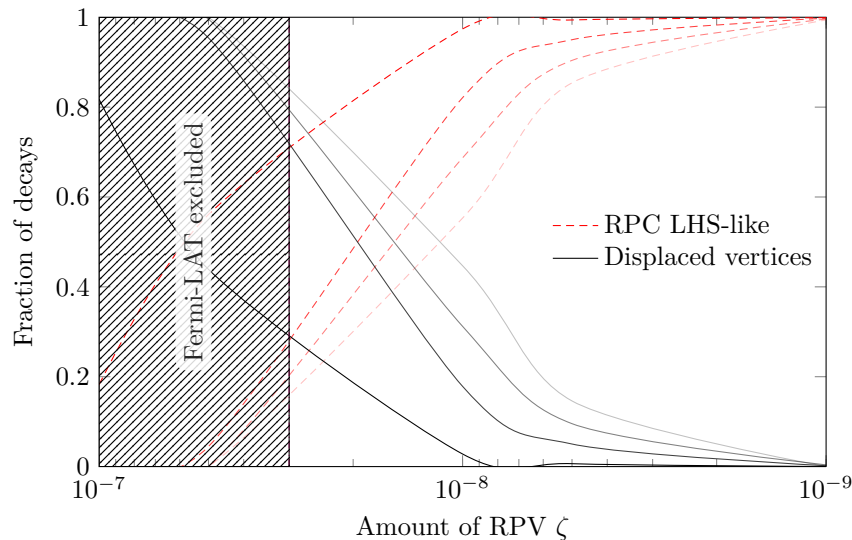
Figure 5.19: Fraction of decays inside and outside of the detector. The four lines represent the four benchmark points $\mu = 100 \ldots 400\,\mathrm{GeV}$, with increasing μ corresponding to lighter lines at smaller values of RPV.

$r \leq 5\,\mathrm{mm}$	Number of neutralino decays before the muon system		
	0	1	2
0	RPC LHS-like	displaced $\mu^+\mu^-$	displaced $\mu^+\mu^-$
1		may be covered by existing SUSY searches	displaced $\mu^+\mu^-$
2			SM-like
Signature	no LHC signature	possibly large MET	no or small MET

(a) Legend: Classification of event types depending on the number of neutralino decays inside the detector (columns) and inside the innermost 5 mm of the tracker (rows). The fractions of events quoted in green belong to the type covered by our search strategy, the fraction of events in red cannot be distinguished from the RPC LHS. The fraction quoted in blue might be covered by existing SUSY searches (see text), and the black events might be misidentified as SM events.

ζ	μ			
	100	200	300	400
1×10^{-7}	**18.2** **40.5** **41.1** 0.059 0.182 0.002	0.046 2.59 **95.6** 0.004 1.72 0.012	0 0.121 **96.3** 0.002 3.52 0.038	0 0.004 **94.4** 0 5.51 0.105
5×10^{-8}	**56.1** **35.5** 8.36 0.042 0.030 0	4.48 **28.6** **66.4** 0.083 0.404 0	0.405 9.64 **89.0** 0.040 0.928 0.002	0.028 2.64 **95.8** 0.016 1.52 0.006
1×10^{-8}	**97.4** 2.58 0.222 0 0 0	**82.1** **16.7** 1.16 0.014 0 0	**68.7** **27.8** 3.41 0.030 0.004 0	**55.3** **37.0** 7.68 0.048 0.024 0
5×10^{-9}	**99.4** 0.643 0.002 0 0 0	**95.0** 4.94 0.083 0.008 0 0	**90.4** 9.23 0.323 0.008 0 0	**85.4** **13.9** 0.709 0.012 0 0
1×10^{-9}	**99.9** 0.018 0 0 0 0	**99.8** 0.204 0 0 0 0	**99.6** 0.391 0 0.002 0 0	**99.4** 0.633 0.002 0.002 0 0

(b) Generator level fractions in % of neutralinos decaying inside and outside of the detector as well as in its innermost part. The meaning of the positions in the subtables and the colour code is explained in Legend (a). Numbers larger than 10 % are bold. A zero entry means that $\leq 0.001\,\%$ of the decays happen in this channel. The tendency of lighter higgsinos with smaller RPV to decay outside the detector follows from relation (4.32).

Table 5.18: Fractions of neutralino decays occurring either within a radius of 5 mm, inside the muon system or outside the detector, depending on the ζ and μ parameters. In Legend (a) we explain the colour code and the meaning of the positions in Table (b).

higgsino	μ			
	100	200	300	400
χ_2^0	106	209	311	413
$\chi_1^\pm$	104	207	309	411
χ_1^0	102	205	307	408

Table 5.19: Mass spectrum of light higgsinos in our four benchmark models with a higgsino mass parameter μ between 100 GeV and 400 GeV. All masses are given in units of GeV.

conserving LHS (see numbers in red).

- The second column in each sub-table shows that when we can have large MET in the event due to one of the neutralinos decaying outside of the detector, very few events will have the other neutralino decaying sufficiently close to the primary vertex for the event to be seen in existing searches for direct production of charginos and neutralinos (see numbers in blue).

- We also see that for a given ζ, increasing higgsino mass will lead to more decays inside the detector.

In Figure 5.19 we give the fraction of higgsinos decaying inside and outside of the detector, depending on the size of ζ.

The leptonic decays of at least one of the neutralinos inside the detector lead to an opposite-sign di-muon signature, which will be exploited in the present work. We will focus on events with two opposite sign muons originating either in a secondary vertex in the tracker, far away from the primary interaction point, or having no associated track at all, being identified solely by the muon system.

5.5.2 Benchmark points

In models with hybrid gauge-gravity mediated SUSY breaking it is possible to realize a spectrum with higgsino masses around the EW scale, Higgs partners around the TeV scale and all other particles at the multi TeV scale, as demonstrated in Section 5.2.1 [46].

The gravity mediated higgsino parameter μ of the superpotential and hence the lightest neutralinos and charginos can be of order 100 GeV. The existing lower bound on the chargino mass of roughly 95 GeV for degenerate spectra comes from Large Electron-Positron Collider (LEP) [79, 146]. In this study we have chosen four benchmark points for which we have varied the higgsino mass parameter μ in three steps from the lower bound of about 100 GeV to 400 GeV, see Table 5.19. The masses of the MSSM Higgs particles are in this case set by the CP-odd Higgs mass parameter m_A, which we have taken to be 800 GeV. All other particles are governed by the gauge mediated parameters m_0 and $m_{1/2}$ which are chosen to be 3 TeV, putting them out of reach of the LHC.

In all our benchmark points the Higgs mass is around 125 GeV, in agreement with the observed Higgs-like resonance at the LHC [6, 7]. Furthermore, while the LHC-beauty (LHCb) result of an excess in the search for the rare decay $B_s^0 \to \mu^+\mu^-$ [147] excludes many models

	μ					μ			
	100	200	300	400		100	200	300	400
$\chi_1^0\chi_1^+$	1640	121	22.8	6.28	$\chi_1^0\chi_1^+$	3350	293	66.0	21.9
$\chi_2^0\chi_1^+$	1530	116	22.2	6.15	$\chi_2^0\chi_1^+$	3130	282	64.3	21.5
$\chi_1^-\chi_1^+$	1300	94.8	17.2	4.58	$\chi_1^-\chi_1^+$	2770	246	53.9	17.4
$\chi_1^0\chi_1^-$	918	55.9	9.23	2.29	$\chi_1^0\chi_1^-$	2090	158	32.0	9.72
$\chi_2^0\chi_1^-$	851	53.6	8.94	2.24	$\chi_2^0\chi_1^-$	1950	152	31.2	9.54
$\chi_1^0\chi_2^0$	1410	91.3	16.1	4.19	$\chi_1^0\chi_2^0$	3030	240	51.0	16.2
σ^{tot}	7649	532.6	96.47	25.73	σ^{tot}	16320	1371	298.4	96.26
$\mathcal{L}_{\mathrm{min}}^{\mathrm{gen}}$	18.3	93.9	518	1940	$\sigma_{14}^{\mathrm{tot}}/\sigma_8^{\mathrm{tot}}$	2.1	2.6	3.1	3.7
$\mathcal{L}_{\mathrm{max}}^{\mathrm{gen}}$	565	263	1450	5440					

(a) $\mathcal{L} = 8\,\mathrm{TeV}$.	(b) $\mathcal{L} = 14\,\mathrm{TeV}$.

Table 5.20: Partial and total NLO production cross sections for our benchmark models at 8 TeV and 14 TeV LHC in units of fb. The minimal and maximal (depending on ζ) integrated luminosity corresponding to the generated number of events at 8 TeV for each model is given in units of fb^{-1}.

with large $\tan\beta$ [148], the LHS is unaffected by this constraint due to the large mass splitting between the μ parameter and the squark masses.

We have used these parameter choices as input values for a full RGE calculation performed with SOFTSUSY. As expected the production cross sections for all supersymmetric particles except the light higgsino states are negligible. The higgsino production cross sections for the four benchmark points are listed in Table 5.20.

5.5.3 Background

The SM processes that dominate the di-muon channel are:

- $\gamma^*/Z^* \to \mu^+\mu^-$

- $t\bar{t}$

- V^*V^*, where $V = W, Z$.

In Table 5.21 we give the NLO cross section for the processes that we have simulated for our study. As we will see, these will be efficiently removed by the requirement of a secondary vertex.

In our analysis, we will require the muons to be isolated, which efficiently removes leptons originating in jets, and we further remove possible contributions from displaced b quarks by a sufficiently large cut on tracks in the inner radius. For low background levels, however, other background sources might come into play. These are:

	$t\bar{t}$	$Z \to \mu\mu$	WW	WZ	ZZ
	[149]	[150]	[113]	[113]	[113]
σ_{NLO}	183	536	57.25	18.55	7.92
$\mathcal{L}^{\mathrm{gen}}$	196	167	360	306	143

Table 5.21: NLO production cross sections for the relevant background processes in units of pb at an energy of 8 TeV as well as the integrated luminosity corresponding to the generated number of events in units of fb^{-1}.

- cosmic muons,

- pion and kaon decays in flight,

- hadronic punch-throughs,

- pileup.

An estimation of such contributions to our background has to be done with real LHC data, and is beyond the scope of this work. We argue here that most of this background, should it contribute, can be removed without significant loss of signal. Cosmic muons can be vetoed against by using the timing information, as discussed in Section 5.4.4, or a cut on back-to-back muons. Punch-throughs are also not simulated in Delphes but should in principle be possible to veto since in this case the muon would be associated with a jet. Most of any possible contribution to displaced muons from decay in flight should be removed by our high PT requirement on muons. Pileup was estimated in a partly similar analysis to give a systematic uncertainty in the event selection efficiency of 2 % [145]. The displacement due to pileup is in general much smaller than the secondary vertices we are expecting. Therefore, such a background can be reduced by increasing the minimal impact parameter value required, which in our case of larger displacements would not lead to a large decrease in signal efficiency.

In the following we therefore neglect these backgrounds to our displaced muon channel. However, as will be described in Section 5.5.5, we will in our statistical analysis allow some margin for systematic uncertainty in case of vanishing estimated background levels by requiring our predicted signal to amount to a certain number of observed events.

5.5.4 Analysis

As in Section 5.4.4 we focus our search solely on the muon objects as we assume that we can trust the detector simulation results in this case even in the presence of secondary vertices. We aim to reconstruct clear signatures where one of the neutralinos decays into a muon and a W boson, which in turn decays into another muon and a neutrino. Thus, we demand two opposite sign muons that are either chamber muons or tracker muons with a secondary vertex far away from the primary interaction point. We remind the reader that displaced muons are not expected in SM processes giving two isolated muons, and we will show in this section that the requirement of large displacements efficiently removes the SM di-muon background. Furthermore, we require that the invariant mass of the two-muon system is not too small, thus suppressing back-to-back signals. This reduces not only the SM background, but also helps to decrease the background of cosmic muons.

cuts	$t\bar{t}$	$Z \to \mu\mu$	WW	WZ	ZZ
$N(\mu) \geq 2$	3057	397	410	361	283
Class 1	2177	385	352	297	256
$m_{\mathrm{inv}}(\mu^+\mu^-) > 5\,\mathrm{GeV}$	1761	385	351	297	256
$d(\mathrm{Vertex}) > 5\,\mathrm{mm}$	11.2	0	0.369	0.281	0.189
$\Delta d(\mathrm{Vertex})_{ij} < 1\,\mathrm{mm}$	0	0	0	0	0
Class 2	0	0	0	0	0
$m_{\mathrm{inv}}(\mu^+\mu^-) > 5\,\mathrm{GeV}$	0	0	0	0	0
Total	0	0	0	0	0

Table 5.22: Cutflow for the main SM di-muon background in units of fb.

Cuts

Only `DELPHES` muon objects with a PT larger than $10\,\mathrm{GeV}$ are passed in our additional muon reconstruction processes described above. We demand that the secondary vertex of the muons lies before the muon system, meaning $r(\mathrm{Vertex}) < 4\,\mathrm{m}$ and $z(\mathrm{Vertex}) < 6\,\mathrm{m}$, where r and z are the radial coordinate perpendicular to the beam and the coordinate parallel to the beam, respectively. We assume that tracks can be reconstructed reliably as long as the secondary vertex lies inside the cylinder defined by $r(\mathrm{Vertex}) < 40\,\mathrm{cm}$ and $z(\mathrm{Vertex}) < 1.3\,\mathrm{m}$. The cut on the pseudorapidity for muons is taken to be $\eta < 2.5$. In addition to the isolation requirements in `DELPHES`, we only select muons that have no overlap with jet objects in angular coordinates $\Delta R > 0.1$, where

$$\Delta R = \sqrt{\Delta\phi^2 + \Delta\eta^2} \, , \tag{5.20}$$

and $\Delta\phi$ and $\Delta\eta$ are the appropriate angle differences between the muon and the jet in the usual detector coordinates. Then we perform a selection cut on the total number of muons (chamber and tracker muons) in the event:

- $N(\mathrm{muons}) \geq 2$.

We define two event classes:

- Class 1: the event contains exactly two tracker muons, *i.e.* $N(\mathrm{tracker\ muons}) = 2$, with opposite charge.

- Class 2: the event does not fulfil the conditions for Class 1 and contains exactly two chamber muons, *i.e.* $N(\mathrm{chamber\ muons}) = 2$, of opposite charge.

As the amount of R-parity breaking decreases, more and more events will fall into the second class. In accordance with the description of the signal presented above, we implement the following cuts on the Class 1 events:

cuts	100		200	
	1×10^{-8}	5×10^{-9}	1×10^{-8}	5×10^{-9}
$N(\mu) \geq 2$	4.26	1.64	3.50	0.82
Class 1	0.219	0.109	0.394	0.096
$m_{\mathrm{inv}}(\mu^+\mu^-) > 5\,\mathrm{GeV}$	0.219	0.109	0.394	0.096
$d(\mathrm{Vertex}) > 5\,\mathrm{mm}$	0.219	0.109	0.394	0.096
$\Delta d(\mathrm{Vertex})_{ij} < 1\,\mathrm{mm}$	0.219	0.109	0.341	0.075
Class 2	3.77	1.31	2.49	0.692
$m_{\mathrm{inv}}(\mu^+\mu^-) > 5\,\mathrm{GeV}$	3.66	1.31	2.49	0.692
Total	3.88	1.42	2.83	0.767

Table 5.23: Cutflow in units of fb for the two lighter benchmark points ($\mu = 100, 200\,\mathrm{GeV}$) with the two most relevant of the analysed values of R-parity breaking ζ.

- $m_{\mathrm{inv}}(\mu^+\mu^-) > 5\,\mathrm{GeV}$: We compute the invariant mass of the muon pair and demand that it is larger than $5\,\mathrm{GeV}$.

- $d(\mathrm{Vertex}) > 5\,\mathrm{mm}$: Each of the tracks associated with the two tracker muons should have a vertex which is further than $5\,\mathrm{mm}$ away from the primary vertex. This value is approximately one order of magnitude larger than the resolution of the inner tracker [119, 127].

- $\Delta d(\mathrm{Vertex})_{ij} < 1\,\mathrm{mm}$: The distance between the two track vertices should be less than $1\,\mathrm{mm}$, in order to capture events where both muons originate in the same secondary vertex.

If the event fails one of the above cuts and fulfils the criteria for Class 2 events it is classified as Class 2:

- $m_{\mathrm{inv}}(\mu^+\mu^-) > 5\,\mathrm{GeV}$: Also in this case we demand that the invariant mass of the muon pair is larger than $5\,\mathrm{GeV}$.

As expected, all of the SM background events are removed by the cut on the minimal distance of the vertex from the primary interaction point and the requirement that the reconstructed secondary vertices are close to each other (see Table 5.22). The LHS model events, however, survive these cuts to such an extent that a signal is detectable (see Table 5.23).

Mass determination

Rejecting the background-only hypothesis is only one contribution to the degree of belief that new physics has been discovered. Whether the signal hypothesis is a plausible one should be tested in other ways as well. Here, we show that the chosen signature allows for the

(a) Large total number of events (#).

(b) Small total number of events (#).
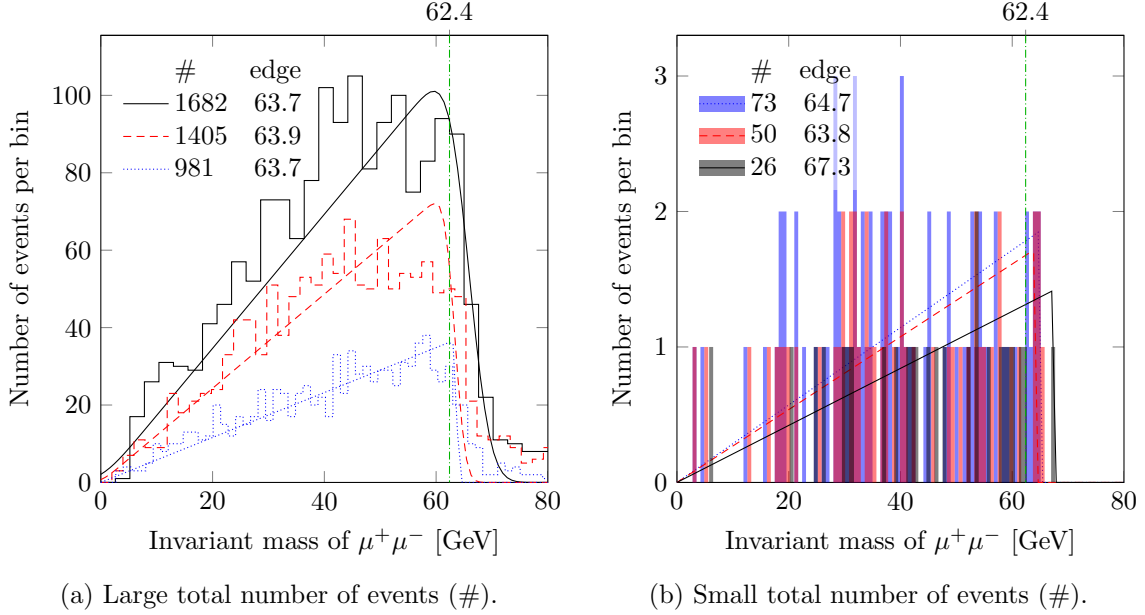
Figure 5.20: Examples of the mass-edge reconstruction when the higgsino mass is $m_{\chi_1^0} = 102\,\text{GeV}$ (benchmarks $\mu = 100\,\text{GeV}$), so that the theoretical value for the edge in the di-muon invariant mass is 62.4 GeV. The values in the legend show that already a small total number of events (#) are sufficient in order to reconstruct the mass edge with an error around 2 GeV.

determination of the neutralino mass via the well-known mass edge method [151, 152]. The mass edge in the di-muon invariant mass distribution is to LO determined by

$$m_{ll}^2 = m_{\chi_1^0}^2 - m_W^2 + \mathcal{O}\left(\frac{m_l}{m_{\chi_1^0}}\right)^2 . \tag{5.21}$$

Following [153] we fold the phase space function with a Gaussian to model the mass edge:

$$T(m_{ll}) = \frac{1}{\sqrt{2\pi}\sigma} \int_0^{m_{\text{cut}}} dy \; y \exp\left(-\frac{1}{2}\left(\frac{m_{ll} - y}{\sigma}\right)^2\right) , \tag{5.22}$$

where the endpoint m_{cut} and the height of the triangle σ are the free parameters to be fitted to the di-lepton invariant mass m_{ll} distribution to reconstruct the di-muon mass edge. We implemented this mass edge formula in the MINUIT class of the ROOT package.

For this method to work, a sufficiently large sample of signal events is needed. In Figure 5.20 we show examples of the mass edge reconstruction for different numbers of observed events in the case of our benchmarks model with $\mu = 100\,\text{GeV}$. We conclude from Figure 5.20b that a total number of events between 26 and 50 should give an accurate estimate of the higgsino mass.

5.5.5   Result

The signal cross sections after cuts for all our LHS benchmark models are given in Table 5.24. The SM background is removed by our cuts, as shown in Table 5.22.

ζ	μ			
	100	200	300	400
5×10^{-8}	90 $\pm$ 2	25.6 $\pm$ 0.5	4.9 $\pm$ 0.1	1.17 $\pm$ 0.03
1×10^{-8}	3.9 $\pm$ 0.5	2.8 $\pm$ 0.2	1.07 $\pm$ 0.05	0.39 $\pm$ 0.01
5×10^{-9}	1.4 $\pm$ 0.3	0.77 $\pm$ 0.09	0.27 $\pm$ 0.02	0.105 $\pm$ 0.007
1×10^{-9}	0.028 $\pm$ 0.007	0.023 $\pm$ 0.009	0.014 $\pm$ 0.003	0.0037 $\pm$ 0.0008

Table 5.24: Signal cross sections after cuts for all benchmark models and different values of the RPV parameter ζ, in units of fb. The errors are Poisson errors and the center-of-mass energy 8 TeV.

When dealing with very low background levels, a Gaussian approximation may not be adequate, and one should assume the number of events to be Poisson distributed. Under the null hypothesis of B background events, the probability of observing N or fewer events is then

$$P(N; B) = \sum_{k=0}^{N} \frac{B^k}{k!} e^{-B} \, , \tag{5.23}$$

given that the expectation value B is the true mean. We denote the expected number of events predicted by the model with S. To estimate the integrated luminosity[8] needed for a 5 sigma detection, one can require that there is a value for the minimum number of observed events $N_{\mathrm{obs}} = N + 1$ such that $1 - P(N; B) < 2.9 \times 10^{-5}$ %, corresponding to five standard deviations in the case of a one-sided Gaussian. In addition, N_{obs} has to satisfy $(1 - P(N; S + B))$ being larger than some probability P_{obs} for observation under the hypothesis of our model.[9]

In our case, the expectation is $B = 0$, and in principle any $S > 0$ would constitute a signal. In a real measurement, however, the estimated background will be known only to a limited precision, and we will require $N_{\mathrm{obs}} \geq 5$ in order to have some margin to allow for systematic uncertainties. In Figure 5.21 we present results assuming a P_{obs} of 50 %, 90 % and 99 %. We see that the integrated luminosities of $\sim 30\,\mathrm{fb}^{-1}$ expected in the 8 TeV run at the LHC would suffice for discovery of the lightest higgsinos with RPV in the range $\zeta \sim 2 \times 10^{-9}$–$2 \times 10^{-8}$, and for ζ above 6×10^{-9} masses of $\mu = 400\,\mathrm{GeV}$ may be reached.

After applying the mass edge method described in section 5.5.4 to one of our benchmark models, we estimate that 30 signal events are sufficient to reconstruct the neutralino mass with a couple of GeV's precision. Figure 5.22 shows the resulting integrated luminosities at which the higgsino mass could be determined at the LHC running at 8 TeV for our benchmark models.

We use our 8 TeV results to estimate the reach when LHC runs at the design centre-of-mass energy of 14 TeV, by the same statistical analysis applied after a naive scaling of the cross sections after cuts with the factors $\sigma_{14}^{\mathrm{tot}}/\sigma_{8}^{\mathrm{tot}}$ presented in Table 5.20. Since the background is assumed to be completely removed by our cuts, the reach at 14 TeV would be significantly improved. Larger higgsino masses can be reached at smaller integrated luminosities, as can

---

[8]The integrated luminosity is $\mathcal{L} = \sigma N$ where σ is the cross section and N the number of events.

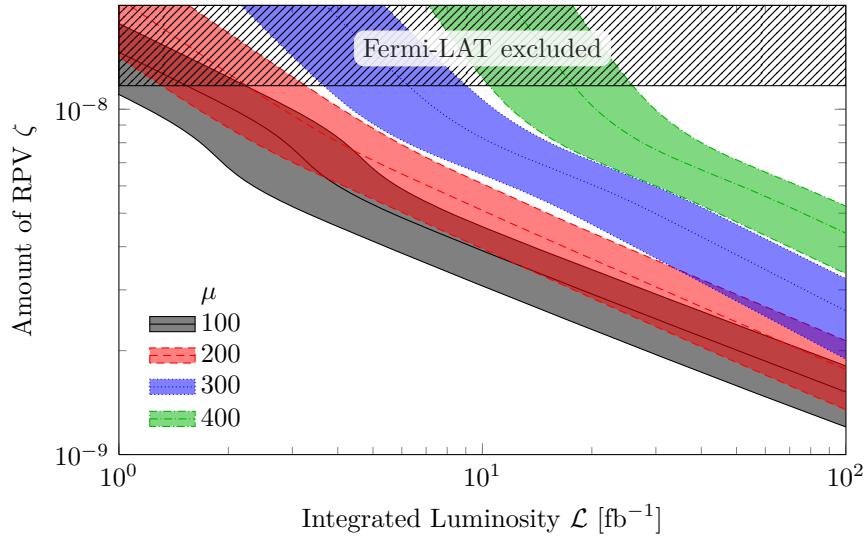[9]For a discussion of the statistical measures used for this kind of study, see Appendix B of [154].

Figure 5.21: Discovery reach with 8 TeV centre-of-mass energy at the LHC for our four benchmark models. Each coloured band represents a value of μ and the lower, middle and upper line on each band corresponds to $P_{\text{obs}} = 50\%$, 90% and 99%, respectively.
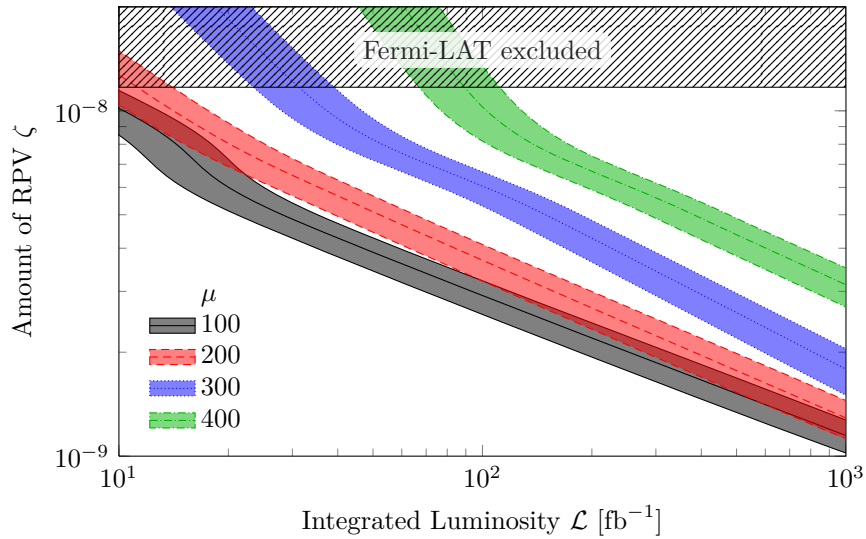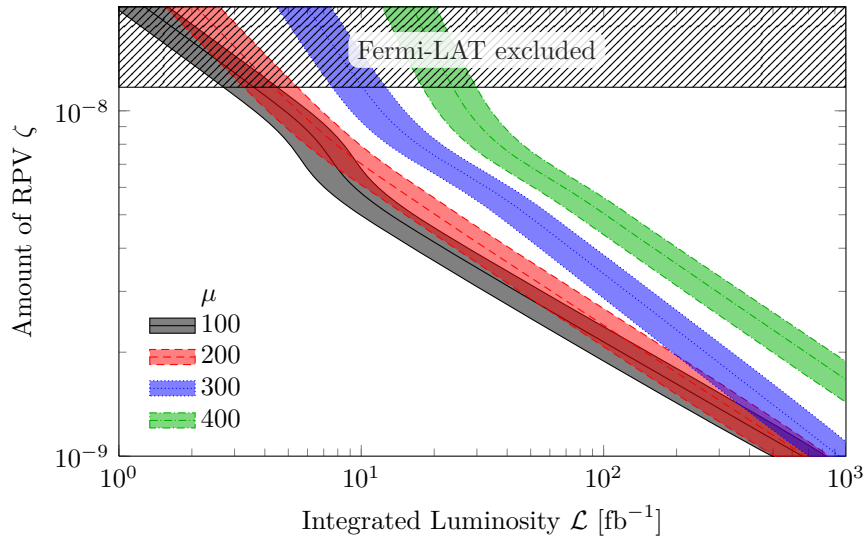

Figure 5.22: Mass reconstruction reach at 8 TeV under the assumption that $S = 40$ events (middle line of each coloured band) are sufficient in order to reconstruct the neutralino mass. The lower and bands correspond to $S = 30$ and $S = 50$ events, respectively, and $P_{\text{obs}} \approx 50\%$.
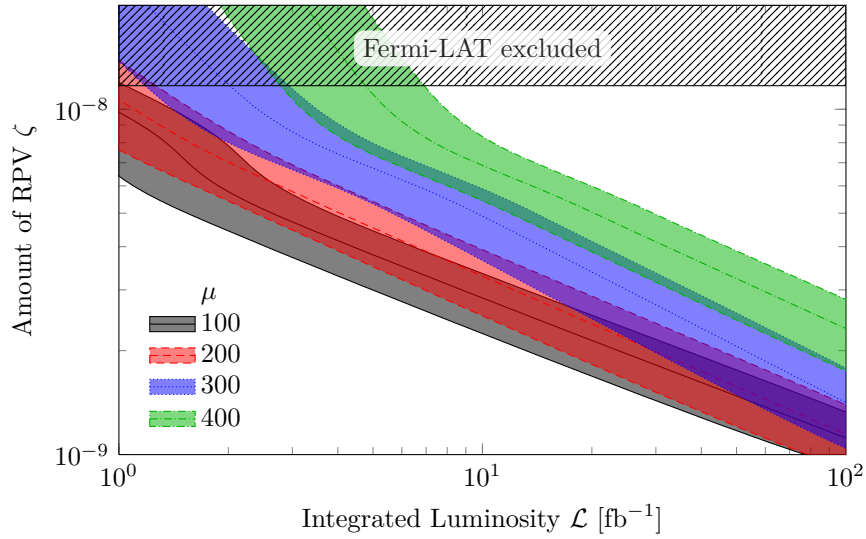
Figure 5.23: Estimation of the $14\,\mathrm{TeV}$ discovery reach based on our $8\,\mathrm{TeV}$ results. Each colored band represents a value of μ and the lower, middle and upper line on each band corresponds to $P_\mathrm{obs} = 50\,\%$, $90\,\%$ and $99\,\%$, respectively.

Figure 5.24: Estimation of the mass reconstruction reach for $14\,\mathrm{TeV}$ based on our $8\,\mathrm{TeV}$ analysis, under the assumption that $S = 40$ events are sufficient in order to reconstruct the neutralino mass. The bands correspond to the interval spanning between 30 and 50 events, and $P_\mathrm{obs} \approx 50\,\%$.

be observed in Figure 5.23. Also the luminosity which is needed in order to reconstruct the neutralino masses is reduced, as can be seen in Figure 5.24. These results are approximate and we expect that changes in *e.g.* the PT cut on the muons may be needed to deal with systematic effects such as increasing pileup.

Chapter 6

Summary and Outlook

We have studied a supersymmetric extension of the SM with small R-parity breaking related to spontaneous $B - L$ breaking, which is consistent with primordial nucleosynthesis, thermal leptogenesis and gravitino DM. We have considered both SUGRA models with universal boundary conditions at the GUT scale, which lead to a scalar tau or a bino-like neutralino as the NLSP, as well as models with hybrid gauge-gravity mediation, which lead to a higgsino-like neutralino as the NLSP. We have analysed bilinear R-parity breaking in a basis of scalar SU(2) doublets, where all bilinear terms vanish. In this basis one has R-parity violating Yukawa and gaugino couplings. They are given in terms of ordinary Yukawa couplings and nine R-parity breaking parameters, which are constrained by the flavour symmetry of the model. Flavour independent processes connected to EW symmetry breaking are described by just one linear combination of these parameters, ζ, which can be used as a overall measure of RPV. The R-parity violating couplings include terms proportional to the up-quark Yukawa couplings, which were not taken into account in previous analyses.

We have derived the branching ratios for gravitino LSP as well as neutralino and scalar tau NLSP decays, along with the quantitative connection between these. Furthermore we have calculated the implications of Fermi-LAT data on the isotropic diffuse gamma-ray flux for superparticle decays at the LHC. In order to establish this connection one needs the relevant R-parity breaking matrix elements of neutral, charged and supercurrents. These matrix elements can be obtained analytically to good approximation, since the diagonalization of the neutralino-neutrino and chargino-lepton mass matrices in powers of the EW scale over the SUSY scale converges well. The analytic expressions for the decay rates make the implications of the Fermi-LAT data for NLSP decays very transparent. It is intriguing that the observation of a photon line in the diffuse gamma-ray flux, together with a measurement of the neutralino lifetime at the LHC, can yield a microscopic determination of the Planck mass, a crucial test of local SUSY.

For a light neutralino NLSP the Fermi-LAT data yield a lower bound of several centimeters. This bound does not depend on the details of the superparticle mass spectrum or the flavour structure of the model. It directly follows from the comparison of two-particle gravitino and neutralino decays. On the contrary, there exists no model-independent lower bound on the scalar tau-decay length. The natural relation between gravitino and scalar tau-decay widths, leading to similar bounds as for neutralino NLSP, can be avoided by fine-tuning. In this case the cosmological constraint that the baryon asymmetry is not washed out leads to the lower bound of some millimeters.

The prospects of finding SUSY at the LHC strongly depends on the masses of the coloured particles. If the lightest of these particles is still in reach of the LHC it leads, in general, to interesting signatures. On the other hand, if the lightest coloured particle is too heavy to be produced at the LHC, neutralino NLSP with masses just above the LEP bound might evade the searches at the CMS and ATLAS detectors.

In order to quantify this statement we have analysed complementary to the usually analysed CMSSM and simplified models with RPC the CMSSM with bilinear RPV as well as models featuring light higgsinos with both, conserved R-parity and relatively light stops as well as broken R-parity and heavy coloured particles.

We have studied the qualitative signatures of these events, the $\beta\gamma$ distribution of the produced NLSPs, the MPT-spectrum and the number of leptons in the final state. A detailed simulation of signal and background events for the generic detector DELPHES (with CMS tune) has been performed with emphasis on the reconstruction of muons. The major uncertainty in the present study is the unknown background from cosmic muons. The crucial new element of our analysis has been the implementation of the finite NLSP decay length.

As representative examples for strongly produced bino-like neutralino NLSP we have considered five benchmark points, HH27–HH80, with gluino and squark masses ranging from $650\,\text{GeV}$ to $1800\,\text{GeV}$.[1] We have determined the range of the RPV parameter ζ which can be probed at the LHC running at the center-of-mass energy of $7\,\text{TeV}$, for varying superparticle masses. As a conservative starting point, we have focused on events with a clean signature: cascade processes with jets where one of the produced neutralino NLSPs decays into a Z boson and a neutrino, with a subsequent decay of the Z boson into a muon pair.

The sensitivity extends from decay lengths of less than a meter, with NLSP decays mostly inside the detector, to values of several kilometers where almost all NLSPs decay outside the detector. The results for the discovery reach for quasi-stable bino-like neutralino NLSPs roughly agree with the simple estimates which one obtains from the branching ratios into the $Z(\mu^+\mu^-)\nu$ final state together with the assumption that these events are background free.

As a second RPV scenario we have investigated the LHC detection prospects for the light higgsino scenario (LHS), in the MSSM extended with bilinear R-parity breaking terms. Because the higgsinos are nearly mass degenerate and the strongly interacting superparticles are out of reach, such a scenario within the usual MSSM is difficult to probe at the LHC. The prospects change if we allow for RPV, which also in this model leads to a consistent cosmology where leptogenesis and gravitino DM can be accounted for without conflict with BBN.

This motivated our study of a di-muon LHC signature with macroscopic and large displaced vertices. We simulated events and detector response for a few benchmark models, varying the value of the higgsino mass parameter μ and the amount of RPV. We found that this scenario can show up already in the data of the $8\,\text{TeV}$ run at the LHC and that the reach in the RPV parameter ζ is improved by up to an order of magnitude compared to the current reach of gamma-ray searches.

We also demonstrated that in the case of a signal, the LHS with RPV hypothesis can be tested further by a mass edge reconstruction. Except for the largest ζ and smallest higgsino masses considered, the luminosity accumulated during the $8\,\text{TeV}$ run may not be enough. However, based on a our rough estimation of the $14\,\text{TeV}$ reach, the higgsino mass in all our

---

[1]The lighter benchmark points considered in this model are already excluded by more recent LHC searches (*cf. e.g.* [155]), the main idea of searching for strongly produced neutralinos in displaced vertices, however, remains unchanged.

benchmark scenarios can be determined in the 14 TeV run, requiring integrated luminosities in the range 30–1000 fb^{-1}. We conclude that for neutralino masses accessible at the LHC values of the R-parity breaking parameter ζ can be probed which are far below the present upper bounds obtained from astrophysics and cosmology.

Given the absence of a signal in the searches for supersymmetry at the LHC it becomes more important to consider also models resulting in signals without large missing transverse energy (the key signature in SUSY searches). We have proposed search strategies for two models leading to signals easily disregarded at the LHC, namely small R-parity violation and light higgsinos with heavy coloured particles.

The prospects of finding possible RPV signals at the LHC are good as long as the overall scale of RPV is not too small. With more advanced simulation software, used by the LHC experiments, the severe restriction to muon final states in the RPV searches can be relaxed and a much larger fraction of events can be used for the analysis. So far the experimental collaborations have focused on large values of RPV, in principle, however, they should be able to extend their searches to values of R-parity breaking proposed in this work.

The search for light higgsinos with very heavy coloured particles and RPC, on the other hand, might be too challenging at the LHC. At a linear collider, however, such a scenario would be detectable.

The complementarity of gamma-ray and LHC signatures for models with RPV may also be used to falsify these models. A future observation of a gamma-ray line consistent with decaying DM would fix the gravitino mass and the value of ζ. If also a LHC signal of a neutralino shows up, which may even be possible in the LHS if the stops are light enough to be produced at the higher center-of-mass energy, the absence of any displaced decays would then render the model with RPV in conflict with experiments.

Acknowledgement

Appendix A

From the electroweak Standard Model to R-parity violating currents

In this chapter we derive formulas needed throughout this work. We begin by introducing our conventions of the EW SM. Afterwards we extend the Higgs sector of the SM to the one of the 2HDM. Looking then at the supersymmetric partners of the Higgs fields and the gauge bosons enables us to derive the currents coupling neutralinos and charginos to the gauge bosons. As we have seen in Section 3.6 the mass matrices of the neutralinos and charginos have to be diagonalized which affects the currents as well. Therefore, we calculate the currents in the mass eigenstate basis, which allows us to give the R-parity violating currents in this basis.

A.1   Electroweak Standard Model

Although the EW SM [156] can be found in every textbook about field theory we will quickly derive basic relations as some of the SUSY RPV results depend on the details of the EW SM and we would like to demonstrate that we have chosen a consistent set of definitions.

   The SM of particle physics is based on the gauge group

$$G_{\mathrm{SM}} = \mathrm{SU}(3)_{\mathrm{c}} \times \mathrm{SU}(2)_{\mathrm{w}} \times \mathrm{U}(1)_{\mathrm{Y}} \;, \tag{A.1}$$

where $\mathrm{SU}(3)_{\mathrm{c}}$ is the strong colour gauge group, $\mathrm{SU}(2)_{\mathrm{w}}$ is the weak iso-spin gauge group and the $\mathrm{U}(1)_{\mathrm{Y}}$ is the Abelian group of hypercharge.

   The covariant derivative of the SM which couples the U(1) field B_μ and the SU(2) field W_μ^i to matter fields is given by

$$D_\mu = \partial_\mu + ig'\mathrm{Y}B_\mu + ig\mathrm{T}^a W_\mu^i = \partial_\mu + \frac{i}{2}\begin{pmatrix} 2g'\mathrm{Y}B + gW_3 & gW_1 - igW_2 \\ gW_1 + igW_2 & g'\mathrm{Y}B - gW_3 \end{pmatrix} \;, \tag{A.2}$$

where g and g' are the coupling constants, Y is the hypercharge of the matter field under consideration and we have used for simplicity the spinorial generators of SU(2) $\mathrm{T}^i = \frac{1}{2}\sigma^i$ which

are proportional to the Pauli matrices

$$\sigma^1 = \begin{pmatrix} 0 & 1 \\ 1 & 0 \end{pmatrix} , \qquad \sigma^2 = \begin{pmatrix} 0 & -i \\ i & 0 \end{pmatrix} , \qquad \sigma^3 = \begin{pmatrix} 1 & 0 \\ 0 & -1 \end{pmatrix} . \qquad (A.3)$$

Due to its potential the scalar Higgs field ϕ develops a VEV v and reads in unitary gauge

$$\phi = \begin{pmatrix} v + \frac{1}{\sqrt{2}}h \\ 0 \end{pmatrix} . \qquad (A.4)$$

Applying the covariant derivative (A.2) to the Higgs field in unitary gauge, leads to

$$D_\mu \phi = \frac{1}{\sqrt{2}} \partial_\mu h + \frac{i}{2} v \begin{pmatrix} gW_\mu^3 - g'B_\mu \\ gW_\mu^1 + igW_\mu^2 \end{pmatrix} = \frac{1}{\sqrt{2}} \partial_\mu h + \frac{i}{2} v \begin{pmatrix} \sqrt{g^2 + g'^2} Z_\mu \\ \sqrt{2} g W_\mu^- \end{pmatrix} , \qquad (A.5)$$

where we have introduced linear combinations of the gauge fields

$$W_\mu^\pm = \frac{1}{\sqrt{2}} \left(W_\mu^1 \mp iW_\mu^2 \right) \qquad\qquad\qquad W_\mu^{\pm\dagger} = W_\mu^\mp , \qquad (A.6a)$$

$$\begin{pmatrix} Z_\mu^0 \\ A_\mu^0 \end{pmatrix} = \frac{1}{\sqrt{g^2 + g'^2}} \begin{pmatrix} g & -g' \\ g' & g \end{pmatrix} \begin{pmatrix} W_\mu^3 \\ B_\mu \end{pmatrix} = \begin{pmatrix} c_w & -s_w \\ s_w & c_w \end{pmatrix} \begin{pmatrix} W_\mu^3 \\ B_\mu \end{pmatrix} , \qquad (A.6b)$$

the sine and cosine of the weak mixing angle are defined by

$$s_w = \frac{g'}{\sqrt{g^2 + g'^2}} , \qquad\qquad c_w = \frac{g}{\sqrt{g^2 + g'^2}} . \qquad (A.7)$$

The adjoint of the covariant derivative is

$$(D_\mu \phi)^\dagger = \frac{1}{\sqrt{2}} \partial_\mu h - \frac{i}{2} v \begin{pmatrix} \sqrt{g^2 + g'^2} Z_\mu \\ \sqrt{2} g W_\mu^+ \end{pmatrix} \qquad (A.8)$$

Hence the mass terms originating in the kinetic Lagrangian of the Higgs field are

$$\begin{aligned}
\mathcal{L} &= (D_\mu \phi)^\dagger D^\mu \phi \\
&\supset \frac{1}{4} v^2 \left((g^2 + g'^2) Z_\mu Z^\mu + 2g^2 W_\mu^- W^{+\mu} \right) \\
&= \frac{1}{2} m_Z^2 Z_\mu Z^\mu + m_W W_\mu^- W^{+\mu} .
\end{aligned} \qquad (A.9)$$

where we have introduced canonically normalized masses for the gauge fields Z_μ and W_μ, whereas the photon A_μ stays massless

$$m_A = 0 , \quad m_W = \frac{1}{\sqrt{2}} gv , \quad m_Z = \frac{1}{\sqrt{2}} \sqrt{g^2 + g'^2} v = \frac{1}{\sqrt{2}} \frac{g'}{s_w} v , \quad m_W = m_Z c_w . \qquad (A.10)$$

With the knowledge of the mass eigenstates we can rewrite the covariant derivative (A.2) as

$$
D_\mu = \partial_\mu + \frac{i}{2}
\begin{pmatrix}
\frac{(2\mathrm{Y}+1)gg'A_\mu - (2\mathrm{Y}g'^2 - g^2)Z_\mu}{\sqrt{g'^2+g^2}} & \sqrt{2}gW_\mu^+ \\
\sqrt{2}gW_\mu^- & \frac{(2\mathrm{Y}-1)gg'A_\mu - (2\mathrm{Y}g'^2 + g^2)Z_\mu}{\sqrt{g'^2+g^2}}
\end{pmatrix}
$$

$$
= \partial_\mu + \frac{i}{2}
\begin{pmatrix}
(2\mathrm{Y}+1)eA_\mu - (2Y s_w g' - c_w g)Z_\mu & \sqrt{2}gW_\mu^+ \\
\sqrt{2}gW_\mu^- & (2\mathrm{Y}-1)eA_\mu - (2Y s_w g' + c_w g)Z_\mu
\end{pmatrix}
$$

$$
= \partial_\mu + \frac{i}{\sqrt{2}}g(W_\mu^+ \mathrm{T}^+ + W_\mu^- \mathrm{T}^-) + ieZ_\mu(t_w^{-1}\mathrm{T}^3 - t_w\mathrm{Y}) + ieA_\mu(\mathrm{T}^3 + \mathrm{Y})
$$

$$
= \partial_\mu + \frac{i}{\sqrt{2}}g(W_\mu^+ \mathrm{T}^+ + W_\mu^- \mathrm{T}^-) + ic_w^{-1}eZ_\mu(s_w^{-1}\mathrm{T}^3 - s_w\mathrm{Q}) + ieA_\mu\mathrm{Q} , \tag{A.11}
$$

where we have introduced the electric charge e, the electric charge quantum number Q and the ladder operators $\mathrm{T}^\pm$

$$
e = \frac{gg'}{\sqrt{g^2 + g'^2}} = s_w g = c_w g' , \qquad \mathrm{Q} = \mathrm{T}^3 + \mathrm{Y} , \qquad \mathrm{T}^\pm = \mathrm{T}^1 \pm i\mathrm{T}^2 . \tag{A.12}
$$

Finally, the fine-structure constant α is given by

$$
e^2 = g^2 s_w^2 = 4\pi\alpha . \tag{A.13}
$$

A.2   Two Higgs doublet model

Fermion masses in the SM are generated by Yukawa couplings to the Higgs field. In the MSSM the superpotential has to be holomorphic, therefore, no Yukawa couplings involving the conjugate of the Higgs field are allowed and a second Higgs field has to come into play. Hence we introduce the standard notation for 2HDMs under the constraint that CP is conserved and no tree level FCNC are present [157, 158]. In this case there are eight fields, three of them are the usual Goldstone bosons, the remaining five are physical fields. The neutral scalar Higgs fields acquire VEVs and are mixing to four eigenstates distinguished by being either CP even or odd and light or heavy

$$
\begin{pmatrix} H_u^0 \\ H_d^0 \end{pmatrix} = \begin{pmatrix} v_u \\ v_d \end{pmatrix} + \frac{1}{\sqrt{2}} \begin{pmatrix} c_\alpha & s_\alpha \\ -s_\alpha & c_\alpha \end{pmatrix} \begin{pmatrix} h^0 \\ H^0 \end{pmatrix} + \frac{i}{\sqrt{2}} \begin{pmatrix} s_{\beta_0} & c_{\beta_0} \\ -c_{\beta_0} & s_{\beta_0} \end{pmatrix} \begin{pmatrix} G^0 \\ A^0 \end{pmatrix} \tag{A.14}
$$

where v_u and v_d are the VEVs of the Higgs fields. They are related to the SM Higgs VEV via

$$
v^2 = v_d^2 + v_u^2 , \qquad v_d = vc_\beta , \qquad v_u = vs_\beta , \qquad \frac{v_u}{v_d} = \tan\beta . \tag{A.15}
$$

In the decoupling limit all but one Higgs field become much heavier than the EW scale $m_{A^0} \gg m_Z$

$$
\alpha \simeq \beta - \frac{\pi}{2} , \qquad c_\alpha \simeq s_\beta , \qquad s_\alpha \simeq -c_\beta . \tag{A.16}
$$

In the decoupling limit we can neglect the heavier fields and the covariant derivative of the two Higgs fields are

$$D_\mu \phi_d = \partial_\mu + \frac{i}{2}\left(-g'B_\mu \begin{pmatrix} 1 \\ 0 \end{pmatrix} + gW_\mu^1 \begin{pmatrix} 0 \\ 1 \end{pmatrix} + gW_\mu^2 \begin{pmatrix} 0 \\ i \end{pmatrix} + gW_\mu^3 \begin{pmatrix} 1 \\ 0 \end{pmatrix}\right)\left(v_d - \frac{s_\alpha}{\sqrt{2}}h^0\right)$$

$$= -\frac{s_\alpha}{\sqrt{2}}\partial_\mu h^0 + \frac{i}{2}vc_\beta \begin{pmatrix} gW_\mu^3 - g'B_\mu \\ gW_\mu^1 + igW_\mu^2 \end{pmatrix} = -\frac{s_\alpha}{\sqrt{2}}\partial_\mu h^0 + \frac{i}{2}vc_\beta \begin{pmatrix} \sqrt{g^2+g'^2}Z_\mu \\ \sqrt{2}gW_\mu^- \end{pmatrix} \quad , \text{ (A.17a)}$$

$$D_\mu \phi_u = \partial_\mu + \frac{i}{2}\left(g'B_\mu \begin{pmatrix} 0 \\ 1 \end{pmatrix} + gW_\mu^1 \begin{pmatrix} 1 \\ 0 \end{pmatrix} + gW_\mu^2 \begin{pmatrix} -i \\ 0 \end{pmatrix} + gW_\mu^3 \begin{pmatrix} 0 \\ -1 \end{pmatrix}\right)\left(v_u + \frac{c_\alpha}{\sqrt{2}}h^0\right)$$

$$= \frac{c_\alpha}{\sqrt{2}}\partial_\mu h^0 + \frac{i}{2}vs_\beta \begin{pmatrix} gW_\mu^1 - igW_\mu^2 \\ g'B_\mu - gW_\mu^3 \end{pmatrix} = \frac{c_\alpha}{\sqrt{2}}\partial_\mu h^0 + \frac{i}{2}vs_\beta \begin{pmatrix} \sqrt{2}gW_\mu^+ \\ -\sqrt{g^2+g'^2}Z_\mu \end{pmatrix} \quad . \text{ (A.17b)}$$

A.3 Minimal supersymmetric standard model

The EW sector of the MSSM is a supersymmetric version of the 2HDM. Therefore, do not only have to take into account the scalar Higgs fields but also the fermionic higgsinos. The covariant derivative of the down type higgsino is given by

$$D_\mu h_d = \partial_\mu \begin{pmatrix} h_d^0 \\ h_d^- \end{pmatrix} + \frac{i}{\sqrt{2}}g\left(W_\mu^+ \begin{pmatrix} h_d^- \\ 0 \end{pmatrix} + W_\mu^- \begin{pmatrix} 0 \\ h_d^0 \end{pmatrix}\right) + \frac{i}{2}\frac{g}{c_w}Z_\mu \begin{pmatrix} h_d^0 \\ -c_{2w}h_d^- \end{pmatrix} + \frac{i}{2}eA_\mu \begin{pmatrix} 0 \\ h_d^- \end{pmatrix} ,$$
$$\text{(A.18)}$$

Whereas the covariant derivative of the up type higgsino is

$$D_\mu h_u = \partial_\mu \begin{pmatrix} h_u^+ \\ h_u^0 \end{pmatrix} + \frac{i}{\sqrt{2}}g\left(W_\mu^+ \begin{pmatrix} h_u^0 \\ 0 \end{pmatrix} + W_\mu^- \begin{pmatrix} 0 \\ h_u^+ \end{pmatrix}\right) + \frac{i}{2}\frac{g}{c_w}Z_\mu \begin{pmatrix} c_{2w}h_u^+ \\ -h_u^0 \end{pmatrix} + \frac{i}{2}eA_\mu \begin{pmatrix} h_u^+ \\ 0 \end{pmatrix} ,$$
$$\text{(A.19)}$$

Finally, as the quantum numbers of the down type Higgs are identical to the lepton superfield, we have to as well take into account the covariant derivative of the lepton doublet

$$D_\mu l_i = \partial_\mu \begin{pmatrix} \nu_i \\ e_i \end{pmatrix} + \frac{i}{\sqrt{2}}g\left(W_\mu^+ \begin{pmatrix} e_i \\ 0 \end{pmatrix} + W_\mu^- \begin{pmatrix} 0 \\ \nu_i \end{pmatrix}\right) + \frac{i}{2}\frac{g}{c_w}Z_\mu \begin{pmatrix} \nu_i \\ -c_{2w}e_i \end{pmatrix} + \frac{i}{2}eA_\mu \begin{pmatrix} 0 \\ e_i \end{pmatrix} ,$$
$$\text{(A.20)}$$

A.4 Neutral and charged currents

For a phenomenological analysis we need the couplings of the gauge fields *i.e.* photon, Z and W boson to charged and neutral matter.

$$\mathcal{L} = -eJ_{e\mu}A^\mu - \frac{g}{c_w}J_{Z\mu}Z^\mu - \frac{g}{\sqrt{2}}J_\mu^- W^{+\mu} - \frac{g}{\sqrt{2}}J_\mu^+ W^{-\mu} - \frac{1}{2M_{\rm P}}\overline{\psi}_\mu S^\mu . \tag{A.21}$$

The couplings of gauge bosons to fermions arise from the covariant derivatives in the fermionic kinetic terms. In the two component notation the kinetic terms have the form

$$\mathcal{L} = i\overline{\lambda}^i \overline{\sigma}^\mu (D_\mu)_i^{\ j} \lambda_j \ , \tag{A.22}$$

In the case of the chiral multiplet we have to consider the higgsinos and the leptons. The kinetic term for the down type higgsino reads

$$h_d^\dagger \overline{\sigma}^\mu D_\mu h_d = \frac{1}{\sqrt{2}} g h_d^{0\dagger} \overline{\sigma}^\mu W_\mu^+ h_d^- + \frac{1}{\sqrt{2}} g h_d^{-\dagger} \overline{\sigma}^\mu W_\mu^- h_d^0 + \frac{1}{2} \frac{g}{c_w} h_d^{0\dagger} \overline{\sigma}^\mu Z_\mu h_d^0$$
$$- \frac{1}{2} \frac{g}{c_w} c_{2w} h_d^{-\dagger} \overline{\sigma}^\mu Z_\mu h_d^- + e h_d^{-\dagger} \overline{\sigma}^\mu A_\mu h_d^- \ . \tag{A.23}$$

The same term for the up type higgsino is given by

$$h_u^\dagger \overline{\sigma}^\mu D_\mu h_u = \frac{1}{\sqrt{2}} g h_u^{+\dagger} \overline{\sigma}^\mu W_\mu^+ h_u^0 + \frac{1}{\sqrt{2}} g h_u^{0\dagger} \overline{\sigma}^\mu W_\mu^- h_u^+ + \frac{1}{2} \frac{g}{c_w} h_u^{+\dagger} c_{2w} \overline{\sigma}^\mu Z_\mu h_u^+$$
$$- \frac{1}{2} \frac{g}{c_w} h_u^{0\dagger} \overline{\sigma}^\mu Z_\mu h_u^0 + e h_u^{+\dagger} \overline{\sigma}^\mu A_\mu h_u^+ \ . \tag{A.24}$$

The kinetic term for the lepton doublet is

$$l_i^\dagger \overline{\sigma}^\mu D_\mu l_i = \frac{1}{\sqrt{2}} g \nu_i^\dagger \overline{\sigma}^\mu W_\mu^+ e_i + \frac{1}{\sqrt{2}} g e_i^\dagger \overline{\sigma}^\mu W_\mu^- \nu_i + \frac{1}{2} \frac{g}{c_w} \nu_i^\dagger \overline{\sigma}^\mu Z_\mu \nu_i$$
$$- \frac{1}{2} \frac{g}{c_w} e_i^\dagger c_{2w} \overline{\sigma}^\mu Z_\mu e_i + e e^\dagger \overline{\sigma}^\mu A_\mu e_i \tag{A.25}$$

and, finally, for the lepton singlet we find

$$e_i^\dagger \overline{\sigma}^\mu D_\mu e_i = s_w^2 \frac{g}{c_w} \overline{e}_i^c \overline{\sigma}^\mu e_i^c Z_\mu - e \overline{e}_i^c \overline{\sigma}^\mu e_i^c A_\mu \ . \tag{A.26}$$

Additionally we have to calculate the kinetic terms of the fermions of the vector multiplet. The bino is not charged under the SM gauge group and does not couple to vector fields. The winos are in the adjoint representation of the SU(2), therefore we need the generators of the adjoint representation [159–161]

$$T^1 = \begin{pmatrix} 0 & 0 & 0 \\ 0 & 0 & -i \\ 0 & i & 0 \end{pmatrix} \ , \qquad T^2 = \begin{pmatrix} 0 & 0 & i \\ 0 & 0 & 0 \\ -i & 0 & 0 \end{pmatrix} \ , \qquad T^3 = \begin{pmatrix} 0 & -i & 0 \\ i & 0 & 0 \\ 0 & 0 & 0 \end{pmatrix} \ . \tag{A.27}$$

This enables us to write the covariant derivative of the wino as

$$D_\mu w_i = \partial_\mu \begin{pmatrix} w_1 \\ w_2 \\ w_3 \end{pmatrix} + \frac{i}{2} g \left(W_\mu^+ \begin{pmatrix} -w_3 \\ -iw_3 \\ \sqrt{2}w^- \end{pmatrix} + W_\mu^- \begin{pmatrix} w_3 \\ -iw_3 \\ -\sqrt{2}w^+ \end{pmatrix} \right) + e \left(t_w^{-1} Z_\mu + A_\mu \right) \begin{pmatrix} -w_2 \\ w_1 \\ 0 \end{pmatrix} \tag{A.28}$$

where we have introduced charged wino eigenstates

$$w^\pm = \frac{1}{\sqrt{2}} \left(w_1 \mp iw_2 \right) \ , \qquad\qquad w^{\pm\dagger} = \frac{1}{\sqrt{2}} \left(w_1^\dagger \pm iw_2^\dagger \right) \ . \tag{A.29}$$

Hence the kinetic term becomes

$$iw^{i\dagger}\bar{\sigma}^{\mu}D_{\mu}w^{i} = iw^{i\dagger}\bar{\sigma}^{\mu}\partial_{\mu}w^{i} + g\left(w^{+\dagger}\bar{\sigma}^{\mu}w^{3} - w_{3}^{\dagger}\bar{\sigma}^{\mu}w^{-}\right)W_{\mu}^{+} \tag{A.30}$$

$$+ g\left(w_{3}^{\dagger}\bar{\sigma}^{\mu}w^{+} - w^{-\dagger}\bar{\sigma}^{\mu}w^{3}\right)W_{\mu}^{-} + e\left(t_{w}^{-1}Z_{\mu} + A_{\mu}\right)\left(w^{-\dagger}w^{-} - w^{+\dagger}w^{+}\right) .$$

We can verify that based on our definition of the Pauli matrices we have chosen the correct definition for the vector representation by noting that the identity

$$w_{i}^{\dagger}T_{ijk}W_{k}^{\mu}w_{j} = 4\,\mathrm{tr}\,w_{i}^{\dagger}\sigma_{i}W_{j}^{\mu}\sigma_{j}w_{k}\sigma_{k} , \tag{A.31}$$

holds. Finally, we are able to collect the various terms, in order to derive the currents in the gauge eigenstate basis

$$\begin{aligned}
J_{e\mu} &= J_{e\mu}^{3} + J_{e\mu}^{2,1} \\
&= \overline{w}^{+}\bar{\sigma}_{\mu}w^{+} - \overline{w}^{-}\bar{\sigma}_{\mu}w^{-} - \bar{e}_{i}\bar{\sigma}_{\mu}e_{i} + \bar{e}_{i}^{c}\bar{\sigma}_{\mu}e_{i}^{c} - \overline{h}_{d}^{-}\bar{\sigma}_{\mu}h_{d}^{-} + \overline{h}_{u}^{+}\bar{\sigma}_{\mu}h_{u}^{+} ,
\end{aligned} \tag{A.32a}$$

$$\begin{aligned}
J_{Z\mu} &= -\frac{1}{2}\overline{h}_{u}^{0}\bar{\sigma}_{\mu}h_{u}^{0} + \frac{1}{2}\overline{h}_{d}^{0}\bar{\sigma}_{\mu}h_{d}^{0} + \frac{1}{2}\overline{\nu}_{i}\bar{\sigma}_{\mu}\nu_{i} \\
&\quad + \overline{w}^{+}\bar{\sigma}_{\mu}w^{+} - \overline{w}^{-}\bar{\sigma}_{\mu}w^{-} - \frac{1}{2}\bar{e}_{i}\bar{\sigma}_{\mu}e_{i} - \frac{1}{2}\overline{h}_{d}^{-}\bar{\sigma}_{\mu}h_{d}^{-} + \frac{1}{2}\overline{h}_{u}^{+}\bar{\sigma}_{\mu}h_{u}^{+} - s_{w}^{2}J_{e\mu}^{2,1} ,
\end{aligned} \tag{A.32b}$$

$$J_{\mu}^{-} = \sqrt{2}\left(\overline{w}^{3}\bar{\sigma}_{\mu}w^{-} - \overline{w}^{+}\bar{\sigma}_{\mu}w^{3}\right) + \overline{\nu}_{i}\bar{\sigma}_{\mu}e_{i} + \overline{h}_{d}^{0}\bar{\sigma}_{\mu}h_{d}^{-} + \overline{h}_{u}^{+}\bar{\sigma}_{\mu}h_{u}^{0} , \tag{A.32c}$$

$$J_{\mu}^{+} = \sqrt{2}\left(\overline{w}^{-}\bar{\sigma}_{\mu}w^{3} - \overline{w}^{3}\bar{\sigma}_{\mu}w^{+}\right) - \bar{e}_{i}\bar{\sigma}_{\mu}\nu_{i} - \overline{h}_{d}^{-}\bar{\sigma}_{\mu}h_{d}^{0} - \overline{h}_{u}^{0}\bar{\sigma}_{\mu}h_{u}^{+} . \tag{A.32d}$$

Having derived the currents we now have to transform them into the mass-eigenstate basis of the fermions.

A.4.1 The currents in the mass eigenstate basis

The masses of the neutral and charged fermions of MSSM are collected in the mass matrices (3.58) and (3.70) and are diagonalized with (3.65) and (3.73). The higgsino and neutrino mass gauge eigenstates read in terms of the mass eigenstates

$$b = U_{1b}^{(\chi^{0})}\chi_{b}^{0} + U_{1j}^{(\chi^{0},\nu)}\nu_{j}' , \tag{A.33}$$

$$w^{3} = U_{2b}^{(\chi^{0})}\chi_{b}^{0} + U_{2j}^{(\chi^{0},\nu)}\nu_{j}' , \qquad w^{-} = U_{1\beta}^{(\chi^{-})}\chi_{\beta}^{-} + U_{1j}^{(\chi^{-},e)}e_{j}' , \quad w^{+} = \widetilde{U}_{1\beta}^{(\chi^{+})}\chi_{\beta}^{+} + \widetilde{U}_{1j}^{(\chi^{+},e^{c})}e_{j}^{c\prime} ,$$

$$h_{u}^{0} = U_{3b}^{(\chi^{0})}\chi_{b}^{0} + U_{3j}^{(\chi^{0},\nu)}\nu_{j}' , \qquad\qquad\qquad h_{u}^{+} = \widetilde{U}_{2\beta}^{(\chi^{+})}\chi_{\beta}^{+} + \widetilde{U}_{2j}^{(\chi^{+},e^{c})}e_{j}^{c\prime} ,$$

$$h_{d}^{0} = U_{4b}^{(\chi^{0})}\chi_{b}^{0} + U_{4j}^{(\chi^{0},\nu)}\nu_{j}' , \qquad h_{d}^{-} = U_{2\beta}^{(\chi^{-})}\chi_{\beta}^{-} + U_{2j}^{(\chi^{-},e)}e_{j}' ,$$

$$\nu_{i} = U_{ib}^{(\nu,\chi^{0})}\chi_{b}^{0} + U_{ij}^{(\nu)}\nu_{j}' , \qquad e_{i} = U_{i\beta}^{(e,\chi^{-})}\chi_{\beta}^{-} + U_{ij}^{(e)}e_{j}' , \qquad e_{i}^{c} = \widetilde{U}_{i\beta}^{(e^{c},\chi^{+})}\chi_{\beta}^{+} + \widetilde{U}_{ij}^{(e^{c})}e_{j}^{c\prime} .$$

Therefore, the photon current in mass eigenstates is

$$\begin{aligned}
J_{e\mu} &= \overline{\chi}_{\alpha}^{+}\widetilde{U}_{1\alpha}^{(\chi^{+})}\bar{\sigma}_{\mu}\widetilde{U}_{1\beta}^{(\chi^{+})}\chi_{\beta}^{+} + \overline{\chi}_{\alpha}^{+}\widetilde{U}_{1\alpha}^{(\chi^{+})}\bar{\sigma}_{\mu}\widetilde{U}_{1j}^{(\chi^{+},e^{c})}e_{j}^{c\prime} + \bar{e}_{i}^{c\prime}\widetilde{U}_{1i}^{(\chi^{+},e^{c})}\bar{\sigma}_{\mu}\widetilde{U}_{1\beta}^{(\chi^{+})}\chi_{\beta}^{+} \\
&\quad + \bar{e}_{i}^{c\prime}\widetilde{U}_{1i}^{(\chi^{+},e^{c})}\bar{\sigma}_{\mu}\widetilde{U}_{1j}^{(\chi^{+},e^{c})}e_{j}^{c\prime} - \overline{\chi}_{\alpha}^{-}U_{1\alpha}^{(\chi^{-})}\bar{\sigma}_{\mu}U_{1\beta}^{(\chi^{-})}\chi_{\beta}^{-} - \overline{\chi}_{\alpha}^{-}U_{1\alpha}^{(\chi^{-})}\bar{\sigma}_{\mu}U_{1j}^{(\chi^{-},e)}e_{j}' \\
&\quad - \bar{e}_{i}'U_{1i}^{(\chi^{-},e)}\bar{\sigma}_{\mu}U_{1\beta}^{(\chi^{-})}\chi_{\beta}^{-} - \bar{e}_{i}'U_{1i}^{(\chi^{-},e)}\bar{\sigma}_{\mu}U_{1j}^{(\chi^{-},e)}e_{j}' - \overline{\chi}_{\alpha}^{-}U_{i\alpha}^{(e,\chi^{-})}\bar{\sigma}_{\mu}U_{i\beta}^{(e,\chi^{-})}\chi_{\beta}^{-} \\
&\quad - \overline{\chi}_{\alpha}^{-}U_{i\alpha}^{(e,\chi^{-})}\bar{\sigma}_{\mu}U_{ij}^{(e)}e_{j}' - \bar{e}_{i}'U_{ki}^{(e)}\bar{\sigma}_{\mu}U_{k\beta}^{(e,\chi^{-})}\chi_{\beta}^{-} - \bar{e}_{i}'U_{ki}^{(e)}\bar{\sigma}_{\mu}U_{kj}^{(e)}e_{j}' \\
&\quad + \overline{\chi}_{\alpha}^{+}\widetilde{U}_{i\alpha}^{(e^{c},\chi^{+})}\bar{\sigma}_{\mu}\widetilde{U}_{i\beta}^{(e^{c},\chi^{+})}\chi_{\beta}^{+} + \overline{\chi}_{\alpha}^{+}\widetilde{U}_{i\alpha}^{(e^{c},\chi^{+})}\bar{\sigma}_{\mu}\widetilde{U}_{ij}^{(e^{c})}e_{j}^{c\prime} + \bar{e}_{i}^{c\prime}\widetilde{U}_{ki}^{(e^{c})}\bar{\sigma}_{\mu}\widetilde{U}_{k\beta}^{(e^{c},\chi^{+})}\chi_{\beta}^{+} \\
&\quad + \bar{e}_{i}^{c\prime}\widetilde{U}_{ki}^{(e^{c})}\bar{\sigma}_{\mu}\widetilde{U}_{kj}^{(e^{c})}e_{j}^{c\prime} - \overline{\chi}_{\alpha}^{-}U_{2\alpha}^{(\chi^{-})}\bar{\sigma}_{\mu}U_{2\beta}^{(\chi^{-})}\chi_{\beta}^{-} - \overline{\chi}_{\alpha}^{-}U_{2\alpha}^{(\chi^{-})}\bar{\sigma}_{\mu}U_{2j}^{(\chi^{-},e)}e_{j}' \\
&\quad - \bar{e}_{i}'U_{2i}^{(\chi^{-},e)}\bar{\sigma}_{\mu}U_{2\beta}^{(\chi^{-})}\chi_{\beta}^{-} - \bar{e}_{i}'U_{2i}^{(\chi^{-},e)}\bar{\sigma}_{\mu}U_{2j}^{(\chi^{-},e)}e_{j}' + \overline{\chi}_{\alpha}^{+}\widetilde{U}_{2\alpha}^{(\chi^{+})}\bar{\sigma}_{\mu}\widetilde{U}_{2\beta}^{(\chi^{+})}\chi_{\beta}^{+} \\
&\quad + \overline{\chi}_{\alpha}^{+}\widetilde{U}_{2\alpha}^{(\chi^{+})}\bar{\sigma}_{\mu}\widetilde{U}_{2j}^{(\chi^{+},e^{c})}e_{j}^{c\prime} + \bar{e}_{i}^{c\prime}\widetilde{U}_{2i}^{(\chi^{+},e^{c})}\bar{\sigma}_{\mu}\widetilde{U}_{2\beta}^{(\chi^{+})}\chi_{\beta}^{+} + \bar{e}_{i}^{c\prime}\widetilde{U}_{2i}^{(\chi^{+},e^{c})}\bar{\sigma}_{\mu}\widetilde{U}_{2j}^{(\chi^{+},e^{c})}e_{j}^{c\prime} ,
\end{aligned} \tag{A.34}$$

which can be combined to

$$J_{e\mu} = \overline{\chi}_\alpha^- \overline{\sigma}_\mu V_{\alpha\beta}^{(\chi^-)} \chi_\beta^- + \overline{\chi}_\alpha^+ \overline{\sigma}_\mu V_{\alpha\beta}^{(\chi^+)} \chi_\beta^+ + \overline{e}_i \overline{\sigma}_\mu V_{ij}^{(e)} e_j + \overline{e}_i^c \overline{\sigma}_\mu V_{ij}^{(e^c)} e_j^c$$
$$+ \left(\overline{\chi}_\alpha^- \overline{\sigma}_\mu V_{\alpha j}^{(\chi^-,e)} e_j + \overline{\chi}_\alpha^+ \overline{\sigma}_\mu V_{\alpha j}^{(\chi^+,e^c)} e_j^c + \text{h.c.} \right) , \tag{A.35}$$

where we have introduced the CKM-like matrices

$$V_{\alpha\beta}^{(\chi^-)} = -U_{1\alpha}^{(\chi^-)} U_{1\beta}^{(\chi^-)} - U_{2\alpha}^{(\chi^-)} U_{2\beta}^{(\chi^-)} - \sum_i U_{i\alpha}^{(e,\chi^-)} U_{i\beta}^{(e,\chi^-)} , \tag{A.36a}$$

$$V_{\alpha\beta}^{(\chi^+)} = \widetilde{U}_{1\alpha}^{(\chi^+)} \widetilde{U}_{1\beta}^{(\chi^+)} + \widetilde{U}_{2\alpha}^{(\chi^+)} \widetilde{U}_{2\beta}^{(\chi^+)} + \sum_i \widetilde{U}_{i\alpha}^{(e^c,\chi^+)} \widetilde{U}_{i\beta}^{(e^c,\chi^+)} , \tag{A.36b}$$

$$V_{ij}^{(e)} = -U_{1i}^{(\chi^-,e)} U_{1j}^{(\chi^-,e)} - U_{2i}^{(\chi^-,e)} U_{2j}^{(\chi^-,e)} - \sum_k U_{ki}^{(e)} U_{kj}^{(e)} , \tag{A.36c}$$

$$V_{ij}^{(e^c)} = \widetilde{U}_{1i}^{(\chi^+,e^c)} \widetilde{U}_{1j}^{(\chi^+,e^c)} + \widetilde{U}_{2i}^{(\chi^+,e^c)} \widetilde{U}_{2j}^{(\chi^+,e^c)} + \sum_k \widetilde{U}_{ki}^{(e^c)} \widetilde{U}_{kj}^{(e^c)} , \tag{A.36d}$$

$$V_{\alpha j}^{(\chi^-,e)} = -U_{1\alpha}^{(\chi^-)} U_{1j}^{(\chi^-,e)} - U_{2\alpha}^{(\chi^-)} U_{2j}^{(\chi^-,e)} - \sum_i U_{i\alpha}^{(e,\chi^-)} U_{ij}^{(e)} , \tag{A.36e}$$

$$V_{\alpha j}^{(\chi^+,e^c)} = \widetilde{U}_{1\alpha}^{(\chi^+)} \widetilde{U}_{1j}^{(\chi^+,e^c)} + \widetilde{U}_{2\alpha}^{(\chi^+)} \widetilde{U}_{2j}^{(\chi^+,e^c)} + \sum_i \widetilde{U}_{i\alpha}^{(e^c,\chi^+)} \widetilde{U}_{ij}^{(e^c)} . \tag{A.36f}$$

On the other hand, the neutral current in the mass eigenstate basis is

$$J_{Z\mu} = -\frac{1}{2} \overline{\chi}_a^0 U_{3a}^{(\chi^0)} \overline{\sigma}_\mu U_{3b}^{(\chi^0)} \chi_b^0 - \frac{1}{2} \overline{\chi}_a^0 U_{3a}^{(\chi^0)} \overline{\sigma}_\mu U_{3j}^{(\chi^0,\nu)} \nu_j' - \frac{1}{2} \overline{\nu}_j' U_{3j}^{(\chi^0,\nu)} \overline{\sigma}_\mu U_{3b}^{(\chi^0)} \chi_b^0$$
$$-\frac{1}{2} \overline{\nu}_i' U_{3i}^{(\chi^0,\nu)} \overline{\sigma}_\mu U_{3j}^{(\chi^0,\nu)} \nu_j' + \frac{1}{2} \overline{\chi}_a^0 U_{4a}^{(\chi^0)} \overline{\sigma}_\mu U_{4b}^{(\chi^0)} \chi_b^0 + \frac{1}{2} \overline{\chi}_a^0 U_{4a}^{(\chi^0)} \overline{\sigma}_\mu U_{4j}^{(\chi^0,\nu)} \nu_j'$$
$$+\frac{1}{2} \overline{\nu}_j' U_{4j}^{(\chi^0,\nu)} \overline{\sigma}_\mu U_{4b}^{(\chi^0)} \chi_b^0 + \frac{1}{2} \overline{\nu}_j' U_{4j}^{(\chi^0,\nu)} \overline{\sigma}_\mu U_{4j}^{(\chi^0,\nu)} \nu_j' + \frac{1}{2} \overline{\chi}_a^0 U_{ia}^{(\nu,\chi^0)} \overline{\sigma}_\mu U_{ib}^{(\nu,\chi^0)} \chi_b^0$$
$$+\frac{1}{2} \overline{\chi}_a^0 U_{ia}^{(\nu,\chi^0)} \overline{\sigma}_\mu U_{ij}^{(\nu)} \nu_j' + \frac{1}{2} \overline{\nu}_j' U_{ij}^{(\nu)} \overline{\sigma}_\mu U_{ib}^{(\nu,\chi^0)} \chi_b^0 + \frac{1}{2} \overline{\nu}_i' U_{ki}^{(\nu)} \overline{\sigma}_\mu U_{kj}^{(\nu)} \nu_j'$$
$$+\overline{\chi}_\alpha^+ \widetilde{U}_{1\alpha}^{(\chi^+)} \overline{\sigma}_\mu \widetilde{U}_{1\beta}^{(\chi^+)} \chi_\beta^+ + \overline{\chi}_\alpha^+ \widetilde{U}_{1\alpha}^{(\chi^+)} \overline{\sigma}_\mu \widetilde{U}_{1j}^{(\chi^+,e^c)} e_j^{c\prime} + \overline{e}_i^{c\prime} \widetilde{U}_{1i}^{(\chi^+,e^c)} \overline{\sigma}_\mu \widetilde{U}_{1\beta}^{(\chi^+)} \chi_\beta^+$$
$$+\overline{e}_i^{c\prime} \widetilde{U}_{1i}^{(\chi^+,e^c)} \overline{\sigma}_\mu \widetilde{U}_{1j}^{(\chi^+,e^c)} e_j^{c\prime} - \overline{\chi}_\alpha^- U_{1\alpha}^{(\chi^-)} \overline{\sigma}_\mu U_{1\beta}^{(\chi^-)} \chi_\beta^- - \overline{\chi}_\alpha^- U_{1\alpha}^{(\chi^-)} \overline{\sigma}_\mu U_{1j}^{(\chi^-,e)} e_j'$$
$$-\overline{e}_i' U_{1i}^{(\chi^-,e)} \overline{\sigma}_\mu U_{1\beta}^{(\chi^-)} \chi_\beta^- - \overline{e}_i' U_{1i}^{(\chi^-,e)} \overline{\sigma}_\mu U_{1j}^{(\chi^-,e)} e_j' - \frac{1}{2} \overline{\chi}_\alpha^- U_{i\alpha}^{(e,\chi^-)} \overline{\sigma}_\mu U_{i\beta}^{(e,\chi^-)} \chi_\beta^-$$
$$-\frac{1}{2} \overline{\chi}_\alpha^- U_{i\alpha}^{(e,\chi^-)} \overline{\sigma}_\mu U_{ij}^{(e)} e_j' - \frac{1}{2} \overline{e}_i' U_{ki}^{(e)} \overline{\sigma}_\mu U_{k\beta}^{(e,\chi^-)} \chi_\beta^- - \frac{1}{2} \overline{e}_i' U_{ki}^{(e)} \overline{\sigma}_\mu U_{kj}^{(e)} e_j'$$
$$-\frac{1}{2} \overline{\chi}_\alpha^- U_{2\alpha}^{(\chi^-)} \overline{\sigma}_\mu U_{2\beta}^{(\chi^-)} \chi_\beta^- - \frac{1}{2} \overline{\chi}_\alpha^- U_{2\alpha}^{(\chi^-)} \overline{\sigma}_\mu U_{2j}^{(\chi^-,e)} e_j' - \frac{1}{2} \overline{e}_i' U_{2i}^{(\chi^-,e)} \overline{\sigma}_\mu U_{2\beta}^{(\chi^-)} \chi_\beta^-$$
$$-\frac{1}{2} \overline{e}_i' U_{2i}^{(\chi^-,e)} \overline{\sigma}_\mu U_{2j}^{(\chi^-,e)} e_j' + \frac{1}{2} \overline{\chi}_\alpha^+ \widetilde{U}_{2\alpha}^{(\chi^+)} \overline{\sigma}_\mu \widetilde{U}_{2\beta}^{(\chi^+)} \chi_\beta^+ + \frac{1}{2} \overline{\chi}_\alpha^+ \widetilde{U}_{2\alpha}^{(\chi^+)} \overline{\sigma}_\mu \widetilde{U}_{2j}^{(\chi^+,e^c)} e_j^{c\prime}$$
$$+\frac{1}{2} \overline{e}_i^{c\prime} \widetilde{U}_{2i}^{(\chi^+,e^c)} \overline{\sigma}_\mu \widetilde{U}_{2\beta}^{(\chi^+)} \chi_\beta^+ + \frac{1}{2} \overline{e}_i^{c\prime} \widetilde{U}_{2i}^{(\chi^+,e^c)} \overline{\sigma}_\mu \widetilde{U}_{2j}^{(\chi^+,e^c)} e_j^{c\prime} - s_w^2 J_{e\mu} . \tag{A.37}$$

This can be combined to

$$J_{Z\mu} = \overline{\chi}_a^0 \overline{\sigma}_\mu V_{ab}^{(\chi^0)} \chi_b^0 + \overline{\chi}_\alpha^- \overline{\sigma}_\mu V_{\alpha\beta}^{(\chi^-)} \chi_\beta^- + \overline{\chi}_\alpha^+ \overline{\sigma}_\mu V_{\alpha\beta}^{(\chi^+)} \chi_\beta^+ + \overline{\nu}_i \overline{\sigma}_\mu V_{ij}^{(\nu)} \nu_j + \overline{e}_i \overline{\sigma}_\mu V_{ij}^{(e)} e_j \tag{A.38}$$
$$+ \overline{e}_i^c \overline{\sigma}_\mu V_{ij}^{(e^c)} e_j^c + \left(\overline{\chi}_a^0 \overline{\sigma}_\mu V_{aj}^{(\chi,\nu)} \nu_j + \overline{\chi}_\alpha^- \overline{\sigma}_\mu V_{\alpha j}^{(\chi^-,e)} e_j + \overline{\chi}_\alpha^+ \overline{\sigma}_\mu V_{\alpha j}^{(\chi^+,e^c)} e_j^c + \text{h.c.} \right) - s_w^2 J_{e\mu} ,$$

where we have introduced the CKM-like matrices

$$V_{ab}^{(\chi^0)} = -\frac{1}{2}U_{3a}^{(\chi^0)}U_{3b}^{(\chi^0)} + \frac{1}{2}U_{4a}^{(\chi^0)}U_{4b}^{(\chi^0)} + \frac{1}{2}\sum_i U_{ia}^{(\nu,\chi^0)}U_{ib}^{(\nu,\chi^0)} \, , \tag{A.39a}$$

$$V_{\alpha\beta}^{(\chi^-)} = -U_{1\alpha}^{(\chi^-)}U_{1\beta}^{(\chi^-)} - \frac{1}{2}U_{2\alpha}^{(\chi^-)}U_{2\beta}^{(\chi^-)} - \frac{1}{2}\sum_i U_{i\alpha}^{(e,\chi^-)}U_{i\beta}^{(e,\chi^-)} \, , \tag{A.39b}$$

$$V_{\alpha\beta}^{(\chi^+)} = \widetilde{U}_{1\alpha}^{(\chi^+)}\widetilde{U}_{1\beta}^{(\chi^+)} + \frac{1}{2}\widetilde{U}_{2\alpha}^{(\chi^+)}\widetilde{U}_{2\beta}^{(\chi^+)} \, , \tag{A.39c}$$

$$V_{ij}^{(\nu)} = -\frac{1}{2}U_{3i}^{(\chi^0,\nu)}U_{3j}^{(\chi^0,\nu)} + \frac{1}{2}U_{4i}^{(\chi^0,\nu)}U_{4j}^{(\chi^0,\nu)} + \frac{1}{2}\sum_k U_{ki}^{(\nu)}U_{kj}^{(\nu)} \, , \tag{A.39d}$$

$$V_{ij}^{(e)} = -U_{1i}^{(\chi^-,e)}U_{1j}^{(\chi^-,e)} - \frac{1}{2}U_{2i}^{(\chi^-,e)}U_{2j}^{(\chi^-,e)} - \frac{1}{2}\sum_k U_{ki}^{(e)}U_{kj}^{(e)} \, , \tag{A.39e}$$

$$V_{ij}^{(e^c)} = \widetilde{U}_{1i}^{(\chi^+,e^c)}\widetilde{U}_{1j}^{(\chi^+,e^c)} + \frac{1}{2}\widetilde{U}_{2i}^{(\chi^+,e^c)}\widetilde{U}_{2j}^{(\chi^+,e^c)} \, , \tag{A.39f}$$

$$V_{aj}^{(\chi,\nu)} = -\frac{1}{2}U_{3a}^{(\chi^0)}U_{3j}^{(\chi^0,\nu)} + \frac{1}{2}U_{4a}^{(\chi^0)}U_{4j}^{(\chi^0,\nu)} + \frac{1}{2}\sum_k U_{ka}^{(\nu,\chi^0)}U_{kj}^{(\nu)} \, , \tag{A.39g}$$

$$V_{\alpha j}^{(\chi^-,e)} = -U_{1\alpha}^{(\chi^-)}U_{1j}^{(\chi^-,e)} - \frac{1}{2}U_{2\alpha}^{(\chi^-)}U_{2j}^{(\chi^-,e)} - \frac{1}{2}\sum_i U_{i\alpha}^{(e,\chi^-)}U_{ij}^{(e)} \, , \tag{A.39h}$$

$$V_{\alpha j}^{(\chi^+,e^c)} = \widetilde{U}_{1\alpha}^{(\chi^+)}\widetilde{U}_{1j}^{(\chi^+,e^c)} + \frac{1}{2}\widetilde{U}_{2\alpha}^{(\chi^+)}\widetilde{U}_{2j}^{(\chi^+,e^c)} \, . \tag{A.39i}$$

Finally, the complete neutral CKM-like matrices are given by

$$V_{ab}^{(\chi^0)} = -\frac{1}{2}U_{3a}^{(\chi^0)}U_{3b}^{(\chi^0)} + \frac{1}{2}U_{4a}^{(\chi^0)}U_{4b}^{(\chi^0)} + \frac{1}{2}\sum_i U_{ia}^{(\nu,\chi^0)}U_{ib}^{(\nu,\chi^0)} \, , \tag{A.40a}$$

$$V_{\alpha\beta}^{(\chi^-)} = (s_w^2 - 1)U_{1\alpha}^{(\chi^-)}U_{1\beta}^{(\chi^-)} + (s_w^2 - \frac{1}{2})U_{2\alpha}^{(\chi^-)}U_{2\beta}^{(\chi^-)} + (s_w^2 - \frac{1}{2})\sum_i U_{i\alpha}^{(e,\chi^-)}U_{i\beta}^{(e,\chi^-)} \, ,$$
$$\tag{A.40b}$$

$$V_{\alpha\beta}^{(\chi^+)} = (1 - s_w^2)\widetilde{U}_{1\alpha}^{(\chi^+)}\widetilde{U}_{1\beta}^{(\chi^+)} + (\frac{1}{2} - s_w^2)\widetilde{U}_{2\alpha}^{(\chi^+)}\widetilde{U}_{2\beta}^{(\chi^+)} - s_w^2\sum_i \widetilde{U}_{i\alpha}^{(e^c,\chi^+)}\widetilde{U}_{i\beta}^{(e^c,\chi^+)} \, , \tag{A.40c}$$

$$V_{ij}^{(\nu)} = -\frac{1}{2}U_{3i}^{(\chi^0,\nu)}U_{3j}^{(\chi^0,\nu)} + \frac{1}{2}U_{4i}^{(\chi^0,\nu)}U_{4j}^{(\chi^0,\nu)} + \frac{1}{2}\sum_k U_{ki}^{(\nu)}U_{kj}^{(\nu)} \, , \tag{A.40d}$$

$$V_{ij}^{(e)} = (s_w^2 - 1)U_{1i}^{(\chi^-,e)}U_{1j}^{(\chi^-,e)} + (s_w^2 - \frac{1}{2})U_{2i}^{(\chi^-,e)}U_{2j}^{(\chi^-,e)} + (s_w^2 - \frac{1}{2})\sum_k U_{ki}^{(e)}U_{kj}^{(e)} \, ,$$
$$\tag{A.40e}$$

$$V_{ij}^{(e^c)} = (1 - s_w^2)\widetilde{U}_{1i}^{(\chi^+,e^c)}\widetilde{U}_{1j}^{(\chi^+,e^c)} + (\frac{1}{2} - s_w^2)\widetilde{U}_{2i}^{(\chi^+,e^c)}\widetilde{U}_{2j}^{(\chi^+,e^c)} - s_w^2\sum_k \widetilde{U}_{ki}^{(e^c)}\widetilde{U}_{kj}^{(e^c)} \, , \tag{A.40f}$$

$$V_{aj}^{(\chi,\nu)} = -\frac{1}{2}U_{3a}^{(\chi^0)}U_{3j}^{(\chi^0,\nu)} + \frac{1}{2}U_{4a}^{(\chi^0)}U_{4j}^{(\chi^0,\nu)} + \frac{1}{2}\sum_k U_{ka}^{(\nu,\chi^0)}U_{kj}^{(\nu)} \, , \tag{A.40g}$$

$$V_{\alpha j}^{(\chi^-,e)} = (s_w^2 - 1)U_{1\alpha}^{(\chi^-)}U_{1j}^{(\chi^-,e)} + (s_w^2 - \frac{1}{2})U_{2\alpha}^{(\chi^-)}U_{2j}^{(\chi^-,e)} + (s_w^2 - \frac{1}{2})\sum_i U_{i\alpha}^{(e,\chi^-)}U_{ij}^{(e)} \, ,$$
$$\tag{A.40h}$$

$$V_{\alpha j}^{(\chi^+,e^c)} = (1 - s_w^2)\widetilde{U}_{1\alpha}^{(\chi^+)}\widetilde{U}_{1j}^{(\chi^+,e^c)} + (\frac{1}{2} - s_w^2)\frac{1}{2}\widetilde{U}_{2\alpha}^{(\chi^+)}\widetilde{U}_{2j}^{(\chi^+,e^c)} - s_w^2\sum_i \widetilde{U}_{i\alpha}^{(e^c,\chi^+)}\widetilde{U}_{ij}^{(e^c)} \, . \tag{A.40i}$$

The charged current is given by

$$
\begin{aligned}
J_\mu^- =\; & \sqrt{2}\; \overline{\chi}_b^0 U_{2b}^{(\chi^0)} \overline{\sigma}_\mu U_{1\beta}^{(\chi^-)} \chi_\beta^- + \sqrt{2}\; \overline{\chi}_b^0 U_{2b}^{(\chi^0)} \overline{\sigma}_\mu U_{1j}^{(\chi^-,e)} e_j' + \sqrt{2}\; \overline{\nu}_j' U_{2j}^{(\chi^0,\nu)} \overline{\sigma}_\mu U_{1\beta}^{(\chi^-)} \chi_\beta^- \\
& + \sqrt{2}\; \overline{\nu}_k' U_{2k}^{(\chi^0,\nu)} \overline{\sigma}_\mu U_{1j}^{(\chi^-,e)} e_j' - \sqrt{2}\; \overline{\chi}_\beta^+ \widetilde{U}_{1\beta}^{(\chi^+)} \overline{\sigma}_\mu U_{2b}^{(\chi^0)} \chi_b^0 - \sqrt{2}\; \overline{\chi}_\beta^+ \widetilde{U}_{1\beta}^{(\chi^+)} \overline{\sigma}_\mu U_{2k}^{(\chi^0,\nu)} \nu_k' \\
& - \sqrt{2}\; \overline{e}_j^{c'} \widetilde{U}_{1j}^{(\chi^+,e^c)} \overline{\sigma}_\mu U_{2b}^{(\chi^0)} \chi_b^0 - \sqrt{2}\; \overline{e}_j^{c'} \widetilde{U}_{1j}^{(\chi^+,e^c)} \overline{\sigma}_\mu U_{2k}^{(\chi^0,\nu)} \nu_k' + \overline{\chi}_b^0 U_{ib}^{(\nu,\chi^0)} \overline{\sigma}_\mu U_{i\beta}^{(e,\chi^-)} \chi_\beta^- \\
& + \overline{\chi}_b^0 U_{ib}^{(\nu,\chi^0)} \overline{\sigma}_\mu U_{ij}^{(e)} e_j' + \overline{\nu}_j' U_{ij}^{(\nu)} \overline{\sigma}_\mu U_{i\beta}^{(e,\chi^-)} \chi_\beta^- + \overline{\nu}_k' U_{ik}^{(\nu)} \overline{\sigma}_\mu U_{ij}^{(e)} e_j' \\
& + \overline{\chi}_b^0 U_{3b}^{(\chi^0)} \overline{\sigma}_\mu U_{2\beta}^{(\chi^-)} \chi_\beta^- + \overline{\chi}_b^0 U_{3b}^{(\chi^0)} \overline{\sigma}_\mu U_{2j}^{(\chi^-,e)} e_j' + \overline{\nu}_j' U_{3j}^{(\chi^0,\nu)} \overline{\sigma}_\mu U_{2\beta}^{(\chi^-)} \chi_\beta^- \\
& + \overline{\nu}_k' U_{3k}^{(\chi^0,\nu)} \overline{\sigma}_\mu U_{2j}^{(\chi^-,e)} e_j' + \overline{\chi}_\beta^+ \widetilde{U}_{2\beta}^{(\chi^+)} \overline{\sigma}_\mu U_{3b}^{(\chi^0)} \chi_b^0 + \overline{\chi}_\beta^+ \widetilde{U}_{2\beta}^{(\chi^+)} \overline{\sigma}_\mu U_{3j}^{(\chi^0,\nu)} \nu_j' \\
& + \overline{e}_j^{c'} \widetilde{U}_{2j}^{(\chi^+,e^c)} \overline{\sigma}_\mu U_{3b}^{(\chi^0)} \chi_b^0 + \overline{e}_j^{c'} \widetilde{U}_{2j}^{(\chi^+,e^c)} \overline{\sigma}_\mu U_{3k}^{(\chi^0,\nu)} \nu_k' \; .
\end{aligned}
\tag{A.41}
$$

This can be combined to

$$
\begin{aligned}
J_\mu^- =\; & \overline{\chi}_a^0 \overline{\sigma}_\mu V_{a\beta}^{(\chi)} \chi_\beta^- + \overline{\chi}_\alpha^+ \overline{\sigma}_\mu V_{\alpha b}^{(\chi)} \chi_b^0 + \overline{\chi}_a^0 \overline{\sigma}_\mu V_{aj}^{(\chi,e)} e_j + \overline{e}_i^c \overline{\sigma}_\mu V_{ib}^{(\chi,e)} \chi_b^0 \\
& + \overline{\nu}_i \overline{\sigma}_\mu V_{i\beta}^{(\nu,\chi)} \chi_\beta^- + \overline{\chi}_\alpha^+ \overline{\sigma}_\mu V_{\alpha j}^{(\nu,\chi)} \nu_j + \overline{\nu}_i \overline{\sigma}_\mu V_{ij}^{(\nu,e)} e_j + \overline{e}_i^c \overline{\sigma}_\mu V_{ij}^{(\nu,e)} \nu_j \; ,
\end{aligned}
\tag{A.42}
$$

where we have introduce the CKM-like matrices

$$
V_{a\beta}^{(\chi)} = \sqrt{2}\; U_{2a}^{(\chi^0)} U_{1\beta}^{(\chi^-)} + U_{3a}^{(\chi^0)} U_{2\beta}^{(\chi^-)} + \sum_k U_{ka}^{(\nu,\chi^0)} U_{k\beta}^{(e,\chi^-)} \; ,
\tag{A.43a}
$$

$$
V_{\alpha b}^{(\chi)} = -\sqrt{2}\; \widetilde{U}_{1\alpha}^{(\chi^+)} U_{2b}^{(\chi^0)} + \widetilde{U}_{2\alpha}^{(\chi^+)} U_{3b}^{(\chi^0)} \; ,
\tag{A.43b}
$$

$$
V_{aj}^{(\chi,e)} = \sqrt{2}\; U_{2a}^{(\chi^0)} U_{1j}^{(\chi^-,e)} + U_{3a}^{(\chi^0)} U_{2j}^{(\chi^-,e)} + \sum_k U_{ka}^{(\nu,\chi^0)} U_{kj}^{(e)} \; ,
\tag{A.43c}
$$

$$
V_{ib}^{(\chi,e)} = -\sqrt{2}\; \widetilde{U}_{1i}^{(\chi^+,e^c)} U_{2b}^{(\chi^0)} + \widetilde{U}_{2i}^{(\chi^+,e^c)} U_{3b}^{(\chi^0)} \; ,
\tag{A.43d}
$$

$$
V_{i\beta}^{(\nu,\chi)} = \sqrt{2}\; U_{2i}^{(\chi^0,\nu)} U_{1\beta}^{(\chi^-)} + U_{3i}^{(\chi^0,\nu)} U_{2\beta}^{(\chi^-)} + \sum_k U_{ki}^{(\nu)} U_{k\beta}^{(e,\chi^-)} \; ,
\tag{A.43e}
$$

$$
V_{\alpha j}^{(\nu,\chi)} = -\sqrt{2}\; \widetilde{U}_{1\alpha}^{(\chi^+)} U_{2j}^{(\chi^0,\nu)} + \widetilde{U}_{2\alpha}^{(\chi^+)} U_{3j}^{(\chi^0,\nu)} \; ,
\tag{A.43f}
$$

$$
V_{ij}^{(\nu,e)} = \sqrt{2}\; U_{2i}^{(\chi^0,\nu)} U_{1j}^{(\chi^-,e)} + U_{3i}^{(\chi^0,\nu)} U_{2j}^{(\chi^-,e)} + \sum_k U_{ki}^{(\nu)} U_{kj}^{(e)} \; ,
\tag{A.43g}
$$

$$
V_{ij}^{(\nu,e)} = -\sqrt{2}\; \widetilde{U}_{1i}^{(\chi^+,e^c)} U_{2j}^{(\chi^0.\nu)} + \widetilde{U}_{2i}^{(\chi^+,e^c)} U_{3j}^{(\chi^0.\nu)} \; .
\tag{A.43h}
$$

Finally, we have to calculate the Higgs to neutralino and neutrino. After rotation into mass eigenstates the coupling induced by the Lagrangian (3.57) reads

$$
\widetilde{V}_{i1}^{(\nu,\chi)} = \sum_j \zeta_j \left(t_w U_{1j}^{(\chi,\nu)} U_{i1}^{(\nu,\chi)} + t_w U_{ij}^{(\nu)} U_{11}^{(\chi)} - U_{2j}^{(\chi,\nu)} U_{i2}^{(\nu,\chi)} - U_{ij}^{(\nu)} U_{21}^{(\chi)} \right) \; .
\tag{A.44}
$$

A.4.2   R-parity violating currents

The following results are approximated by an expansion in ζ and ϵ, where $\epsilon = m_Z / \tilde{m}$ and $\tilde{m}$ the largest mass parameters of either M_1, M_2 or μ. The parameter choice affects neither the expansion of $U^{(n)}$ nor the mass eigenstates. For the RPV part of the neutral CKM-like matrix

we find

$$V_{aj}^{(\chi,\nu)} = -\frac{1}{2}\zeta_j m_Z \begin{pmatrix} \frac{s_w}{M_1} \\ -\frac{c_w}{M_2} \\ \frac{m_Z}{\sqrt{2}\mu}v_1 \\ \frac{m_Z}{\sqrt{2}\mu}v_2 \end{pmatrix} \left(1 + \mathcal{O}\left(\frac{m_Z}{\tilde{m}}\right)\right) , \tag{A.45}$$

with abbreviations

$$v_1 = (s_\beta + c_\beta)\frac{M_1 c_w^2 + M_2 s_w^2 - \mu}{(M_1 - \mu)(M_2 - \mu)} - (s_\beta - c_\beta)\left(\frac{s_w^2}{M_1} + \frac{c_w^2}{M_2}\right) , \tag{A.46a}$$

$$v_2 = (s_\beta - c_\beta)\frac{M_1 c_w^2 + M_2 s_w^2 + \mu}{(M_1 + \mu)(M_2 + \mu)} - (s_\beta + c_\beta)\left(\frac{s_w^2}{M_1} + \frac{c_w^2}{M_2}\right) . \tag{A.46b}$$

Numerically, the relative errors are smaller than 0.10, 0.20, 0.15, 0.05 for $a = 1, \ldots, 4$. For the RPV part of the charged CKM-like matrix we find

$$V_{aj}^{(\chi,e)} = -\zeta_j m_Z \begin{pmatrix} \frac{s_w}{M_1} \\ \frac{c_w}{M_2} \\ \frac{m_Z}{\sqrt{2}\mu}\widetilde{v}_1 \\ \frac{m_Z}{\sqrt{2}\mu}\widetilde{v}_2 \end{pmatrix} \left(1 + \mathcal{O}\left(\frac{m_Z}{\tilde{m}}\right)\right) , \tag{A.47}$$

with abbreviations[1]

$$\widetilde{v}_1 = (s_\beta + c_\beta)\frac{M_1 c_w^2 + M_2 s_w^2 - \mu}{(M_1 - \mu)(M_2 - \mu)} - 2(s_\beta + c_\beta)\frac{\mu c_w^2}{M_2(M_2 - \mu)} + 2s_\beta \frac{c_w^2}{M_2} , \tag{A.48a}$$

$$\widetilde{v}_2 = (s_\beta - c_\beta)\frac{M_1 c_w^2 + M_2 s_w^2 + \mu}{(M_1 + \mu)(M_2 + \mu)} - 2(s_\beta + \frac{\mu}{M_2}c_\beta)\frac{M_1 + \mu}{(M_1 + \mu)(M_2 + \mu)}c_w^2 . \tag{A.48b}$$

Here we again neglected corrections that involve the Yukawa couplings h_{ii}^e. The numerical corrections to the NLO contributions to $V_{ai}^{(\chi,e)}$ are smaller than 0.05, 0.15, 0.20 for $a = 1, 2, 3$, respectively. For $a = 4$ we reach the limit of our numerical precision. The RPV part of the matrix coupling Higgs to neutrino and neutralino reads

$$\widetilde{V}_{i1}^{(\nu,\chi)} = \zeta_i \begin{pmatrix} -t_w \\ 1 \\ \frac{m_Z}{\sqrt{2}}(s_\beta + c_\beta)\frac{(M_1 - M_2)c_w + (M_2 - \mu)s_w t_w}{(\mu - M_1)(M_2 - \mu)} \\ \frac{m_Z}{\sqrt{2}}(s_\beta - c_\beta)\frac{(\mu + M_1)c_w + (M_2 + \mu)s_w t_w}{(\mu + M_1)(M_2 + \mu)} \end{pmatrix} \left(1 + \mathcal{O}\left(\frac{m_Z}{\tilde{m}}\right)\right) . \tag{A.49}$$

---

[1]The formula for $\widetilde{v}_1$ differs slightly from the version in [1], due to a typo therein.

Appendix B

Free gauge fields

In the following we would like to demonstrate a consisted way how to construct the action S for free gauge fields ϕ_μ

$$S = \int d^4x \mathcal{L} \left(\phi_\mu, \partial_\nu \phi_\mu \right) \ . \tag{B.1}$$

To that end, we replace the scalar field in the Klein-Gordon Lagrangian with a vector field A_μ and a tensor field $h_{\mu\nu}$, respectively, as well as the spinor in the Dirac Lagrangian with a spinor-vector ψ_μ. Since there are more than one Lorentz invariant combinations, we write down the most general linear combination of Lorentz scalars. Varying the action with respect to the gauge fields $\phi_\mu = A_\mu$, ψ_μ, $h_{\mu\nu}$

$$\delta S = \int d^4x \left(\frac{\partial \mathcal{L}}{\partial \phi_\mu} - \partial_\nu \frac{\partial \mathcal{L}}{\partial \partial_\nu \phi_\mu} \right) \delta \phi_\mu \ , \tag{B.2}$$

and demanding invariance under gauge transformation $\delta \phi_\mu \to f_\mu \Lambda$ fully constraints the free parameter of the action. For the massless action it is enough to introduce the gauge transformation $f_\mu = \partial_\mu$ (applied to both indices in the case of the tensor field). For the massive spinor-vector and tensor field, however, the gauge transformation must be extended to be functions of $f_\mu = f(\partial_\mu, \gamma_\mu)$ and $f_{\mu\nu} = f(\partial_\mu, \partial_\nu, \eta_{\mu\nu})$, respectively. The mass terms, however, break gauge invariance in all three cases.

In the massless case, the derived constraints single out one certain gauge condition, which leads to the massless Klein-Gordon and Dirac equation, respectively. As we would like to know how many degrees of freedom (DOFs) we have to gauge in the massless case, we also calculate the differences of DOFs between the massive and massless fields with the Stückelberg technique.

B.1 Vector field

In order to demonstrate the method we will apply this procedure to a vector field $A^\mu(x)$. Therefore, we need the most general Lorentz invariant extension of the Klein-Gordon Lagrangian which is still quadratic in $A_\mu(x)$

$$\mathcal{L} = \partial_\mu A_\nu(x) \left(a\eta^{\mu\nu}\eta^{\rho\sigma} + b\eta^{\mu\rho}\eta^{\nu\sigma} \right) \partial_\rho A_\sigma(x) + m^2 A^\nu(x) A_\nu(x) \ , \tag{B.3}$$

where a and b are free parameters. Demanding invariance under the gauge transformation

$$A^\mu(x) \rightarrow A^\mu(x) + \partial^\mu \Lambda(x) \ . \tag{B.4}$$

leads to the equation

$$(a+b)\partial_\nu \partial^2 A^\nu(x) - m^2 \partial_\nu A^\nu(x) = 0 \ . \tag{B.5}$$

We see that the invariance under gauge transformation can be fulfilled by massless fields $m = 0$ for $a = -b$. In order to make the anti-symmetry manifest one usually introduces the anti-symmetric field strength tensor

$$F_{\mu\nu}(x) = \partial_{[\mu} A_{\nu]}(x) = \partial_\mu A_\nu(x) - \partial_\nu A_\mu(x) \ . \tag{B.6}$$

The Lagrangian is now the usual Proca Lagrangian [162]

$$\mathcal{L} = -\frac{1}{4} F_{\mu\nu}(x) F^{\mu\nu}(x) + \frac{1}{2} m^2 A_\mu(x) A^\mu(x) \ , \tag{B.7}$$

extremizing leads to the Proca-equation

$$\partial_\mu F^{\mu\nu}(x) + m^2 A^\nu(x) = 0 \ . \tag{B.8}$$

We have seen that the mass term breaks gauge invariance, but instead of setting $m = 0$ we can constrain the massive vector field by

$$\partial_\nu A^\nu(x) = 0 \ . \tag{B.9}$$

This constraint simplifies the Proca equation

$$\partial^2 A^\nu(x) + m^2 A^\nu(x) = 0 \ . \tag{B.10}$$

and results in the Klein-Gordon equation for a massive vector field. This equation has four DOFs. Together with the constraint (B.9) it shows that the massive vector field has three DOFs.

B.1.1   Stückelberg Lagrangian

In the massless limit $m \rightarrow 0$ the Proca Lagrangian (B.7) becomes the Maxwell Lagrangian [163]

$$\mathcal{L} = -\frac{1}{4} F_{\mu\nu}(x) F^{\mu\nu}(x) \ , \tag{B.11}$$

which is invariant under the gauge transformation (B.4) even without the constraint (B.9). The introduction of a scalar Stückelberg field $\phi(x)$ makes also the Proca equation independent of the constraint (B.4) and circumvents this abrupt change at $m \rightarrow 0$

$$A^\mu(x) \rightarrow A^\mu(x) + \frac{\partial^\mu}{m} \phi(x) \ , \tag{B.12}$$

where we have kept track of the canonical mass dimensions by dividing the Stückelberg field by m. The resulting Lagrangian is the Stückelberg Lagrangian [164]

$$\mathcal{L} = -\frac{1}{4}F_{\mu\nu}(x)F^{\mu\nu}(x) + \frac{1}{2}m^2 A^\mu(x)A_\mu(x) + m A^\mu(x)\partial_\mu\phi(x) + \frac{1}{2}\partial^\mu\phi(x)\partial_\mu\phi(x) , \quad \text{(B.13)}$$

which still has three DOFs and is invariant under the gauge transformation

$$\delta A_\mu(x) = \partial_\mu\Lambda(x) , \qquad\qquad \delta\phi(x) = -m\Lambda(x) . \qquad\qquad \text{(B.14)}$$

Going to unitary gauge $\phi(x) = 0$ leads back to the Proca Lagrangian (B.7). The massless limit, on the other hand, leads now to the Lagrangian of a massless vector field and a massless scalar field

$$\mathcal{L} = -\frac{1}{4}F_{\mu\nu}(x)F^{\mu\nu}(x) + \frac{1}{2}\partial^\mu\phi(x)\partial_\mu\phi(x) . \qquad\qquad \text{(B.15)}$$

We see that for the massless vector field we have to gauge one DOF.

B.1.2   Maxwell equation

The massless vector field obeys the Maxwell equation

$$\partial_\mu F^{\mu\nu}(x) = 0 , \qquad\qquad\qquad \text{(B.16)}$$

and must be gauge fixed. As gauge condition one can *e.g.* demand that also for the massless vector field the constraint (B.9) is fulfilled (Lorenz gauge [165]). Applying this gauge to the Maxwell equation

$$\partial^2 A^\nu(x) = 0 , \qquad\qquad\qquad \text{(B.17)}$$

leads to the Klein-Gordon equation for a massless vector field.

B.2   Rarita-Schwinger field

A spinor-vector $\psi_\mu(x)$ transforms simultaneously under the spinor and the vector representation of the Lorentz group (for an overview see *e.g.* [166]). Therefore, we have to extend the Dirac Lagrangian with the goal to incorporate the extra vector indices without changing the linearity in the derivative.[1] This can be achieved either by reassigning the vector indices in $\slashed{\partial}$ with the metric or by using three γ-matrices instead of one

$$\mathcal{L} = \overline{\psi}_\mu(x)i\left(a\gamma^\mu\gamma^\nu\gamma^\rho + b\gamma^\mu\eta^{\nu\rho} + c\gamma^\nu\eta^{\mu\rho} + d\gamma^\rho\eta^{\mu\nu}\right)\partial_\nu\psi_\rho(x) \qquad\qquad \text{(B.18)}$$
$$= ia\overline{\psi}_\mu(x)\gamma^\mu\slashed{\partial}\gamma^\rho\psi_\rho(x) + ib\overline{\psi}_\mu(x)\gamma^\mu\partial^\rho\psi_\rho(x) + ic\overline{\psi}_\mu(x)\slashed{\partial}\psi^\mu(x) + id\overline{\psi}_\mu(x)\partial^\mu\gamma^\rho\psi_\rho(x) .$$

where we have introduced four parameters $a \dots d$ and for simplicity postponed the discussion of the mass term. Demanding invariance under the gauge transformation

$$\psi_\mu(x) \rightarrow \psi_\mu(x) + \partial_\mu\chi(x) , \qquad\qquad\qquad \text{(B.19)}$$

---

[1]In order to describe neutral-spinor vectors *e.g.* the gravitino, the Majorana reality condition $\psi_\mu^c = \psi_\mu$ has to be imposed.

leads to the equations

$$(a+d)i\partial^2\gamma^\rho\psi_\rho(x) + (b+c)i\slashed{\partial}\partial^\rho\psi_\rho(x) = 0 \ , \tag{B.20a}$$

$$(a+b)i\overline{\psi}_\mu(x)\gamma^\mu\partial^2 + (c+d)i\overline{\psi}_\mu(x)\partial^\mu\slashed{\partial} = 0 \ . \tag{B.20b}$$

These constraints can be fulfilled by $a=-b=c=-d$ and determine the form of the kinetic term of the Rarita-Schwinger Lagrangian

$$\begin{aligned}
\mathcal{L} &= a\overline{\psi}_\mu(x)i\left(\gamma^\mu\slashed{\partial}\gamma^\rho\psi_\rho(x) - \gamma^\mu\partial^\rho\psi_\rho(x) + \slashed{\partial}\psi_\rho(x) - \partial^\mu\gamma^\rho\psi^\mu(x)\right) \\
&= a\overline{\psi}_\mu(x)i\left(\gamma^\mu\gamma^\nu\gamma^\rho - \gamma^\mu\eta^{\nu\rho} + \gamma^\nu\eta^{\mu\rho} - \gamma^\rho\eta^{\mu\nu}\right)\partial_\nu\psi_\rho(x) \\
&= a\overline{\psi}_\mu(x)i\gamma^{\mu\nu\rho}\partial_\nu\psi_\rho(x) \ ,
\end{aligned} \tag{B.21}$$

where we have introduced the anti-symmetrised combination of three γ-matrices

$$\gamma^{\mu\nu\rho} = \gamma^{[\mu}\gamma^\nu\gamma^{\rho]} = \gamma^\mu\gamma^\nu\gamma^\rho - \gamma^\mu\eta^{\nu\rho} + \gamma^\nu\eta^{\mu\rho} - \gamma^\rho\eta^{\mu\nu} = -i\epsilon^{\mu\nu\rho\sigma}\gamma_\sigma\gamma^5 \ . \tag{B.22}$$

The equation of motion (EOM) for a massless spinor-vector reads

$$0 = i\gamma^{\mu\nu\rho}\partial_\nu\psi_\rho(x) \ . \tag{B.23}$$

B.2.1 Massive Rarita-Schwinger Lagrangian

Now we are adding the most general linear combination of Lorentz invariant mass terms

$$\begin{aligned}
\mathcal{L} &= \overline{\psi}_\mu(x)\left(ai\gamma^{\mu\nu\rho}\partial_\nu + em\gamma^\mu\gamma^\rho + fm\eta^{\mu\rho}\right)\psi_\rho(x) \\
&= ai\overline{\psi}_\mu(x)\gamma^{\mu\nu\rho}\partial_\nu\psi_\rho(x) + me\overline{\psi}_\mu(x)\gamma^\mu\gamma^\rho\psi_\rho(x) + mf\overline{\psi}_\mu(x)\psi^\mu(x) \ . \tag{B.24}
\end{aligned}$$

Invariance under gauge transformation (B.19) can only be ensured for $e=f=0$ or $m=0$. Demanding, however, invariance under the extended transformation

$$\psi_\mu(x) \to \psi_\mu(x) + \frac{\partial_\mu}{m}\chi(x) - i\gamma_\mu\chi(x) \ , \tag{B.25}$$

leads to

$$(2a+e)\slashed{\partial}\gamma^\rho\psi_\rho - (2a-f)\partial^\rho\psi_\rho + (4e+f)im\gamma^\rho\psi_\rho = 0 \ . \tag{B.26}$$

Hence the Lagrangian is invariant for massless fields $m=0$ with $e=-f=-2a$. Therefore, the Rarita-Schwinger Lagrangian for a massive spinor-vector is given by [167]

$$\mathcal{L} = \overline{\psi}_\mu(x)\left(i\gamma^{\mu\nu\rho}\partial_\nu - \frac{1}{2}m\gamma^{\mu\rho}\right)\psi_\rho(x) \ , \tag{B.27}$$

and the mass term breaks the gauge invariance. We have used the anti-symmetrised combination of two γ-matrices

$$\gamma^{\mu\nu} = \gamma^{[\mu}\gamma^{\nu]} = \frac{1}{2}\left[\gamma^\mu, \gamma^\nu\right]_- = \gamma^\mu\gamma^\nu - \eta^{\mu\nu} \ , \qquad \gamma^{\mu\nu\rho}\gamma_\rho = 2\gamma^{\mu\nu} \ , \qquad \gamma^{\mu\nu}\gamma_\nu = 3\gamma^\mu \ . \tag{B.28}$$

The EOM reads

$$0 = i\gamma^{\mu\nu\rho}\partial_\nu\psi_\rho(x) - \frac{1}{2}m\gamma^{\mu\rho}\psi_\rho(x) \ , \tag{B.29}$$

and its divergence leads to the relation

$$\gamma^{\nu\rho}\partial_\nu\psi_\rho(x) = \slashed{\partial}\gamma^\mu\psi_\mu - \partial^\mu\psi_\mu = 0 \ , \tag{B.30}$$

The mass term breaks the invariance under the transformation (B.25), however, instead of setting $m = 0$ we can constrain the massive spinor-vector field by

$$\gamma^\rho\psi_\rho = 0 \ . \tag{B.31}$$

Using this constraint in the Equation (B.30) leads to the additional relation

$$\partial^\rho\psi_\rho(x) = 0 \ . \tag{B.32}$$

Finally, applying these two constraints to the Rarita-Schwinger equation (B.29) shows that the massive Rarita-Schwinger field obeys the Dirac equation

$$(i\slashed{\partial} - m)\psi^\mu(x) = 0 \ , \tag{B.33}$$

The Dirac equation for a spinor-vector (B.33) represents 16 DOFs. The two constraints (B.31) and (B.32) reduce this by four constraints each. Hence we end up with eight DOFs for the massive Dirac Rarita-Schwinger field.

B.2.2   Stückelberg Rarita-Schwinger Lagrangian

The Lagrangian of the massless Rarita-Schwinger field is invariant under the transformation (B.25) even without the additional constraint (B.31). As in the case of the vector field we would like to avoid this change for $m \to 0$ by introducing a Stückelberg field $\psi'(x)$ [168]

$$\psi_\mu(x) \to \psi_\mu(x) + \frac{\partial_\mu}{m}\psi'(x) \ . \tag{B.34}$$

This field shift leads to mixing terms

$$\Delta\mathcal{L} = -\frac{1}{2}\overline{\psi}_\mu(x)\gamma^{\mu\rho}\partial_\rho\psi'(x) + \text{h.c.} \tag{B.35}$$

In contrast to the result of applying the same technique to the vector field, this does not lead to a kinetic term for the spinor field, but introduces kinetic mixing between the spinor-vector and the spinor field. In this case, however, we are able to make use of the second transformation in (B.25) by introducing the Stückelberg field $\psi''(x)$

$$\psi_\mu(x) \to \psi_\mu(x) + \gamma_\mu\psi''(x) \ , \tag{B.36}$$

which adds to the Lagrangian the terms

$$\Delta\mathcal{L} = 3\overline{\psi}''(x)\left(i\gamma^\mu\partial_\mu - m\right)\psi''(x) + \overline{\psi}_\mu(x)\left(2i\gamma^{\mu\nu}\partial_\nu - \frac{3}{2}m\gamma^\mu\right)\psi''(x) + \text{h.c.} \tag{B.37}$$

Possible mixing terms originating from the combined transformation

$$\psi_\mu(x) \to \psi_\mu(x) + \frac{\partial_\mu}{m}\psi'(x) + \gamma_\mu\psi''(x) \ , \tag{B.38}$$

vanish. Finally, the field redefinitions

$$\psi'(x) \to \frac{2\sqrt{2}}{\sqrt{3}} i\psi(x) \;, \qquad\qquad \psi''(x) \to \frac{1}{\sqrt{6}}\psi(x) \;, \qquad (B.39)$$

lead to a canonical kinetic term for the spinor field and eliminate the kinetic mixing. The Lagrangian is now given by

$$\mathcal{L} = \overline{\psi}_\mu(x) \left(i\gamma^{\mu\nu\rho}\partial_\nu - \frac{1}{2} m\gamma^{\mu\rho} \right) \psi_\rho(x) + \overline{\psi}(x) \left(i\gamma^\mu\partial_\mu - m \right) \psi(x)$$
$$- \left(\frac{\sqrt{3}}{2\sqrt{2}} m\overline{\psi}_\mu(x)\gamma^\mu\psi(x) + \text{h.c.} \right) \;, \qquad (B.40)$$

and is invariant under the transformation

$$\delta\psi_\mu(x) = \left(\gamma_\mu + 4i\frac{\partial_\mu}{m} \right) \chi(x) \;, \qquad\qquad \delta\psi(x) = -\sqrt{6}\chi(x) \;. \qquad (B.41)$$

For unitary gauge $\psi(x) \to 0$ the Lagrangian becomes the usual Rarita-Schwinger Lagrangian and for $m \to 0$ the Lagrangian becomes the Lagrangian of massless spinor-vector and and a massless spinor.

$$\mathcal{L} = \overline{\psi}_\mu(x) i\gamma^{\mu\nu\rho}\partial_\nu\psi_\rho(x) + \overline{\psi}(x) i\gamma^\mu\partial_\mu\psi(x) \;, \qquad (B.42)$$

Hence we deduce that the massless Dirac spinor-vector has four DOFs.

B.2.3   Massless Rarita-Schwinger field

Now we are turning our attention to the massless spinor-vector. First we notice that we are able to re-express the Lagrangian in terms of the γ^5-matrix and the Levi-Civita symbol (*cf.* Equation (B.22))

$$\mathcal{L} = \overline{\psi}_\mu(x)\epsilon^{\mu\nu\rho\sigma}\gamma^5\gamma_\nu\partial_\rho\psi_\sigma(x) \;. \qquad (B.43)$$

In order to simplify the EOM of the massless Rarita-Schwinger field (B.23) we further notice that the contraction of the EOM with a γ-matrix leads to the relation (B.30), which in turn reduces the EOM

$$\slashed{\partial}\psi^\mu - \partial^\mu\gamma^\rho\psi_\rho = 0 \;. \qquad (B.44)$$

Furthermore we have observed that the massless Lagrangian does not depend on the constraint (B.31) in order to be invariant under the transformation (B.25), therefore an obvious gauge condition is given by demanding that the constraint (B.31) holds as well in the massless case, which leads to

$$\slashed{\partial}\psi^\mu = 0 \;, \qquad (B.45)$$

and shows that also the massless spinor-vector obeys the Dirac equation.

B.3 Tensor field

Let us finally derive the Lagrangian describing a symmetric tensor field $h^{\mu\nu}(x) = h^{\nu\mu}(x)$. For simplicity we first derive the massless Lagrangian. The most general kinetic Lagrangian quadratic in the field is given by

$$
\begin{aligned}
\mathcal{L} &= \partial_\mu h_{\nu\rho}(x) \left\{ a\eta^{\mu\sigma}\eta^{\nu\tau}\eta^{\rho\lambda} + b\left[y\eta^{\mu\nu}\eta^{\rho\tau}\eta^{\sigma\lambda} + (1-y)\eta^{\mu\rho}\eta^{\nu\tau}\eta^{\sigma\lambda} \right] \right. \\
&\quad \left. + c\left[z\eta^{\mu\tau}\eta^{\nu\rho}\eta^{\sigma\lambda} + (1-z)\eta^{\mu\nu}\eta^{\rho\sigma}\eta^{\tau\lambda} \right] + d\eta^{\mu\sigma}\eta^{\nu\rho}\eta^{\tau\lambda} \right\} \partial_\sigma h_{\tau\lambda}(x) \\
&= a\partial^\sigma h_{\nu\rho}(x)\partial_\sigma h^{\nu\rho}(x) + b\partial^\nu h_{\nu\rho}(x)\partial_\lambda h^{\rho\lambda}(x) + c\partial^\nu h_{\nu\rho}(x)\partial^\rho h(x) + d\partial^\sigma h(x)\partial_\sigma h(x) , \quad \text{(B.46)}
\end{aligned}
$$

where $h(x) = h^\mu_\mu(x) = \eta_{\mu\nu}h^{\mu\nu}(x)$ and $a, \ldots, d$ are constants appearing in the Lagrangian, whereas y and z are constants, which only appear in the variation of the Lagrangian. Furthermore we have already taken the symmetry in the tensor field and the derivatives into account. Demanding invariance under gauge transformation with regard to the first index

$$
h_{\nu\rho}(x) \rightarrow h_{\nu\rho}(x) + \partial_\nu\xi_\rho(x) . \quad \text{(B.47)}
$$

leads to

$$
0 = \left((a+by)\partial_\nu\partial^2 h^{\nu\rho}(x) + (b(1-y)+cz)\,\partial_\nu\partial^\rho\partial_\sigma h^{\nu\sigma}(x) + (c(1-z)+d)\,\partial^2\partial^\rho h(x) \right)\xi_\rho \quad \text{(B.48)}
$$

Demanding on the other hand invariance under gauge transformation with regard to the second index

$$
h_{\nu\rho}(x) \rightarrow h_{\nu\rho}(x) + \partial_\rho\xi_\nu(x) . \quad \text{(B.49)}
$$

leads to

$$
0 = \left((a+b(1-y))\,\partial_\rho\partial^2 h^{\nu\rho}(x) + (by+cz)\partial_\rho\partial^\nu\partial_\lambda h^{\rho\lambda}(x) + (c(1-z)+d)\,\partial^\nu\partial^2 h(x) \right)\xi_\nu . \quad \text{(B.50)}
$$

Under the assumption that $z = y$ the combined gauge transformation

$$
h_{\nu\rho}(x) \rightarrow h_{\nu\rho}(x) + \partial_\nu\xi_\rho(x) + \partial_\rho\xi_\nu(x) , \quad \text{(B.51)}
$$

determines the constants to be $a = -\frac{1}{2}b = \frac{1}{2}c = -d$ and $y = \frac{1}{2}$. The Lagrangian reads

$$
\mathcal{L}_0 = a\left(\partial_\mu h_{\nu\rho}(x)\partial^\mu h^{\nu\rho}(x) - 2\partial_\mu h_{\nu\rho}(x)\partial^\nu h^{\mu\rho}(x) + 2\partial_\mu h(x)\partial^\rho h^{\mu\rho}(x) - \partial_\mu h(x)\partial^\mu h(x) \right) , \quad \text{(B.52)}
$$

which leads to the EOM of a massless tensor field

$$
\partial^2 h^{\nu\rho}(x) - \partial_\mu\partial^\nu h^{\mu\rho}(x) + \eta^{\nu\rho}\partial_\mu\partial_\sigma h^{\mu\sigma}(x) - \partial_\mu\partial^\rho h^{\mu\nu}(x) + \partial^\nu\partial^\rho h(x) - \eta^{\nu\rho}\partial^2 h(x) = 0 . \quad \text{(B.53)}
$$

B.3.1 Fierz Pauli Lagrangian

Let us now turn to the massive tensor field. We find two possible mass terms quadratic in $h_{\mu\nu}(x)$

$$\Delta\mathcal{L} = m^2 h_{\nu\rho}(x) \left(e\eta^{\nu\tau}\eta^{\rho\lambda} + f\eta^{\nu\rho}\eta^{\tau\lambda} \right) h_{\tau\lambda}(x)$$
$$= m^2 \left(e h_{\nu\rho}(x) h^{\nu\rho}(x) + f h^2(x) \right) , \tag{B.54}$$

with two constants e and f. Demanding invariance under gauge transformation (B.51) leads to either $e = f = 0$ or $m = 0$. Invariance under the extended transformation

$$h_{\mu\nu}(x) \to h_{\mu\nu}(x) + \frac{\partial_\mu}{m}\xi_\nu(x) + \frac{\partial_\nu}{m}\xi_\mu(x) + \frac{\partial_\mu\partial_\nu}{m^2}\Lambda(x) + \eta_{\mu\nu}\Lambda(x) , \tag{B.55}$$

leads to

$$(2a + e)\partial_\mu\partial_\sigma h^{\mu\sigma}(x) - (2a - f)\partial^2 h(x) - m\left(e\partial_\rho h^{\nu\rho}(x) + f\partial^\nu h(x)\right) - m^2(e + 4f)h(x) = 0 , \tag{B.56}$$

which is invariant for $e = -f = -2a$ and $m = 0$. Hence all constants except for a overall scaling are fixed and we see that only the mass term breaks the invariance. The Fierz-Pauli Lagrangian for a massive tensor field reads now [169]

$$\mathcal{L} = -\frac{1}{2}\partial_\rho h_{\mu\nu}(x)\partial^\rho h^{\mu\nu}(x) + \partial_\mu h_{\nu\rho}(x)\partial^\nu h^{\mu\rho}(x) - \partial_\mu h^{\mu\nu}(x)\partial_\nu h(x) + \frac{1}{2}\partial_\rho h(x)\partial^\rho h(x)$$
$$-\frac{1}{2}m^2\left(h_{\mu\nu}(x)h^{\mu\nu} - h^2(x)\right) , \tag{B.57}$$

and extremizing results in the Fierz-Pauli equation for a massive tensor field

$$0 = \partial_\rho\partial^\rho h_{\mu\nu}(x) - \partial_\rho\partial_\mu h^\rho{}_\nu(x) - \partial_\rho\partial_\nu h^\rho{}_\mu(x) + \eta_{\mu\nu}\partial_\rho\partial_\sigma h^{\rho\sigma}(x) + \partial_\mu\partial_\nu h(x) - \eta_{\mu\nu}\partial_\rho\partial^\rho h(x)$$
$$+ m^2\left(h_{\mu\nu}(x) - \eta_{\mu\nu}h(x)\right) . \tag{B.58}$$

We have seen, that the mass terms break the gauge invariance of the Fierz Pauli Lagrangian, however, instead of setting $m = 0$ we can constrain the massive tensor field to obey

$$\partial^\nu h_{\mu\nu}(x) = \partial_\mu h(x) , \qquad\qquad h(x) = 0 . \tag{B.59}$$

This simplifies the Fierz Pauli EOM

$$\left(\partial^2 + m^2\right)h^{\mu\nu}(x) = 0 , \tag{B.60}$$

which becomes the Klein-Gordon equation. Hence for a real symmetric tensor the Klein-Gordon equation gives ten DOFs, which is reduced to five DOF by the constraints (B.59).

B.3.2 Stückelberg Fierz-Pauli Lagrangian

The Lagrangian of the massless tensor field is invariant under the transformation (B.55) even without the additional constraint (B.59). In order to keep track of the DOFs at $m \to 0$ we introduce Stückelberg fields (following [170])

$$h_{\mu\nu}(x) \to h_{\mu\nu}(x) + \frac{\partial_\mu}{m}A_\nu(x) + \frac{\partial_\nu}{m}A_\mu(x) , \tag{B.61}$$

This introduces new terms to the Fierz-Pauli Lagrangian

$$\mathcal{L} = \mathcal{L}_0 - \frac{1}{2}m^2 \left(h_{\mu\nu}(x)h^{\mu\nu}(x) - h^2(x) \right)$$
$$- \frac{1}{2}F_{\mu\nu}(x)F^{\mu\nu}(x) - 2m \left(h_{\mu\nu}(x)\partial^\mu A^\nu(x) - h(x)\partial_\mu A^\mu(x) \right) \ , \qquad \text{(B.62)}$$

which now has the gauge symmetry

$$\delta h_{\mu\nu}(x) = \partial_\mu \xi_\nu(x) + \partial_\nu \xi_\mu(x) \ , \qquad\qquad \delta A_\mu(x) = -m\xi_\mu(x) \ . \qquad \text{(B.63)}$$

Gauge fixing $A_\mu(x) = 0$ leads to the original Lagrangian. Rescaling the vector field

$$A_\mu(x) \rightarrow \frac{1}{\sqrt{2}}A_\mu(x) \ , \qquad\qquad\qquad\qquad \text{(B.64)}$$

leads to a Lagrangian with canonical kinetic terms

$$\mathcal{L} = \mathcal{L}_0 - \frac{1}{2}m^2 \left(h_{\mu\nu}(x)h^{\mu\nu}(x) - h^2(x) \right) - \frac{1}{4}F_{\mu\nu}(x)F^{\mu\nu}(x)$$
$$- \sqrt{2}m \left(h_{\mu\nu}(x)\partial^\mu A^\nu(x) - h(x)\partial_\mu A^\mu(x) \right) \ . \qquad \text{(B.65)}$$

The massless limit, however, still possesses a gauge freedom not present in the massive Lagrangian

$$A_\mu(x) \rightarrow A_\mu(x) + \partial_\mu \Lambda(x) \ . \qquad\qquad\qquad \text{(B.66)}$$

Therefore, we have to introduce a further Stückelberg field

$$A_\mu(x) \rightarrow A_\mu(x) + \frac{\partial_\mu}{m}\phi'(x) \ . \qquad\qquad\qquad \text{(B.67)}$$

The Lagrangian is then given by

$$\mathcal{L} = \mathcal{L}_0 - \frac{1}{2}m^2 \left(h_{\mu\nu}(x)h^{\mu\nu}(x) - h^2(x) \right) - \frac{1}{4}F_{\mu\nu}(x)F^{\mu\nu}(x) \qquad \text{(B.68)}$$
$$- \sqrt{2}m \left(h_{\mu\nu}(x)\partial^\mu A^\nu(x) - h(x)\partial_\mu A^\mu(x) \right) - \sqrt{2}\left(h_{\mu\nu}(x)\partial^\mu \partial^\nu \phi'(x) - h(x)\partial^2 \phi'(x) \right) \ ,$$

and exhibits the gauge symmetries

$$\delta h_{\mu\nu}(x) = \partial_\mu \xi_\nu(x) + \partial_\nu \xi_\mu(x) \ , \qquad\qquad \delta A_\mu(x) = -m\xi_\mu(x) \ , \qquad \text{(B.69a)}$$
$$\delta A_\mu(x) = \partial_\mu \Lambda(x) \ , \qquad\qquad\qquad\qquad \delta\phi'(x) = -m\Lambda(x) \ . \qquad \text{(B.69b)}$$

Gauge fixing $\phi'(x) = 0$ leads to the previous Lagrangian, the scalar and the tensor field, however, are kinetically coupled. We resolve this by the final field shift

$$h_{\mu\nu}(x) = h_{\mu\nu}(x) + \eta_{\mu\nu}\phi''(x) \ , \qquad\qquad\qquad \text{(B.70)}$$

which leads to

$$\mathcal{L} = \mathcal{L}_0 - \frac{1}{2}m^2 \left(h_{\mu\nu}(x)h^{\mu\nu}(x) - h^2(x) \right) - \frac{1}{4}F_{\mu\nu}(x)F^{\mu\nu}(x)$$
$$- \sqrt{2}m \left(h_{\mu\nu}(x)\partial^\mu A^\nu(x) - h(x)\partial_\mu A^\mu(x) \right) - \sqrt{2}\left(h_{\mu\nu}(x)\partial^\mu \partial^\nu \phi'(x) - h(x)\partial^2 \phi'(x) \right)$$
$$+ 3\partial_\mu \phi''(x)\partial^\mu \phi'' + 3\sqrt{2}\phi''(x)\partial^2 \phi'(x) + 2\partial^\mu h(x)\partial_\mu \phi''(x) + 2\partial_\mu h^{\mu\nu}(x)\partial_\nu \phi''(x)$$
$$+ 6m^2 \phi''^2(x) + 3m^2 \phi''(x)h(x) + 3\sqrt{2}m\phi''(x)\partial^\mu A_\mu(x) \ , \qquad \text{(B.71)}$$

Finally, by rescaling the scalar fields in order to have a canonical kinetic term for the scalar field with vanishing kinetic mixing between the scalar and the tensor field

$$\phi'(x) \to -\sqrt{\frac{2}{3}}\phi(x) \, , \qquad\qquad \phi''(x) \to \frac{1}{\sqrt{3}}\phi(x) \, , \qquad (B.72)$$

we arrive at the desired Lagrangian

$$\mathcal{L} = \mathcal{L}_0 - \frac{1}{2}m^2 \left(h_{\mu\nu}(x)h^{\mu\nu}(x) - h^2(x) \right) - \frac{1}{4}F_{\mu\nu}(x)F^{\mu\nu}(x) - \partial^\mu\phi\partial_\mu\phi + 2m^2\phi^2(x)$$
$$- \sqrt{2}m \left(h_{\mu\nu}(x)\partial^\mu A^\nu(x) - h(x)\partial_\mu A^\mu(x) \right) + \sqrt{6}m\phi(x)\partial_\mu A^\mu(x) + \sqrt{3}m^2 h(x)\phi(x) \quad (B.73)$$

Unitary gauge $A_\mu(x)$, $\phi(x) \to 0$ gives the Fierz-Pauli Lagrangian and taking the massless limit $m \to 0$ leads to the Lagrangian of a massless tensor field, a massless vector field and a massless scalar field

$$\mathcal{L} = \mathcal{L}_0 - \frac{1}{4}F_{\mu\nu}(x)F^{\mu\nu}(x) - \partial^\mu\phi(x)\partial_\mu\phi(x) \, . \qquad (B.74)$$

Therefore, we see that the real massless tensor field has two DOFs.

B.3.3 Massless tensor field

Contracting the EOM of the massless tensor field (B.53) with the metric results in

$$\partial_\mu\partial_\nu h^{\mu\nu}(x) - \partial^2 h(x) = 0 \, , \qquad (B.75)$$

which can be used in order to simplify the EOM

$$\partial^2 h^{\nu\rho}(x) - \partial_\mu\partial^\nu h^{\mu\rho}(x) - \partial_\mu\partial^\rho h^{\mu\nu}(x) + \partial^\nu\partial^\rho h(x) = 0 \, . \qquad (B.76)$$

We have seen that we have to eliminate three DOFs by gauging the massless tensor field. Demanding the viability of the constraint (B.59) also in the massless case simplifies the EOM

$$\partial^2 h_{\mu\nu}(x) = 0 \, . \qquad (B.77)$$

Therefore, in the so called transverse traceless gauge, also the massless tensor field obeys the Klein-Gordon equation.

B.4 Momentum space

In order to perform actual calculations we are interested in the Fourier transform of the fields

$$\phi_\mu(x) = \phi_\mu^+(p, s)e^{-ipx} \, , \qquad (B.78)$$

where s runs over the spin DOFs derived in the previous sections. The various constraints we have derived hold as well in momentum space. Furthermore we will need the polarisation tensor, which is the spin sum over the product of two gauge fields

$$\Phi_{\mu\nu}^\pm(p) = \sum_s \phi_\mu^{\dagger\pm}(p, s)\phi_\nu^\pm(p, s) \, . \qquad (B.79)$$

Due to the normalization of the fields the contraction of the polarization tensor with the metric leads to

$$\eta^{\mu\nu}\Phi_{\mu\nu}^\pm(p) = s\mathcal{N} \, . \qquad (B.80)$$

and $\mathcal{N}$ depends on the normalization.

B.4.1 Spinor

In Section 3.8 we have calculated the decay widths and branching ratios of the lightest and next-to-lightest supersymmetric particle. As these supersymmetric fermions are Majorana fermions it turns out to be advantageous to perform this calculation in the two-component spinor notation. Here we summarise the formulas which are important for our calculations, the details of the two-component spinor notation are given in [80]. Dirac spinors $u(p)$ and $v(p)$ are normalized according to

$$\overline{u}(p,s)u(p,s') = 2md_{ss'} \ , \qquad\qquad \overline{v}(p,s)v(p,s') = -2md_{ss'} \ , \qquad (B.81)$$

and the spin sum is given by

$$\sum_s \overline{u}(p,s)u(p,s) = \gamma p + m \ . \qquad \sum_s \overline{v}(p,s)v(p,s) = \gamma p - m \ . \qquad (B.82)$$

Weyl Spinors $x(p)$ and $y(p)$ are normalized according to

$$\sum_s x(p,s)x^\dagger(p,s) = p\sigma \ , \qquad\qquad \sum_s y(p,s)y^\dagger(p,s) = p\sigma \ , \qquad (B.83a)$$

$$\sum_s x^\dagger(p,s)x(p,s) = p\overline{\sigma} \ , \qquad\qquad \sum_s y^\dagger(p,s)y(p,s) = p\overline{\sigma} \ , \qquad (B.83b)$$

$$\sum_s x(p,s)y(p,s) = m \ , \qquad\qquad \sum_s y^\dagger(p,s)x^\dagger(p,s) = m \ , \qquad (B.83c)$$

$$\sum_s y(p,s)x(p,s) = -m \ , \qquad\qquad \sum_s x^\dagger(p,s)y^\dagger(p,s) = -m \ , \qquad (B.83d)$$

We need the trace over a even number of σ-matrices

$$\operatorname{tr} \sigma^\mu \overline{\sigma}^\nu = \operatorname{tr} \overline{\sigma}^\mu \sigma^\nu = 2g^{\mu\nu} \ , \qquad (B.84a)$$

$$\operatorname{tr} \sigma^\mu \overline{\sigma}^\nu \sigma^\rho \overline{\sigma}^\sigma = 2\left(g^{\mu\nu}g^{\rho\sigma} - g^{\mu\rho}g^{\nu\sigma} + g^{\mu\sigma}g^{\nu\rho} + i\epsilon^{\mu\nu\rho\sigma}\right) \ , \qquad (B.84b)$$

$$\operatorname{tr} \overline{\sigma}^\mu \sigma^\nu \overline{\sigma}^\rho \sigma^\sigma = 2\left(g^{\mu\nu}g^{\rho\sigma} - g^{\mu\rho}g^{\nu\sigma} + g^{\mu\sigma}g^{\nu\rho} - i\epsilon^{\mu\nu\rho\sigma}\right) \ . \qquad (B.84c)$$

Higher products of σ-matrices can be derived via

$$[\sigma^\mu, \overline{\sigma}^\nu]_+ = 2\eta^{\mu\nu} \ . \qquad (B.85)$$

B.4.2 Vector

In momentum space the constraint for a massive vector field reads

$$p_\mu \epsilon^\mu(p,s) = 0 \ . \qquad (B.86)$$

The most general polarization tensor is given by

$$\Pi^\pm_{\mu\nu}(p) = a\eta_{\mu\nu} + bp_\mu p_\nu \ , \qquad (B.87)$$

The polarization tensor is constraint by

$$p^\mu p^\nu \Pi^\pm_{\mu\nu}(p) = 0 \ , \qquad\qquad \eta^{\mu\nu}\Pi_{\mu\nu}(p) = 3\mathcal{N} \ . \qquad (B.88)$$

which leads to

$$\Pi_{\mu\nu}(p) = -\eta_{\mu\nu} + \frac{p_\mu p_\nu}{m^2} \ , \tag{B.89}$$

where we have already used the proper normalization $\mathcal{N} = -1$

In the massless case every contraction which contains two momenta is bound to vanish, a full calculation after gauge fixing reveals, that the polarization tensor is just given by

$$\Pi_{\mu\nu}(p) = -\eta_{\mu\nu} \ . \tag{B.90}$$

B.4.3   Spinor-vector

The EOM of spinor-vectors is constrained by

$$p_\mu \psi^\mu(p,s) = 0 \ , \qquad\qquad \gamma_\mu \psi^\mu(p,s) = 0 \ . \tag{B.91}$$

The most general polarization tensor reads

$$P_{\mu\nu}^\pm(p) = a\eta_{\mu\nu} + b\gamma_\mu\gamma_\nu + cp_\mu\gamma_\mu + d\gamma_\mu p_\nu + ep_\mu p_\nu \ . \tag{B.92}$$

where we have used five constants $a \ldots e$ which have to be calculated using the five constraints

$$\eta^{\mu\nu}P_{\mu\nu}^\pm(p) = 4\mathcal{N} \ , \quad \gamma^\mu\gamma^\nu P_{\mu\nu}^\pm(p) = p^\mu\gamma^\nu P_{\mu\nu}^\pm(p) = \gamma^\mu p^\nu P_{\mu\nu}^\pm(p) = p^\mu p^\nu P_{\mu\nu}^\pm(p) = 0 \ , \quad \text{(B.93)}$$

which leads to

$$
\begin{aligned}
P_{\mu\nu}^\pm(p) &= (m \mp p\gamma)\left(\Pi_{\mu\nu}(p) - \frac{1}{3}\Pi_{\mu\sigma}(p)\gamma^\sigma \Pi_{\nu\lambda}(p)\gamma^\lambda\right) \\
&= (m + p\gamma)\left(-\eta_{\mu\nu} + \frac{1}{3}\gamma_\mu\gamma_\nu - \frac{1}{3}(p\gamma)\frac{p_\mu\gamma_\mu}{m^2} - \frac{1}{3}(p\gamma)\frac{\gamma_\mu p_\nu}{m^2} + \frac{2}{3}\frac{p_\mu p_\nu}{m^2}\right) \ .
\end{aligned} \tag{B.94}
$$

where we have already applied the four spinor normalization $\mathcal{N} = -\frac{1}{2}(m + p\gamma)$.

B.4.4   Tensor

For the tensor field the most general polarisation tensor is given by

$$
\begin{aligned}
\Pi_{\mu\nu\rho\sigma}(p) = {}& a\eta_{\mu\nu}\eta_{\rho\sigma} + b\eta_{\mu\rho}\eta_{\nu\sigma} + c\eta_{\mu\sigma}\eta_{\nu\rho} + d\eta_{\mu\nu}p_\rho p_\sigma + e\eta_{\mu\rho}p_\nu p_\sigma \\
&+ f\eta_{\mu\sigma}p_\nu p_\rho + g\eta_{\nu\rho}p_\mu p_\sigma + h\eta_{\nu\sigma}p_\mu p_\rho + i\eta_{\rho\sigma}p_\mu p_\nu + jp_\mu p_\nu p_\rho p_\sigma \ ,
\end{aligned} \tag{B.95}
$$

where we have introduced ten constants $a \ldots j$, which have to be fixed by applying the ten constraints, which originate in the tracelessness, the initial value condition and the normalization

$$\eta_{\mu\rho}\eta_{\nu\sigma}\Pi^{\mu\nu\rho\sigma}(p) = \eta_{\mu\sigma}\eta_{\nu\rho}\Pi^{\mu\nu\rho\sigma}(p) = 5\mathcal{N} \ , \tag{B.96a}$$

$$\eta_{\mu\nu}\eta_{\rho\sigma}\Pi^{\mu\nu\rho\sigma}(p) = p_\mu p_\nu p_\rho p_\sigma \Pi^{\mu\nu\rho\sigma}(p) = 0 \ , \tag{B.96b}$$

$$\eta_{\mu\nu}p_\rho p_\sigma \Pi^{\mu\nu\rho\sigma}(p) = \eta_{\mu\rho}p_\nu p_\sigma \Pi^{\mu\nu\rho\sigma}(p) = \eta_{\mu\sigma}p_\nu p_\rho \Pi^{\mu\nu\rho\sigma}(p) = 0 \ , \tag{B.96c}$$

$$\eta_{\nu\rho}p_\mu p_\sigma \Pi^{\mu\nu\rho\sigma}(p) = \eta_{\nu\sigma}p_\mu p_\rho \Pi^{\mu\nu\rho\sigma}(p) = \eta_{\rho\sigma}p_\mu p_\nu \Pi^{\mu\nu\rho\sigma}(p) = 0 \ , \tag{B.96d}$$

which leads to the polarisation tensor

$$
\begin{aligned}
\Pi_{\mu\nu\rho\sigma}(p) = & \frac{1}{2} \left(\Pi_{\mu\rho}(p)\Pi_{\nu\sigma}(p) + \Pi_{\mu\sigma}(p)\Pi_{\nu\rho}(p) \right) - \frac{1}{3}\Pi_{\mu\nu}(p)\Pi_{\rho\sigma}(p) \\
= & -\frac{1}{3}\eta_{\mu\nu}\eta_{\rho\sigma} + \frac{1}{2}\eta_{\mu\rho}\eta_{\nu\sigma} + \frac{1}{2}\eta_{\mu\sigma}\eta_{\nu\rho} + \frac{1}{3}\frac{\eta_{\mu\nu}p_\rho p_\sigma}{m^2} - \frac{1}{2}\frac{\eta_{\mu\rho}p_\nu p_\sigma}{m^2} \\
& -\frac{1}{2}\frac{\eta_{\mu\sigma}p_\nu p_\rho}{m^2} - \frac{1}{2}\frac{\eta_{\nu\rho}p_\mu p_\sigma}{m^2} - \frac{1}{2}\frac{\eta_{\nu\sigma}p_\mu p_\rho}{m^2} + \frac{1}{3}\frac{\eta_{\rho\sigma}p_\mu p_\nu}{m^2} + \frac{2}{3}\frac{p_\mu p_\nu p_\rho p_\sigma}{m^4} \ ,
\end{aligned}
\tag{B.97}
$$

where we have already used the proper normalization $\mathcal{N} = -1$.

List of Acronyms

List of Figures

List of Tables

Publications

Most of the results presented in this work have been published in the following papers.

[1] S. Bobrovskyi, W. Buchmüller, J. Hajer and J. Schmidt. 'Broken R-Parity in the Sky and at the LHC'. In: *JHEP* 1010 (2010), p. 061. DOI: 10.1007/JHEP10(2010)061. arXiv: 1007.5007 [hep-ph] (cit. on pp. 28, 52, 114).

[2] S. Bobrovskyi, W. Buchmüller, J. Hajer and J. Schmidt. 'Quasi-stable neutralinos at the LHC'. In: *JHEP* 1109 (2011), p. 119. DOI: 10.1007/JHEP09(2011)119. arXiv: 1107.0926 [hep-ph].

[3] S. Bobrovskyi, F. Brümmer, W. Buchmüller and J. Hajer. 'Searching for light higgsinos with b-jets and missing leptons'. In: *JHEP* 1201 (2012), p. 122. DOI: 10.1007/JHEP01(2012)122. arXiv: 1111.6005 [hep-ph].

[4] S. Bobrovskyi, J. Hajer and S. Rydbeck. 'Long-lived higgsinos as probes of gravitino dark matter at the LHC'. In: *JHEP* 1302 (2013), p. 133. DOI: 10.1007/JHEP02(2013)133. arXiv: 1211.5584 [hep-ph].

Bibliography

[5]   P. W. Higgs. 'Broken symmetries, massless particles and gauge fields'. In: *Phys.Lett.* 12 (1964), pp. 132–133. DOI: 10.1016/0031-9163(64)91136-9 (cit. on p. 5).

[6]   *ATLAS Collaboration*: G. Aad et al. 'Observation of a new particle in the search for the Standard Model Higgs boson with the ATLAS detector at the LHC'. In: *Phys.Lett.B* (2012). arXiv: 1207.7214 (hep-ex) (cit. on pp. 5, 92).

[7]   *CMS Collaboration*: S. Chatrchyan et al. 'Observation of a new boson at a mass of 125 GeV with the CMS experiment at the LHC'. In: *Phys.Lett.B* (2012). arXiv: 1207.7235 [hep-ex] (cit. on pp. 5, 92).

[8]   L. Bergstrom. 'Nonbaryonic dark matter: Observational evidence and detection methods'. In: *Rept.Prog.Phys.* 63 (2000), p. 793. DOI: 10.1088/0034-4885. arXiv: hep-ph/0002126 [hep-ph] (cit. on p. 5).

[9]   H. Baer and X. Tata. *Weak scale supersymmetry: From superfields to scattering events.* 2006 (cit. on p. 5).

[10] *Super-Kamiokande Collaboration*: Y. Fukuda et al. 'Neutrino induced upward stopping muons in Super-Kamiokande'. In: *Phys.Lett.* B467 (1999), pp. 185–193. DOI: 10.1016/S0370-2693(99)01188-0. arXiv: hep-ex/9908049 [hep-ex] (cit. on pp. 5, 15).

[11] M. Fukugita and T. Yanagida. 'Baryogenesis Without Grand Unification'. In: *Phys.Lett.* B174 (1986), p. 45. DOI: 10.1016/0370-2693(86)91126-3 (cit. on p. 5).

[12] S. Davidson and A. Ibarra. 'A Lower bound on the right-handed neutrino mass from leptogenesis'. In: *Phys.Lett.* B535 (2002), pp. 25–32. DOI: 10.1016/S0370-2693(02)01735-5. arXiv: hep-ph/0202239 [hep-ph] (cit. on p. 5).

[13] W. Buchmüller, P. Di Bari and M. Plumacher. 'Leptogenesis for pedestrians'. In: *Annals Phys.* 315 (2005), pp. 305–351. DOI: 10.1016/j.aop.2004.02.003. arXiv: hep-ph/0401240 [hep-ph] (cit. on p. 5).

[14] W. Buchmüller, R. Peccei and T. Yanagida. 'Leptogenesis as the origin of matter'. In: *Ann.Rev.Nucl.Part.Sci.* 55 (2005), pp. 311–355. DOI: 10.1146/annurev.nucl.55.090704.151558. arXiv: hep-ph/0502169 [hep-ph] (cit. on p. 5).

[15] D. Z. Freedman, P. van Nieuwenhuizen and S. Ferrara. 'Progress Toward a Theory of Supergravity'. In: *Phys.Rev.* D13 (1976), pp. 3214–3218. DOI: 10.1103/PhysRevD.13.3214 (cit. on p. 5).

[16] S. Weinberg. 'Cosmological Constraints on the Scale of Supersymmetry Breaking'. In: *Phys.Rev.Lett.* 48 (1982), p. 1303. DOI: 10.1103/PhysRevLett.48.1303 (cit. on p. 5).

[17]   J. R. Ellis, D. V. Nanopoulos and S. Sarkar. 'The Cosmology of Decaying Gravitinos'.
       In: *Nucl.Phys.* B259 (1985), p. 175. DOI: `10.1016/0550-3213(85)90306-2` (cit. on
       p. 5).

[18]   M. Kawasaki and T. Moroi. 'Gravitino production in the inflationary universe and the
       effects on big bang nucleosynthesis'. In: *Prog.Theor.Phys.* 93 (1995), pp. 879–900. DOI:
       `10.1143/PTP.93.879`. arXiv: `hep-ph/9403364 [hep-ph]` (cit. on p. 5).

[19]   M. Kawasaki, K. Kohri and T. Moroi. 'Hadronic decay of late - decaying particles
       and Big-Bang Nucleosynthesis'. In: *Phys.Lett.* B625 (2005), pp. 7–12. DOI: `10.1016/j.`
       `physletb.2005.08.045`. arXiv: `astro-ph/0402490 [astro-ph]` (cit. on p. 5).

[20]   M. Kawasaki, K. Kohri and T. Moroi. 'Big-Bang nucleosynthesis and hadronic decay
       of long-lived massive particles'. In: *Phys.Rev.* D71 (2005), p. 083502. DOI: `10.1103/`
       `PhysRevD.71.083502`. arXiv: `astro-ph/0408426 [astro-ph]` (cit. on pp. 5, 50).

[21]   K. Jedamzik. 'Big bang nucleosynthesis constraints on hadronically and electromag-
       netically decaying relic neutral particles'. In: *Phys.Rev.* D74 (2006), p. 103509. DOI:
       `10.1103/PhysRevD.74.103509`. arXiv: `hep-ph/0604251 [hep-ph]` (cit. on p. 5).

[22]   H. Pagels and J. R. Primack. 'Supersymmetry, Cosmology and New TeV Physics'. In:
       Phys.Rev.Lett. 48 (1982), p. 223. DOI: `10.1103/PhysRevLett.48.223` (cit. on p. 5).

[23]   M. Bolz, W. Büchmuller and M. Plumacher. 'Baryon asymmetry and dark matter'. In:
       Phys.Lett. B443 (1998), pp. 209–213. DOI: `10.1016/S0370-2693(98)01342-2`. arXiv:
       `hep-ph/9809381 [hep-ph]` (cit. on p. 5).

[24]   J. L. Feng. 'Supersymmetry and cosmology'. In: *Annals Phys.* 315 (2005), pp. 2–51.
       DOI: `10.1016/j.aop.2004.09.014` (cit. on p. 6).

[25]   B. A. Campbell, S. Davidson, J. R. Ellis and K. A. Olive. 'Cosmological baryon
       asymmetry constraints on extensions of the standard model'. In: *Phys.Lett.* B256
       (1991), p. 457. DOI: `10.1016/0370-2693(91)91795-W` (cit. on pp. 6, 50).

[26]   W. Fischler, G. Giudice, R. Leigh and S. Paban. 'Constraints on the baryogenesis scale
       from neutrino masses'. In: *Phys.Lett.* B258 (1991), pp. 45–48. DOI: `10.1016/0370-`
       `2693(91)91207-C` (cit. on pp. 6, 50).

[27]   H. K. Dreiner and G. G. Ross. 'Sphaleron erasure of primordial baryogenesis'. In:
       Nucl.Phys. B410 (1993), pp. 188–216. DOI: `10.1016/0550-3213(93)90579-E`. arXiv:
       `hep-ph/9207221 [hep-ph]` (cit. on pp. 6, 50).

[28]   M. Endo, K. Hamaguchi and S. Iwamoto. 'Lepton Flavor Violation and Cosmological
       Constraints on R-parity Violation'. In: *JCAP* 1002 (2010), p. 032. DOI: `10.1088/1475-`
       `7516`. arXiv: `0912.0585 [hep-ph]` (cit. on pp. 6, 50, 55).

[29]   W. Buchmüller, L. Covi, K. Hamaguchi, A. Ibarra and T. Yanagida. 'Gravitino Dark
       Matter in R-Parity Breaking Vacua'. In: *JHEP* 0703 (2007), p. 037. DOI: `10.1088/1126-`
       `6708`. arXiv: `hep-ph/0702184 [HEP-PH]` (cit. on pp. 6, 19, 21, 44, 51).

[30]   L. J. Hall and M. Suzuki. 'Explicit R-Parity Breaking in Supersymmetric Models'. In:
       Nucl. Phys. B231 (1984), p. 419. DOI: `10.1016/0550-3213(84)90513-3` (cit. on p. 6).

[31]   B. C. Allanach, A. Dedes and H. K. Dreiner. 'R-parity violating minimal supergravity
       model'. In: *Phys.Rev.* D69 (2004), p. 115002. DOI: `10.1103/PhysRevD.69.115002;10.`
       `1103/PhysRevD.72.079902`. arXiv: `hep-ph/0309196 [hep-ph]` (cit. on pp. 6, 22).

[32] R. Barbier, C. Berat, M. Besancon, M. Chemtob, A. Deandrea et al. 'R-parity violating supersymmetry'. In: *Phys.Rept.* 420 (2005), pp. 1–202. DOI: 10.1016/j.physrep.2005.08.006. arXiv: hep-ph/0406039 [hep-ph] (cit. on pp. 6, 17).

[33] F. de Campos, O. Eboli, M. Magro, W. Porod, D. Restrepo et al. 'Probing bilinear R-parity violating supergravity at the LHC'. In: *JHEP* 0805 (2008), p. 048. DOI: 10.1088/1126-6708. arXiv: 0712.2156 [hep-ph] (cit. on p. 6).

[34] F. Takayama and M. Yamaguchi. 'Gravitino dark matter without R-parity'. In: *Phys.-Lett.* B485 (2000), pp. 388–392. DOI: 10.1016/S0370-2693(00)00726-7. arXiv: hep-ph/0005214 [hep-ph] (cit. on pp. 6, 29).

[35] W. Buchmüller, M. Endo and T. Shindou. 'Superparticle Mass Window from Leptogenesis and Decaying Gravitino Dark Matter'. In: *JHEP* 0811 (2008), p. 079. DOI: 10.1088/1126-6708. arXiv: 0809.4667 [hep-ph] (cit. on pp. 6, 50).

[36] G. Bertone, W. Buchmüller, L. Covi and A. Ibarra. 'Gamma-Rays from Decaying Dark Matter'. In: *JCAP* 0711 (2007), p. 003. DOI: 10.1088/1475-7516. arXiv: 0709.2299 [astro-ph] (cit. on p. 6).

[37] A. Ibarra and D. Tran. 'Gamma Ray Spectrum from Gravitino Dark Matter Decay'. In: *Phys.Rev.Lett.* 100 (2008), p. 061301. DOI: 10.1103/PhysRevLett.100.061301. arXiv: 0709.4593 [astro-ph] (cit. on p. 6).

[38] S. Lola, P. Osland and A. R. Raklev. 'Radiative gravitino decays from R-parity violation'. In: *Phys. Lett.* B656 (2007), pp. 83–90. DOI: 10.1016/j.physletb.2007.09.048. arXiv: 0707.2510 [hep-ph] (cit. on p. 6).

[39] K. Ishiwata, S. Matsumoto and T. Moroi. 'High Energy Cosmic Rays from the Decay of Gravitino Dark Matter'. In: *Phys.Rev.* D78 (2008), p. 063505. DOI: 10.1103/PhysRevD.78.063505. arXiv: 0805.1133 [hep-ph] (cit. on p. 6).

[40] W. Buchmüller, A. Ibarra, T. Shindou, F. Takayama and D. Tran. 'Probing Gravitino Dark Matter with PAMELA and Fermi'. In: *JCAP* 0909 (2009), p. 021. DOI: 10.1088/1475-7516. arXiv: 0906.1187 [hep-ph] (cit. on pp. 6, 31).

[41] N.-E. Bomark, S. Lola, P. Osland and A. Raklev. 'Photon, Neutrino and Charged Particle Spectra from R-violating Gravitino Decays'. In: *Phys.Lett.* B686 (2010), pp. 152–161. DOI: 10.1016/j.physletb.2010.02.050. arXiv: 0911.3376 [hep-ph] (cit. on p. 6).

[42] K.-Y. Choi, D. Restrepo, C. E. Yaguna and O. Zapata. 'Indirect detection of gravitino dark matter including its three-body decays'. In: *JCAP* 1010 (2010), p. 033. DOI: 10.1088/1475-7516. arXiv: 1007.1728 [hep-ph] (cit. on p. 6).

[43] *Fermi-LAT Collaboration*: A. A. Abdo et al. 'Fermi LAT Search for Photon Lines from 30 to 200 GeV and Dark Matter Implications'. In: *Phys. Rev. Lett.* 104 (2010), p. 091302. DOI: 10.1103/PhysRevLett.104.091302. arXiv: 1001.4836 [astro-ph.HE] (cit. on p. 6).

[44] *Fermi-LAT Collaboration*: A. A. Abdo et al. 'The Spectrum of the Isotropic Diffuse Gamma-Ray Emission Derived From First-Year Fermi Large Area Telescope Data'. In: *Phys. Rev. Lett.* 104 (2010), p. 101101. DOI: 10.1103/PhysRevLett.104.101101. arXiv: 1002.3603 [astro-ph.HE] (cit. on p. 6).

[45] W. Buchmüller and M. Garny. 'Decaying vs Annihilating Dark Matter in Light of a Tentative Gamma-Ray Line'. In: *JCAP* 1208 (2012), p. 035. DOI: 10.1088/1475-7516. arXiv: 1206.7056 [hep-ph] (cit. on pp. 6, 29, 41).

[46] F. Brümmer and W. Buchmüller. 'Light Higgsinos as Heralds of Higher-Dimensional Unification'. In: *JHEP* 1107 (2011), p. 010. DOI: 10.1007/JHEP07(2011)010. arXiv: 1105.0802 [hep-ph] (cit. on pp. 6, 13, 57, 92).

[54] P. W. Graham, D. E. Kaplan, S. Rajendran and P. Saraswat. 'Displaced Supersymmetry'. In: *JHEP* 1207 (2012), p. 149. DOI: 10.1007/JHEP07(2012)149. arXiv: 1204.6038 [hep-ph] (cit. on p. 6).

[47] K. Ishiwata, T. Ito and T. Moroi. 'Long-Lived Unstable Superparticles at the LHC'. In: *Phys.Lett.* B669 (2008), pp. 28–33. DOI: 10.1016/j.physletb.2008.09.024. arXiv: 0807.0975 [hep-ph] (cit. on pp. 6, 55, 85, 87).

[48] S. Asai, K. Hamaguchi and S. Shirai. 'Measuring lifetimes of long-lived charged massive particles stopped in LHC detectors'. In: *Phys.Rev.Lett.* 103 (2009), p. 141803. DOI: 10.1103/PhysRevLett.103.141803. arXiv: 0902.3754 [hep-ph] (cit. on pp. 6, 55).

[49] K. Desch, S. Fleischmann, P. Wienemann, H. K. Dreiner and S. Grab. 'Stau as the Lightest Supersymmetric Particle in R-Parity Violating SUSY Models: Discovery Potential with Early LHC Data'. In: *Phys. Rev.* D83 (2011), p. 015013. DOI: 10.1103/PhysRevD.83.015013. arXiv: 1008.1580 [hep-ph] (cit. on p. 6).

[50] P. Meade, M. Reece and D. Shih. 'Long-Lived Neutralino NLSPs'. In: *JHEP* 10 (2010), p. 067. DOI: 10.1007/JHEP10(2010)067. arXiv: 1006.4575 [hep-ph] (cit. on pp. 6, 77).

[51] N.-E. Bomark, D. Choudhury, S. Lola and P. Osland. 'Flavour Structure of R-violating Neutralino Decays at the LHC' (2011). arXiv: 1105.4022 [hep-ph] (cit. on p. 6).

[52] M. Hirsch, W. Porod and D. Restrepo. 'Collider signals of gravitino dark matter in bilinearly broken R-parity'. In: *JHEP* 0503 (2005), p. 062. DOI: 10.1088/1126-6708. arXiv: hep-ph/0503059 [hep-ph] (cit. on p. 6).

[53] P. Ghosh, D. E. Lopez-Fogliani, V. A. Mitsou, C. Munoz and R. R. de Austri. 'Displaced multileptons at the LHC – probing a 125 GeV new boson in $\mu\nu$SSM' (2012). arXiv: 1211.3177 [hep-ph] (cit. on p. 6).

[55] B. Allanach, A. Dedes and H. K. Dreiner. 'Two loop supersymmetric renormalization group equations including R-parity violation and aspects of unification'. In: *Phys.Rev.* D60 (1999), p. 056002. DOI: 10.1103/PhysRevD.60.056002,10.1103/PhysRevD.86.039906. arXiv: hep-ph/9902251 [hep-ph] (cit. on pp. 9, 12).

[56] J. Wess and J. Bagger. 'Supersymmetry and supergravity' (1992), p. 259 (cit. on pp. 8, 29).

[57] S. P. Martin. 'A Supersymmetry primer' (1997). arXiv: hep-ph/9709356 [hep-ph] (cit. on p. 10).

[58] P. R. Auvil and J. J. Brehm. 'Wave Functions for Particles of Higher Spin'. In: *Phys. Rev.* 145 (4 May 1966), pp. 1152–1153. DOI: 10.1103/PhysRev.145.1152. URL: http://link.aps.org/doi/10.1103/PhysRev.145.1152 (cit. on p. 11).

[59] S. Ferrara, L. Girardello and F. Palumbo. 'A General Mass Formula in Broken Super-symmetry'. In: *Phys.Rev.* D20 (1979), p. 403. DOI: `10.1103/PhysRevD.20.403` (cit. on p. 11).

[60] G. Giudice and R. Rattazzi. 'Theories with gauge mediated supersymmetry breaking'. In: *Phys.Rept.* 322 (1999), pp. 419–499. DOI: `10.1016/S0370-1573(99)00042-3`. arXiv: `hep-ph/9801271 [hep-ph]` (cit. on p. 13).

[61] G. Giudice and A. Masiero. 'A Natural Solution to the mu Problem in Supergravity Theories'. In: *Phys.Lett.* B206 (1988), pp. 480–484. DOI: `10.1016/0370-2693(88)91613-9` (cit. on pp. 13, 20).

[62] Z. Lalak, S. Pokorski and K. Turzynski. 'Gravity in Gauge Mediation'. In: *JHEP* 0810 (2008), p. 016. DOI: `10.1088/1126-6708/2008/10/016`. arXiv: `0808.0470 [hep-ph]` (cit. on p. 13).

[63] J. Schechter and J. Valle. 'Neutrinoless Double beta Decay in SU(2) x U(1) Theories'. In: *Phys.Rev.* D25 (1982), p. 2951. DOI: `10.1103/PhysRevD.25.2951` (cit. on p. 15).

[64] P. Minkowski. '$\mu \rightarrow e\gamma$ at a Rate of One Out of 1-Billion Muon Decays?' In: *Phys.Lett.* B67 (1977), p. 421. DOI: `10.1016/0370-2693(77)90435-X` (cit. on p. 15).

[65] T. Yanagida. 'horizontal symmetry and masses of neutrinos'. In: *Conf.Proc.* C7902131 (1979), p. 95 (cit. on p. 15).

[66] M. Gell-Mann, P. Ramond and R. Slansky. 'Complex spinors and unified theories'. In: *Conf.Proc.* C790927 (1979), pp. 315–321 (cit. on p. 15).

[67] P. Fayet. 'Supergauge Invariant Extension of the Higgs Mechanism and a Model for the electron and Its Neutrino'. In: *Nucl.Phys.* B90 (1975), pp. 104–124. DOI: `10.1016/0550-3213(75)90636-7` (cit. on p. 16).

[68] P. Fayet. 'Mixing Between Gravitational and Weak Interactions Through the Massive Gravitino'. In: *Phys.Lett.* B70 (1977), p. 461. DOI: `10.1016/0370-2693(77)90414-2` (cit. on p. 16).

[69] P. Fayet. 'About the origins of the supersymmetric standard model'. In: *Nucl.Phys.-Proc.Suppl.* 101 (2001), pp. 81–98. DOI: `10.1016/S0920-5632(01)01495-5`. arXiv: `hep-ph/0107228 [hep-ph]` (cit. on p. 16).

[70] *Super-Kamiokande Collaboration*: H. Nishino et al. 'Search for Proton Decay via $p \rightarrow e^+\pi^0$ and $p \rightarrow \mu^+\pi^0$ in a Large Water Cherenkov Detector'. In: *Phys.Rev.Lett.* 102 (2009), p. 141801. DOI: `10.1103/PhysRevLett.102.141801`. arXiv: `0903.0676 [hep-ex]` (cit. on p. 17).

[71] G. D'Ambrosio, G. Giudice, G. Isidori and A. Strumia. 'Minimal flavor violation: An Effective field theory approach'. In: *Nucl.Phys.* B645 (2002), pp. 155–187. DOI: `10.1016/S0550-3213(02)00836-2`. arXiv: `hep-ph/0207036 [hep-ph]` (cit. on p. 17).

[72] E. Nikolidakis and C. Smith. 'Minimal Flavor Violation, Seesaw, and R-parity'. In: *Phys.Rev.* D77 (2008), p. 015021. DOI: `10.1103/PhysRevD.77.015021`. arXiv: `0710.3129 [hep-ph]` (cit. on p. 17).

[73] C. Csaki, Y. Grossman and B. Heidenreich. 'MFV SUSY: A Natural Theory for R-Parity Violation'. In: *Phys.Rev.* D85 (2012), p. 095009. DOI: `10.1103/PhysRevD.85.095009`. arXiv: `1111.1239 [hep-ph]` (cit. on p. 18).

[74] V. Cirigliano, B. Grinstein, G. Isidori and M. B. Wise. 'Minimal flavor violation in the lepton sector'. In: *Nucl.Phys.* B728 (2005), pp. 121–134. DOI: `10.1016/j.nuclphysb.2005.08.037`. arXiv: `hep-ph/0507001 [hep-ph]` (cit. on p. 18).

[75] W. Buchmüller and T. Yanagida. 'Quark lepton mass hierarchies and the baryon asymmetry'. In: *Phys.Lett.* B445 (1999), pp. 399–402. DOI: `10.1016/S0370-2693(98)01480-4`. arXiv: `hep-ph/9810308 [hep-ph]` (cit. on p. 21).

[76] W. Buchmüller, D. Delepine and L. T. Handoko. 'Neutrino mixing and flavor changing processes'. In: *Nucl.Phys.* B576 (2000), pp. 445–465. DOI: `10.1016/S0550-3213(00)00095-X`. arXiv: `hep-ph/9912317 [hep-ph]` (cit. on p. 21).

[77] J. Hajer. 'Gravitino and scalar tau-lepton decays in supersymmetric models with broken R-parity'. Diploma-Thesis. 2010. DOI: `10.3204/DESY-THESIS-2010-021` (cit. on p. 22).

[78] T. Moroi. 'Effects of the gravitino on the inflationary universe' (1995). arXiv: `hep-ph/9503210 [hep-ph]` (cit. on p. 29).

[79] *Particle Data Group*: J. Beringer et al. 'Review of Particle Physics (RPP)'. In: *Phys.Rev.* D86 (2012), p. 010001. DOI: `10.1103/PhysRevD.86.010001` (cit. on pp. 31, 92).

[80] H. K. Dreiner, H. E. Haber and S. P. Martin. 'Two-component spinor techniques and Feynman rules for quantum field theory and supersymmetry'. In: *Phys.Rept.* 494 (2010), pp. 1–196. DOI: `10.1016/j.physrep.2010.05.002`. arXiv: `0812.1594 [hep-ph]` (cit. on pp. 31, 32, 125).

[81] B. Mukhopadhyaya, S. Roy and F. Vissani. 'Correlation between neutrino oscillations and collider signals of supersymmetry in an R-parity violating model'. In: *Phys.Lett.* B443 (1998), pp. 191–195. DOI: `10.1016/S0370-2693(98)01288-X`. arXiv: `hep-ph/9808265 [hep-ph]` (cit. on p. 33).

[82] S. Bobrovskyi. 'Gravitinos and hidden supersymmetry at the LHC'. PhD-Thesis. DESY. ReportNumber: `DESY-THESIS-2012-032` (cit. on pp. 33, 52).

[83] V. D. Barger and R. Phillips. 'Collider Physics' (1987). ReportNumber: `ISBN-9780201149456` (cit. on p. 35).

[84] J. R. Ellis, K. A. Olive, Y. Santoso and V. C. Spanos. 'Gravitino dark matter in the CMSSM'. In: *Phys.Lett.* B588 (2004), pp. 7–16. DOI: `10.1016/j.physletb.2004.03.021`. arXiv: `hep-ph/0312262 [hep-ph]` (cit. on p. 36).

[85] J. L. Feng, S. Su and F. Takayama. 'Supergravity with a gravitino LSP'. In: *Phys.Rev.* D70 (2004), p. 075019. DOI: `10.1103/PhysRevD.70.075019`. arXiv: `hep-ph/0404231 [hep-ph]` (cit. on p. 36).

[86] L. Roszkowski, R. Ruiz de Austri and K.-Y. Choi. 'Gravitino dark matter in the CMSSM and implications for leptogenesis and the LHC'. In: *JHEP* 0508 (2005), p. 080. DOI: `10.1088/1126-6708/2005/08/080`. arXiv: `hep-ph/0408227 [hep-ph]` (cit. on p. 36).

[87] D. G. Cerdeno, K.-Y. Choi, K. Jedamzik, L. Roszkowski and R. Ruiz de Austri. 'Gravitino dark matter in the CMSSM with improved constraints from BBN'. In: *JCAP* 0606 (2006), p. 005. DOI: `10.1088/1475-7516/2006/06/005`. arXiv: `hep-ph/0509275 [hep-ph]` (cit. on p. 36).

[88] G. Barenboim and G. Panotopoulos. 'Gravitino dark matter in the constrained next-to-minimal supersymmetric standard model with neutralino next-to-lightest superpartner'. In: *JHEP* 1009 (2010), p. 011. DOI: 10.1007/JHEP09(2010)011. arXiv: 1004.4525 [hep-ph] (cit. on p. 36).

[89] L. Covi, M. Grefe, A. Ibarra and D. Tran. 'Unstable Gravitino Dark Matter and Neutrino Flux'. In: *JCAP* 0901 (2009), p. 029. DOI: 10.1088/1475-7516. arXiv: 0809.5030 [hep-ph] (cit. on p. 41).

[90] M. Grefe. 'Neutrino signals from gravitino dark matter with broken R-parity'. Diploma-Thesis. 2008. DOI: 10.3204/DESY-THESIS-2008-043 (cit. on p. 41).

[91] W. Buchmüller, K. Hamaguchi, M. Ratz and T. Yanagida. 'Supergravity at colliders'. In: *Phys.Lett.* B588 (2004), pp. 90–98. DOI: 10.1016/j.physletb.2004.03.016. arXiv: hep-ph/0402179 [hep-ph] (cit. on p. 44).

[92] J. L. Feng, S.-f. Su and F. Takayama. 'SuperWIMP gravitino dark matter from slepton and sneutrino decays'. In: *Phys.Rev.* D70 (2004), p. 063514. DOI: 10.1103/PhysRevD.70.063514. arXiv: hep-ph/0404198 [hep-ph] (cit. on p. 50).

[93] F. D. Steffen. 'Gravitino dark matter and cosmological constraints'. In: *JCAP* 0609 (2006), p. 001. DOI: 10.1088/1475-7516. arXiv: hep-ph/0605306 [hep-ph] (cit. on p. 50).

[94] M. Bolz. 'Thermal production of gravitinos'. PhD-Thesis. DESY, 2000. ReportNumber: DESY-THESIS-2000-013 (cit. on p. 50).

[95] F. Brümmer and W. Buchmüller. 'The Fermi scale as a focus point of high-scale gauge mediation'. In: *JHEP* 1205 (2012), p. 006. DOI: 10.1007/JHEP05(2012)006. arXiv: 1201.4338 [hep-ph] (cit. on p. 50).

[96] W. Buchmüller, K. Schmitz and G. Vertongen. 'Entropy, baryon asymmetry and dark matter from heavy neutrino decays'. In: *Nucl.Phys.* B851 (2011), pp. 481–532. DOI: 10.1016/j.nuclphysb.2011.06.004. arXiv: 1104.2750 [hep-ph] (cit. on p. 51).

[97] W. Buchmüller, V. Domcke and K. Schmitz. 'Spontaneous B-L Breaking as the Origin of the Hot Early Universe'. In: *Nucl.Phys.* B862 (2012), pp. 587–632. DOI: 10.1016/j.nuclphysb.2012.05.001. arXiv: 1202.6679 [hep-ph] (cit. on p. 51).

[98] G. Vertongen and C. Weniger. 'Hunting Dark Matter Gamma-Ray Lines with the Fermi LAT'. In: *JCAP* 1105 (2011), p. 027. DOI: 10.1088/1475-7516. arXiv: 1101.2610 [hep-ph] (cit. on pp. 51, 85).

[99] *Fermi-LAT Collaboration*: M. Ackermann et al. 'Fermi LAT Search for Dark Matter in Gamma-ray Lines and the Inclusive Photon Spectrum'. In: *Phys.Rev.* D86 (2012), p. 022002. DOI: 10.1103/PhysRevD.86.022002. arXiv: 1205.2739 [astro-ph.HE] (cit. on p. 51).

[100] M. Cirelli, E. Moulin, P. Panci, P. D. Serpico and A. Viana. 'Gamma ray constraints on Decaying Dark Matter'. In: *Phys.Rev.* D86 (2012), p. 083506. DOI: 10.1103/PhysRevD.86.083506;10.1103/PhysRevD.86.109901. arXiv: 1205.5283 [astro-ph.CO] (cit. on p. 51).

[101] B. C. Allanach and M. A. Bernhardt. 'Including R-parity violation in the numerical computation of the spectrum of the minimal supersymmetric standard model: SOFTSUSY 3.0'. In: *Comput. Phys. Commun.* 181 (2010), pp. 232–245. DOI: 10.1016/j.cpc.2009.09.015. arXiv: 0903.1805 [hep-ph] (cit. on p. 56).

[102] B. C. Allanach. 'SOFTSUSY: a program for calculating supersymmetric spectra'. In: *Comput.Phys.Commun.* 143 (2002), pp. 305–331. DOI: 10.1016/S0010-4655(01)00460-X. arXiv: hep-ph/0104145 [hep-ph] (cit. on p. 56).

[103] M. Muhlleitner. 'SDECAY: A Fortran code for SUSY particle decays in the MSSM'. In: *Acta Phys. Polon.* B35 (2004), pp. 2753–2766. arXiv: hep-ph/0409200 (cit. on p. 56).

[104] J. Alwall, P. Demin, S. de Visscher, R. Frederix, M. Herquet et al. 'MADGRAPH/MADEVENT v4: The New Web Generation'. In: *JHEP* 0709 (2007), p. 028. DOI: 10.1088/1126-6708. arXiv: 0706.2334 [hep-ph] (cit. on p. 56).

[105] T. Sjostrand, S. Mrenna and P. Z. Skands. 'PYTHIA 6.4 Physics and Manual'. In: *JHEP* 0605 (2006), p. 026. DOI: 10.1088/1126-6708. arXiv: hep-ph/0603175 [hep-ph] (cit. on p. 56).

[106] J. Pumplin, D. Stump, J. Huston, H. Lai, P. M. Nadolsky et al. 'New generation of parton distributions with uncertainties from global QCD analysis'. In: *JHEP* 0207 (2002), p. 012. arXiv: hep-ph/0201195 [hep-ph] (cit. on p. 56).

[107] S. Ovyn, X. Rouby and V. Lemaitre. 'DELPHES, a framework for fast simulation of a generic collider experiment' (2009). arXiv: 0903.2225 [hep-ph] (cit. on p. 56).

[108] G. L. Kane. 'A Higgsino-LSP world'. In: *Perspectives on supersymmetry* (1998), pp. 352–354 (cit. on p. 56).

[109] C. Csáki, A. Falkowski, Y. Nomura and T. Volansky. 'New Approach to the mu-Bmu Problem of Gauge-Mediated Supersymmetry Breaking'. In: *Phys.Rev.Lett.* 102 (2009), p. 111801. DOI: 10.1103/PhysRevLett.102.111801. arXiv: 0809.4492 [hep-ph] (cit. on p. 56).

[110] A. De Simone, R. Franceschini, G. F. Giudice, D. Pappadopulo and R. Rattazzi. 'Lopsided Gauge Mediation'. In: *JHEP* 1105 (2011), p. 112. DOI: 10.1007/JHEP05(2011)112. arXiv: 1103.6033 [hep-ph] (cit. on p. 56).

[111] H. Baer, V. Barger and P. Huang. 'Hidden SUSY at the LHC: the light higgsino-world scenario and the role of a lepton collider'. In: *JHEP* 1111 (2011), p. 031. DOI: 10.1007/JHEP11(2011)031. arXiv: 1107.5581 [hep-ph] (cit. on pp. 59, 89).

[112] N. Kidonakis. 'Top quark pair and single top production at Tevatron and LHC energies'. In: *PoS* ICHEP2010 (2010), p. 059. arXiv: 1008.2460 [hep-ph] (cit. on pp. 63, 80).

[113] J. M. Campbell, R. K. Ellis and C. Williams. 'Vector boson pair production at the LHC'. In: *JHEP* 1107 (2011), p. 018. DOI: 10.1007/JHEP07(2011)018. arXiv: 1105.0020 [hep-ph] (cit. on pp. 63, 80, 94).

[114] P. Torrielli and S. Frixione. 'Matching NLO QCD computations with PYTHIA using MC@NLO'. In: *JHEP* 1004 (2010), p. 110. DOI: 10.1007/JHEP04(2010)110. arXiv: 1002.4293 [hep-ph] (cit. on p. 63).

[115] L. Randall and D. Tucker-Smith. 'Dijet Searches for Supersymmetry at the LHC'. In: *Phys.Rev.Lett.* 101 (2008), p. 221803. DOI: 10.1103/PhysRevLett.101.221803. arXiv: 0806.1049 [hep-ph] (cit. on p. 62).

[116] CMS Collaboration. 'SUSY searches with dijet events'. In: *CMS Physics Analysis Summary SUS-08-005* (Oct. 2008) (cit. on p. 62).

[117] CMS Collaboration. 'Search strategy for exclusive multi-jet events from supersymmetry at CMS'. In: *CMS Physics Analysis Summary SUS-09-001* (July 2009) (cit. on pp. 62, 63).

[118] *ATLAS Collaboration*: G. Aad et al. 'The ATLAS Experiment at the CERN Large Hadron Collider'. In: *JINST* 3 (2008), S08003. DOI: `10.1088/1748-0221` (cit. on p. 69).

[119] *CMS Collaboration*: G. Bayatian et al. 'CMS physics: Technical design report' (2006). ReportNumber: `CERN-LHCC-2006-001, CMS-TDR-008-1` (cit. on pp. 69, 81, 96).

[120] *ATLAS Collaboration*: G. Aad et al. 'Search for supersymmetric particles in events with lepton pairs and large missing transverse momentum in $\sqrt{s} = 7$ TeV proton-proton collisions with the ATLAS experiment'. In: *Eur.Phys.J.* C71 (2011), p. 1682. DOI: `10.1140/epjc`. arXiv: `1103.6214` `[hep-ex]` (cit. on pp. 74, 77).

[121] *CMS Collaboration*: S. Chatrchyan et al. 'Search for Physics Beyond the Standard Model in Opposite-Sign Dilepton Events at $\sqrt{s} = 7$ TeV'. In: *JHEP* 1106 (2011), p. 026. DOI: `10.1007/JHEP06(2011)026`. arXiv: `1103.1348` `[hep-ex]` (cit. on pp. 74, 79).

[122] *CMS Collaboration*: S. Chatrchyan et al. 'Search for new physics with same-sign isolated dilepton events with jets and missing transverse energy at the LHC' (2011). arXiv: `1104.3168` `[hep-ex]` (cit. on p. 74).

[123] *CMS Collaboration*: G. Bayatian et al. 'CMS technical design report, volume II: Physics performance'. In: *J.Phys.G* G34 (2007), pp. 995–1579. DOI: `10.1088/0954-3899` (cit. on p. 78).

[124] W. Beenakker, R. Hopker and M. Spira. 'PROSPINO: A program for the PROduction of Supersymmetric Particles In Next-to-leading Order QCD' (1996). arXiv: `hep-ph/9611232` (cit. on p. 78).

[125] T. Binoth, G. Ossola, C. Papadopoulos and R. Pittau. 'NLO QCD corrections to tri-boson production'. In: *JHEP* 0806 (2008), p. 082. DOI: `10.1088/1126-6708`. arXiv: `0804.0350` `[hep-ph]` (cit. on p. 80).

[126] R. Gavin, Y. Li, F. Petriello and S. Quackenbush. 'FEWZ 2.0: A code for hadronic Z production at next-to-next-to-leading order' (2010). arXiv: `1011.3540` `[hep-ph]` (cit. on p. 80).

[127] *ATLAS Collaboration*: G. Aad et al. 'Expected Performance of the ATLAS Experiment – Detector, Trigger and Physics' (2009). arXiv: `0901.0512` `[hep-ex]` (cit. on pp. 79, 81, 96).

[128] G. Cowan, K. Cranmer, E. Gross and O. Vitells. 'Asymptotic formulae for likelihood-based tests of new physics'. In: *Eur.Phys.J.* C71 (2011), p. 1554. DOI: `10.1140/epjc`. arXiv: `1007.1727` `[physics.data-an]` (cit. on p. 82).

[129] G. Cowan. *SigCalc*. URL: `http://www.pp.rhul.ac.uk/~cowan/stat/SigCalc` (cit. on p. 82).

[130] *ATLAS Collaboration*: G. Aad et al. 'Search for direct slepton and gaugino production in final states with two leptons and missing transverse momentum with the ATLAS detector in *pp* collisions at $\sqrt{s} = 7$ TeV' (2012). arXiv: `1208.2884` `[hep-ex]` (cit. on p. 89).

[131]   *ATLAS Collaboration*: G. Aad et al. 'Search for direct production of charginos and
        neutralinos in events with three leptons and missing transverse momentum in $\sqrt{s} =$
        7 TeV *pp* collisions with the ATLAS detector' (2012). arXiv: `1208.3144` `[hep-ex]`
        (cit. on p. 89).

[132]   *CMS Collaboration*: S. Chatrchyan et al. 'Search for electroweak production of charginos
        and neutralinos using leptonic final states in *pp* collisions at $\sqrt{s} = 7$ TeV' (2012). arXiv:
        `1209.6620` `[hep-ex]` (cit. on p. 89).

[133]   *ATLAS Collaboration*: G. Aad et al. 'Search for a heavy neutral particle decaying into
        an electron and a muon using $1\,\text{fb}^{-1}$ of ATLAS data'. In: *Eur.Phys.J.* C71 (2011),
        p. 1809. DOI: `10.1140/epjc`. arXiv: `1109.3089` `[hep-ex]` (cit. on p. 89).

[134]   *ATLAS Collaboration*: G. Aad et al. 'Search for displaced vertices arising from decays
        of new heavy particles in 7 TeV *pp* collisions at ATLAS'. In: *Phys.Lett.* B707 (2012),
        pp. 478–496. DOI: `10.1016/j.physletb.2011.12.057`. arXiv: `1109.2242` `[hep-ex]`
        (cit. on p. 89).

[135]   *ATLAS Collaboration*. 'Search for Supersymmetry in events with four or more lep-
        tons in $13\,\text{fb}^{-1}$ *pp* collisions at $\sqrt{s} = 8$ TeV with the ATLAS detector' (Nov. 2012).
        ReportNumber: `ATLAS-CONF-2012-153` (cit. on p. 89).

[136]   *ATLAS Collaboration*: G. Aad et al. 'Searches for heavy long-lived sleptons and R-
        Hadrons with the ATLAS detector in *pp* collisions at $\sqrt{s} = 7$ TeV' (2012). arXiv:
        `1211.1597` `[hep-ex]` (cit. on p. 89).

[137]   *ATLAS Collaboration*: G. Aad et al. 'Search for long-lived, heavy particles in final
        states with a muon and multi-track displaced vertex in proton-proton collisions at
        $\sqrt{s} = 7$ TeV with the ATLAS detector' (2012). arXiv: `1210.7451` `[hep-ex]` (cit. on
        p. 89).

[138]   *ATLAS Collaboration*: G. Aad et al. 'Search for pair production of massive particles
        decaying into three quarks with the ATLAS detector in $\sqrt{s} = 7$ TeV *pp* collisions at
        the LHC' (2012). arXiv: `1210.4813` `[hep-ex]` (cit. on p. 89).

[139]   *ATLAS Collaboration*: G. Aad et al. 'Search for R-parity-violating supersymmetry in
        events with four or more leptons in $\sqrt{s} = 7$ TeV *pp* collisions with the ATLAS detector'
        (2012). arXiv: `1210.4457` `[hep-ex]` (cit. on p. 89).

[140]   *ATLAS Collaboration*: G. Aad et al. 'Search for lepton flavour violation in the emu
        continuum with the ATLAS detector in $\sqrt{s} = 7$ TeV *pp* collisions at the LHC'. In:
        Eur.Phys.J. C72 (2012), p. 2040. DOI: `10.1140/epjc`. arXiv: `1205.0725` `[hep-ex]`
        (cit. on p. 89).

[141]   *CMS Collaboration*. 'Search for RPV supersymmetry with three or more leptons and
        b-tags' (2012). ReportNumber: `CMS-PAS-SUS-12-027` (cit. on p. 89).

[142]   *ATLAS Collaboration*: G. Aad et al. 'Search for a light Higgs boson decaying to long-
        lived weakly-interacting particles in proton-proton collisions at $\sqrt{s} = 7$ TeV with the
        ATLAS detector'. In: *Phys.Rev.Lett.* 108 (2012), p. 251801. DOI: `10.1103/PhysRevLett.`
        `108.251801`. arXiv: `1203.1303` `[hep-ex]` (cit. on p. 89).

[143]   *ATLAS Collaboration*: G. Aad et al. 'Search for displaced muonic lepton jets from light
        Higgs boson decay in proton-proton collisions at $\sqrt{s} = 7$ TeV with the ATLAS detector'
        (2012). arXiv: `1210.0435` `[hep-ex]` (cit. on p. 89).

[144]   *CMS Collaboration*: S. Chatrchyan et al. 'Search for new physics with long-lived particles decaying to photons and missing energy in *pp* collisions at $\sqrt{s} = 7\,\text{TeV}$' (2012). arXiv: `1207.0627 [hep-ex]` (cit. on p. 89).

[145]   *CMS Collaboration*: S. Chatrchyan et al. 'Search in leptonic channels for heavy resonances decaying to long-lived neutral particles' (2012). arXiv: `1211.2472 [hep-ex]` (cit. on pp. 89, 94).

[146]   *ALEPH, DELPHI, L3 OPAL experiments*: LEP2 SUSY Working Group. 'Combined LEP Chargino Results, up to 208 GeV' (2001). URL: `http://lepsusy.web.cern.ch/lepsusy/www/inos_moriond01/charginos_pub.html` (cit. on p. 92).

[147]   *LHCb Collaboration*: R. Aaij et al. 'First evidence for the decay $B_s^0 \to \mu^+\mu^-$' (2012). arXiv: `1211.2674 [hep-ex]` (cit. on p. 92).

[148]   W. Altmannshofer, M. Carena, N. Shah and F. Yu. 'Indirect Probes of the MSSM after the Higgs Discovery' (2012). arXiv: `1211.1976 [hep-ph]` (cit. on p. 93).

[149]   K. Melnikov and M. Schulze. 'NLO QCD corrections to top quark pair production and decay at hadron colliders'. In: *JHEP* 0908 (2009), p. 049. DOI: `10.1088/1126-6708`. arXiv: `0907.3090 [hep-ph]` (cit. on p. 94).

[150]   J. M. Campbell, R. K. Ellis and D. L. Rainwater. 'Next-to-leading order QCD predictions for $W + 2$ jet and $Z + 2$ jet production at the CERN LHC'. In: *Phys.Rev.* D68 (2003), p. 094021. DOI: `10.1103/PhysRevD.68.094021`. arXiv: `hep-ph/0308195 [hep-ph]` (cit. on p. 94).

[151]   I. Hinchliffe, F. Paige, M. Shapiro, J. Soderqvist and W. Yao. 'Precision SUSY measurements at CERN LHC'. In: *Phys.Rev.* D55 (1997), pp. 5520–5540. DOI: `10.1103/PhysRevD.55.5520`. arXiv: `hep-ph/9610544 [hep-ph]` (cit. on p. 97).

[152]   B. C. Allanach, C. Lester, M. A. Parker and B. Webber. 'Measuring sparticle masses in nonuniversal string inspired models at the LHC'. In: *JHEP* 0009 (2000), p. 004. arXiv: `hep-ph/0007009 [hep-ph]` (cit. on p. 97).

[153]   *CMS Collaboration*. 'Discovery potential and measurement of a dilepton mass edge in SUSY events at $\sqrt{s} = 10\,\text{TeV}$' (2009). ReportNumber: `CMS-PAS-SUS-09-002` (cit. on p. 97).

[154]   M. Gustafsson, S. Rydbeck, L. Lopez-Honorez and E. Lundstrom. 'Status of the Inert Doublet Model and the Role of multileptons at the LHC'. In: *Phys.Rev.* D86 (2012), p. 075019. DOI: `10.1103/PhysRevD.86.075019`. arXiv: `1206.6316 [hep-ph]` (cit. on p. 98).

[155]   *CMS Collaboration*: S. Chatrchyan et al. 'Interpretation of searches for supersymmetry with simplified models' (2013). arXiv: `1301.2175 [hep-ex]` (cit. on p. 103).

[156]   S. Weinberg. 'A Model of Leptons'. In: *Phys.Rev.Lett.* 19 (1967), pp. 1264–1266. DOI: `10.1103/PhysRevLett.19.1264` (cit. on p. 105).

[157]   G. Branco, P. Ferreira, L. Lavoura, M. Rebelo, M. Sher et al. 'Theory and phenomenology of two-Higgs-doublet models'. In: *Phys.Rept.* 516 (2012), pp. 1–102. DOI: `10.1016/j.physrep.2012.02.002`. arXiv: `1106.0034 [hep-ph]` (cit. on p. 107).

[158]   A. Djouadi. 'The Anatomy of electro-weak symmetry breaking II: The Higgs bosons in the minimal supersymmetric model'. In: *Phys.Rept.* 459 (2008), pp. 1–241. DOI: `10.1016/j.physrep.2007.10.005`. arXiv: `hep-ph/0503173 [hep-ph]` (cit. on p. 107).

[159]   H. Georgi. *Lie Algebras in Particle Physics – From Isospin to Unified Theories*. Vol. 54. Front.Phys., 1999, pp. 1–255 (cit. on p. 109).

[160]   H. Jones. *Groups, representations and physics*. Taylor & Francis Group, 1998 (cit. on p. 109).

[161]   P. Ramond. *Group theory: A physicist's survey*. Cambridge, 2010 (cit. on p. 109).

[162]   A. Proca. 1936 (cit. on p. 116).

[163]   J. C. Maxwell. 'A dynamical theory of the electromagnetic field'. In: *Phil.Trans.Roy.-Soc.Lond.* 155 (1865), pp. 459–512 (cit. on p. 116).

[164]   E. Stückelberg. 'Interaction forces in electrodynamics and in the field theory of nuclear forces'. In: *Helv.Phys.Acta* 11 (1938), pp. 299–328 (cit. on p. 117).

[165]   L. Lorenz. 'On the identity of the vibrations of light with electrical currents'. In: *Phil.Mag.* 34 (1867), p. 287 (cit. on p. 117).

[166]   S. Weinberg. *The quantum theory of fields. Vol. 3: Supersymmetry*. 2000. ISBN-9780521670555 (cit. on p. 117).

[167]   W. Rarita and J. Schwinger. 'On a theory of particles with half integral spin'. In: *Phys.Rev.* 60 (1941), p. 61. DOI: 10.1103/PhysRev.60.61 (cit. on p. 118).

[168]   H. Watanabe, H. Shimodaira and S. Kamefuchi. 'The Stückelberg formalism for Rarita-Schwinger field with spin 3/2'. In: *Nuclear Physics B* 2.3 (1967), pp. 360–368 (cit. on p. 119).

[169]   M. Fierz and W. Pauli. 'On relativistic wave equations for particles of arbitrary spin in an electromagnetic field'. In: *Proc.Roy.Soc.Lond.* A173 (1939), pp. 211–232 (cit. on p. 122).

[170]   K. Hinterbichler. 'Theoretical Aspects of Massive Gravity'. In: *Rev.Mod.Phys.* 84 (2012), pp. 671–710. DOI: 10.1103/RevModPhys.84.671. arXiv: 1105.3735 [hep-th] (cit. on p. 122).